

APPLIED PHYSICS REVIEWS

Luminescence properties of defects in GaN

Michael A. Reshchikov^{a)} and Hadis Morkoç

Department of Electrical Engineering and Physics Department, Virginia Commonwealth University, Richmond, Virginia 23284

(Received 13 July 2004; accepted 18 January 2005; published online 15 March 2005)

Gallium nitride (GaN) and its allied binaries InN and AlN as well as their ternary compounds have gained an unprecedented attention due to their wide-ranging applications encompassing green, blue, violet, and ultraviolet (UV) emitters and detectors (in photon ranges inaccessible by other semiconductors) and high-power amplifiers. However, even the best of the three binaries, GaN, contains many structural and point defects caused to a large extent by lattice and stacking mismatch with substrates. These defects notably affect the electrical and optical properties of the host material and can seriously degrade the performance and reliability of devices made based on these nitride semiconductors. Even though GaN broke the long-standing paradigm that high density of dislocations precludes acceptable device performance, point defects have taken the center stage as they exacerbate efforts to increase the efficiency of emitters, increase laser operation lifetime, and lead to anomalies in electronic devices. The point defects include native isolated defects (vacancies, interstitial, and antisites), intentional or unintentional impurities, as well as complexes involving different combinations of the isolated defects. Further improvements in device performance and longevity hinge on an in-depth understanding of point defects and their reduction. In this review a comprehensive and critical analysis of point defects in GaN, particularly their manifestation in luminescence, is presented. In addition to a comprehensive analysis of native point defects, the signatures of intentionally and unintentionally introduced impurities are addressed. The review discusses in detail the characteristics and the origin of the major luminescence bands including the ultraviolet, blue, green, yellow, and red bands in undoped GaN. The effects of important group-II impurities, such as Zn and Mg on the photoluminescence of GaN, are treated in detail. Similarly, but to a lesser extent, the effects of other impurities, such as C, Si, H, O, Be, Mn, Cd, etc., on the luminescence properties of GaN are also reviewed. Further, atypical luminescence lines which are tentatively attributed to the surface and structural defects are discussed. The effect of surfaces and surface preparation, particularly wet and dry etching, exposure to UV light in vacuum or controlled gas ambient, annealing, and ion implantation on the characteristics of the defect-related emissions is described. © 2005 American Institute of Physics. [DOI: 10.1063/1.1868059]

TABLE OF CONTENTS

I. INTRODUCTION.....	3	2. Substitutional acceptors.....	8
II. FORMATION AND ENERGY LEVELS OF POINT DEFECTS IN GaN.....	5	3. Isoelectronic impurities.....	9
A. Theoretical approach.....	5	4. Hydrogen.....	9
B. Native point defects.....	6	D. Complexes.....	9
1. Vacancies.....	6	1. Shallow donor—gallium vacancy complexes.....	10
a. Gallium vacancy.....	7	2. Shallow acceptor—nitrogen vacancy complexes.....	10
b. Nitrogen vacancy.....	7	3. Hydrogen-related complexes.....	10
c. Divacancy.....	7	4. Other complexes.....	11
2. Interstitials and antisite defects.....	7	E. Role of dislocations in the point defect formation.....	11
a. Gallium interstitial.....	7	III. LUMINESCENCE METHODS.....	12
b. Nitrogen interstitial.....	7	A. Steady-state photoluminescence.....	12
c. Gallium antisite.....	8	1. Recombination statistics.....	12
d. Nitrogen antisite.....	8	2. Effect of temperature on PL intensity.....	13
C. Impurities.....	8	3. Estimates of quantum efficiency.....	14
1. Shallow donors.....	8	4. Effect of excitation intensity on PL intensity.....	14

5. Estimates of acceptor concentration in <i>n</i> -type GaN.....	15	d. Resonant excitation and vibrational properties.....	51
B. Time-resolved luminescence.....	15	e. ODMR and defect identification.....	52
C. Vibrational properties of deep-level defects..	16	2. Green, yellow, and red luminescence bands.....	52
D. Photoluminescence excitation spectra.....	17	B. Luminescence in Mg-doped GaN.....	52
E. Spatially and depth-resolved cathodoluminescence.....	18	1. Ultraviolet luminescence band in lightly Mg-doped GaN.....	53
F. Optically detected magnetic resonance.....	18	2. Effect of potential fluctuations on PL.....	54
IV. LUMINESCENCE RELATED TO POINT DEFECTS IN UNDOPED GaN.....	18	3. UVL and BL bands in compensated and heavily Mg-doped GaN.....	56
A. Yellow luminescence band.....	19	a. Effects of growth conditions and annealing.....	56
1. Effect of temperature.....	20	b. Effect of excitation intensity.....	57
2. Effect of excitation intensity.....	22	c. Effect of temperature.....	58
3. Effect of hydrostatic pressure.....	22	d. Time-resolved PL.....	60
4. Effect of electron irradiation.....	23	e. Effect of hydrostatic pressure.....	60
5. Time-resolved PL.....	23	f. Effect of electron irradiation.....	60
6. Resonant excitation.....	25	g. Optically detected magnetic resonance..	61
7. Vibrational model of the YL.....	26	h. DLTS, positron annihilation, and the infrared spectra.....	61
8. Comparison with the positron annihilation results.....	26	4. Yellow and red luminescence bands.....	62
9. ODMR on the YL.....	27	5. Luminescence in GaN:Mg codoped with shallow donors.....	62
10. Effect of doping on the YL.....	27	6. Identification of defects in Mg-doped GaN.....	62
B. Yellow and green luminescence in high-purity GaN.....	28	C. Luminescence in GaN doped with other impurities.....	62
1. Effect of excitation intensity.....	29	1. Doping with shallow donors.....	62
2. Resonant excitation.....	30	a. Silicon doping.....	62
3. Time-resolved PL.....	31	b. Oxygen doping.....	63
4. Effect of temperature.....	33	c. Selenium doping.....	63
C. Ultraviolet (shallow DAP) band.....	34	d. Germanium doping.....	63
1. Steady-state PL.....	34	2. Doping with acceptors.....	63
2. Time-resolved PL.....	36	a. Carbon doping.....	63
3. ODMR and identification of the shallow acceptor.....	37	b. Beryllium doping.....	64
D. Blue luminescence band.....	38	c. Calcium doping.....	64
1. Steady-state PL.....	38	d. Cadmium doping.....	65
2. Time-resolved PL.....	40	e. Manganese doping.....	65
3. Spatially and depth-resolved cathodoluminescence.....	40	f. Other acceptors in GaN.....	65
4. Origin of the BL band in undoped GaN..	40	3. Doping with isoelectronic impurities.....	65
E. Red luminescence band.....	41	a. Arsenic doping.....	65
F. Red and green luminescence bands in Ga-rich GaN grown by MBE.....	42	b. Phosphorus doping.....	66
1. Effect of excitation intensity.....	42	4. Radiative defects introduced by irradiation.....	66
2. Effect of temperature.....	43	5. Transition and rare-earth elements.....	67
3. Time-resolved PL.....	44	a. Transition metals.....	67
4. Resonant excitation of the GL2 and RL2 bands.....	45	b. Rare-earth elements.....	67
5. Origin and model of the GL2 and RL2 bands.....	45	VI. DEFECT-RELATED LUMINESCENCE IN CUBIC GaN.....	67
G. Other broad bands in undoped GaN.....	46	A. Undoped material.....	67
H. Characteristics and identification of radiative defects in undoped GaN.....	47	1. Exciton emission.....	67
V. INTENTIONALLY INTRODUCED IMPURITIES AND NATIVE DEFECTS.....	48	2. Shallow DAP band.....	67
A. Luminescence in Zn-doped GaN.....	48	3. Deep defects.....	68
1. Blue luminescence band.....	49	B. Doped material.....	68
a. Effect of temperature.....	49	1. Carbon doping.....	68
b. Effect of excitation intensity.....	50	2. Magnesium doping.....	69
c. Time-resolved PL.....	51	3. Silicon doping.....	69
		VII. EXCITONS BOUND TO POINT DEFECTS....	69

A. Free excitons.....	69
B. Bound excitons.....	71
1. Excitons bound to shallow donors.....	71
2. Excitons bound to acceptors.....	73
3. Haynes rule in GaN.....	74
VIII. UNUSUAL LUMINESCENCE LINES IN GaN.....	75
A. Y_i lines.....	75
1. Effects of sample treatments and experimental conditions on the Y_i lines...	76
a. Effect of hot wet chemical etching....	76
b. Effect of photoelectrochemical etching.....	77
c. Evolution of PL and memory effect....	77
d. Effect of excitation intensity.....	77
e. Effect of temperature.....	77
2. Characteristics of the Y_i lines.....	78
a. The 3.45-eV line (Y_1).....	78
b. The 3.42-eV line (Y_2).....	79
c. The 3.38-eV line (Y_3).....	79
d. The 3.35-eV line (Y_4).....	79
e. The 3.34-eV line (Y_5).....	79
f. The 3.32-eV line (Y_6).....	79
g. The 3.21-eV line (Y_7).....	80
h. The 3.08-, 2.85-, 2.80- and 2.66-eV lines (Y_8 – Y_{11}).....	80
3. Y_i lines and structural defects.....	80
a. Atomic force microscopy.....	80
b. X-ray diffraction.....	80
c. Transmission electron microscopy.....	81
B. Oil-related 3.31- and 3.36-eV lines.....	81
C. Identification of the Y_i lines.....	82
IX. UNSTABLE LUMINESCENCE FROM DEFECTS.....	82
A. Unstable luminescence bands.....	82
1. Blue band from the etched GaN surface..	83
2. Blue and yellow unstable bands.....	83
B. Manifestation of surface states in photoluminescence.....	85
1. Band bending at the surface of GaN.....	85
2. Effect of UV illumination on PL.....	86
3. Effect of ambient on intensity and shape of PL bands.....	86
4. Effect of passivation on PL.....	87
X. SUMMARY.....	88

I. INTRODUCTION

Gallium nitride and its alloys with InN and AlN have emerged as important semiconductor materials with applications to green, blue, and ultraviolet portions of the spectrum as emitters and detectors and as high-power/temperature radio frequency electronic devices. However, further improvements in device performance hinge on understanding and reduction of extended and point defects. The lack of native substrates makes the fabrication of efficient and reliable devices particularly difficult, which is typified by dislocation

densities in the range of 10^9 – 10^{10} cm^{-2} on sapphire substrates unless special precautions are taken. Isolated point defects and defects related to dislocations are responsible for a variety of ailments in devices. In detectors, they manifest themselves as excess dark current, noise, and reduced responsivity. In light-emitting devices, they reduce radiative efficiency and operation lifetime. Furthermore, the point defects and complexes are generally the culprits for parasitic current paths. Moreover, they decrease the gain and increase the noise—particularly the low-frequency noise—in electronic devices, increase the threshold current, the slope efficiency and operation lifetime of lasers, and are source of instability particularly in devices relying on charge control and high electric fields such as field-effect transistors.

It is customary to bring a variety of techniques to probe the optical and electrical signatures associated with point defects. Luminescence is a very strong tool for detection and identification of point defects in semiconductors, especially in wide-band-gap varieties where application of electrical characterization is limited because of large activation energies that are beyond the reach of thermal means. In spite of considerable progress made in the last decade in light-emitting and electronic devices based on GaN, understanding and identification of point defects remain surprisingly enigmatic. One of the reasons is a vast number of controversial results in the literature. Therefore, a critical review of the state of understanding of point defects, particularly the issues dealing with their manifestation in luminescence experiments, is very timely. Even though the optical properties of GaN have been reviewed by Monemar,^{1–4} only a small fraction of those reviews concerned themselves with defect-associated luminescence in GaN. It should also be noted that a brief review of point defects and their optical properties in GaN can be found in earlier reviews and books prepared as part of the general properties of GaN.^{5–13} In many original works and reviews, analysis of the luminescence is limited to excitonic emission, a field which is well understood, leaving out an earnest discussion of point defects in GaN which still remain unidentified. Traditionally by *point defects* one means native defects, impurities, and complexes with the size comparable to the nearest atomic distance. Besides point defects, the crystal lattice may contain *extended defects*, such as dislocations, clusters, domains, voids, etc. The latter commonly do not contribute to the luminescence, although may significantly affect the optical and electronic properties of the material by trapping carriers or gettering the point defects.

In order to illustrate the myriad of optical transitions that could be and have been observed in the luminescence spectra of GaN associated with defects, we present a table summarizing them (Table I) as well as a figure (Fig. 1) showing a schematic description of the related transitions and energy positions within the gap of the defect levels we are about to discuss in detail throughout the review. In addition to the luminescence energy-band positions, Table I tabulates their nomenclature and provides brief comments and references to the sections of this review where these lines and bands are discussed in detail. The energy position of the luminescence lines and bands may depend on strain in thin GaN layers, temperature, and excitation intensity. Therefore, in Table I

^aElectronic mail: mreshchi@vcu.edu

TABLE I. List of main luminescence lines and bands in GaN.

Maximum position (eV)	Nomenclature	Doping	Comments	Reference to the text (pages)
3.478	FE, X_A	Undoped		69–71
3.471	DBE, D^0X_A	Undoped, Si	A few close lines	71–75
3.466	ABE, A^0X_A	Undoped, Mg	Best FWHM <0.1 meV	73–75
3.44–3.46	TES	Undoped	Plethora of lines	71–72
3.455	ABE	Zn	A weaker peak at 3.39 eV	49, 71–72
3.45–3.46	Y_1	Undoped	Correlates with inversion domains	75–82
3.41–3.42	Y_2	Undoped		75–82
3.397		Be	e-A type	64
3.387	FE-LO	Undoped		69–71
3.38	DBE-LO	Undoped		71–73
3.38		Be	DAP type	64
3.37–3.38	Y_3	Undoped	Undoped	75–82
3.375	ABE-LO	Undoped		73–74
3.364	ABE-LO	Zn		49, 71–72
3.35–3.36	Y_4	Undoped		75–82
3.34	Y_5	Undoped		75–82
3.30–3.32	Y_6	Undoped		75–82
3.295	FE-2LO	Undoped		69–71
3.288	DBE-2LO	Undoped		71–75
3.283	ABE-2LO	Undoped		71–75
3.28	UVL	Undoped	e-A type	34–37
3.272	ABE-2LO	Zn		49, 71–72
3.27	DBE		DBE in cubic GaN	67–68
3.26	UVL	Undoped, Si	DAP type	19, 34–37, 47–48, 63
3.1–3.26	UVL	Mg	e-A and DAP	53, 54, 56–62
3.21–3.23	Y_7	Undoped		75–82
3.16			Shallow DAP in cubic GaN	67–68
3.08	Y_8	Undoped		80
3.08		C	In cubic GaN	68–69
3.0–3.05	BL	C	Broad	63–64
2.9–3.0	BL	Undoped, Fe	Broad, unstable intensity	83–84
2.9	BL	P	Broad, with fine structure	66
2.88	BL	Undoped	Broad, with fine structure	19, 38–41, 47–48
2.88	BL	Zn	Broad, with fine structure	48–52
2.86	Y_9	Undoped		80
2.8	Y_{10}	Undoped		80
2.8	BL	Cd	Broad, with fine structure	64–65
2.7–2.8	BL	Mg	Broad, large shifts	56–62
2.6–2.8	BL	Undoped	Broad, surface related	83
2.68	Y_{11}	Undoped		80
2.6	GL	As	Broad, with fine structure	65–66
2.6	GL	Zn	Broad	48, 52
2.56	AL	Undoped	Broad	47
2.51	GL3	Undoped	Broad	47
2.5		Ca	Broad	64
2.4–2.5		Mg–O	Broad	62
2.48	GL	Undoped	Broad	29–34
2.43		Hg	Broad	65
2.36	GL2	Undoped	Broad	19, 42–48
2.2–2.3	YL	Undoped, C	Broad	19–34, 47–48, 63
1.9–2.1		C	Broad, in cubic GaN	68–69
1.8–2.0	RL	Undoped	Broad	19, 41, 47–48
1.85	RL2	Undoped	Broad	19, 42–48
1.8		Zn	Broad	48, 52
1.7–1.8		Mg	Broad	62
1.66		Undoped	Broad	42
1.64		C	Broad	63–64
1.3		(Fe)	Sharp	67
1.27		Mn	Broad	65
1.193		(Ti,Cr)?	Sharp	67
0.95		Undoped	Sharp, irradiation induced	66
0.85–0.88		Undoped	Sharp, irradiation induced	66

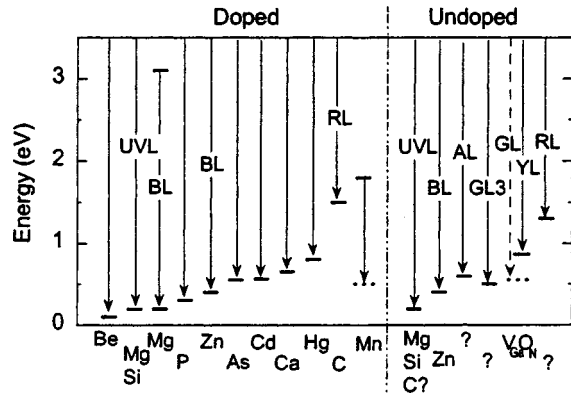


FIG. 1. Radiative transitions associated with major doping impurities (see Sec. V) and unintentionally introduced defects (Sec. IV) in GaN. For the $V_{\text{Ga}}\text{O}_\text{N}$ complex, two charge states are shown (Sec. IV B). Transitions resulting in the GL2 and RL2 bands are assumed to be internal and the related defect levels are unknown (Sec. IV F).

we give the energy positions corresponding to the strain-free GaN at low temperatures and excitation intensities. In the case of dispersion in the reported data for a particular luminescence band, we give the most commonly observed energy position. In Fig. 1, the positions of the energy levels are shown in scale, whereas the radiative transitions, depicted by the arrows, correspond to the zero-phonon line, which has higher photon energy than the maximum of the broad luminescence band due to the Stokes shift.

The arrangement of this review is as follows: in Sec. II the theoretical predictions from the first-principles calculations regarding the formation probability and energy levels of main point defects in GaN are reviewed. Although the accuracy of the predictions may not be sufficiently high, these efforts as a minimum provide a first-order idea on what kind of defects we may expect in GaN while undertaking the task of analyzing the luminescence data. Section III presents basics of the luminescence methods employed. In Sec. IV, the properties of the main luminescence bands in unintentionally doped GaN are reviewed. The plethora of data published in literature are classified and analyzed, particularly dealing with the notorious yellow luminescence in undoped GaN. The results of different works are often controversial and need careful analysis. In this section, we present some previously unpublished data obtained in our laboratory in order to assist the reader to better formulate a model for a complete picture.

Luminescence from defects intentionally introduced in GaN (by doping, postgrowth implantation, or by irradiation damage) is analyzed in Sec. V. Among the numerous impurities we give particular attention to magnesium and zinc since these two impurities are of paramount importance for GaN-based devices and the published luminescence properties of GaN doped with Zn and Mg are very controversial. Impurities, such as transition metals and rare-earth elements, are reviewed very briefly, being beyond the scope of the theme of this review since the luminescence properties of semiconductors doped with these impurities are almost independent of the host material, being determined mostly by internal transitions associated with these elements but modified some by the crystal field of the host material. Section VI

briefly reviews luminescence from the other metastable phase of GaN—zinc-blende or cubic GaN. This crystal polytype is not well developed and not widely used. Consequently, much less space is devoted to defects in cubic GaN.

We also briefly review the near-band-edge luminescence related to recombination of excitons in GaN in Sec. VII, in part for completeness and in part to distinguish the *typical* excitonic lines from the *unusual* luminescence lines appearing in the same energy range. The properties of the unusual luminescence lines, inclusive of those that are now attributed to artifacts mistakenly reported in the literature as being related to GaN, are discussed in Sec. VIII. In some cases, the luminescence in GaN evolves under ultraviolet illumination. The changes may be quite large and they are usually detected on time scales ranging from a few seconds to several hours. These changes may be due to metastability of point defects or some light-induced changes at or near the surface of GaN. In this vein, unstable luminescence and the effect of different ambient on luminescence are presented in Sec. IX. Finally, Sec. X brings this comprehensive review to a close with a brief summary.

II. FORMATION AND ENERGY LEVELS OF POINT DEFECTS IN GaN

In this section, the salient features of theoretical calculations that may help to identify luminescence bands in undoped and doped GaN are reviewed. In early studies, Jenkins and Dow,¹⁴ based on an empirical tight-binding theory, have estimated the energy levels of vacancies and antisites in GaN. In the past decade since then, *ab initio* computational methods significantly improved the accuracy of predictions of the defect energy levels in GaN. Neugebauer and Van de Walle,^{15–17} and Boguslawski *et al.*,¹⁸ have estimated not only the energy levels of the main point defects in GaN but also their formation energies and possible range of concentrations. Thereafter many theoretical groups employed and developed the first-principles calculations germane to nitrides for improved predictions and exploring the likelihood of formation of numerous point and structural defects in this material.^{19–24}

A. Theoretical approach

The concentration c of a point defect in the semiconductor formed at a temperature T under thermodynamic equilibrium conditions is determined by its formation energy E^f as

$$c = N_{\text{sites}} \exp\left(\frac{S^f}{k} - \frac{E^f}{kT}\right), \quad (1)$$

where N_{sites} is the concentration of sites in the lattice where the particular defect can be incorporated ($N_{\text{sites}} \approx 4.4 \times 10^{22} \text{ cm}^{-3}$ for the substitutional defects in GaN) and S^f is the formation entropy, which is about $6k$.^{19,20} When the defects or their constituents are impurities, Eq. (1) gives an upper limit of their possible concentrations on the assumption that the impurities are abundantly available during the growth. Although the growth is a nonequilibrium process, at sufficiently high growth or annealing temperatures the conditions may be approximated as in equilibrium. Equation (1)

shows that E^f is the key parameter for estimating likelihood of defect formation. Obviously, the defects with high formation energies have less probability to form.

The formation energy can be calculated in the formalism of Zhang and Northrup²⁵ as

$$E^f(q, E_F) = E^{\text{tot}}(q) - E_{\text{bulk}}^{\text{tot}} - \sum_i n_i \mu_i + qE_F, \quad (2)$$

where $E^{\text{tot}}(q)$ is the total energy of a supercell containing one defect in the charge state q , $E_{\text{bulk}}^{\text{tot}}$ is the total energy of the defect-free supercell, n_i is the number of atoms of type i in this supercell, μ_i is the chemical potential of atoms of type i , E_F (the Fermi level) is the electron chemical potential with respect to the valence-band maximum. The chemical potentials for Ga and N are usually considered for extreme growth or annealing conditions: $\mu_{\text{Ga}} = \mu_{\text{Ga(bulk)}}$ for the Ga-rich case and $\mu_{\text{N}} = \mu_{\text{N}_2}$ for the N-rich case. Note that these values are not independent in that $\mu_{\text{Ga}} + \mu_{\text{N}} = \mu_{\text{GaN}}$. The formation energy of the charged defects depends on the charge and the Fermi level at the time of defect formation (during growth or annealing). As can be seen from Eq. (2), the formation energy of the positively (negatively) charged defects increases (decreases) as the Fermi level moves from the valence-band maximum towards the conduction band. The slope of this variation is proportional to the charge state of the defect. The energy at which the levels corresponding to different charge states intersect determines the ionization level of the defect. Note that the calculations of the total energy may in general give an error of up to a few tenths of eV, and a variety of corrections is often used to improve the accuracy. The details on the first-principles calculations used for defects in GaN can be found in the recent review by Van de Walle and Neugebauer.²⁶

The above approach enables one to calculate not only the formation energies and positions of the defect levels but also the binding and dissociation energies of complex defects, local modes of vibrations, and migration barriers or diffusivity of point defects. Any agreement between different groups, using slightly different approaches, increases confidence in the reliability of the results.

B. Native point defects

Native defects are always present in semiconductors and notably affect the electrical and optical properties of the host material. They are often formed as compensation sources when dopants are introduced, or as a result of nonstoichiometric growth or annealing. The isolated native defects take the form of vacancies, interstitials, and antisites. Complex defects formed through interaction of isolated native defects, and combinations of native defects and impurities are considered in Sec. II D.

Figure 2 shows the calculated formation energies for all isolated native point defects in GaN as a function of the Fermi level in all stable charge states. The transition levels so calculated for the native defects are illustrated in Fig. 3. The slope of each line in Fig. 2 represents a charge of the defect. For each charge state only the segment giving the lowest overall energy is shown. The changes in slope of the lines

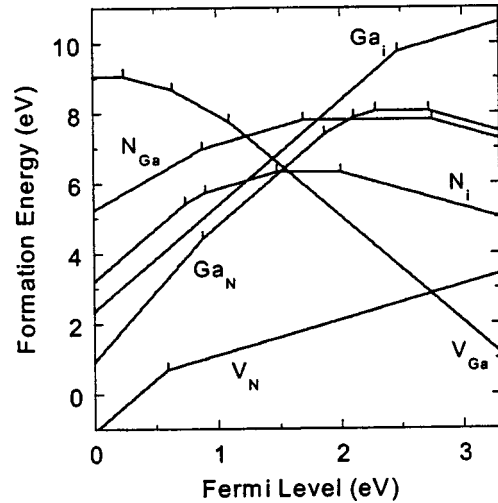


FIG. 2. Formation energies as a function of Fermi level for native point defects in GaN. Ga-rich conditions are assumed. The zero of Fermi level corresponds to the top of the valence band. Only segments corresponding to the lowest-energy charge states are shown. Adapted with permission from Limpijumong and Van de Walle, Phys. Rev. B 69, 035207 (2004). Copyright (2004) by the American Physical Society.

represent the energy level of the defect (Fig. 3) that can be measured experimentally. It is clear from Fig. 2 that self-interstitial and antisite defects have very high formation energies and thus are unlikely to occur in GaN during growth at least in n -type GaN. Gallium and nitrogen vacancies may be abundant in n - and p -type GaN, respectively. It must be noted, however, that electron irradiation or ion implantation can create the defects which have high formation energy in large concentrations.

1. Vacancies

Similar to the case of GaAs,²⁷ vacancies in GaN are multiply charged defects, and several defect levels may appear in the energy gap (Fig. 3). A gallium vacancy (V_{Ga}) may be the dominant native defect in n -type GaN, whereas the nitrogen vacancy (V_{N}) may be abundantly formed in p -type

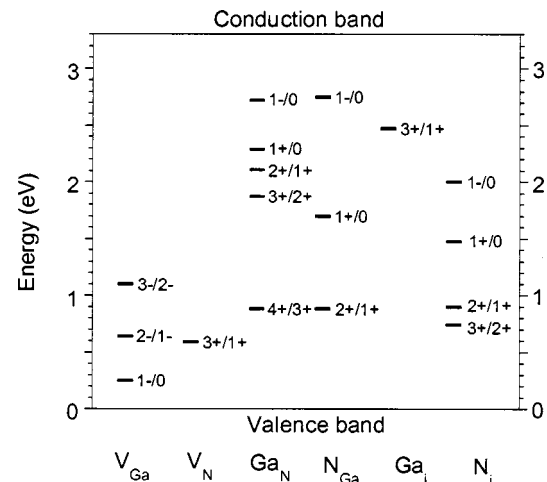


FIG. 3. Transition levels for native defects in GaN, determined from formation energies displayed in Fig. 2. Adapted with permission from Limpijumong and Van de Walle, Phys. Rev. B 69, 035207 (2004). Copyright (2004) by the American Physical Society.

GaN. Evidently N-rich conditions favor formation of V_{Ga} , while in the Ga-rich case the formation of V_{Ga} is facilitated.

a. Gallium vacancy. The gallium vacancy has relatively low formation energy in *n*-type GaN when the Fermi level is close to the conduction band. Being an acceptorlike defect, the V_{Ga} acts as a compensating center. The $2-/3-$, $-/2-$, and $0/-$ transition levels of V_{Ga} are estimated at 1.10, 0.64, and 0.25 eV, respectively (Fig. 3).²¹ Slightly larger values of the ionization energies (about 1.5, 1.0, and 0.5 eV, respectively) have been reported by other authors.^{22,28} However, the formation energies of V_{Ga}^{3-} are consistently low when the Fermi level is close to the conduction band. In *n*-type GaN the Ga vacancy is completely filled with electrons, and capture of a photogenerated hole, e.g., during photoluminescence measurements, may lead to radiative transition of an electron from the conduction band or from a shallow donor level to the $3-/2-$ level of V_{Ga} . The calculated migration barrier for V_{Ga}^{3-} is relatively low: 1.9 eV.²¹ Therefore, the Ga vacancies are mobile in a wide range of temperatures typically used during growth or thermal annealing. It is likely that they migrate and form complexes with more stable defects.

b. Nitrogen vacancy. Early calculations predicted the energy levels of the nitrogen vacancy to be close to or inside the conduction band.^{14,15,18} In fact, owing to these early calculations, the *n*-type conductivity in undoped GaN has for a considerable period of time been attributed to V_{N} ,¹⁴ an attribution which is still in circulation. However, the first-principles calculations showed that V_{N} might be formed in detectable concentrations in *n*-type GaN only under Ga-rich conditions.^{15,18} In this scenario, an electron from the resonance $0/-$ state would autoionize to the bottom of the conduction band, where it would form an effective-masslike state bound by the Coulomb tail of the vacancy potential.^{15,18} Thus V_{N} acts as a donor. There is only one transition level for V_{N} in the gap which is the $3+/+$ state situated at about 0.5 ± 0.2 eV above the valence-band maximum (Fig. 3).^{21,29} The $2+$ charge state is unstable, and transition from $+$ to $3+$ charge state causes a large lattice relaxation.^{21,24,29} The migration barrier for the charge states $3+$ and $+$ is estimated at 2.6 and 4.3 eV, respectively.²¹ Similar to the case of V_{Ga} , the relatively low migration barriers (at least for V_{N}^{3+}) could pave the way for the formation of complexes between V_{N} and more stable defects during high-temperature growth or annealing, especially in *p*-type GaN where the $3+$ state may dominate.

c. Divacancy. A divacancy ($V_{\text{Ga}}V_{\text{N}}$) has relatively high formation energy in GaN and is unlikely to form in large concentrations (Fig. 4). This particular defect, if formed, is expected to produce at least two deep levels in the energy gap of GaN and behaves as a double acceptor in *n*-type and as a double donor in *p*-type GaN.²²

2. Interstitials and antisite defects

Formation of interstitial and antisite defects is often considered to have a low probability in GaN due to the small lattice constant of GaN and the large size mismatch between

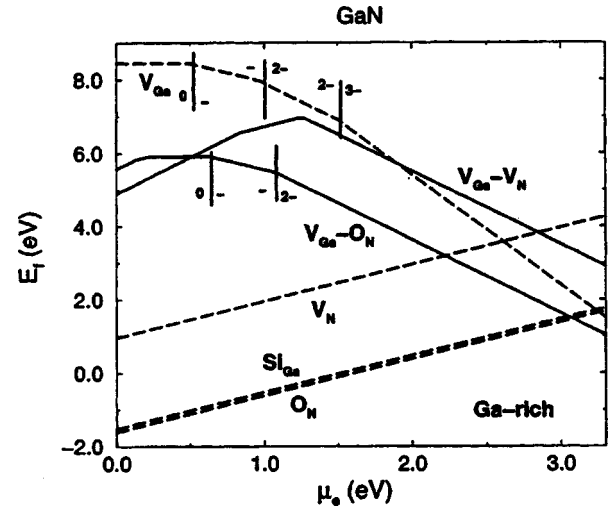


FIG. 4. Calculated formation energies and ionization levels for the defects in GaN in the Ga-rich case. The dashed lines correspond to isolated point defects and the solid lines to defect complexes, respectively. Reprinted with permission from Mattila and Nieminen, Phys. Rev. B 55, 9571 (1997). Copyright (1997) by the American Physical Society.

Ga and N atoms.³⁰ However, under certain conditions some of these defects may form but in very small concentrations.

a. Gallium interstitial. The large size of the Ga atom leads to high formation energies of the Ga interstitial (Ga_i) and associated fairly large lattice relaxations. Only the octahedral site is stable for Ga_i .²¹ Although in *n*-type or under N-rich conditions the formation of Ga_i is improbable in thermodynamic equilibrium, it may form under electron irradiation in GaN or under conditions used for *p*-type growth (Fig. 2). Similar to V_{N} , Ga_i is a donor with the resonance $+/0$ state in the conduction band and a $3+/+$ state deep in the band gap (Fig. 3).^{18,21} The $3+/+$ energy level is predicted at about 2.5 eV above the valence band.²¹ A metastable behavior is possible for the $3+$ state.²¹ The migration barrier for Ga_i is estimated as approximately 0.9 eV,²¹ in agreement with the experimental results of Chow *et al.*³¹ who have discovered the mobile Ga_i in irradiated GaN at temperatures below room temperature (Sec. V C 4). Note that the optically detected electron-paramagnetic-resonance (ODEPR) experiments in Ref. 31 apparently detected the $2+$ charge state of Ga_i , which was predicted to be unstable.²¹ It is possible that the metastable $2+$ state could be activated by optical excitation.²¹ High mobility of Ga_i even at room temperature implies that Ga_i is trapped by some other defect(s) and does not exist in GaN as an isolated defect in equilibrium.

b. Nitrogen interstitial. The nitrogen interstitial (N_i) forms a N-N bond.^{15,18,21,24} It has a high formation energy, especially in Ga-rich conditions (Fig. 2). Up to four stable levels corresponding to different charge states of N_i can be formed in the energy gap (Fig. 3).²¹ The N-N bond distance monotonically decreases with an increasing charge of N_i , approaching the bond distance in a N_2 molecule in the case of N_i^{3+} .^{15,21} Note that the two N atoms share one N site in apparently equal relation. The highest stable level ($-/0$) is expected at about 2 eV above the valence-band maximum.²¹ Therefore, in *n*-type GaN, N_i will act as a simple acceptor. However, the formation energy of this defect is too high in

GaN grown under equilibrium Ga-rich conditions. The migration barrier for N_i is only about 1.5 eV for the $-$ and $3+$ charge states,²¹ so that diffusion of nitrogen interstitials is likely to occur in GaN at temperatures slightly above room temperature.

c. Gallium antisite. The gallium antisite (Ga_N) introduces a few deep levels in GaN (Fig. 3).^{18,21} The $4+/3+$ level of Ga_N is expected at about 0.9 eV above the valence band.²¹ Therefore, in p -type GaN this native defect may be responsible for significant compensation if the Ga-rich conditions are used. Large outward lattice relaxation around the Ga_N has been noted by several theorists.^{18,23}

d. Nitrogen antisite. The nitrogen antisite (N_{Ga}) apparently introduces three²¹ or perhaps even four³² deep levels in the energy gap of GaN (Fig. 3). It can behave as a compensating double donor in p -type GaN or an acceptor in n -type GaN. The formation energy of N_{Ga} is very high regardless of the position of the Fermi level, especially under Ga-rich conditions (Fig. 2). It should be pointed out that Mattila *et al.*³² predicted a reasonably low formation energy of N_{Ga}^{3-} in strongly n -type GaN grown under N-rich conditions.

The neutral N_{Ga} defect may exhibit a metastable behavior, similar to its analog in GaAs which is known as the EL2 defect.^{33,34} Mattila *et al.*³² and Gorczyca *et al.*²³ predicted that the neutral N_{Ga} defect can transform into $V_{Ga}N_i$ defect in cubic GaN.

C. Impurities

Generally, C, Si, and Ge on the Ga sites and O, S, and Se on the N sites are considered as shallow donors in GaN, whereas Be, Mg, Ca, Zn, and Cd on the Ga sites and C, Si, and Ge on the N sites could potentially give rise to relatively shallow acceptors in this semiconductor. Below we briefly review the formation energies and energy levels calculated from first principles and by using the effective-mass method. While the former could predict which defect is easier to form, the latter could provide a much better accuracy in determining the ionization energy.

1. Shallow donors

Wang and Chen³⁵ calculated the energy levels of substitutional shallow donors in GaN in the effective-mass approximation accounting for such effects as mass anisotropy, central-cell potential correction, and the conduction-band-edge wave function of the host material. They deduced the following donor ionization energies in wurtzite GaN: 34.0, 30.8, and 31.1 meV for C, Si, and Ge on the Ga site, and 32.4, 29.5, and 29.5 meV for O, S, and Se on the N sites. Boguslawski and Bernholc²⁰ considered substitutional C, Si, and Ge impurities in wurtzite GaN in the framework of first-principles calculations. They have found that formation energies of Si_{Ga} and Ge_{Ga} donors are reasonably small (0.9 and 2.3 eV, respectively, for Ga-rich conditions), while formation of C_{Ga} donor has a low probability. In various theoretical investigations the formation energy of neutral C_{Ga} has been estimated as 4–4.7 eV for the N-rich case and 5.7–6.5 eV for the Ga-rich case.^{20,23,36} Neugebauer and Van de Walle¹⁷ and Mattila and Nieminen²² have obtained small formation ener-

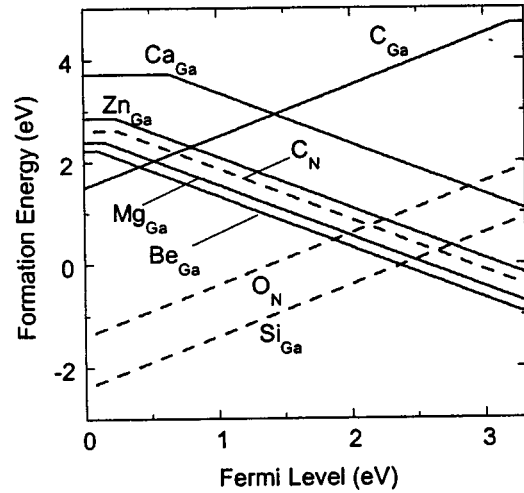


FIG. 5. Calculated formation energies as a function of Fermi level for shallow donors and acceptors in GaN grown in the most favorable for these dopants conditions (except for Si_{Ga} which should have even lower formation energy in Ga-rich conditions). Solid lines—Ga-rich case, dashed lines—N-rich case. The zero of Fermi level corresponds to the top of the valence band. The data for Ca, Zn, Mg, and Be are taken from Ref. 30, C—from Ref. 36, and O and Si—from Ref. 53 with kind permission from the authors.

gies for O_N and Si_{Ga} donors (both below 2 eV in the Ga-rich case). With decreasing the Fermi level, the formation energy of the shallow donors linearly decreases (Fig. 5), so we may expect an even easier formation of the substitutional shallow donors in high-resistivity or p -type GaN if these impurities are present in the growth environment.

2. Substitutional acceptors

Ionization energies of the main substitutional acceptors in wurtzite and also zinc-blende GaN have been calculated in the effective-mass approximation by Mireles and Ulloa³⁷ and Wang and Chen,³⁸ the results of which are presented in Table II.

As tabulated in Table II, the main candidates for the shallow acceptors are Be_{Ga} , Mg_{Ga} , C_N , and Si_N . Pödör³⁹ concluded from the analysis of the electronegativity differences between the acceptor atoms and the host atoms that the ionization energy of Be_{Ga} is the smallest among the likely acceptors and is only slightly greater than the effective-mass value estimated by the same author as 85 meV. In the order of increasing ionization energies, the other Ga-substitutional acceptors are Mg, Zn, Cd, and Hg, as follows from the elec-

TABLE II. Calculated acceptor ionization energies (in meV) for wurtzite (wz) and zinc-blende (zb) GaN.

Acceptor	E_A (wz) (Ref. 38)	E_A (wz) (Ref. 37)	E_A (zb) (Ref. 38)	E_A (zb) (Ref. 37)
Be_{Ga}	187	204	183	133
Mg_{Ga}	224	215	220	139
Ca_{Ga}	302	259	297	162
Zn_{Ga}	364	331	357	178
Cd_{Ga}	625		620	
C_N	152	230	143	147
Si_N	224	203	220	132
Ge_N	281		276	

tronegativity difference between these impurities and Ga atom.³⁹ Park and Chadi²⁹ examined the atomic and electronic structures of substitutional Be, Mg, and C acceptors in GaN through first-principles calculations and concluded that these impurities would give effective-mass states in GaN, not AX states. The calculated formation energies of some of these substitutional acceptors are shown in Fig. 5. The formation energies of Mg_{Ga} and Be_{Ga} and their ionization energies are the lowest. One problem for Be, however, is that the atom is too small and can incorporate efficiently on the interstitial site, where it acts as a double donor.^{30,40-42} Therefore, among the group-II impurities, Mg and Be are the most promising *p*-type dopants for GaN, and Be appears to be the best candidate, provided that the conditions that suppress formation of Be_i donors can be established. This is technologically challenging to say the least. The formation energies of acceptors from group-IV impurities, such as Si_{N} and Ge_{N} , are relatively high, so that formation of these acceptors is unlikely in GaN under equilibrium conditions.^{20,30} The formation energy of C_{N} could be sufficiently low in Ga-rich conditions.^{19,20,23,36,43} However, the C_{N} acceptor might be compensated by interstitial C when the Fermi level is close to the conduction band.³⁶ Note also that the formation energies of the acceptors decrease with increasing Fermi level, so that we may expect efficient formation of C_{N} and Si_{N} acceptors in undoped or *n*-type doped GaN when these impurities are present in the growth environment.

Neugebauer and Van de Walle³⁰ also examined the formation energies of acceptors from group-I impurities, such as K_{Ga} , Na_{Ga} , and Li_{Ga} . They predicted that these acceptors have relatively high formation energies and large ionization energies, and are therefore not likely to be candidates for successful *p*-type dopants. Moreover, the formation energies of the Na and Li interstitials are much lower in *p*-type GaN, so that these alkali impurities would rather behave as single donors.³⁰

3. Isoelectronic impurities

Arsenic and phosphorus could substitute nitrogen atoms in GaN to form isovalent defects, As_{N} and P_{N} . In silicon, germanium, and most of III-V semiconductors isovalent impurities do not introduce deep energy levels in the band gap. However, the theory predicts formation of deep gap states by isovalent impurities in GaN, similar to the situation in II-VI compounds, due to large size mismatch of the isovalent atoms in GaN.^{44,45} The first-principles calculations have shown that the As_{N} and P_{N} defects may exist in neutral, +, and 2+ charge states in GaN. Mattila and Zunger⁴⁵ predicted the 2+/ + and $\text{+}/0$ energy levels of As_{N} to be 0.24 and 0.41 eV above the valence-band maximum, and those of P_{N} to be 0.09 and 0.22 eV, respectively.⁴⁵ Van de Walle and Neugebauer⁴⁶ obtained the values for the same as 0.11 and 0.31 eV for the 2+/ + and $\text{+}/0$ levels of As_{N} , respectively. The formation energy of As_{N} is quite large, and under the most favorable conditions (Ga rich and Fermi level above 2.3 eV), the first-principles calculations predict the formation energy of As_{N} of about 4.5 eV. In *p*-type GaN, and/or in N-rich conditions, formation of As_{Ga} antisite-type defect is much more likely.⁴⁶ This defect is a double donor with the

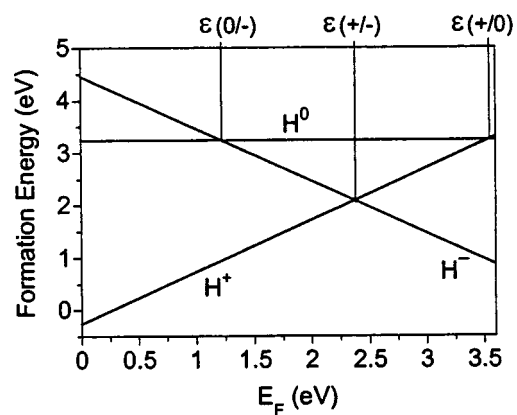


FIG. 6. Calculated formation energy of interstitial hydrogen in wurtzite GaN as a function of Fermi level. $E_F=0$ corresponds to the valence-band maximum, and formation energies are referenced to the energy of a H_2 molecule. Reprinted with permission from Van de Walle, Phys. Status Solidi B 235, 89 (2003).

2+/ + level at about 2.5 eV above the valence-band maximum. In addition, the formation energy is very small when the Fermi level is close to the valence band.⁴⁶ Therefore, the presence of As can cause significant compensation during growth of *p*-type GaN.

4. Hydrogen

Monatomic interstitial hydrogen is predicted to exist in two charge states in GaN: H^+ and H^- , whereas the H^0 state is unstable (Fig. 6).⁴⁷⁻⁴⁹ H^+ prefers the N antibonding site, whereas for H^- the Ga antibonding site is the most energetically stable. H^+ is expected to be mobile even at room temperature due to a small migration barrier (about 0.7 eV), while H^- has a very limited mobility in GaN due to a very large migration barrier (about 3.4 eV).⁴⁷ It follows from Fig. 6 that the solubility of H is considerably higher under *p*-type conditions (where it exists as H^+) than under *n*-type conditions (where it is H^-). The value of the negative-U effect (transition of H^- into H^+) is extremely high (-2.4 eV), larger than in any other semiconductor.⁴⁷ In contrast with Si or GaAs, the H_2 molecule has low stability and high formation energy in GaN.⁴⁷ Since hydrogen is abundantly present in most of GaN growth processes, such as metal-organic chemical-vapor deposition (MOCVD), hydrate vapor-phase epitaxy (HVPE), and ammonia-based molecular-beam epitaxy (MBE), and easily migrates, especially in *p* type, it should form stable complexes with other defects in GaN, playing an important role in the material properties (see Sec. II D 3).

D. Complexes

From the results of calculations presented in Sec. II B we expect that none of the simple native defects could exist in GaN in substantial concentrations. However, complexes between native defects and impurities, including hydrogen, are expected to be the dominant unintentionally introduced defects.

1. Shallow donor—gallium vacancy complexes

The gallium vacancy is the dominant native defect in n -type (in particular, undoped) GaN because the formation energy of V_{Ga} is low in this case (Fig. 2). However, as noted in Sec. II B 1, V_{Ga} could easily diffuse even at moderate temperatures of growth or thermal annealing and would readily form complexes with other defects. It should be underscored that formation of complexes is driven by electrostatic forces. The impurities that are most likely to form stable complexes with V_{Ga} are donors. A negatively charged acceptor (the charge of V_{Ga} is 3- in n -type GaN) and a positively charged donor are attracted to each other. According to the calculations of Neugebauer and Van de Walle,¹⁷ $V_{\text{Ga}}\text{O}_\text{N}$ and $V_{\text{Ga}}\text{Si}_\text{Ga}$ complexes act as double acceptors in GaN, and their $-2-$ energy levels (at 1.1 and 0.9 eV, respectively) are close to the $2-/3-$ transition level of the isolated V_{Ga} (at 1.1 eV). The electronic structure of Ga vacancy dominates the electronic structure of the V_{Ga} -shallow donor complexes, very similar to the situation in n -type GaAs.^{50–52} Formation of the $V_{\text{Ga}}\text{O}_\text{N}$ complex is even more favorable than formation of isolated V_{Ga} .¹⁷ Similar results have been obtained by Mattila and Nieminen,²² who compared the formation energies of the isolated V_{Ga} and the $V_{\text{Ga}}\text{O}_\text{N}$ complex for different positions of the Fermi level (Fig. 4). The $V_{\text{Ga}}\text{O}_\text{N}$ complex has a binding energy of ~ 1.8 eV, as compared to ~ 0.23 eV for the $V_{\text{Ga}}\text{Si}_\text{Ga}$ complex.¹⁷ This indicates that the $V_{\text{Ga}}\text{O}_\text{N}$ complex is much more stable and it may be the dominant compensating acceptor in n -type GaN. The $V_{\text{Ga}}\text{C}_\text{N}$ complex has a low formation energy, but is unstable in n -type GaN because both constituents are acceptors and repel each other.^{17,36}

2. Shallow acceptor—nitrogen vacancy complexes

The situation with N vacancy and shallow acceptors in p -type GaN is essentially the same as for the Ga vacancy, and shallow donors in n -type GaN. N vacancy, V_N , being a mobile and dominant compensating donor in p -type GaN, would be attracted by negatively charged acceptors during growth and cooling down or thermal annealing. The binding energy for a neutral $\text{Mg}_\text{Ga}V_\text{N}$ complex is about 0.5 eV,^{29,53} although Gorczyca *et al.*⁵⁴ obtained a value of 2.8 eV. The formation energy of the $\text{Mg}_\text{Ga}V_\text{N}$ complex is significantly lower than the sum of the formation energies of the isolated Mg_Ga and V_N .⁵⁴ Park and Chadi²⁹ assumed that the $\text{Mg}_\text{Ga}V_\text{N}$ complex is responsible for the persistent photoconductivity in GaN:Mg⁵⁵ and attributed the bistability to the neutral and 2+ states of this complex. Van de Walle *et al.*⁵³ argued that the relatively low binding energy of the $\text{Mg}_\text{Ga}V_\text{N}$ complex prevents abundant formation of these complexes in p -type GaN in thermal equilibrium. However, their formation can be enhanced by kinetically driven processes on the sample surface during growth. It is not clear where in the band gap the energy level of $\text{Mg}_\text{Ga}V_\text{N}$ is. Kaufmann *et al.*⁵⁶ assumed that $\text{Mg}_\text{Ga}V_\text{N}$ is a deep donor with an energy level at about 0.4 eV below the conduction band. Park and Chadi²⁹ estimated the energy level of $(\text{Mg}_\text{Ga}V_\text{N})^{2+}$ at about 0.7 eV above the valence band, while Gorczyca *et al.*⁵⁴ obtained an energy level much closer to the valence band. Note that in the latter

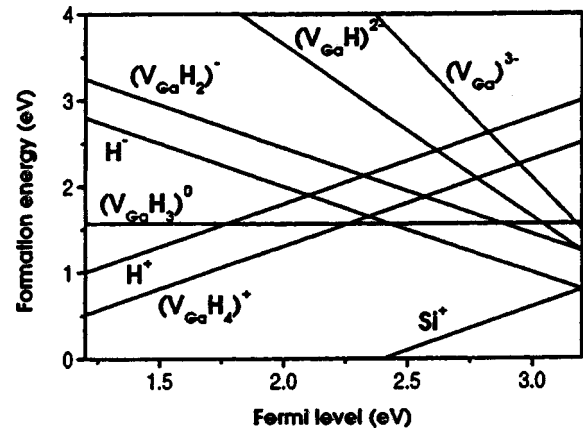


FIG. 7. Calculated formation energies of hydrogenated Ga vacancies in GaN as a function of Fermi energy. The formation energies of the isolated vacancy (V_{Ga}), of interstitial H^+ and H^- , and of the Si donor are also included. Reprinted with permission from Van de Walle, Phys. Rev. B 56, 10020 (1997). Copyright (1997) by the American Physical Society.

report the energy level of V_N was also much lower than that obtained in Refs. 29 and 53. Similar to the $\text{Mg}_\text{Ga}V_\text{N}$ complexes in GaN:Mg, the $\text{Be}_\text{Ga}V_\text{N}$ complexes are expected to form in Be-doped GaN.⁵⁷

Lee and Chang⁵⁸ examined the possibility of formation of Mg_iV_N complexes in p -type GaN. While incorporation of the isolated Mg_i is unlikely in GaN due to large atomic radius of Mg, formation of the Mg_iV_N complexes has low enough formation energy when the Fermi level is close to the valence band.⁵⁸ The charge state of the Mg_iV_N complex is 3+ in this case, and therefore it can efficiently compensate Mg_Ga acceptors.⁵⁸ The energy level of the Mg_iV_N complex (or even three close levels) is about 2.8 eV above the valence-band maximum. Similar results have been obtained by Gorczyca *et al.*⁵⁴ Therefore, Mg_iV_N might be the compensating donor in p -type GaN:Mg, apparently not $\text{Mg}_\text{Ga}V_\text{N}$. The energy level of the compensating donor has been determined in the photoluminescence study of Kaufmann *et al.*⁵⁶ at about 0.4 eV below the conduction band. Note that the Mg_iV_N complex could be formed only under Ga-rich conditions and when the Fermi level is very close to the valence band.⁵⁸ This means that passivation with hydrogen or N-rich conditions would prevent formation of this compensating donor. Lee and Chang⁵⁸ also assumed that hydrogen passivation can stabilize formation of the Mg_iV_N complex at higher positions of the Fermi level. However, this conclusion is somewhat questionable.⁵⁴

3. Hydrogen-related complexes

As is commonly the case with other semiconductors, hydrogen readily forms complexes with defects in GaN also. In addition, the formation energies of the hydrogenated defects are often relatively lower. In n -type GaN, hydrogen atoms could be bound to a Ga vacancy, in as many configuration as four, to form complexes such as $(V_{\text{Ga}}\text{H})^{2-}$, $(V_{\text{Ga}}\text{H}_2)^-$, $(V_{\text{Ga}}\text{H}_3)^0$, and $(V_{\text{Ga}}\text{H}_4)^+$.⁵⁹ The first three complexes are acceptors, whereas the last one is a single donor. The formation energies of the $V_{\text{Ga}}\text{H}_n$ complexes are shown in Fig. 7. With the exception of the $(V_{\text{Ga}}\text{H}_4)^+$ complex, the hydrogenated

vacancies have lower formation energies than the isolated V_{Ga} , which points to the importance of these complexes in GaN. The calculated energy levels of the $(V_{\text{Ga}}\text{H})^{2-}$ and $(V_{\text{Ga}}\text{H}_2)^-$ complexes (at about 1.0 eV above the valence band) are close to that of the isolated V_{Ga} , while the level of $(V_{\text{Ga}}\text{H}_3)^0$ is near the valence-band maximum.⁵⁹ It must be pointed out that in n -type GaN, formation of complexes with several H atoms, such as $(V_{\text{Ga}}\text{H}_3)^0$ and $(V_{\text{Ga}}\text{H}_4)^+$, is unlikely since in n -type GaN the isolated hydrogen atom exists as H^- which would be repelled from the negatively charged Ga vacancy.⁵⁹ Dissociation of the $V_{\text{Ga}}\text{H}_n$ complexes is unlikely due to the large associated binding energies.⁵⁹ Therefore, once formed during growth in the presence of hydrogen, these complexes cannot dissociate during postgrowth thermal annealing.

In p -type GaN, hydrogen passivates the dominant acceptor (Mg_{Ga}), as well as the dominant compensating donor (V_{N}).^{47,59} In the case of Mg, the electrically neutral Mg–H complex has a binding energy of 0.7 eV, with the H atom located in an antibonding site behind the N neighbor of the acceptor.⁴⁷ During postgrowth annealing, the Mg–H complex dissociates, and H diffuses either to the surface or to the extended defects.⁴⁷ Similarly, in Be-doped GaN, the Be–H complexes may form with a binding energy of 1.81 eV and a dissociation energy of 2.51 eV.⁴⁰ A postgrowth annealing would also be required to remove the hydrogen from Be acceptors.

The N vacancy in p -type GaN may also be passivated by hydrogen during the growth to form the $(V_{\text{N}}\text{H})^{2+}$ complex with the binding energy of 1.56 eV.⁵⁹ The formation energy of the $(V_{\text{N}}\text{H})^{2+}$ complex is lower than the formation of the isolated H^+ and V_{N} when the Fermi level is low in the gap.⁵⁹ The $V_{\text{N}}\text{H}$ complexes can be formed only during growth as diffusion of H^+ towards V_{N} is highly unlikely in p -type GaN since they repel each other. Formation of the $(V_{\text{N}}\text{H}_2)^+$ complex is also possible, while the $(V_{\text{N}}\text{H}_3)^0$ complex is unstable.⁶⁰ The $V_{\text{N}}\text{H}$ complex is expected to have a $2+/0$ transition level at about 2.5 eV above the valence band and a $0/2-$ level close to the conduction band,⁶⁰ while earlier calculations predicted the $0/+$ transition level of $V_{\text{N}}\text{H}$ to be near or in resonance with the conduction band.⁵⁹ Both V_{N}^{3+} and $(V_{\text{N}}\text{H})^{2+}$ could be formed in abundance in p -type GaN and compensate the dominant acceptor. Note that the hydrogenated vacancies may lose their hydrogen after the sample is grown, either during cooling down or during postgrowth annealing, and V_{N}^{3+} could also migrate during high-temperature annealing.²¹

4. Other complexes

The other element, in addition to H, that is unintentionally present in any growth systems is O which must be dealt with. While O is a ubiquitous problem for all semiconductors, O in GaN takes on a new dimension. The O atom in N site is a shallow donor in GaN and it might hamper attempts to obtain p -type material in addition to causing undesirable background donors. The formation energy of the $\text{Mg}_{\text{Ga}}\text{O}_{\text{N}}$ complexes is very low.⁵⁴ Therefore, these complexes can readily form in Mg-doped GaN when oxygen is present in the growth environment. Gorczyca *et al.*⁵⁴ predicted that for-

mation of these complexes would result in semi-insulating GaN, since both O_{N} and Mg_{Ga} levels would be pushed out of the energy gap. However, the relatively low binding energy of the $\text{Mg}_{\text{Ga}}\text{O}_{\text{N}}$ complex (0.6 eV) is unfavorable for the complex formation, unless the kinetically driven processes on the surface result in the preferential incorporation of $\text{Mg}_{\text{Ga}}\text{O}_{\text{N}}$.⁵³

In Be-doped GaN, $\text{Be}_{\text{Ga}}\text{O}_{\text{N}}$ complex could be formed, which is neutral.^{40,41} Moreover, the $\text{Be}_{\text{Ga}}\text{O}_{\text{N}}\text{Be}_{\text{Ga}}$ complex could be formed with the $0/-$ transition level at 0.14 eV above the valence-band maximum.⁴⁰ Along with the formation of Be_i^{2+} donors, the $(\text{Be}_{\text{Ga}}\text{Be}_i)^+$ donor complexes might form in Be-doped GaN which end up compensating the Be acceptor.⁴⁰ However, the postgrowth annealing at temperatures above 600 °C should result in dissociation of these complexes.⁴⁰

E. Role of dislocations in the point defect formation

Due to large lattice mismatch, heteroepitaxy of GaN on sapphire substrates results in films containing threading dislocations with the densities from $\sim 10^8$ to $\sim 10^{10}$ cm^{-2} , depending on growth method and conditions, and whether dislocation reducing methods are employed. The situation is not much different if other substrates with seemingly smaller lattice mismatches are used. These dislocations are mainly parallel to the c axis, and their Burgers vectors are equal to \mathbf{a} (edge-type), \mathbf{c} (screw-type), or $\mathbf{a} + \mathbf{c}$ (mixed-type). The first-principles calculations enable comparison of formation energies and structures of different types of dislocations and point defects that can be trapped by the stress fields associated with the dislocations.

In contrast to the earlier prediction that threading dislocations are electrically inactive in GaN,⁶¹ later calculations indicated that various types of dislocations may introduce numerous energy levels in the gap.^{62–64} In particular, threading dislocations are expected to behave as deep donors in n -type material and deep acceptors in p type.⁶² Under Ga-rich conditions dislocations decorated with Ga vacancies have the lowest formation energy in n -type GaN, while in N-rich conditions dislocations decorated with Ga vacancies have the lowest formation energy in p -type GaN.^{62,65} To a first extent these results are consistent with the experimental findings from a scanning-capacitance microscopy study, indicating the presence of negatively charged dislocations in n -type GaN.⁶⁶ Note that deep donors in n -type material and deep acceptors in p -type material usually do not contribute to luminescence,⁶⁷ therefore dislocations are not expected to manifest themselves in luminescence experiments, unless point defects are trapped at them due to the large stress fields near dislocations.

The behavior of point defects trapped at threading-edge dislocations in GaN was examined by Elsner *et al.*⁶⁸ First-principles calculations indicated that V_{Ga} and its complexes with one or more O_{N} have very low formation energies at different positions near the threading-edge dislocations. The results indicate that the formation energies of V_{Ga} , O_{N} , and their complexes at different sites near the threading-edge dislocation are much lower than the formation energies of the corresponding defects in the bulk. Energy levels of the de-

fects trapped at dislocations generally shift as compared to the point defects in bulk, however, the shift is not large.⁶⁸ In short, the stress field of threading-edge dislocations is likely to trap Ga vacancies, oxygen, and their complexes. A variety of the V_{Ga} -containing complexes may form acceptorlike defect levels in the lower half of the band gap and therefore be responsible for some transitions observed in luminescence experiments. Note that a similar situation might take place in p -type GaN, where the dislocations may trap V_{N} and V_{N} -related complexes.

III. LUMINESCENCE METHODS

Photoluminescence (PL) and cathodoluminescence (CL) have been the most widely used experimental methods applied to investigations of GaN. Defects in GaN have been studied by analyzing the steady-state PL (SSPL), time-resolved PL (TRPL), and PL excitation (PLE) spectra. Optically detected magnetic resonance (ODMR), a variant of the PL technique, along with the positron annihilation method has been extensively used for identification of point defects in GaN.

A. Steady-state photoluminescence

The SSPL spectroscopy is widely used for qualitative analysis of GaN and its alloys. Commonly, the SSPL is generated in GaN by illuminating it with a He–Cd laser (325 nm) beam with optical power levels of up to approximately 60 mW. In investigating defects, however, special precaution must be taken to employ a sufficiently low excitation density since the defect-related PL often saturates at power densities of the order of 10^{-2} – 10^{-1} W/cm². Failure to do so would very likely cause skewing of the PL spectrum in favor of excitonic emission at higher excitation densities, giving the false impression about the relative strength of defect-induced transitions. Similarly, focusing the laser beam and using small slit widths of a monochromator for the entire PL spectrum would also distort the PL in favor of excitonic transitions. In such a case, the chromatic dispersion of lenses used to collect the PL, as well as the different effective sizes of the emission spots for the ultraviolet (UV) and visible emission attributed, in particular, to photon-recycling process,⁶⁹ may lead to a marked, but artificial, enhancement of the UV (near band edge) over the visible part in the PL spectrum (mainly defect-related).

Qualitative terms, such as “very intense PL that confirms high quality of the material,” are omnipresent in the literature regarding GaN. However, there have been very few attempts to estimate the absolute value of the PL intensity or its quantum efficiency (QE) for a quantitative analysis. Although the direct measurement of the QE is not straightforward, attempts have been made to estimate this important parameter for GaN.^{70,67} Göldner *et al.*⁷⁰ simultaneously detected the calorimetric absorption (measure of nonradiative recombination which results in heating of the sample), transmission, reflection, and excitation power, and reported the QE to be below 20% for thin GaN layers grown by MOCVD on sapphire and up to 75% for bulk GaN crystal grown by HVPE. An indirect method based on quantitative analysis of

the competition of radiative and nonradiative recombination channels was suggested by Reshchikov and Korotkov,⁶⁷ and is presented in Sec. III A 3.

Quantitative studies of point defects in GaN by PL have rarely been undertaken. Often, qualitative estimations of the acceptor concentration in n -type GaN were made by comparing the ratios between the defect and near-band-edge emission intensities.^{71,72} However, this ratio is shown to depend not only on the defect concentration but also on the experimental conditions, in particular, on the excitation intensity,^{67,73,74} as was mentioned above. Temperature dependence of the defect-related PL intensity in GaN has often been used to determine the nature of a given optical transition. For example, the donor-acceptor-pair (DAP) transitions have been distinguished from the conduction-band-acceptor (e-A) transitions by the thermal behavior of PL.^{75–77} However, the thermal behavior of PL may be complicated by a competition between several recombination channels as is shown below using a simple phenomenological approach.⁶⁷

1. Recombination statistics

Let us now consider an n -type semiconductor containing several radiative acceptors A_i with concentrations N_{A_i} . The electron-hole pairs are excited with a generation rate G [cm⁻³ s⁻¹]. The concentration of the photogenerated holes in the valence band is p , the concentration of equilibrium (n_0) and photogenerated (δn) free electrons is $n = n_0 + \delta n$. After optical excitation, the holes are captured by acceptors at the rate $C_{pi} N_{A_i} p$, where C_{pi} [cm³ s⁻¹] is the hole-capture coefficient for the i th acceptor and N_{A_i} is the concentration of ionized acceptors of type i . A competing process is the formation of excitons with the rate $C_{ex} n p$, where the coefficient C_{ex} describes the efficiency of the exciton formation. In addition to radiative processes, some of the holes recombine nonradiatively. For simplicity, the nonradiative recombination rate can be introduced as $C_{ps} N_S p$, where C_{ps} and N_S are the average hole-capture coefficient and the concentration of the nonradiative centers, respectively. Thus, in general, the hole-capture rate can be expressed as $C_i N_i p$, where $C_i = C_{ex}$, C_{pi} , or C_{ps} and $N_i = n$, N_{A_i} , or N_S for excitons, radiative acceptors, and nonradiative defects, respectively.

At elevated temperatures, the bound holes may return to the valence band as a result of thermal activation or exciton dissociation. The probability of this process, Q_i [s⁻¹], is proportional to $\exp(-E_i/kT)$, where E_i is the thermal activation energy for the radiative acceptors (E_{A_i}), nonradiative centers (E_S), or the exciton dissociation energy (E_{ex}). Taking into account all these processes (Fig. 8), the detailed balance equation for the hole concentration in the valence band in steady state in the case of N recombination channels can be written in the form

$$\frac{\partial p}{\partial t} = G - \sum_{i=1}^N C_i N_i p + \sum_{i=1}^N Q_i N_i^0 = 0, \quad (3)$$

where $N_i^0 = N_{A_i}^0$, N_S^0 , and N_{ex} is the concentration of holes bound to radiative acceptors, nonradiative centers, or forming excitons, respectively. At sufficiently low excitation in-

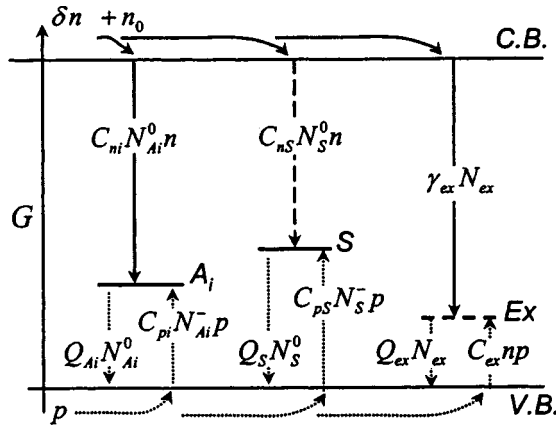


FIG. 8. Schematic of the main transitions in n -type GaN in conditions of PL. Electron-hole pairs ($\delta n = p$) are created with the rate G by optical excitation. The photogenerated holes are captured by radiative acceptors (one acceptor level A_i is shown), nonradiative defects (S), and form excitons (Ex). The level for excitons is conventional, meaning only that some energy is required to dissociate the excitons. The solid and dotted lines show the transitions of electrons and holes, respectively. Optical transitions are shown by the straight solid lines; recombination of holes at nonradiative centers with free electrons is shown with a dashed line. Rates for all the transitions are noted.

tensities, $N_i^0 \ll N_i^- \approx N_i$, the steady-state equation for the concentration of holes bound to the i th defect can be written as

$$\frac{\partial N_i^0}{\partial t} = C_i N_i p - \frac{N_i^0}{\tau_{R_i}} - Q_i N_i^0 = 0, \quad (4)$$

where the second term describes recombination via the i th channel and the parameter τ_{R_i} characterizes the recombination lifetime (in general case it may evolve in time in transient processes).

The capture rates are usually much faster than recombination rates. As a result, the efficiency of each of the recombination channels is proportional to the rate of capture of the minority carriers (holes in n -type GaN). Therefore, in the low-temperature limit, where both the thermal release of the bound holes and the exciton dissociation are negligible, the QE of each recombination channel, $\eta_i(0)$, is given by the ratio of hole-capture rate for a specific recombination channel to the total escape rate of holes from the valence band

$$\eta_i(0) = \frac{C_i N_i p}{\sum_{j=1}^N C_j N_j p} = \frac{C_i N_i}{\sum_{j=1}^N C_j N_j}. \quad (5)$$

With the above assumptions, an expression for the intensity of PL via each defect can be determined as⁶⁷

$$I_i^{\text{PL}} = \frac{N_i^0}{\tau_{R_i}} = \eta_i G = \frac{\eta_i^*}{1 + (1 - \eta_i^*) \tau_{R_i} Q_i} G, \quad (6)$$

where

$$\eta_i^* = \eta_i(0) \left[1 - \sum_{j \neq i}^N \frac{\eta_j(0) \tau_{R_j} Q_j}{1 + \tau_{R_j} Q_j} \right]^{-1}, \quad (7)$$

and η_i is the QE of the i th channel accounting for dissociation of excitons and thermal escape of holes from the defects to the valence band.

2. Effect of temperature on PL intensity

It is evident from Eqs. (6) and (7) that the temperature dependence of the PL intensity in n -type GaN is largely determined by exciton dissociation and thermal escape of holes from the defects to the valence band. Although the exact expressions for the exciton dissociation can also be derived,⁷⁸ it is much easier to account for the contribution of the exciton dissociation into the defect-related PL (the term $\tau_{R_{ex}} Q_{ex}$) by taking the temperature dependence of the integrated exciton emission intensity from the experiment.⁶⁷

The probability of thermal activation of holes from an acceptor, Q_{A_i} , can be obtained from a detailed balance as

$$Q_{A_i} = C_{pi} g^{-1} N_V \exp\left(-\frac{E_{A_i}}{kT}\right) \quad (8)$$

with

$$N_V = 2 \left(\frac{m_h kT}{2\pi \hbar^2} \right)^{3/2} \quad (9)$$

and

$$C_{pi} = \sigma_{pi} v_p = \sigma_{pi} \sqrt{\frac{8kT}{\pi m_h}}, \quad (10)$$

where g is the degeneracy factor of the acceptor level, N_V is the density of states in the valence band, m_h is the effective mass of the holes in the valence band, v_p is the hole thermal velocity, and σ_{pi} is, by definition, the hole-capture cross section of the i th acceptor. An analysis of Eqs. (6) and (8) shows that the temperature dependence of PL intensity for the i th acceptor involves a region of thermal quenching with an activation energy E_{A_i} at temperatures T satisfying the condition $(1 - \eta_i^*) \tau_{R_i} Q_i > 1$. Variation of the parameter η_i^* in the region of thermal quenching of PL related to i th acceptor can be ignored if the quenching regions for different defects do not overlap significantly. Parameters E_{A_i} and C_{pi} (or σ_{pi}) can be obtained by fitting Eq. (6) to the experimental dependence of the PL intensity in the region of thermal quenching of the PL band related to the i th acceptor. Note that the value of E_{A_i} calculated from the fit to the experimental data using Eq. (6) is somewhat different from the ionization energy obtained from the slope of the Arrhenius plot of $I^{\text{PL}}(T^{-1})$ due to the temperature dependence of N_V and C_{pi} . The temperature dependence of the acceptor energy level may also lead to some discrepancy between the value of E_{A_i} at temperatures of PL quenching and the value of $E_{A_i}(T=0)$ obtained from the low-temperature spectroscopy.

An analysis of Eqs. (6)–(8) also indicates that the integrated PL intensity for the given recombination channel at a given temperature depends on the quenching state of the rest of the recombination channels. Therefore, several increases

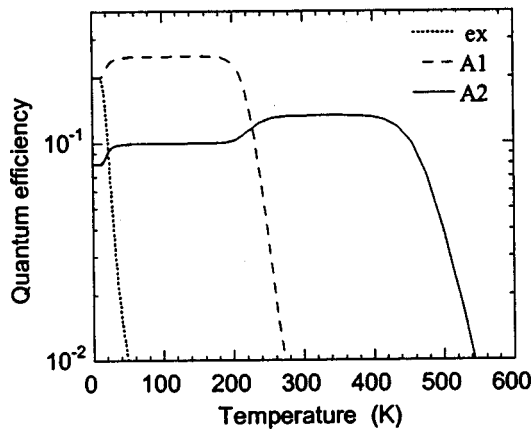


FIG. 9. Calculated temperature dependencies of the PL QE for three radiative recombination channels in GaN: excitonic (ex) and via two acceptors (A1 and A2). The dependences were calculated using Eqs. (6)–(10) with the following parameters: $\eta_{\text{ex}}(0)=0.2$; $\eta_{A1}(0)=0.2$; $\eta_{A2}(0)=0.08$; $\tau_{\text{rex}}Q_{\text{ex}}=250 \exp(-10 \text{ meV}/kT)$, $\tau_{R1}=10^{-5} \text{ s}$, $\tau_{R2}=5 \times 10^{-5} \text{ s}$, $C_{p1}=10^{-6} \text{ cm}^3 \text{ s}^{-1}$, $C_{p2}=4 \times 10^{-7} \text{ cm}^3 \text{ s}^{-1}$, $E_{A1}=0.34 \text{ eV}$, $E_{A2}=0.8 \text{ eV}$. Reprinted with permission from Reshchikov and Korotkov, Phys. Rev. B **64**, 115205 (2001). Copyright (2001) by the American Physical Society.

of the PL intensity are expected in the form of intensity steps corresponding to thermal quenching of other PL bands. An example of the calculated temperature dependencies of PL intensity related to three radiative recombination channels is shown in Fig. 9. The increase in PL intensity in the region of thermal quenching of a particular recombination channel is associated with the redistribution of the released holes among all unquenched channels. The complete quenching of the i th channel results in the stepwise increase of the PL intensity from other recombination channels R_i times, if the overlap of the quenching regions can be neglected. A simple expression for R_i can be obtained from Eqs. (6) and (7)

$$R_i \approx 1 + \frac{\eta_i(0)}{1 - \sum_j \eta_j(0)}, \quad (11)$$

where the summation is taken over the recombination channels which have been thermally quenched prior to the quenching of the i th channel.

Besides the above analysis of the PL intensity, the temperature dependencies of the PL band line shape and peak position can sometimes provide useful information on the nature of transitions and the type of a defect. The effect of temperature on the PL spectrum related to a deep-level defect is discussed in Sec. III D. The PL bands caused by DAP recombination are expected to shift to higher photon energies (blueshift) with increasing temperature due to thermal escape of electrons from long-lived distant pairs contributing at the low-energy side of a PL band due to weaker Coulomb interaction.^{79,80} However, one should be careful with the interpretation of the shift since defects with strong electron-phonon coupling often exhibit a blueshift owing to the particulars of their adiabatic potentials.⁸¹ Moreover, the PL bands from DAPs with relatively deep donors and acceptors may exhibit red or blueshift with temperature, depending on the excitation conditions.^{80,82}

3. Estimates of quantum efficiency

The QE of PL can be estimated from the temperature dependence of the PL intensity using Eq. (11). The relative values of $\eta_i(0)$ can be obtained at low temperatures as the integrated PL intensities for all the PL bands.⁶⁷ The absolute value of $\eta_i(0)$ can be calculated from the value of the stepwise increase in PL intensity for any band, which is related to the thermal quenching of the i th channel

$$\eta_i(0) = \left[\frac{1}{R_i - 1} + \frac{\sum_j I_j^{\text{PL}}(0)}{I_i^{\text{PL}}} \right]^{-1}, \quad (12)$$

where the summation is taken over the channels quenched prior to quenching of the i th channel.

The internal QEs estimated by this method in undoped GaN layers agree well with the values obtained by direct measurement of the laser and PL power levels with correction for reflection and the geometry of the PL collection setup.⁶⁷ In this review, we give the values of the QEs for different GaN samples calibrated by using the same standard, whenever the data allow.

4. Effect of excitation intensity on PL intensity

High and even moderate excitation power levels could saturate the defect-related PL since the defect concentration and lifetime are finite. Let us now consider the case when thermalization of the holes trapped by the i th acceptor is negligible and assume that only the i th acceptor is subject to saturation by nonequilibrium holes in the considered excitation range. Then, from the steady-state rate equations similar to Eqs. (3) and (4) one can obtain an expression for the PL intensity related to the i th acceptor as⁶⁷

$$I_i^{\text{PL}} = \frac{N_i^0}{\tau_{R_i}} = \frac{1}{2} \left(G + \frac{N_i}{\eta_i \tau_{R_i}} \right) - \frac{1}{2} \sqrt{\left(G + \frac{N_i}{\eta_i \tau_{R_i}} \right)^2 - \frac{4GN_i}{\tau_{R_i}}}, \quad (13)$$

which for the case of low QE of the i th channel ($\eta_i \ll 1$) simplifies to

$$I_i^{\text{PL}} \approx \frac{G}{\frac{G\tau_{R_i}}{N_i} + \frac{1}{\eta_i}}. \quad (14)$$

For low-excitation rates ($G\tau_{R_i}\eta_i \ll N_i$), the $I_i^{\text{PL}}(G)$ dependence is linear and at high excitation rates it is expected to saturate at the value of $N_i\tau_{R_i}^{-1}$. Instead of complete saturation, a square-root dependence of the PL intensity is often observed for defects in GaN at excitation densities above the range of 10^{-2} – 1 W/cm^2 .^{67,74,83}

The square-root dependence of the defect-related PL intensity as a function of the excitation power is expected at high-excitation densities when the concentrations of photo-excited carriers (δn and p) exceed the free-electron concentration in dark (n_0).^{67,74} However, the excitation density necessary to inject δn , $p \sim 10^{18}\text{-cm}^{-3}$ nonequilibrium carriers (typical concentration of free electrons in GaN at room temperature), is about 10^5 W/cm^2 ,⁸⁴ which is much higher than that commonly used in defect-related PL studies. One of the

reasons for the square-root dependence of the defect-related PL at moderate excitation powers is recombination through nonradiative donors that may be present in GaN in relatively high concentrations, particularly near the surface.⁶⁷ Another possibility is the reabsorption of the UV emission by deep-level defects, which is known as photon recycling.

5. Estimates of acceptor concentration in n-type GaN

Once the hole-capture coefficients C_{pi} are evaluated for different acceptors (Sec. IV H for defects in undoped GaN), the ratio between the concentrations of each acceptor can be determined from an analysis of the low-temperature PL spectrum. This is a simple and effective method for estimating the relative concentrations of unintentional acceptors in n-type GaN, and one that could be widely employed for a sample characterization. Indeed, all that is necessary is the ability to measure the PL spectrum at sufficiently low temperatures and excitation intensities⁸⁵ followed by finding the integrated intensity for each band in relative units. Then, the ratio between the concentrations of the i th and j th acceptors can be found as⁶⁷

$$\frac{N_{A_i}}{N_{A_j}} = \frac{I_i^{\text{PL}} C_{pi}}{I_j^{\text{PL}} C_{pj}}. \quad (15)$$

To determine the absolute values of the acceptor concentrations, the concentration of one of the acceptors should be found independently by fitting the dependence of the PL intensity on excitation intensity, as described in Sec. III A 4.

B. Time-resolved luminescence

By measuring the PL intensity at a given photon energy as a function of time delay after an excitation pulse, valuable insight can be garnered about the recombination mechanisms. A full emission spectrum can also be measured at different decay times. A spectral analysis helps to distinguish the overlapped PL bands and investigate the evolution of the PL band shape and its shift with time.

The luminescence decay in GaN is often nonexponential, especially at low temperatures. The most plausible cause for the nonexponential decay of PL is the DAP recombination. When an electron bound to a donor recombines with a photogenerated hole bound to an acceptor, the radiative recombination rate W is not constant but depends exponentially on the separation, R , between the donor and acceptor involved,^{79,86}

$$W(R) = W_{\text{max}} \exp\left(-\frac{2R}{a_D}\right). \quad (16)$$

where W_{max} is the transition probability in the limit $R \rightarrow 0$ and a_D is the Bohr radius for a more weakly bound particle (an electron on the shallow donor in GaN). It is evident from Eq. (16) that the lifetime of the bound hole, $\tau = W^{-1}$, is much longer for distant pairs than for close ones. This results in an increase of the instantaneous lifetime of the measured PL with the time delay. The transient PL depends on the details of the spatial distribution of pairs. Thomas *et al.*⁷⁹ obtained

the following expression for the PL intensity decay in the case of a random distribution of DAP:

$$I(t) \propto N \exp\left\{4\pi N \int_0^\infty [e^{-W(R)t} - 1] R^2 dR\right\} \times \int_0^\infty W(R) e^{-W(R)t} R^2 dR, \quad (17)$$

where N is the concentration of the majority constituent in DAPs. Equation (17) combined with Eq. (16) describes well the nonexponential decay of low-temperature PL in undoped GaN.^{76,87}

From simple reasoning, we expect an increase of W_{max} with increasing ionization energy of an acceptor E_A due to increasing localization of the bound hole. Indeed, the maximum rate of the DAP transitions in the effective-mass approximation upon neglecting many-body effects is given by^{80,88}

$$W_{\text{max}} = 64A \left(\frac{a_A}{a_D}\right)^3, \quad (18)$$

where the parameter A depends on the optical properties of the semiconductor and on the photon energy $\hbar\omega$ ($A[\text{s}^{-1}] \approx 4.5 \times 10^8 \hbar\omega$ [eV] for GaN), and a_A is the Bohr radius for the bound hole given by⁸⁹

$$a_A = \frac{\hbar}{\sqrt{2m_h E_A}}. \quad (19)$$

Although the effective-mass approximation may not be a good choice for deep-level defects, it nevertheless provides surprisingly good results.^{88,90}

Note that potential fluctuations, typically present in highly compensated and/or heavily doped semiconductors as a result of the random charge distribution,⁹¹ also result in a nonexponential PL decay. This is due to localization of carriers in potential wells, very similar in nature to their localization on spatially separated donors and acceptors. The problem of the potential fluctuations is discussed in more detail in Sec. V B 2.

With increasing time delay, PL bands originating from the DAP-type transitions, especially those involving deep donors, are expected to shift to lower energies.^{79,80} This effect is caused by a faster recombination in close pairs, which contribute to the high-energy side of the band due to a stronger Coulomb interaction. The deeper the donor, the larger the shift is expected, but it still remains below the value of ionization energy of the donor.⁸⁰ The absence of a noticeable shift of a PL band with the time delay may indicate that shallow donors are involved.

With increasing temperature, the electrons from shallow donors thermalize to the conduction band, and the DAP transitions are gradually replaced by transitions from the conduction band to the same acceptor (e-A transitions). For the e-A transitions, the decay is commonly exponential and the characteristic radiative lifetime, τ_R , depends on the free-electron concentration n_0 , provided that $n_0 \gg \delta n$. The electron-capture coefficient for the acceptor C_n can then be expressed as

$$\tau_R = \frac{1}{C_n n_0}. \quad (20)$$

The electron-capture coefficient in the effective-mass approximation for a neutral defect can be approximately estimated as⁸⁰

$$C_n = 64\pi A a_A^3. \quad (21)$$

In the transition temperature range where the decay gradually transforms from nonexponential to exponential, the average or effective lifetime of PL, τ_R^* , can be introduced.⁸⁷ It is defined as the time delay corresponding to the position of a maximum in the dependence $t \times I^{PL}(t)$, where $I^{PL}(t)$ is the PL intensity at time t . In the case of the DAP recombination, τ_R^* is the time of transition between the pairs, giving the largest contribution to the PL after pulse excitation. In the case of the e-A transitions, τ_R^* is the characteristic time of decay [PL intensity decays as $\exp(-t/\tau_R^*)$].

In the temperature range where the SSPL intensity quenches, the lifetime of PL usually decreases with an activation energy corresponding to thermalization of holes from an acceptor to the valence band. In general, the PL lifetime (τ_{PL}) with allowance made for thermalization of holes can be expressed as⁹²

$$\tau_{PL}^{-1} = \tau_R^{-1} + \tau_q^{-1} = C_n n_0 + K \exp\left(-\frac{E_A}{kT}\right), \quad (22)$$

where E_A is the ionization energy of the acceptor, τ_q is the characteristic time of the hole escape to the valence band, and the coefficient K depends on the hole-capture characteristics of the acceptor.

Similar to Eq. (10) for nonradiative capture of holes, we can define the capture cross section for electrons, σ_n , as

$$\sigma_n = C_n v_n^{-1} \approx C_n \left(\frac{8kT}{\pi m_n}\right)^{-1/2}, \quad (23)$$

where v_n and m_n are the velocity and effective mass of free electrons [$m_n = 0.22m_0$ for GaN (Ref. 93)]. Note that whether C_n and C_p or σ_n and σ_p are temperature dependent or not is still an open question for defects in GaN.

C. Vibrational properties of deep-level defects

In contrast to the shallow defects, recombination of carriers at deep-level defects usually results in broad PL bands due strong electron-phonon coupling. This mechanism can simply be illustrated as follows: For a deep acceptor, the hole wave function is localized at one of the bonds and its asymmetrical location would cause the atoms to shift from their ideal sites, as shown in Fig. 10. After recombination of the bound hole with a free electron or electron at a spatially separated donor, the atoms would move to their original sites because all the bonds are restored and equivalent (Fig. 10). The atomic relaxation causes vibration of the lattice, i.e., emission of phonons. The radiative emission energy is reduced by the energy released through phonon emission. In different recombination processes, the number of emitted phonons is different, which results in a broad PL band.

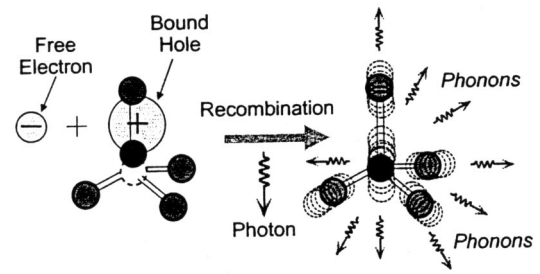


FIG. 10. Schematic representation of a recombination of the localized hole with a free electron, resulting in emission of a photon and several phonons.

The measure of the electron-phonon coupling is the Huang–Rhys factor, S .⁹⁴ The larger the S , the stronger the electron-phonon coupling is and the broader the PL band is. The so-called configuration coordinate (CC) model^{95–97} is often used to illustrate and even quantitatively describe recombination involving a localized carrier. The simplest one-dimensional CC diagram is illustrated in Fig. 11. In this diagram, adiabatic potentials represent the total potential energy, including electron and nuclear, of the defect. The equilibrium positions of the ground and excited states are displaced according to the strength of the electron-phonon coupling. In the simplest case, the electronic state interacts with a single localized vibrational mode of frequency ω_0 . In general, the phonon frequencies in the ground and excited states may be different and are represented by the terms ω_0^g and ω_0^e , respectively. At low temperatures ($kT \ll \hbar\omega_0^e$) optical transitions take place from the zero vibrational level of the excited state, and the maximum of the emission (E_{\max}) corresponds to the solid vertical line AB indicated in Fig. 11. After emitting a photon, the system relaxes to the zero vibrational level of the ground state by emitting several phonons with energies $\hbar\omega_0^g$ in the crystal (transition $B \rightarrow C$). Probability of optical transition from the zero level of the excited state to the n vibrational level ($n=0, 1, 2, \dots$) of the ground state is determined by the Poisson distribution

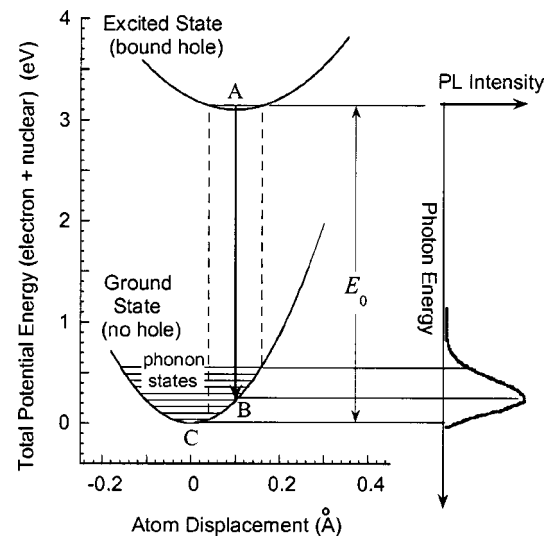


FIG. 11. An example of the CC diagram and resulting PL spectrum.

$$W_{0 \rightarrow n} = e^{-S} \frac{S^n}{n!}. \quad (24)$$

In the case of strong electron-phonon coupling ($S \gg 1$), S represents the mean number of the emitted phonons for each photon absorption or emission process. The larger the S , the wider the band and the less resolved transitions corresponding to different vibration levels are. In general, the Huang–Rhys factor, S , is different for absorption and emission, S_{ab} and S_{em} , and yet in the one-dimensional CC approximation a simple relation between these values can be obtained

$$\frac{S_{ab}}{S_{em}} = \frac{\hbar \omega_0^e}{\hbar \omega_0^g}. \quad (25)$$

The full width at half maximum (FWHM or W) of the PL band depends on temperature T and in the one-dimensional CC model $W(T)$ is given by

$$W(T) = W(0) \sqrt{\coth\left(\frac{\hbar \omega_0^e}{2kT}\right)} \\ = \left(\sqrt{8 \ln 2} \frac{S_{em} \hbar \omega_0^g}{\sqrt{S_{ab}}} \right) \sqrt{\coth\left(\frac{\hbar \omega_0^e}{2kT}\right)}. \quad (26)$$

At high temperatures, the bandwidth is proportional to $T^{1/2}$ and at low temperatures it is temperature independent. Thus, it is possible to find parameters $W(0)$ and $\hbar \omega_0^e$ from the temperature dependence of the FWHM of a PL band. Further, if the position of the zero-phonon line (E_0) is known, one can estimate the quantity ($\hbar \omega_0^g S_{em}$) with the accuracy of $\frac{1}{2}(\hbar \omega_0^g - \hbar \omega_0^e)$:

$$\hbar \omega_0^g S_{em} = (E_0 - E_{max}) + \frac{1}{2} \hbar \omega_0^g \approx (E_0 - E_{max}) + \frac{1}{2} \hbar \omega_0^e, \quad (27)$$

and then find parameters $\hbar \omega_0^g$, S_{em} , and S_{ab} using Eqs. (25) and (26).

The temperature-related shift, $\Delta E_{em} = E_{em}(T) - E_{em}(0)$, of the broad PL band may have little or no correlation to the band-gap reduction. The following expression for ΔE_{em} is derived in the one-dimensional CC approximation for a defect with strong electron-phonon coupling⁸¹

$$\Delta E_{em} = \left[\frac{\omega_g^2 - \omega_e^2}{\omega_e^2} + \frac{8\omega_e^4}{\omega_e^2(\omega_g^2 + \omega_e^2)} \right] \left(\frac{E_{abs} - E_{em}}{E_{em}} \right) kT. \quad (28)$$

Thus, a shift to higher or lower energies can be observed for the broad PL bands with increasing temperature, depending on the particulars of the adiabatic potentials of the recombination centers.

It is important to note that in the cases of e-A and DAP transitions involving shallow donors, the shapes of the adiabatic potentials are determined solely by the adiabatic characteristics of the acceptor since its wave function is more localized. Therefore, no difference in the shape of the PL band can be noted between the e-A and DAP transitions in the first approximation. Only the positions of the PL bands would be shifted by the ionization energy of the donor. However, this shift often remains unnoticed due to the large PL bandwidth and strong temperature dependence of the band position.

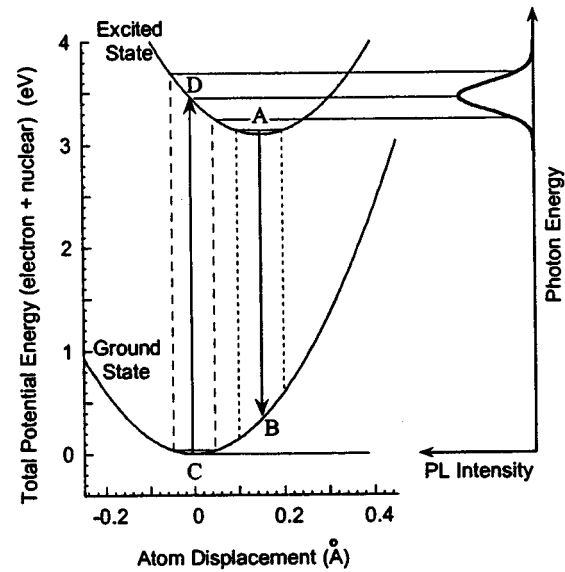


FIG. 12. An example of the CC diagram and resulting PLE spectrum.

D. Photoluminescence excitation spectra

PLE spectrum for a particular PL band can be obtained by using a tunable laser or a broad band lamp combined with an additional monochromator as the excitation source. The monochromator dispersing the PL is set to a particular wavelength, which is usually at the maximum of the analyzed PL band, and the wavelength of the excitation source is varied in order to obtain the excitation spectrum. The PLE spectrum is expected to coincide with the absorption spectrum with the difference that in the latter case several different transitions may contribute and complicate the spectral analysis. Photoionization of a defect is an inverse process to the luminescence, and in n -type GaN it involves a transition of an electron from an acceptor level to the conduction band, or to the excited state of the defect. In p -type GaN, we may expect a very similar photoionization of an electron from the valence band to a deep donor, followed by a recombination between this electron and a free hole. Note that the photoionization spectra measured by PLE, absorption, photocapacitance, or photoconductivity methods should have more or less similar shapes since the mechanism of the photoexcitation is the same in all the above cases.

Broad PL bands arising from deep-level defects with strong electron-phonon couplings usually result in broad bands in the PLE spectrum also. This is illustrated schematically in Fig. 12. At low temperatures, the system in the ground state (represented by an acceptorlike defect filled with electrons in n -type GaN and the surrounding neighboring atoms) stays at zero level and oscillates. The energy provided by the optical excitation source can bring the system to an excited state (solid line CD in Fig. 12). The transition $C \rightarrow D$ in our example corresponds to a transition of an electron from the acceptor level to the conduction band or to the excited state of the acceptor near the conduction band if any. The electron transition is much faster than the motion of atoms (adiabatic approximation). Therefore, the transition is vertical in the CC diagram. Depending on the phase of the

zero-level oscillations, the system may be closer or farther from the equilibrium point in the excited state (as shown by the dashed lines on both sides of transition CD). Therefore, after numerous photoexcitation processes the absorption energy evolves into a broad band. In the case of a strong electron-phonon coupling, which causes the minima of the ground and excited states to be sufficiently displaced, the shape of the absorption band is nearly Gaussian. However, for a weak electron-phonon coupling and small displacement of the adiabatic potential minima the shape of the absorption band is asymmetric with an abrupt edge near the zero-phonon transition line, E_0 . After the excitation, the system relaxes to its minimal energy position by emitting several local or lattice phonons (transition $D \rightarrow A$). Then the system stays at the zero level at low temperatures and after a period of time (PL lifetime) it returns to the ground state by emission of a photon ($A \rightarrow B$) and consequent emission of a few phonons ($B \rightarrow C$).

For transitions of electrons from the defect level to the conduction band the shape of the PLE or absorption spectrum may depart from the Gaussian shape and have an extended shoulder at the high-energy side due to the possible transitions to the quasicontinuous states in the conduction band. When the energy of the excitation becomes equal or exceeds the band gap, transitions of electrons from the valence band to the conduction band and subsequent nonradiative capture of a hole by a deep acceptor (nonresonant excitation of the acceptor) would give a step in the PLE spectrum corresponding to the band-to-band absorption. The relative contribution of the resonant and nonresonant transitions in the PLE spectrum depends on the thickness of the sample and specific values of the nonradiative and optical (photoionization) capture cross sections for a particular acceptor. The energy displacement of the emission and absorption maxima (Stokes shift) facilitates the measurement of the PLE spectra.

The PLE spectra from deep-level defects, including contributions from the resonant and nonresonant excitations, have been studied in GaN (Refs. 76 and 98–100), and are discussed in Secs. IV A 6 and IV B 2.

E. Spatially and depth-resolved cathodoluminescence

CL is produced by absorption of high-energy electrons and resultant spontaneous emission of light corresponding to specific transitions in a semiconductor. It can be detected as a CL spectrum or as a distribution of CL intensity over a certain area of the semiconductor surface (CL image). The latter case is conveniently facilitated by a combination of a scanning electron microscope and a luminescence collection system. When an incident electron beam bombards the semiconductor under test, it first causes the emission of secondary electrons from a thin surface layer which is on the order of 10 nm causing that region to be positively charged.¹⁰¹ The secondary electrons also penetrate into the sample to some depth which depends on the acceleration voltage (V_b). This negatively charged layer is much thicker than the positively charged surface layer from which the secondary electrons escaped. The electron penetration depth in GaN increases

from about 0.2 to more than 4 μm as V_b is increased from 5 to 35 kV.^{102,103} Note that the energy-loss depth profile maximizes at approximately 30% of the penetration depth.¹⁰⁴ The penetration depth increases with increasing V_b , and the electron-hole pair generation rate is proportional to the beam power ($E_b I_b$). The CL intensity is determined not only by the generation rate but also by the penetration depth through the process of self-absorption,¹⁰⁵ surface recombination, competition of different recombination mechanisms, and migration of charges with time.^{101,103}

Depth-resolved CL experiments are usually conducted under constant beam power or constant power-density conditions. The penetration depth is varied by varying the accelerating voltage. Depth-dependent CL spectra can be taken also from the edge of a cleaved sample. Since the radiated area is about 0.1–1 μm^2 , depth profiling is especially conducive for thick layers or bulk samples since electrons cannot penetrate deeper than $\sim 5 \mu\text{m}$.

To obtain a CL image at a certain photon energy which can be varied, the electron beam is scanned over an area of up to 0.1 \times 0.1 mm^2 . Such images may help identify the luminescence bands and determine their spatial distribution and relation to structural defects.

F. Optically detected magnetic resonance

Electron paramagnetic resonance (EPR) and its variant, ODMR, provide information on the ground state and microscopic origin of defects through obtaining the values and angular dependencies of the Zeeman splitting (g tensor) and interpretation of any hyperfine structure. Compared to EPR, ODMR relates the magnetic information to particular luminescence bands and assists their identification.

The g value of the free electron is $g_e = 2.0023$. In the first-order perturbation theory the deviation of the g value for a particular center is given by $\lambda/\Delta E$, where λ is the spin-orbit interaction constant.¹⁰⁶ Usually donors show g values smaller than free electrons, and acceptors have a positive g shift. However, there are exceptions to this simple rule.¹⁰⁷ Donors in GaN are typically characterized by g factors between 1.949 and 1.962, showing a small anisotropy ($g_{\parallel} - g_{\perp} \sim 0.003 - 0.006$). Acceptors are characterized by a relatively larger value and anisotropy of the g factor.^{108,109}

IV. LUMINESCENCE RELATED TO POINT DEFECTS IN UNDOPED GaN

Typical low-temperature PL spectra from selected unintentionally doped GaN samples are shown in Fig. 13. In addition to the near-band-edge emission due to bound and free exciton transitions and their phonon replicas, the PL spectrum from undoped GaN almost always contains a broad yellow luminescence (YL) band with a maximum at about 2.2 eV (Fig. 13). The YL band is by far the most studied PL band in GaN. Despite this inordinate effort, it is still not clear how many and what kind of defects contribute to that broad emission band (see Sec. IV A). In high-purity GaN grown by HVPE, the YL band is replaced by a green luminescence (GL) band at about 2.5 eV under certain experimental

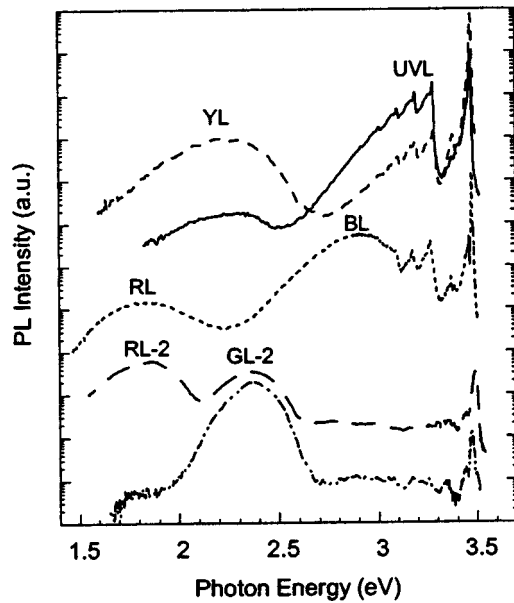


FIG. 13. PL spectra from undoped GaN at 15 K. The spectra are plotted in logarithmic scale and displaced vertically for better viewing.

conditions.^{110–114} The GL band is attributed to another charge state of the defect¹¹² responsible for the YL band, the details of which are discussed in Sec. IV B.

Another PL band, observed in undoped GaN at low temperatures, is known as the shallow DAP band.¹¹⁵ This band is characterized by a relatively sharp peak at about 3.25–3.27 eV followed by several replicas at energies which are multiples of the LO phonon energy in GaN (Fig. 13). The nomenclature chosen has its roots in the fact that at low temperatures that band is caused by transitions from the shallow donors to the shallow acceptors. At elevated temperatures, the DAP-type transitions are gradually replaced by the e-A transitions involving the same shallow acceptor. Since the shapes of the DAP and e-A bands are similar and these transitions cannot always be delineated from each other, we will refer hereafter both the shallow DAP and e-A bands as the ultraviolet luminescence (UVL) band. Unlike the YL band, which remains nearly unchanged with increasing temperature at least up to the room temperature, the UVL band quenches at temperatures above ~ 150 K and typically cannot be detected at room temperature. Properties of the UVL band are examined in Sec. IV C.

In GaN layers grown by MOCVD or HVPE, another broad band, the blue luminescence (BL) band, is often observed in the low-temperature PL spectrum at about 2.9 eV (Fig. 13). This band begins to quench above 200 K, and at low temperatures it exhibits a characteristic fine structure.¹¹⁶ We present a detailed description of the BL band in Sec. IV D.

In undoped GaN grown by HVPE or MOCVD methods, a red luminescence (RL) band is sometimes observed at about 1.8 eV (Fig. 13), often as a shoulder to the YL band. In Sec. IV E, we present some data regarding the RL band in GaN.

Two broad bands, a green one at about 2.5 eV and a red one at 1.9 eV, have been detected^{99,117} only in high-resistivity

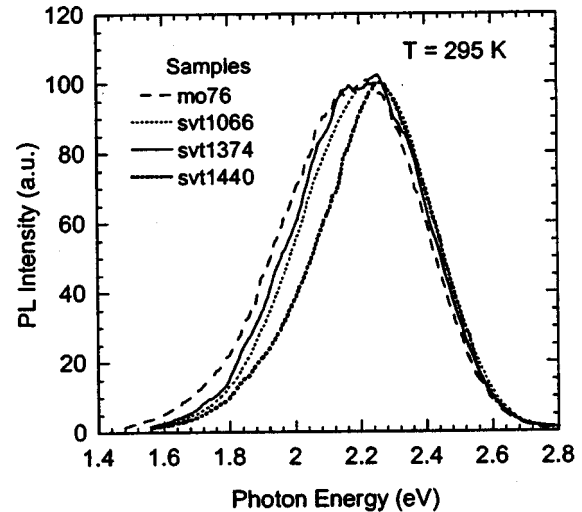


FIG. 14. Normalized room-temperature PL spectra of the MOCVD-grown sample (mo76) and three representative MBE-grown GaN layers. All the spectra were measured in identical conditions with an excitation density of 0.1 W/cm^2 . Weak oscillations of intensity are caused by light interferences.

GaN samples grown by MBE under extremely Ga-rich conditions. These bands exhibit properties very different from those of the RL band in GaN grown by MOCVD or HVPE and the GL band in GaN grown by HVPE. To avoid any confusion, these bands will be denoted hereafter as RL2 and GL2 bands, respectively (Fig. 13). The properties of these bands are presented in Sec. IV F.

In some investigations, a few less common PL bands have been observed in the visible part of the spectrum, as discussed in Sec. IV G. The contribution of all the above-mentioned defect-related bands varies from sample to sample, and no clear correlation is yet established until present between the appearance of most of these bands and presence of particular defects in the GaN samples.

The defects discussed in Sec. IV are presumably point defects which are more or less uniformly distributed inside the GaN layer, i.e., bulk defects. As has been shown, the surfaces also affect luminescence substantially. Some PL bands appear only after specific treatment of the GaN surface. We present a detailed description of such bands, in particular, the surface-related blue band, in Sec. IX A. PL from undoped GaN sometimes also contains sharp peaks that cannot be attributed to well-known exciton or defect-related transitions. These features are commonly assigned to manifestation of structural (extended) defects. These unusual PL lines in undoped GaN are discussed in Sec. VIII.

A. Yellow luminescence band

In most of the unintentionally and intentionally doped *n*-type GaN samples grown by the various techniques available, the room-temperature PL spectrum contains a near-band-edge emission at about 3.42 eV and the YL band peaking at 2.20–2.25 eV (Fig. 14). The YL band has been the topic of literally hundreds of publications. Only the investigations with meaningful contributions are discussed here. The YL band in GaN is always broad, nearly Gaussian with FWHM of about 350–450 meV, and structureless even at the

lowest measurement temperatures. However, the exact position and shape of the YL band are sometimes sample dependent. Although a few attempts have so far been made to resolve two or more bands^{118–120} or phonon-related fine structure in the broad YL band,^{121,122} we believe that the departure of the YL shape from Gaussian may be related to the particulars of the spectral response of the optical system used in some cases and to the interference effects in others.

There are several, albeit contradictory, results in the literature concerning the origin of the YL band and the effects of doping on its intensity. In early experiments of Pankove and Hutchby¹²³ 35 elements were implanted in GaN and most of them resulted in appearance or enhancement of the YL band. From that investigation, one can glean the obvious that the YL is related not to a specific impurity but to some native defect introduced by the implantation damage. First-principle calculations predict that several V_{Ga} -related defects may be responsible for YL in undoped GaN (Sec. II). Positron annihilation experiments strongly support the prediction of the theory that V_{Ga} is abundantly formed in n -type GaN.^{124–133} Substantial decrease and even disappearance of the YL with p -type doping also favors its assignment to a defect containing V_{Ga} .^{123,134} Ogino and Aoki⁹⁸ have found that Si and O doping do not affect the relative YL intensity, while doping with carbon enhanced this emission. These authors attributed the YL band to a complex involving a Ga vacancy and a C atom substituted for the nearest neighbor of the Ga sites. Several other experimental groups also attributed the YL band to C impurity or a complex involving carbon.^{135–140} The origin of the YL in undoped GaN is discussed in more detail in Secs. IV A 10 and IV H after the main properties of this band are treated.

Not only the identity of the YL-related defect but also the type of transitions responsible for the YL, as well as the question of whether the related defects are located in depth or at the surface of GaN, have been the subject of spirited discussion for many years. In the earliest detailed study of YL,⁹⁸ the band was attributed to a radiative transition from a shallow donor to a deep acceptor, presumably the $V_{\text{Ga}}C_{\text{N}}$ complex. The band shape, position, and activation energy of its thermal quenching have been explained consistently within a simple CC model with the acceptor level being located about 0.86 eV above the valence band.⁹⁸ The debates began some 15 years later when Glaser *et al.*¹⁴¹ explained their ODMR results associated with this band using an alternative model. This model is based on a two-stage process involving nonradiative capture of an electron by a deep double donor followed by radiative recombination between the electron at the deep donor and a hole at a shallow acceptor. Although this model appears very improbable from basic PL reasoning (see Sec. III A), it was seemingly confirmed by a few experimental groups¹⁴² and cited plentifully in many investigations devoted to YL in GaN. Other investigations making use of time-resolved PL,^{76,143,144} photocapacitance and optical deep-level transient spectroscopy (DLTS),^{145,146} Raman scattering,^{147,148} hydrostatic pressure,^{149,150} and PL excitation⁷⁶ did not support the model of Glaser *et al.*¹⁴¹

The questions on (i) whether YL originates from bulk or surface defects, (ii) what the depth distribution of the YL-

related defects is, and (iii) whether YL is related to point or structural defects have received extensive coverage. CL measurements indicated that the YL band is enhanced with increasing probe depth toward the substrate,¹⁵¹ in accordance with the observation of stronger YL near the GaN/sapphire interface when the sample is illuminated from the front side and the backside.^{152,153} Etching experiments demonstrated nearly independence of the YL intensity on depth into the layer.^{154,155} In contrast, photovoltage spectroscopy was used to argue in favor of surface defects being responsible for the YL band.^{156,157} Both correlation¹⁵⁸ and anticorrelation¹⁵⁹ between YL and structural defects in GaN have been reported.

Slightly different positions and shapes of the YL in different investigations may in part be related to a lack of correction for the spectral response of measurement systems. A point of interest is, however, that in one report different positions of the YL bands, obtained with the same setup, have been cited.¹⁰⁰ Superposition of several unresolved bands may affect the position and shape of the broad YL band. We observed a small shift (up to 50 meV) between bands very similar in shape (Fig. 14). The YL band in these samples did not shift with increasing excitation power and its intensity was nearly independent of temperature in the range of 15–300 K. As it will be shown below, the slightly different positions of the YL band found in the literature can simply be due to varying effects of structural defects on apparently the same point defect. Although formation of defects with slightly different spatial structure, various interactions between the point and structural defects, and even substantial contributions of surface states, which are spread in energy, in some samples cannot be ruled out without an extensive study. Below we present the main properties of the YL band in GaN that we believe will help shed some much needed light to identify the defect(s) responsible for the YL band or a set of unresolved YL bands in undoped GaN.

1. Effect of temperature

The effect of temperature on the intensity, shape, and position of the YL band has been the topic of many reports.^{67,76,98,137,143,152,160–165} The temperature dependence of the YL intensity, in comparison with the integrated PL intensities of the exciton emission, inclusive of all the emissions in the range of 3.3–3.5 eV and the BL band, is shown in Fig. 15. In the samples with high QE, a fast decrease of the exciton band intensity at temperatures from 15 to about 60 K is accompanied by the corresponding increase in the defect-related PL intensities in agreement with Eqs. (6) and (7). In the temperature range of 200–260 K a quenching of the BL band in the sample with the highest QE is accompanied by an increase in the intensity of the YL and exciton bands (the latter is seen as a shoulder in Fig. 15). A similar increase of the YL band intensity has been observed with increasing temperature from 10 to about 100 K (Refs. 161 and 165) and is attributed to a trap of 13.7 meV below the shallow donor.¹⁶¹ It should be noted, however, that the observed effect can be explained without invoking any traps. Indeed, as shown in Sec. III A 2, the quenching of the integrated exciton emission with an activation energy of about 13 meV (Ref. 67) results in enhancement of other PL bands

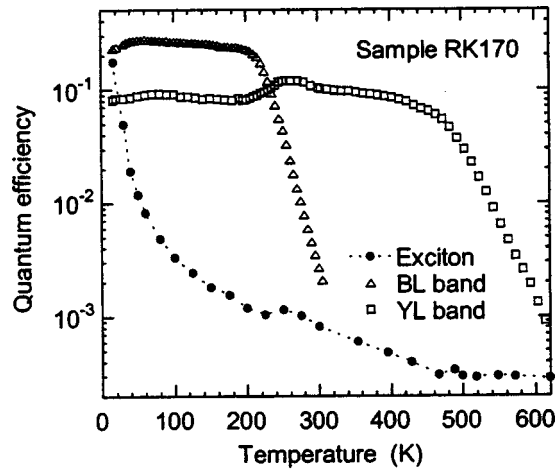


FIG. 15. Temperature dependencies of QE of the YL, BL, and exciton emission at excitation density of 2×10^{-4} W/cm². Reprinted with permission from Reshchikov and Korotkov, Phys. Rev. B **64**, 115205 (2001). Copyright (2001) by the American Physical Society.

with a similar activation energy. Therefore, the “unusual” increase of the YL intensity reported in Refs. 67, 161, and 165 is a consequence of a good sample quality, as categorized by high radiative efficiency of exciton emission and low excitation intensity conditions. Similar to the low-temperature increase of the YL intensity due to the quenching of exciton emission, the increase in YL intensity in the temperature range from 200 to 260 K, as depicted in Fig. 15, indicates a redistribution of holes released to the valence band due to thermal quenching of BL.

A slow variation of the YL intensity in the temperature ranges between quenching of this and other bands (for example, for $T=60\text{--}200$ K and $T=260\text{--}480$ K in Fig. 15) can be attributed to a slow variation of the hole-capture cross section for YL related or other defects, including nonradiative ones.⁶⁷ Various relative concentrations and types of defects in different samples may explain slightly different temperature dependencies of the YL intensity in different reports.^{76,98,137,143,152,161,162} Note, however, that the variation of the YL intensity below room temperature is not related to ionization of the shallow donor, as sometimes suggested.^{76,152,162} Indeed, according to carrier statistics in n -type GaN (Sec. III A), ionization of shallow donors may lead to replacement of the DAP recombination mechanism by the e-A mechanism and to variation of the PL lifetime. However, the intensity of the PL should be independent of these changes since it is determined only by capture of holes in n -type GaN.⁶⁷

In a few reports, the effect of temperature on the YL intensity has been studied up to very high temperatures, above 450–480 K, where drastic quenching of the YL takes place (Fig. 16).^{67,98,160,163,164} Although the reported values for the activation energy of this process vary from 58 meV (Ref. 163) to 1040 meV,¹⁶⁴ a close inspection of the data in these reports shows that the experimental results are very close and all the data can be explained by ionization of an acceptor with an activation energy of about 0.85 ± 0.2 eV. In particular, the value of 0.86 ± 0.04 eV has been obtained for C-doped GaN at temperatures above 480 K from quenching

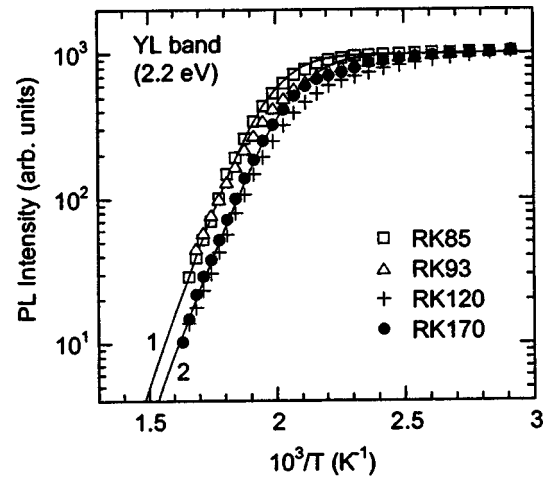


FIG. 16. Temperature-induced variation of the intensity of the YL band in the region of its quenching. The solid curves demonstrate fits by using Eqs. (5)–(7). Reprinted with permission from Reshchikov and Korotkov, Phys. Rev. B **64**, 115205 (2001). Copyright (2001) by the American Physical Society.

representing two orders-of-magnitude decrease.⁹⁸ A narrow range of activation energies (from 0.75 to 0.89 eV) and the same range of YL quenching (480–620 K) have been reported for several undoped GaN layers grown by MOCVD.^{67,160} Note that the value of 0.81 ± 0.03 eV obtained in Ref. 67 accounts for the temperature dependence of the density of states in the valence band ($T^{3/2}$) and thermal velocity of holes ($T^{1/2}$), which reduces the apparent activation energy, measured as a slope in Arrhenius plot, by about 0.09 eV. Thus, for comparison with other reports we change the above value to 0.90 ± 0.03 eV. Determination of the activation energy for the YL intensity in the MBE-grown undoped GaN as 0.058 ± 0.001 eV (Ref. 163) is evidently an oversight, since the YL intensity decreased by a factor of about 10 in the temperature range between 523 and 623 K [see Fig. 1(a) in Ref. 163], which leads to an activation energy in the range of 0.8–0.9 eV and is consistent with that reported in Refs. 67, 98, and 160. Finally, two samples grown by MBE, both undoped and C doped, showed quite different activation energies of 0.65 ± 0.04 and 1.04 ± 0.06 eV, respectively. This result has been attributed to apparently different defects responsible for the YL in undoped and C-doped GaN. Although these results merit careful attention, and the idea of different acceptors in undoped and C-doped GaN deserves detailed consideration, the quantitative data of Ref. 164 should be treated with caution due to lack of statistics and possibility of experimental artifacts. For example, a very high-excitation density of 20 W/cm², employed in Ref. 164, may saturate acceptors with holes, leading to a distortion of the temperature dependence of the PL intensity.⁶⁷ Contributions from blackbody radiation can also affect the measured PL intensity at high temperatures,¹⁶³ especially in the samples with weak YL.

Variation of the shape and position of YL with temperature has been the topic of several publications.^{98,137,160,162,163} The position of the YL band did not change within an accuracy of 20–40 meV when the temperature varied from about 10–30 to 300 K,¹³⁷ or 380 K,^{98,160} and also in the range from

300 to almost 600 K.¹⁶³ It should be kept in mind that the band gap reduces by more than 100 meV from cryogenic temperatures to 380 K and by about another 130 meV from 300 to 600 K.¹⁶³ Insensitivity of the PL peak shift to the band-gap variation is typical for defects with strong electron-phonon coupling.⁸¹ The FWHM of the YL band increases with temperature and can be described by Eq. (26). The obtained fitting parameters within the one-dimensional CC model of the YL emission are $W(0)=380$ meV (Ref. 160) and 430 meV (Ref. 98) and $\hbar\omega_0^e=52$ meV (Ref. 160) and 40 meV (Ref. 98) (see a more in-depth discussion in Sec. IV A 7). It is interesting to note that there is some discrepancy in the literature about the effect of temperature on the width and peak position of the YL band. In particular, Zhang and Kuech¹³⁷ reported a *decrease* of the FWHM from about 510 eV at 50–100 K to 475 meV at 300 K and a monotonic shift of the peak position by about 25 meV to a *higher* photon energy in the same temperature range in C-doped GaN. Moreover, the temperature variation of these parameters was substantially different for the YL in undoped GaN. In contrast, Ogino and Aoki⁹⁸ observed an *increase* of the FWHM from 430 to 540 meV and a shift of the peak position by about 30 meV to a *lower* photon energies in the same temperature range in C-doped GaN. The discrepancy in the absolute values of the FWHM of the broad YL band and its peak position may be attributed to a lack of accurate accounting for the spectral response of the measurement system and any interference effects. However, the diversity in the relative changes obtained for the samples grown under different conditions and/or different doping deserves a closer attention in an effort to better identify the YL band.

Variation of the YL intensity in a wide temperature range, including its quenching with temperature, allows us to estimate the hole-capture coefficient C_p and the hole-capture cross section σ_p for the acceptor responsible for YL (Sec. III A). These parameters can be obtained by fitting Eqs. (6)–(10) to the experimentally observed dependence of the YL intensity on temperature, provided that the excitation intensity is small enough to avoid saturation of the related acceptors by holes, and the lifetime of the YL is known. Note that the parameter η_i^* in denominator of Eq. (6) can be ignored since it is usually much less than unity. Moreover, a knowledge of the absolute PL intensity is not important in this fit. Examples of the fits to the temperature dependencies of the YL intensity in the quenching region for several undoped GaN samples are shown in Fig. 16. From these fits, parameters C_p and σ_p for the acceptor responsible for the YL band have been estimated as $(3.3\pm 1.6)\times 10^{-7}$ cm³ s⁻¹ and $(2.7\pm 1.3)\times 10^{-14}$ cm², respectively.⁶⁷ Note that the capture cross section is very large, indicating that the acceptor may be multiply charged, and thus attracts holes very efficiently. We will return to the analysis of these parameters in Sec. IV H.

2. Effect of excitation intensity

Information obtained from the dependence of the PL intensity on the excitation intensity can be used for determining the acceptor concentrations in GaN, as described in Sec. III A 5, as well as establishing the type of transition in-

involved. At low excitation levels, the intensity on the YL in *n*-type GaN is proportional to the excitation intensity. Above a critical excitation density (P_{cr}) the dependence becomes sublinear.^{67,73,74,166} The value of P_{cr} depends on a few parameters that can be estimated from the analysis of the PL data.⁶⁷

To estimate the acceptor concentration from PL data, one must first estimate the QE of the related PL band by direct measurements or by employing the method suggested in Ref. 67, as described in Sec. III A 3. The generation rate of the photoexcited carriers, G , can be estimated from the excitation density if the effective thickness of the layer subject to excitation is known. The absorption coefficient α at 325 nm is $\approx(1.2-1.5)\times 10^5$ cm⁻¹ in GaN,¹⁶⁷ therefore the carriers are efficiently created in about the 0.1- μ m region of the surface layer only. The hole diffusion length is about 0.1–0.3 μ m in thin GaN layers at room temperature,¹⁶⁸⁻¹⁷¹ approaching 1 μ m in thick HVPE-grown GaN.¹⁷⁰ Consequently, the effective thickness can be taken in the range of 0.1–1 μ m, depending on the sample quality. Finally, the PL lifetime should be measured, preferably at elevated temperatures (e.g., at room temperature for the YL) to avoid the analysis of nonexponential decays due to DAP-type transitions.⁸⁷ A typical dependence of the YL intensity on excitation intensity consists of a linear increase of the PL intensity followed by saturation above $G\approx 10^{21}$ cm⁻³ s⁻¹ (excitation density $\sim 10^{-2}$ W/cm²).⁶⁷ A square-root dependence is observed for higher generation rates.^{67,74,166} From the fit of Eq. (13) to the experimental data, the concentration of the acceptor responsible for the YL band has been estimated to be in mid- 10^{15} cm⁻³ for GaN layers grown by MOCVD.⁶⁷ The square-root dependence of the YL intensity on excitation power, observed in the high-excitation region, has been explained by a significant concentration of nonradiative deep donors near the surface.⁶⁷ However, as mentioned in Sec. III A 4, some other reasons including geometrical factors and photon recycling may be responsible for the square-root dependence of the PL at moderate excitation powers.

A small shift of the YL band with excitation intensity has also been reported.^{98,172} At low temperatures, the YL shifted to higher energy by about 10 meV as the excitation intensity was increased by a factor of 10 in C-doped GaN,⁹⁸ and by up to 15 meV (and up to 35 meV) as the excitation intensity was varied by four orders of magnitude in Si-doped GaN with low (and high) concentrations of Si.¹⁷² The relatively small shift can be attributed to the DAP nature of YL at low temperatures. As the excitation intensity is increased, distant pairs emitting at lower photon energies due to weaker Coulomb interaction contribute less due to their earlier saturation with holes, since the PL lifetime for distant pairs is longer than for close ones. Small shifts in energy indicate that the donor is shallow.

3. Effect of hydrostatic pressure

Experiments with uniaxial and hydrostatic pressures could provide useful information on the identification of a defect or at least the type of transitions causing the defect-related PL. In particular, application of hydrostatic pressure induces shifts of PL bands. If the shift is similar to the shift of the band gap, the PL can be attributed to transitions from

the conduction band or from a shallow donor to an acceptor level. Indeed, the pressure shift of the shallow donor level is about the same as the shift of the conduction-band minimum, whereas the pressure shift of an acceptor level should be similar to the shift of the top of the valence band, or even a weak negative shift of the acceptor level with respect to the top of the valence band may be expected.¹⁷³ A much weaker pressure shift of a given PL band is expected for transitions from a deep donor to an acceptor, or for internal transitions within the defect. The effect of hydrostatic pressure on YL was studied for bulk GaN unintentionally doped with oxygen^{149,150} and nominally undoped GaN layers grown by MBE (Refs. 149 and 150) and MOCVD (Refs. 174–176) on sapphire. All these reports noted large shifts of YL at least up to 6 GPa having a pressure coefficient between 30 and 40 meV/GPa, which is very similar to the shift of the band gap having a pressure coefficient of about 40 meV/GPa.^{149,150,174,175} At pressures above approximately 20 GPa, the shift of the YL band saturated, which has been attributed to an emergence of a resonance level from the conduction band into the gap, leading to a change of the mechanism of the YL in that transitions from the conduction band to a deep acceptor level, were replaced by transitions from the resonant level to the same acceptor.^{149,150}

The intensity of the YL band decreased with pressure^{174–176} and became barely measurable at 18 GPa.¹⁷⁶ An interesting observation is that with cooling to low temperatures under hydrostatic pressure, the YL intensity strongly decreases,¹⁷⁶ which is to be contrasted with its small increase upon cooling under ambient pressure. Michael *et al.*¹⁷⁶ explained this effect by contribution of two DAP-type transitions involving the same acceptor and two different donors, with one of them having a DX-like behavior.

4. Effect of electron irradiation

Electron irradiation is widely used in studies of semiconductors because it artificially creates point defects that may be present in an as-grown material but in an amount insufficient for their analysis.¹⁷⁷ Look¹⁷⁷ has estimated that the electron energy of the order of 1 MeV is already high enough to create V_N-N_i and $V_{Ga}-Ga_i$ Frenkel pairs. However, Kuriyama *et al.*¹⁶² argued that much higher energies may be needed to create Ga vacancies. Saarinen *et al.*¹⁷⁸ have established experimentally that 2-MeV electron irradiation at 300 K does create Ga vacancies in GaN. The electron irradiation with relatively low power can be used also as a source of electron-hole pairs to probe point defects at different depths in the luminescence experiments. So, low-energy electron-excited nanoscale luminescence (LEEN) employing energies from 100 eV to 5 keV,¹⁷⁹ and CL typically employing energies between 1 and 35 keV,^{103,180–183} have been extensively employed to investigate defects in GaN. More results obtained by LEEN and CL investigations of GaN are presented in Secs. IV D 3, IV E, and V B 3 f. Here we limit ourselves to showing how irradiation with relatively high energy of electrons, in the range of 2.5–30 MeV, affects YL in *n*-type GaN.

After irradiation with 2.5-MeV electrons to a dose of about 10^{18} cm⁻², the YL intensity markedly decreased.^{184,185}

However, the decrease in the near-band-edge emission was much stronger.¹⁸⁵ Irradiation with 7-MeV electrons caused a substantial increase of the YL intensity and decrease of the near-band-edge emission.¹⁸⁶ The variation of PL intensity in Ref. 186 was proportional to the electron dose in the range from 10^{15} to 10^{17} cm⁻². Irradiation with 30-MeV electrons completely destroyed PL in the entire spectrum. However, a subsequent annealing at temperatures ranging from 500 to 1000 °C led to substantial increase of the YL intensity of up to five times compared to the value in as-grown sample.¹⁶² An increase of the YL intensity after electron irradiation was attributed to the creation of Ga vacancies in GaN.^{162,186} High stability of YL with annealing was explained¹⁶² by the formation of gallium vacancy-shallow donor ($V_{Ga}D$) complexes that are much more stable than isolated V_{Ga} .

Fast proton irradiation of GaN at room temperature has been performed by using 25- and 55-MeV protons.¹⁸⁷ While the YL intensity after irradiation increased in the 160- μ m-thick freestanding template grown by HVPE, no increase was observed for the 10- μ m-thick GaN layer grown by HVPE on sapphire and in MBE-grown GaN layer. The YL intensity in the freestanding template gradually increased with increasing proton fluence from 1×10^{14} to 2.7×10^{14} cm⁻². The enhancement of YL has been attributed to a radiation-induced creation of Ga vacancies in GaN.¹⁸⁷

5. Time-resolved PL

As discussed in Sec. III B, TRPL has the potential to give clues to recombination mechanism in effect, e.g., whether it is e-A or DAP transition, and whether deep-level or shallow defects constitute the DAP. TRPL may also give a clue in identifying the deep acceptor through the values of the electron-capture cross section. It also helps in delineating the PL bands which are overlapped in the SSPL spectrum. Transient PL for the YL band in GaN has been investigated by several authors,^{76,87,110,142,143,152,161,166,188–192} and the results have often been controversial. For example, the reported PL lifetime for the YL ranges from 20 ps (Ref. 166) and 1 ns (Ref. 143) to the microseconds (50–700 μ s) (Refs. 87 and 142) and even up to 300 ms.¹⁶¹ Measurements at 15 K revealed a nonexponential decay of the YL band, typical for the DAP transitions,^{76,87,142,152,190} whereas at room temperature the decay was nearly exponential.⁸⁷ Single exponential decay with a characteristic time of 250–260 μ s has been observed in time-resolved CL experiments at 87 K.¹⁸⁹ Below we present TRPL results for the YL band in undoped GaN and comment on the unusually small and large values of the reported lifetimes of this emission.

A typical intensity decay curve for the YL band is shown in Fig. 17 along with the decays of other PL bands present in the same sample. The instantaneous lifetime of PL changes from several microseconds to milliseconds at low temperatures. The decay curves are nonexponential at 15 K and become nearly exponential above 150 K. The nonexponential decay is a signature of the DAP recombination, as discussed in Sec. III B. The DAP transitions are expected at low temperatures, and e-A transitions are expected at elevated temperatures when ionization of the shallow donor is significant. Excellent fits of the PL decay to Eq. (17) for the YL band

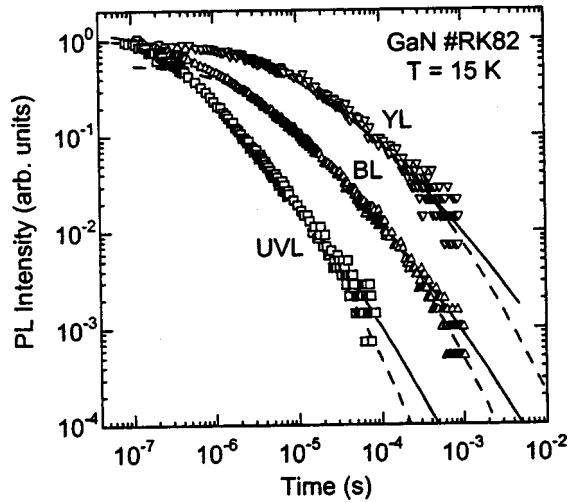


FIG. 17. Intensity of the YL, BL, and UVL bands at 15 K in undoped GaN grown by MOCVD. The curves are calculated using Eq. (17). Reprinted with permission from Korotkov *et al.*, *Physica B* 273, 80 (1999). Copyright (1999) by Elsevier.

with minimal number of fitting parameters, demonstrated in Refs. 188 and 76, support the assignment of this band to transitions from a shallow donor to a deep acceptor at low temperatures. The value of W_{\max} in a set of four samples was obtained to be on the order of 10^6 s^{-1} (Ref. 188), although a much higher value of $2.5 \times 10^7 \text{ s}^{-1}$ has also been reported.⁷⁶

The time-resolved PL spectra for different delay times are shown in Fig. 18. No difference is seen between the SSPL and TRPL spectra for small delay times.¹⁸⁸ With increasing delay time, no shift or change in the band shape is observed within the experimental accuracy of $<30 \text{ meV}$. Similar results have been reported in Refs. 76 and 191. The PL bands originating from the DAP transitions involving deep donors are expected to redshift significantly with delay time.^{79,80} This is a result of the faster recombination in close pairs, which contribute to the high-energy side of the band

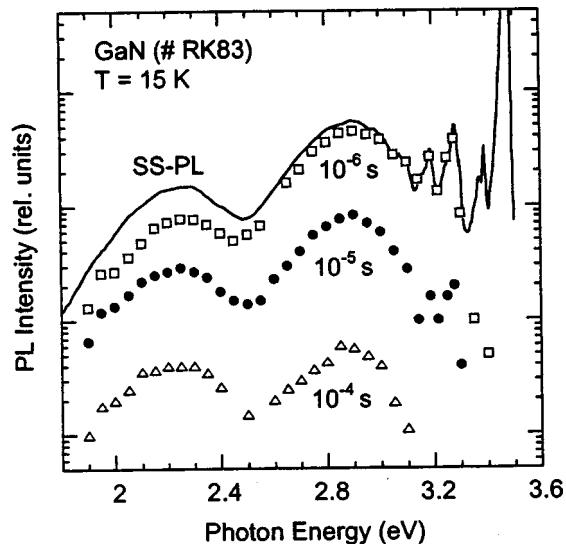


FIG. 18. Steady-state PL spectrum (solid curve) and time-resolved PL spectra (points) at time delays of 10^{-6} , 10^{-5} , and 10^{-4} s for undoped GaN sample grown by MOCVD. Reprinted with permission from Korotkov *et al.*, *Physica B* 273, 80 (1999). Copyright (1999) by Elsevier.

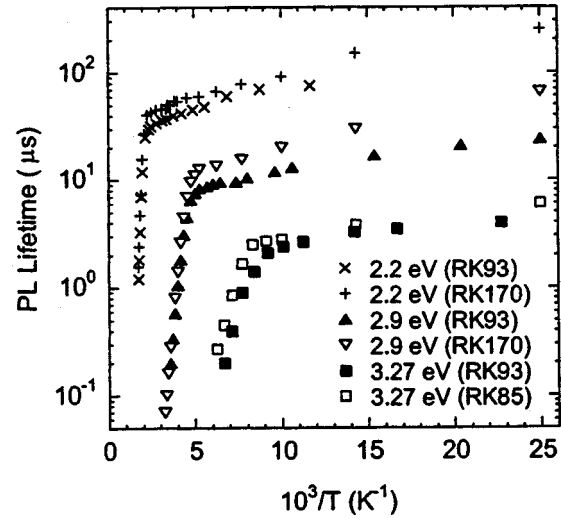


FIG. 19. Temperature dependence of the effective lifetime of the YL (2.2 eV), BL (2.9 eV), and UVL (3.27 eV) bands in undoped GaN grown by MOCVD. Reprinted with permission from Korotkov *et al.*, *Physica B* 325, 1 (2003). Copyright (2003) by Elsevier.

due to stronger Coulomb interaction. The deeper the donor, the larger the possible shift, but it still remains below the value of the ionization energy of the donor.⁸⁰ The absence of a noticeable shift of the bands with time delay indicates that only shallow donors are involved. However, the shift of the YL band to a lower photon energy by about 30–40 meV at a delay time of about 1 ms compared to the YL band position in the SSPL spectrum has been observed by Monteiro *et al.*,¹⁹² who attributed this observation to a competition of two bands peaking at 2.05 and 2.28 eV. An attempt to resolve the 2.27- and 2.04-eV peaks in the decay of the YL band was made also by Chtchekine *et al.*¹⁴² Further, an apparent shift of the YL band maximum from 2.25 to 2.35 eV at a delay time of $\sim 10 \text{ ms}$ after a light pulse has been observed in undoped GaN and attributed to the emergence of another band at 2.35 eV having a decay time of the order of 300 ms.¹⁶¹ The complex nature of the YL band has also been noted in time-resolved CL studies where two bands at 2.03 and 2.22 eV have apparently been resolved by transient measurements.¹⁸⁹

The measured decay curve undergoes a considerable change and becomes nearly exponential with increasing temperature.⁸⁷ Therefore, the recombination mechanism also changes with temperature. The concentration of free electrons increases and the DAP transitions are gradually replaced by the e-A transitions at temperatures above 100–200 K. The change in the recombination mechanism at temperatures above 100 K is consistent with the Hall data for undoped *n*-type GaN. Temperature dependence of the effective lifetime of PL, τ_R^* (as defined in Sec. III B), for the YL band in comparison with τ_R^* for other bands in *n*-type GaN is shown in Fig. 19. The effective lifetime of PL has a weak temperature dependence up to $\sim 500 \text{ K}$ for the YL band. In a larger set of samples, the value of τ_R^* ranged from 25 to 60 μs at 300 K. The longer lifetime was observed in the samples with lower free-electron concentrations,⁸⁷ in agreement with theory [see Eq. (20) in Sec. III B].

In the temperature region where the SSPL intensity quenches, the lifetime of PL decreases sharply (Fig. 19) with activation energies close to those found from the PL intensity quenching.^{87,188} Thermalization of holes from the acceptors to the valence band at temperatures above ~ 500 K for the YL band (and above 120 and 200 K for the UVL and BL bands, respectively) is responsible for the fast decrease of the PL lifetime [see Eq. (22) in Sec. III B].

The electron-capture coefficient C_n and the electron-capture cross section σ_n derived for the YL band by using Eqs. (20) and (23) are $(6.2 \pm 1.2) \times 10^{-14} \text{ cm}^3 \text{ s}^{-1}$ and $(2.7 \pm 0.5) \times 10^{-21} \text{ cm}^2$, respectively.⁸⁷ These values are very small which support the assertion that the ground state of the acceptor, responsible for the YL band in *n*-type GaN, is a multiply negatively charged defect such as an isolated V_{Ga} or its complex with a shallow donor. The small values of C_n and σ_n , which result in long PL lifetime, are also consistent with very large values of C_p and σ_p , which likewise result in fast capture of holes for the same acceptor⁶⁷ (see Sec. IV A 1).

Finally, commenting on extremely short decays of the YL reported in the literature,^{143,166} it should be noted that according to Eq. (20), the lifetime of the e-A transitions for a particular acceptor cannot be much different in samples with comparable concentrations of free electrons. Therefore, the extremely low lifetimes cannot be explained by the e-A transitions if the same acceptor is involved. The DAP transitions are usually even slower. Note that at high excitation levels, when the defect-related PL saturates, a very fast decay component can be observed that is related to the exciton band tail at the position of the defect-related PL band.⁸⁷

6. Resonant excitation

There have been relatively few attempts made to measure PLE spectra of deep-level defects in GaN. A few more investigations employed resonant excitation without measuring the PLE spectrum. Further most of these studies are related to the YL band. Ogino and Aoki⁹⁸ pioneered in applying PLE spectroscopy to the investigation of the YL band in the C-doped GaN needlelike crystals. Later a similar PLE spectrum was obtained in undoped GaN layers grown by MOCVD,⁷⁶ MBE,⁹⁹ and HVPE (Ref. 152) on sapphire substrates as well as in undoped GaN freestanding templates.¹⁰⁰

Figure 20 shows the PLE spectra for the YL band at cryogenic and room temperatures measured in the 2.5- μm -thick undoped GaN layer grown by MBE on sapphire. Various groups^{76,98,152} reported similar spectra for undoped and C-doped GaN. The PLE spectrum consists of two characteristic regions: a slow increase of PL intensity with variation of $\hbar\omega_{\text{exc}}$ from 2.7 to ~ 3.3 eV and a fast increase at higher photon energies. The slow increase is related to the resonant excitation of the YL-related defect involving transition of an electron from the acceptor level to the conduction band, and the fast increase is attributed to the interband transitions followed by nonradiative capture of the photogenerated hole by the defect. Note that the resonant excitation part of the spectrum is nearly independent of temperature, while the interband transitions shift significantly towards the low-temperature gap energy and become sharper with decreasing temperature. The resonant part of the PLE spectrum can be

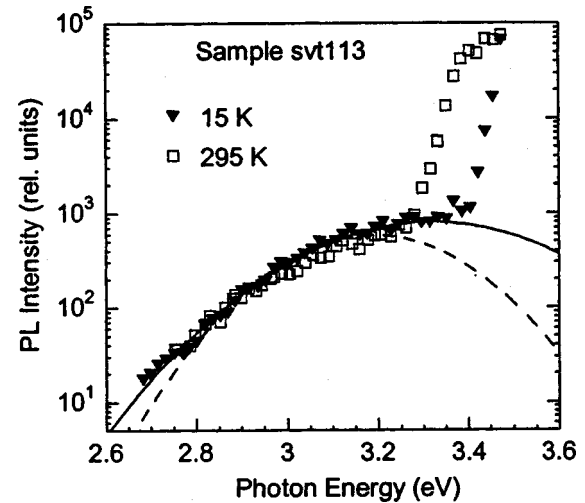


FIG. 20. PLE spectra for the YL in the 2.5- μm -thick MBE-grown GaN layer at 15 and 295 K. The solid curve is a Gaussian fit with maximum at 3.32 eV and FWHM of 0.52 eV. The broken line is a Gaussian fit with maximum at 3.19 eV and FWHM of 0.40 eV. Reprinted with permission from Reshchikov *et al.*, Mater. Res. Soc. Symp. Proc. 693, I6.19 (2002).

fitted with a Gaussian curve according to the CC model for a defect with strong electron-phonon coupling (see Sec. III C). The position (3.32 eV) and FWHM (0.52 eV) of the fitted curve in Fig. 20 are similar to the values found by Ogino and Aoki [3.19 and 0.40 eV, respectively, at 4.2 K (Ref. 98)]. The fit with the latter parameters is shown for comparison in Fig. 20. Note that only the part of the Gaussian curve has been observed in the PLE spectrum, hampering a precise estimate of these parameters. The shape of the resonant PLE curve is the same for undoped and C-doped samples regardless of the sample preparation technique employed.^{76,98–100,152}

To determine whether the PLE spectrum is related to one defect or due to a superposition of emissions from defects with different vibrational properties, one should compare the PL spectra at different excitation energies. In some investigations,^{98,99,191} the same shape and position of the YL band were observed at different excitation energies. The zero-phonon energy, below which the excitation of the YL band is impossible, has been estimated as 2.64 ± 0.05 eV.^{98,99} The threshold for the YL excitation could be estimated as ~ 2.4 – 2.5 eV from Refs. 76 and 152. However, it is not clear if the YL was the one that was excited at $\hbar\omega_{\text{exc}} < 2.64$ eV, not some background emission from the sapphire substrate is what was observed. In conflict with the above results, Calleja *et al.*¹⁴⁶ reported only a moderate decrease of the YL intensity in undoped GaN layer on sapphire when the excitation energy was decreased down to 2.41 eV. The band shifted from ~ 2.20 to about 2.10 eV with variation of $\hbar\omega_{\text{exc}}$ from 2.7 to 2.41 eV, and the shift was attributed to the coexistence of several defects with similar ionization energy.¹⁴⁶ Drastically different results from all above were reported by Colton *et al.*^{119,120} Those authors observed a linear shift of the YL band as the excitation energy was gradually varied from 2.2 to 2.7 eV. Note that the YL band in these reports did not resemble the usual YL band and consisted of several relatively sharp peaks. The shift of these peaks was identical to

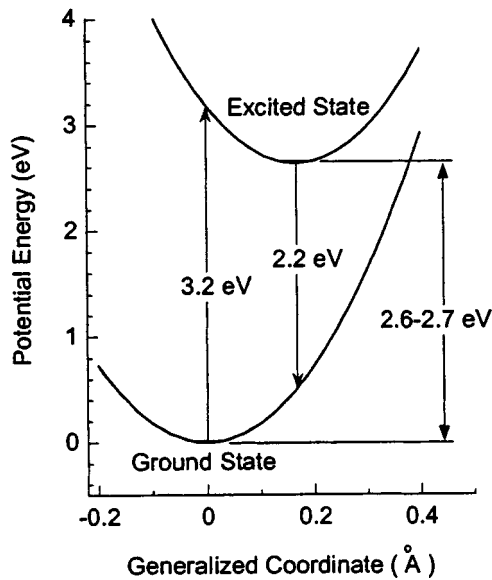


FIG. 21. One-dimensional CC diagram for the YL in GaN.

the shift of $\hbar\omega_{\text{exc}}$ of the laser, which might point to an artifact for the peaks observed in Refs. 119 and 120.

A comparison of the absolute intensity of the YL band, excited resonantly under identical conditions in the 2.5- μm -thick GaN layer grown by MBE, 10- μm -thick GaN layer grown by HVPE, and in a 200- μm -thick HVPE-grown GaN freestanding template, allowed us to estimate the concentration of the YL-related defect in these samples.^{99,100} The concentration of the YL-related defect is of the order of $\sim 1 \times 10^{15} \text{ cm}^{-3}$ in HVPE-grown samples, and about 200 times higher in the MBE-grown sample, the PLE spectrum of which is shown in Fig. 20.

7. Vibrational model of the YL

An absence of the YL band shift with changing excitation energy from 2.9 to 3.81 eV (Ref. 99) indicates that at least in some particular samples the YL peak is related to a single defect rather than to closely spaced states with a broad distribution.¹⁴⁶ Indeed, a strong electron-phonon coupling alone can explain the displacement and large width of the PL and PLE bands. The position and the FWHM of the excitation and emission curves provide valuable information for the construction of adiabatic potentials for the YL-related defect in the ground and excited states. Additional information can be gained from an analysis of the temperature behavior of the YL band (see Sec. IV A 1 a). Figure 21 schematically shows the one-dimensional CC diagram for the YL-related acceptor. The potential minima of the excited and ground states of the analyzed deep acceptor are displaced in space, termed the lattice relaxation. According to the CC model, the zero-phonon energy (E_0), or the energy difference between these minima, is the smallest excitation energy and the largest emission energy that can be observed at low temperatures in the PLE and PL spectra of the YL band, respectively. The values of E_0 , E_{em} , E_{ab} , $W_{\text{em}}(0)$, $W_{\text{ab}}(0)$, $\hbar\omega_0^g$, $\hbar\omega_0^e$, S_{em} , and S_{ab} have been estimated as 2.64 eV, 2.13 eV, 3.19 eV, 430 meV, 400 meV, 40 meV, 41 meV, 12.8, and 13.4, respectively.⁹⁸ Note that these parameters consistently ex-

plain a large set of experimental results including the temperature dependence of the position and width of the YL band, the shape, and position of the emission and excitation bands.⁹⁸ Slightly different values of $W_{\text{em}}(0)$, E_{em} , and $\hbar\omega_0^e$ (380 meV, 2.21 eV, and 52 meV, respectively), obtained from the position and temperature dependence of the FWHM of the YL band in MOCVD-grown GaN layer, led to slightly different values of $\hbar\omega_0^g$, S_{em} , and S_{ab} (55 meV, 8.0, and 8.4, respectively).¹⁶⁰ The parameter $E_0=2.64$ eV was adopted from Ref. 98. However, by taking $E_0=2.70$ eV, which is consistent with the results for the MOCVD-grown layer,^{99,100} one can obtain $\hbar\omega_0^g=51$ meV, $S_{\text{em}}=10.3$, and $S_{\text{ab}}=10.2$ from the data of Ref. 160. The latter parameters are in better agreement with the position and shape of the YL excitation spectrum depicted in Fig. 20. A much simplified analysis of vibrational properties of the YL band, based largely on theoretical predictions, yielded a Huang–Rhys factor of 6.5 for the YL band in GaN.¹⁹³ Of course, the accuracy of all the above-estimated parameters is not high, and moreover, the simplified picture of the electron-phonon coupling gives some average for the phonon modes of the defect involved.

The ground state of the defect in Fig. 21 corresponds to an acceptor completely filled with electrons in n -type GaN. The resonance excitation, which is possible above $E_0=2.6\text{--}2.7$ eV, transfers an electron to the conduction band, leaving a bound hole at the acceptor. In the excited state (depicting a hole at the acceptor) the defect system relaxes to its minimum, and the excess energy is emitted in the form of phonons. After the system spends substantial time while oscillating in the excited state at low temperatures, the acceptor may capture a free electron or electron from a distant shallow donor, and emission with the average energy $E_{\text{em}}\approx 2.2$ eV ensues. The emission band is broad due to zero-level oscillations and a substantial spatial shift of the adiabatic potential minima. The cycle is completed by relaxation of the system to its potential minimum in the ground state by emitting phonons.

8. Comparison with the positron annihilation results

Positrons in solids are trapped at neutral and negative vacancy defects, which can be experimentally detected by measuring the positron lifetime.¹⁹⁴ Positron annihilation experiments revealed that n -type GaN usually contains relatively high concentration of Ga vacancies, whereas p -type GaN lacks them.^{124–133,164,178,195} Saarinen *et al.*¹⁹⁵ have found that in undoped GaN grown by MOCVD, the concentration of V_{Ga} increases from 10^{16} to 10^{19} cm^{-3} as the Ga/N ratio used during growth is increased from 10^3 to 10^4 in successive layers. The above results are consistent with theoretical predictions (see Sec. II). Moreover, Saarinen *et al.*¹²⁵ established a correlation between the concentration of the V_{Ga} and the intensity of the YL. Although there were only four samples in that study, and the intensity of the YL was not necessarily proportional to the concentration of the YL-related defect in different samples as evident from the consideration of carrier statistics discussed in Sec. III A, a perfect correlation allowed the authors of Ref. 125 to conclude that V_{Ga} is responsible for the YL in n -type GaN. Early positron annihilation experiments, however, could not answer if

isolated V_{Ga} or V_{Ga} involved in a complex, such as $V_{\text{Ga}}\text{O}_\text{N}$ or $V_{\text{Ga}}\text{Si}_{\text{Ga}}$, is present in n -type GaN. According to calculations, both the isolated V_{Ga} and V_{Ga} -donor complexes are abundantly created in n -type GaN (see Sec. II). However, it was not clear if an isolated V_{Ga} is stable enough to survive during cooling down of the crystals without forming a complex with donors noting that the stability of the $V_{\text{Ga}}\text{D}$ complexes is much higher. To address this problem, Saarinen *et al.*^{129,178} created V_{Ga} in bulk GaN crystals, containing high concentration of oxygen, by 2-MeV electron irradiation at room temperature and subsequently annealed the samples at different temperatures. The concentration of V_{Ga} increased linearly with irradiation fluence up to 10^{18} cm^{-2} . The created $V_{\text{Ga}}\text{-Ga}_i$ Frenkel pairs are expected to break at relatively low temperature since the Ga interstitial is already mobile at room temperature.³¹ Annealing experiments demonstrated that V_{Ga} becomes mobile in a temperature window of 500–600 K, a band which is much lower than the typical GaN growth temperatures. These results indicated that the isolated V_{Ga} would not survive during cooling down of the samples and the observations should associate with other defects, most probably with shallow donors that attract triply negatively charged mobile V_{Ga} by their positive charge. Another controversial question to be addressed is whether the $V_{\text{Ga}}\text{O}_\text{N}$ or $V_{\text{Ga}}\text{Si}_{\text{Ga}}$ is preferably formed during growth if both shallow donors are present in equal amounts. Calculations predict that the formation energy of the $V_{\text{Ga}}\text{O}_\text{N}$ complex is much lower (see Sec. II). In line with this prediction, Oila *et al.*¹²⁷ discovered that in O-doped GaN, either bulk or epilayer, the concentration of V_{Ga} is very high (about 10^{18} cm^{-3}), whereas in Si-doped GaN the Ga vacancies are undetectable (not more than 10^{16} cm^{-3}). This result was naturally interpreted as V_{Ga} easily forming a complex with oxygen and failing to complex with silicon. However, Uedono *et al.*¹²⁸ reported that the concentration of V_{Ga} increases with Si doping, although one cannot rule out the possibility that the samples had been contaminated with oxygen.

In another report,¹³¹ positron annihilation, secondary-ion-mass spectroscopy (SIMS), and PL were employed to study the V_{Ga} -related defects in undoped and Si-doped (containing also oxygen) GaN, grown by MBE on GaN template prepared by HVPE. From the analysis of W and S parameters, extracted from the positron annihilation time experiments, Laukkanen *et al.*¹³¹ have concluded that the V_{Ga} -related defect in the MBE-grown samples is not the same as that observed in MOCVD layers. This new defect displayed properties similar to a vacancy cluster, and its concentration decreased with Si doping.¹³¹ Interestingly, the YL intensity increased with increasing concentration of Si in these samples, implying no connection between the vacancy clusters and the YL band. Annealing experiments indicated that the vacancy clusters are stable up to at least 1050 K, ruling out their identification as isolated V_{Ga} .¹³¹ Note that the vacancy clusters with open space larger than divacancies ($V_{\text{Ga}}V_{\text{N}}$) have also been detected by positron annihilation in undoped MOCVD-grown GaN.¹²⁸ Finally, a decrease of the V_{Ga} -related defects from more than 10^{19} to $2 \times 10^{16}\text{ cm}^{-3}$ has been observed in the HVPE-grown layers when the distance from the GaN/sapphire interface region increased.¹³³ The

depth profile of oxygen was similar to that of V_{Ga} , implying that V_{Ga} is likely to associate with oxygen in these samples. In the thickest freestanding 300- μm sample, the concentration of V_{Ga} decreased to $2 \times 10^{15}\text{ cm}^{-3}$, perfectly matching the total acceptor concentration^{196,197} and the concentration of the YL-related acceptors in these samples¹¹² (see also PL results in Sec. IV B).

In contrast with the above investigations where the YL correlated with concentrations of V_{Ga} , O_N , and Si_{Ga} , Armitage *et al.*¹⁶⁴ reported that the YL band is weaker in the undoped GaN sample with relatively higher concentration of oxygen and V_{Ga} , as compared to the C-doped sample. This result may indicate that the $V_{\text{Ga}}\text{O}_\text{N}$ complex (or the $V_{\text{Ga}}\text{Si}_{\text{Ga}}$ complex which is expected to behave nearly identically but is less probable to form) is not the only defect responsible for the broad emission near 2.2 eV in n -type GaN.

9. ODMR on the YL

Glaser *et al.*^{141,198} detected two increasing luminescence resonances for the YL band. A strong and sharp resonance with $g_{\parallel}=1.9515 \pm 0.0002$ and $g_{\perp}=1.9485 \pm 0.0002$ was attributed to the effective-mass donor, while a broader resonance with $g_{\parallel}=1.989 \pm 0.001$ and $g_{\perp}=1.992 \pm 0.001$ was attributed to a deep donor. The proposed model of the YL, as being due to optical transitions from the deep donor to a shallow acceptor (accompanied by a nonradiative spin-dependent transition from the shallow donor to a singly ionized double-donor state),^{141,198} failed to agree with numerous results supporting solely the shallow donor-deep acceptor model for the YL band.^{67,76,143–150} In particular, transitions from the deep donor to the shallow acceptor would have an extremely low probability in undoped GaN due to negligible overlap of the hole and electron wave functions at distant deep donors and acceptors.

Koschnick *et al.*¹⁴⁴ performed mapping of YL by ODMR over the sample area. The YL intensity was distributed uniformly, whereas the intensity ratio of the two dominant ODMR signals (with $g_{\parallel}=1.9515$ and 1.989) varied strongly. This experimental finding indicated that the two dominant ODMR signals cannot belong to transition between two defects which results in YL. The authors of Ref. 144 proposed that the resonances are due to two relatively shallow donors competing for recombination with the hole bound to a deep acceptor. As for the missing signal from the deep acceptor, it was speculated that it is barely seen as a weak broad signal underneath the donor signals.¹⁴⁴ Attribution of the signal with $g_{\parallel}=1.952$ to the shallow donor (O_N) has also been supported by ODMR studies under high hydrostatic pressure.¹⁷⁶

10. Effect of doping on the YL

There have been many attempts aimed at revealing the origin of the YL band by intentional doping. Pankove and Hutchby¹²³ implanted 35 elements in GaN and 23 of them led to a strong YL band peaking at 2.15 ± 0.03 eV. Implantation with carbon resulted in the strongest YL band, although the intensity of the YL band in the Li-, Be-, Al-, and Si-doped GaN was also very high.¹²³ Skromme and co-workers^{199–202} also observed a substantial increase of the

YL band in GaN implanted with C or Be, but not with Ar, Al, P, O, N, P, As, Ne, or Mg. Note that Dewsnip *et al.*²⁰³ also reported an enhancement of the YL in Be-doped GaN.

Ogino and Aoki⁹⁸ have established that C doping enhances YL greatly, whereas Si and O doping did not affect the YL intensity in their experiment. Several other experimental groups observed enhancement of the YL band in C-doped GaN and attributed the YL band to C impurity or a complex involving carbon.^{135–140,164,204–206} Although the peak position and shape of the YL band in the C-doped samples were similar to those in undoped GaN, different temperature dependencies for these parameters were observed in undoped and C-doped GaN.¹³⁷ It appears that C introduces a defect contributing to the YL band in C-doped GaN, whereas the V_{Ga} -containing complex, such as $V_{\text{Ga}}\text{O}_{\text{N}}$, is responsible for the YL band in undoped GaN, although the position and shape of the YL from two different defects may be quite similar.¹⁶⁴ It is also plausible that the C-related defect also contains V_{Ga} . For instance, if the $V_{\text{Ga}}\text{C}_{\text{Ga}}$ is formed in GaN, it would have nearly the same properties as $V_{\text{Ga}}\text{O}_{\text{N}}$ since both O_{N} and C_{Ga} are shallow donors. However, the first-principles theory predicts a low probability of formation for C_{Ga} in *n*-type GaN (Sec. II).

The effect of Si doping on the absolute and relative intensities of the YL band has also been studied extensively. In concert with results of Pankove and Hutchby,¹²³ Dai *et al.*²⁰⁷ reported a significant enhancement of YL in GaN after implantation with Si and postannealing. In several other investigations, Si doping caused an increase in the YL intensity.^{71,131,172,208} Important to note, however, is that the ratio of the YL intensity to the near-band-edge emission intensity increased in some experiments,^{208,209} but decreased in others,^{131,207,210} or remained nearly unchanged.⁷¹ At very high levels of *n*-type doping ($n_0 > 10^{19} \text{ cm}^{-3}$), the YL intensity decreased in Si-doped^{209,211} and Ge-doped GaN.²¹² The suppression of the YL band has been attributed to the substitution of V_{Ga} by donors in Ga sites.²¹²

Doping with another shallow donor, Se_{N} , also resulted in an enhancement of the YL band.^{213,214} Chen *et al.*²¹³ reported that Se doping decreased the Ga/N ratio substantially and moreover, they attributed the YL band to the N_{Ga} antisite. It is obvious, however, that the concentration of V_{Ga} also increases with decreasing Ga/N ratio. Therefore, creation of the V_{Ga} -related acceptors is also able to explain the observed enhancement of the YL band in Se-doped GaN.

What can be gleaned from the above discussion is that there is still no model which fully describes the defect or defects that are responsible for the YL band in undoped or *n*-type doped GaN. On the one hand, there are extensive data supporting the assignment of the YL band emission to a native defect, which also can be introduced by implantation damage or irradiation. In this case, the $V_{\text{Ga}}\text{O}_{\text{N}}$ complex is the main candidate, as well as V_{Ga} and $V_{\text{Ga}}\text{O}_{\text{N}}$ trapped at dislocations or other structural defects. On the other hand, carbon is a strong candidate for the YL-related defect in C-doped GaN. Although experimentally difficult, an investigation of the YL band GaN with controllably different concentrations of C and V_{Ga} is desperately needed to delineate the root cause for the YL emission in GaN.

What is firmly established is that the YL band in all *n*-type GaN samples is related to transitions from the conduction band or from a shallow donor to a deep acceptor. The ionization energy of this acceptor is about 0.8–0.9 eV. Its capture cross section for holes is much larger than that for electrons. Thus, it might be a multiply charged acceptor. From this point of view, the V_{Ga} -shallow donor complex is a very strong candidate. The shape of the YL band and its position in this case should be determined by V_{Ga} due to its strong electron-phonon coupling. The situation is very similar to the V_{Ga} -shallow donor complexes in GaAs, where the shallow donors mostly change the charge state of V_{Ga} but barely affect the energy level and vibrational characteristics of the defect.²¹⁵ Similarly, the properties of V_{Ga} may not be strongly affected by the strain field of a dislocation that may trap the V_{Ga} -containing complex. It is important to understand that in $V_{\text{Ga}}D$ complex the transitions take place not from D to V_{Ga} as often interpreted, but from a distant donor or from the conduction band to the $V_{\text{Ga}}D$ complex because in such a complex the hole wave function would cover both defects.

B. Yellow and green luminescence in high-purity GaN

Thick GaN layers grown by HVPE demonstrate substantially improved quality,¹² as determined by structural, electrical, and optical characterizations, and paved the way for investigating defects with more confidence. Liliental-Weber *et al.*²¹⁶ showed that the dislocation density drastically decreases with increasing thickness of GaN. The concentration of point defects, including impurities and Ga vacancies, also gradually decreases with distance from the GaN/sapphire interface.^{133,217,218} Among thick GaN layers grown by different groups, 200–300- μm -thick laser-separated freestanding GaN templates grown by HVPE at Samsung Advanced Institute of Technology (SAIT) in Korea have the superior quality to date, combining the highest bulk mobility of electrons,^{196,197,219} the lowest concentration of uncontrolled donors ($0.6\text{--}1.8 \times 10^{16} \text{ cm}^{-3}$) and acceptors ($1.7\text{--}2.4 \times 10^{15} \text{ cm}^{-3}$),^{196,197,219} very low density of dislocations near the Ga face (less than 10^6 cm^{-2}),^{220,221} and exceptional optical properties.^{222,223} We studied PL from a few GaN templates prepared at SAIT and observed that PL results were very reproducible in different samples. Some of these templates were also studied by positron annihilation,¹³³ Hall effect,^{196,197,219} and SIMS (Ref. 223) methods. The comprehensive study of very similar GaN templates allows us to use the results from various investigations in order to reliably quantify the PL results.

The low-temperature PL spectrum from the freestanding GaN templates produced by SAIT contains multiple exciton peaks above 3.3 eV,^{222–224} the UVL band with the main peak at 3.26 eV, and a broad yellow-green band (Fig. 22). Very weak BL (at about 2.9 eV) and RL (at about 1.8 eV) are masked by neighboring bands in these samples but can be detected under special conditions (in TRPL, under resonant excitation of PL, or at intermediate temperatures). At room temperature, most of the bands thermally quench. Only the near-band-edge emission peaking at about 3.41 eV and the

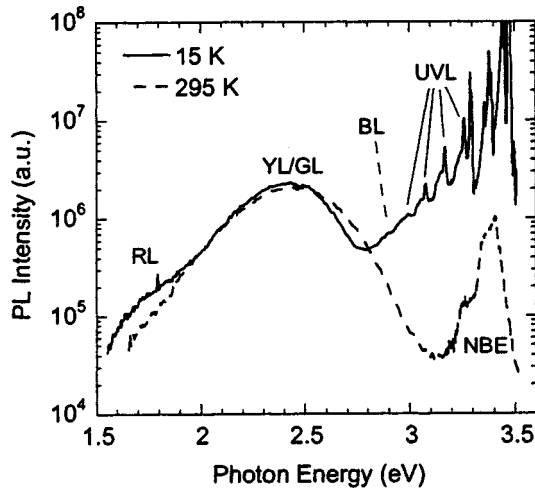


FIG. 22. PL spectra from a freestanding GaN template at 15 and 295 K. Exciton part at 15 K is cut in order to present better the defect-related bands. See Ref. 222 for details of the exciton part.

broad yellow-green band can be observed at room temperature (Fig. 22). The shape and position of the broad band depend on the excitation intensity and excitation energy, while it can always be deconvolved in two bands, namely, the YL band peaking at about 2.22 eV and the GL band with a maximum at about 2.48 eV.^{111,112} Below, the detailed results of study of the YL and GL bands in a high-purity GaN freestanding template grown by HVPE are presented. All the results can be explained using a model whereby the YL and GL are related to two charge states of the same defect, presumably the $V_{\text{Ga}}\text{O}_{\text{N}}$ complex.

1. Effect of excitation intensity

Figure 23 shows the room-temperature PL spectrum of a GaN template at different excitation densities. The broad band maximum shifts from about 2.22 to 2.47 eV to increas-

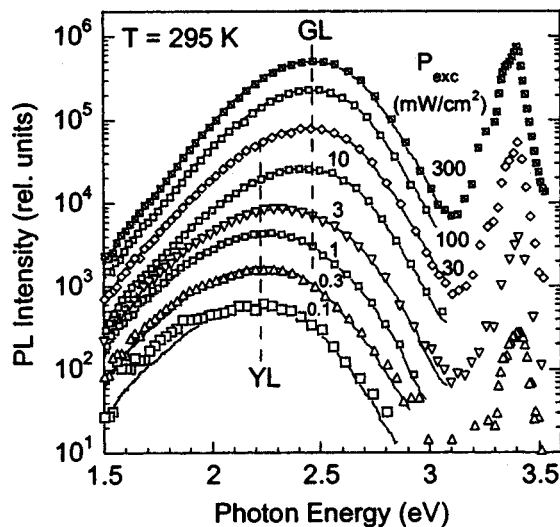


FIG. 23. Room-temperature PL spectrum of a freestanding GaN template (Ga face) at different excitation densities. Points are experimental data (only every tenth point is shown for clarity); solid curves - fit using modeled YL and GL bands with their relative contribution given in Fig. 24. Reprinted with permission from Reshchikov *et al.*, Appl. Phys. Lett. 81, 4970 (2002). Copyright (2002) by the American Institute of Physics.

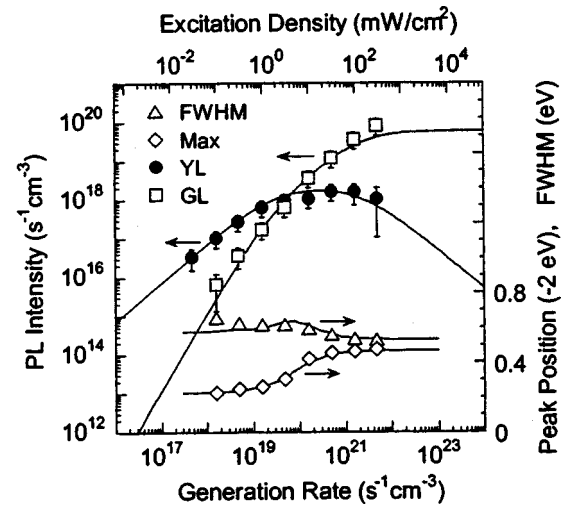


FIG. 24. Dependence of the integrated intensity of the YL and GL bands on excitation intensity. The points are experimental data obtained from deconvolution of the spectra shown in Fig. 23 onto two bands (YL and GL). The solid lines represent a fit with the following parameters: $C_{n1} = 10^{-13} \text{ cm}^3 \text{ s}^{-1}$, $C_{n2} = 2.5 \times 10^{-12} \text{ cm}^3 \text{ s}^{-1}$, $C_{p1} = 3.3 \times 10^{-7} \text{ cm}^3 \text{ s}^{-1}$, $C_{p2} = 1.5 \times 10^{-7} \text{ cm}^3 \text{ s}^{-1}$, $B = 5 \times 10^{-7} \text{ cm}^3 \text{ s}^{-1}$, $N_A = 1.5 \times 10^{15} \text{ cm}^{-3}$, $n_0 = 1.3 \times 10^{16} \text{ cm}^{-3}$. Also shown are the FWHM and position of maximum (after deduction of 2 eV for appearance) of the experimentally observed broad band (points) and the same values simulated by using the modeled shapes of the YL and GL bands and their relative contributions. Reprinted with permission from Reshchikov *et al.*, Appl. Phys. Lett. 81, 4970 (2002). Copyright (2002) by the American Institute of Physics.

ing excitation level. In contrast to the monotonic shift of the PL band with excitation intensity, which is typical for deep DAP transitions,⁸² a rapid shift of the band maximum between 1 and 10 mW/cm^2 has been observed (Fig. 23). Self-consistent deconvolution of the broad band at different excitation intensities revealed¹¹² that it is composed of two bands: (i) a nearly Gaussian-shaped YL band with a maximum at 2.22 eV and FWHM of about 0.58 eV and (ii) slightly asymmetric GL band with a maximum at 2.48 eV and FWHM of about 0.53 eV. With increasing P_{exc} , the YL intensity increases linearly and saturates above $P_{\text{exc}} = 1 \text{ mW}/\text{cm}^2$, whereas the GL intensity is approximately quadratic in P_{exc} at low-excitation densities and linear in P_{exc} above $\sim 10 \text{ mW}/\text{cm}^2$ (Fig. 24). A consideration of the balance equations, similar to those presented in Sec. III A 1, shows that the above behavior of the defect-related PL is a hallmark of two charge states of the same defect.¹¹²

As one would expect from the viewpoint of probability, the concentrations of the acceptors binding one and two holes are, respectively, linear and quadratic functions of P_{exc} at low excitation intensities. Figures 23 and 24 demonstrate the fit of rate equations, developed for the case of two charge states of an acceptor, to the experimental data.¹¹² The concentration of the acceptor was estimated as $N_A = 1.5 \times 10^{15} \text{ cm}^{-3}$ from this fit. This value is in excellent agreement with the acceptor concentration in the studied freestanding templates determined from the Hall-effect data ($2.4 \times 10^{15} \text{ cm}^{-3}$) (Ref. 196) and with the concentration of the V_{Ga} -containing defects found for similar samples from the positron lifetime experiments ($2 \times 10^{15} \text{ cm}^{-3}$).¹³³ Other parameters, found from the fitting, are given in the caption of Fig. 24. The assignment of the YL and GL bands to the

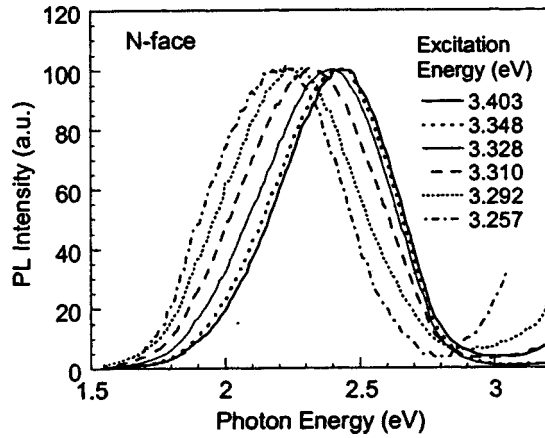


FIG. 25. PL spectrum in the defect range taken for below-band excitation at different photon energies. The excitation density is about 0.2 W/cm^2 . Reprinted with permission from Reshchikov *et al.*, Appl. Phys. Lett. **78**, 3041 (2001). Copyright (2001) by the American Institute of Physics.

2-/- and -/0 states of the $V_{\text{Ga}}\text{O}_{\text{N}}$ complex is consistent with the obtained values of their capture cross sections for electrons and holes. Indeed, electrons are much more likely captured by $(V_{\text{Ga}}\text{O}_{\text{N}})^0$ than by $(V_{\text{Ga}}\text{O}_{\text{N}})^-$, whereas the difference between $(V_{\text{Ga}}\text{O}_{\text{N}})^{2-}$ and $(V_{\text{Ga}}\text{O}_{\text{N}})^-$ for the capture of holes is not so important. Further, the predicted energy separation between the 2-/- and -/0 states of the $V_{\text{Ga}}\text{O}_{\text{N}}$ (0.45 eV) (Ref. 22) is reasonably close to the difference in positions of the GL and YL bands (about 0.26 eV).

We observed similar transformation of the YL into GL band in several freestanding GaN templates, both at room and cryogenic temperatures, as well as in relatively thin high-quality GaN layers grown by HVPE on sapphire. However, the GL band has never been observed in thin undoped GaN layers grown by MBE or MOCVD. The observation of the GL band only in certain samples can be explained by higher purity of these samples. Indeed, saturation of the acceptor-related PL is promoted by low concentration of the acceptor, long lifetime of the acceptor-related PL (which is inversely related to the shallow donor concentration), and high efficiency of radiative recombination (requiring low density of dislocations, perfect surface preparation, and large diffusion length).⁶⁷ All these parameters in the freestanding GaN templates grown by SAIT satisfy the conditions set forth above for observing the GL band.¹² The lack of the GL band in thin GaN films with inferior quality could also be explained if the $V_{\text{Ga}}\text{O}_{\text{N}}$ complexes were preferably bound to dislocations⁶⁸ that may affect the charge state and other characteristics of the defect. We should emphasize that in various GaN samples different defects may contribute to emission in the visible range.

2. Resonant excitation

Figure 25 shows the room-temperature PL spectrum from a freestanding GaN template taken at different excitation energies. With increasing excitation energy, the spectrum gradually shifts from about 2.2 eV (yellow emission) to 2.43 eV (green emission) on both N and Ga faces. Figure 26 depicts the variation of the position of the band maximum and its FWHM as a function of the photon excitation energy

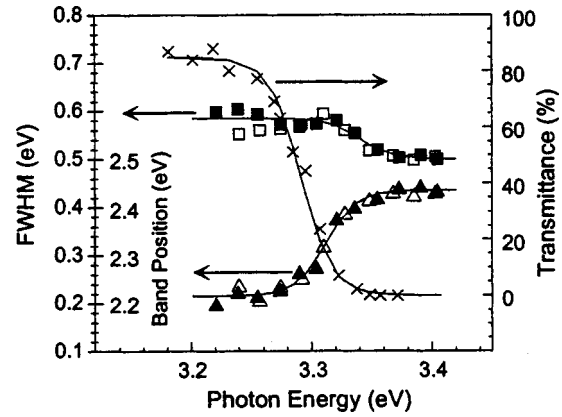


FIG. 26. Position of the broad band maximum, FWHM, and sample transparency for the freestanding GaN template as a function of the incident light energy at room temperature. The excitation density is about 0.2 W/cm^2 . The full squares and triangles are for the Ga face. The open squares and triangles are for the N face. The solid lines are guides to the eye. Reprinted with permission from Reshchikov *et al.*, Appl. Phys. Lett. **78**, 3041 (2001). Copyright (2001) by the American Institute of Physics.

along with the transmittance of the sample. The variation of the shape and position of the band strongly correlates with the transmittance curve. For $\hbar\omega_{\text{exc}} < 3.26 \text{ eV}$, where the absorption coefficient is of the order of or less than 10 cm^{-1} , the position of the band maximum saturates at about 2.2 eV, and the band FWHM is about 590 meV. For $\hbar\omega_{\text{exc}} > 3.35 \text{ eV}$, where the absorption coefficient exceeds $\sim 10^3 \text{ cm}^{-1}$, the position of the band maximum saturates at about 2.43 eV, and the band FWHM is about 500 meV. For $\hbar\omega_{\text{exc}} < 3.26 \text{ eV}$, only a small fraction of the excitation light is absorbed in the sample, while for $\hbar\omega_{\text{exc}} > 3.35 \text{ eV}$ the excitation light is absorbed in a thin (of the order of or less than $10 \mu\text{m}$) surface layer.

The above observations were originally explained¹¹¹ by assuming that two different defects are responsible for the YL and GL bands. The YL-related defect was assumed to have a relatively high concentration in the first $1 \mu\text{m}$ from the surface, whereas the GL-related defect was assumed to be distributed uniformly throughout the bulk GaN. However, the model of two charge states of the same defect, presented above, can easily explain the results of resonant excitation. Indeed, the YL band dominates at resonant excitation below 3.3 eV because the absorption coefficient is very small at these photon energies¹¹¹ and the acceptors cannot be saturated. The GL appears at higher photon energies and dominates above 3.3 eV when the excitation power is high enough because the absorption of GaN increases markedly in this range¹¹¹ and the defects can be saturated. Presented below are the results of a PLE study in a wide temperature range that are also consistent with the above model of the YL and GL bands.

Figure 27 shows the PLE spectra of the YL band in the GaN freestanding template at different temperatures. As in the case of the YL band in the MBE-grown GaN layer (Fig. 20), the PLE spectrum consists of two characteristic regions: a slow increase of the PL intensity with variation of $\hbar\omega_{\text{exc}}$ from 2.7 to $\sim 3.3 \text{ eV}$ which is attributed to the resonant excitation, and a fast increase at higher photon energies which

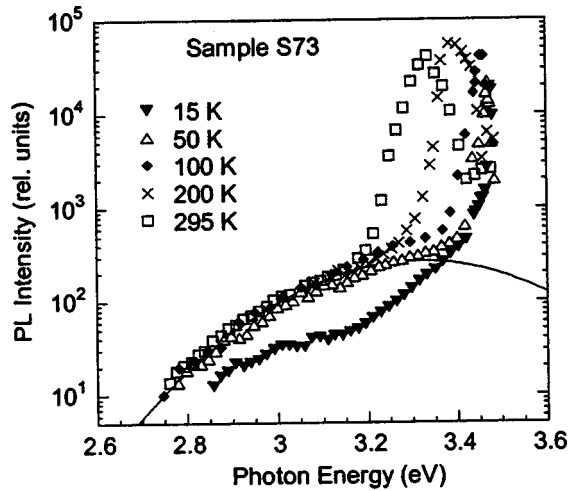


FIG. 27. PLE spectra for the YL in the freestanding GaN template at different temperatures. The solid curve is a Gaussian fit with maximum at 3.32 eV and FWHM of 0.52 eV. Reprinted with permission from Reshchikov *et al.*, Mater Res. Soc. Symp. Proc. **693**, 16.19 (2002).

is attributed to the interband transitions.¹⁰⁰ The resonant part of the PLE spectrum was fitted with a Gaussian curve with the same parameters as for the YL band in the MBE-grown sample. In the PL spectrum of the freestanding GaN at resonant excitation we also resolved the RL band (Fig. 28), appearing as a weak shoulder to the YL band in Figs. 22 and 23. We did not observe the GL band at resonant excitation. It appeared only at high excitation intensities and at photon energies corresponding to strong absorption. This observation agrees with the assignment of the GL band to another charge state of the YL-related defect that is difficult to saturate with holes by resonant excitation.

While the YL band intensity under resonant excitation in the MBE-grown sample was completely independent of temperature (Fig. 20), it sharply changes in the temperature range of 30–50 K in the freestanding template, being temperature independent at higher and lower temperatures (Fig. 27).¹⁰⁰ An activation energy of 15 meV, determined from a

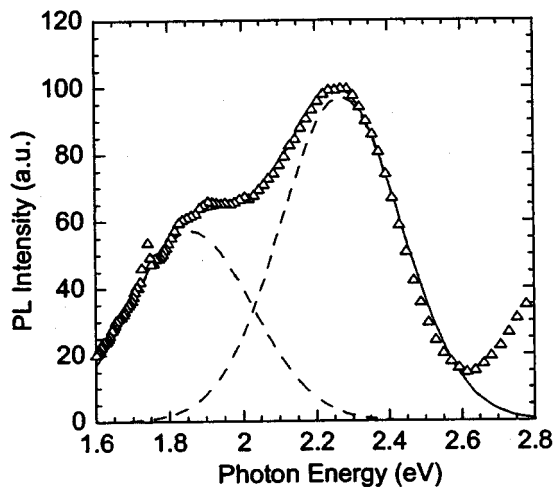


FIG. 28. PL spectrum from the freestanding GaN template excited with below-band-gap energy (3.44 eV) at 50 K. Points—experiment. Dashed lines—Gaussians peaking at 1.86 and 2.27 eV and having FWHM of 390 meV. The solid curve is the sum of two Gaussians.

fit, was tentatively attributed to a barrier in the adiabatic potential of the defect.¹⁰⁰ We can suggest the following interpretation of the decrease of YL intensity of about 5 times with decreasing temperature. Similar to predictions for V_{Ga} in GaAs,²²⁵ Ga vacancy in GaN may have a metastable state along one of the adjacent N atoms. If the barrier in the ground state is small enough, reorientation between the four equivalent configurations would be allowed above some critical temperature (for instance, above 50 K), whereas in the excited state (a hole bound to the acceptor) the barrier might be too high, so that reorientation of the distortion is not observed even at very high temperatures. We assume that, as in GaAs,⁵⁰ the effect of O_{N} donor on the V_{Ga} distortion is weak, especially in the ground state of the defect. Assuming that the minima of three equivalent configurations lie 15 meV below the minimum of the fourth configuration in the ground state, and that excitation of only the defect distorted along c axis leads to the radiative recombination while the rest of the three configurations are nonradiative, we can qualitatively explain why the intensity drastically changes at 30–50 K. In this picture, the defect in potentially radiative state may reorient into nonradiative state and get trapped in it for long at low temperature.

3. Time-resolved PL

A pulse nitrogen laser was used in the TRPL experiments to excite the freestanding GaN template.^{110,113} While the GL band was detected for short delay times (up to 10 μs), for longer delay times the GL completely disappeared and the YL emerged due to a much slower decay. The low-temperature TRPL spectra at different delay times are shown in Fig. 29 in comparison with the SSPL spectra excited with nitrogen and He–Cd lasers. For short times following pulsed excitation, the GL band with a maximum at about 2.45 eV dominates the PL spectrum at 15 K. The shape and position of the GL band remain nearly unchanged up to about 10 μs .^{110,113} However, at longer delay times the GL band disappears, giving way to the YL band peaking at 2.2 eV. Also, the RL band observed at about 1.8 eV and the BL band observed at about 2.9 eV could be seen as shoulders of the YL band and the UVL band at long delay times (Fig. 29).

A striking feature of the PL behavior is a clearly visible persistence of light emission after the excitation is completely turned off. The PL intensity decay of the green-yellow band at 2.2 eV, in comparison with that of the BL and UVL bands at 15 K, is shown in Fig. 30. The decays are nonexponential as would be expected for the DAP transitions in low-temperature PL of GaN. The time dependence of the emission at 2.2 eV exhibits a steep drop between 10^{-5} and 10^{-4} s followed by a nonexponential decay, which is slower than t^{-1} . Remarkably, in the same time interval the GL transforms into YL, as shown in Fig. 29. It is clear that the PL decays below and above 10^{-4} s at 2.2 eV are associated with two different emissions, namely, GL and YL bands, respectively. A fast quenching of the GL band and a very slow decay of the YL band are consistent with the assignment of these bands to two charge states of the same defect, presum-

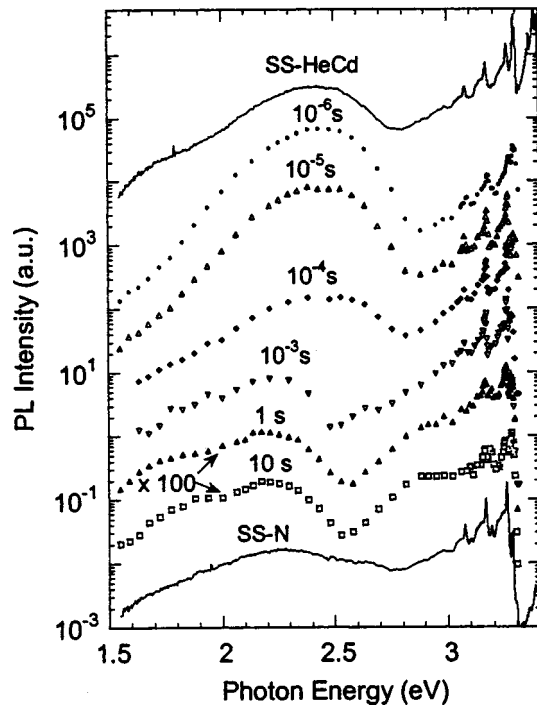


FIG. 29. Steady-state PL spectra (solid curves) obtained from a freestanding GaN under excitation with pulsed nitrogen (SS-N) and cw He-Cd (SS-HeCd) lasers, and time-resolved PL spectra at different time delays (points). $T=15$ K. Reprinted with permission from Reshchikov *et al.*, Appl. Phys. Lett. 83, 266 (2003). Copyright (2003) by the American Institute of Physics.

ably $(V_{\text{Ga}}\text{O}_\text{N})^{0/-}$ and $(V_{\text{Ga}}\text{O}_\text{N})^{-2/-}$, respectively.¹¹² The RL and BL bands also exhibit a persistent behavior, as can be seen in Fig. 29.

Several mechanisms may lead to persistent PL. The most common ones are DAP transitions,⁷⁹ potential fluctuations,²²⁶ and trapping and detrapping by shallow traps.²²⁷ We may completely neglect potential fluctuations in the studied

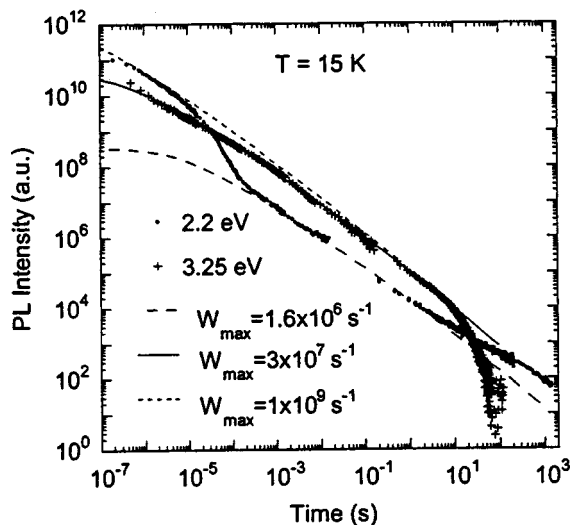


FIG. 30. PL intensity decay of the UVL (3.25 eV), BL (2.9 eV), and GL–YL (at 2.2 eV) in freestanding GaN grown by HVPE. The curves are calculated using Eq. (17) with the following parameters: $N_D=1.8 \times 10^{16} \text{ cm}^{-3}$, $a_D=2.4 \text{ nm}$, and $W_{\text{max}}=10^6$, 3×10^7 , and 10^9 s^{-1} , as shown in the figure. Reprinted with permission from Reshchikov *et al.*, Physica B 340–342, 444 (2003). Copyright (2003) by Elsevier.

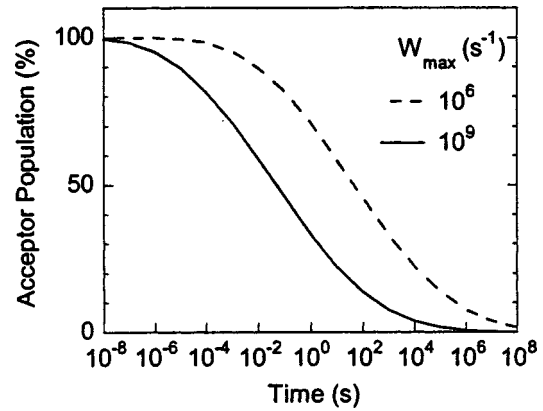


FIG. 31. Population of an acceptor with holes after excitation pulse in the DAP model (Ref. 79) with the same parameters as in Fig. 30. Note that W_{max} covers the range estimated for different acceptors in GaN. Reprinted with permission from Reshchikov *et al.*, Physica B 340–342, 444 (2003). Copyright (2003) by Elsevier.

samples because the concentration of defects and compensation ratio are very small. Furthermore, there is no experimental evidence for shallow traps in GaN. However, the DAP mechanism looks very attractive because in the studied high-purity samples the distances between donors and acceptors are large enough to provide long-lived PL in conditions of very low concentration of free carriers at low temperatures.

The decay curves were fitted by the Thomas–Hopfield expression for the case of low compensation [Eq. (17)] with $N_D=1.8 \times 10^{16} \text{ cm}^{-3}$, $a_D=25 \text{ \AA}$, and W_{max} being the only fitting parameter.¹¹³ The calculated curves with three values of W_{max} are shown in Fig. 30 as typical examples rather than the best fit. The fitting parameters are reasonable and close to the parameters found earlier for DAP transitions involving different acceptors in GaN.⁸⁷ As may be seen, the curve shape is not very sensitive to W_{max} , especially for the values of W_{max} above 10^7 s^{-1} . Nevertheless, we may conclude qualitatively that W_{max} for the GL is apparently very large, of the order of 10^8 – 10^{10} s^{-1} .^{110,113} Deviation of the UVL and YL emission decays from the classical DAP-type decay for times above 10 s (Fig. 30) can be explained by a redistribution of electrons thermally emitted to the conduction band.¹¹³ For the case of long delay times, an electron may thermally escape from a particular shallow donor and be captured by another shallow donor. If the electron is captured by a donor located closer to a neutral acceptor, the recombination will occur faster. Otherwise it will be emitted again to the conduction band and captured by another ionized donor. This is a reasonable explanation for the shallow DAP transition involving a simple acceptor. In contrast, the acceptor responsible for the YL band is negative when it binds a hole,¹¹² and its Coulomb potential would repel free electrons emitted from the donors. Therefore, we may expect slowing down of the YL recombination when the emission of electrons from the shallow donors becomes efficient (for times above 10 s).

It is interesting to note that for the studied freestanding GaN about half of the deep acceptors responsible for the YL band are filled with holes 1 min after ceasing the excitation light, and about 20% of the acceptors would hold the hole even after 1 h (Fig. 31).¹¹⁴

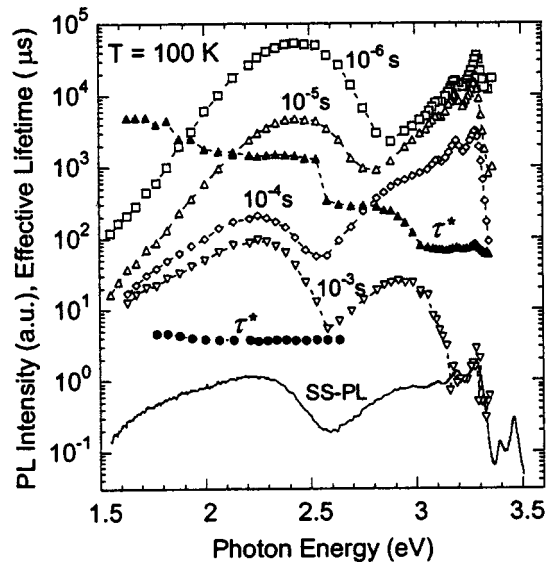


FIG. 32. Steady-state (SS) PL spectrum (solid line) and PL spectrum at time delays of 10^{-6} , 10^{-5} , 10^{-4} , and 10^{-3} s (open points) in freestanding GaN at 100 K. Effective lifetime is also shown (closed points). Reprinted with permission from Reshchikov *et al.*, Physica B **340–342**, 448 (2003). Copyright (2003) by Elsevier.

4. Effect of temperature

With increasing temperature, the DAP transitions give way to transitions from the conduction band to the same acceptors (e-A type) in undoped GaN.⁸⁷ As this takes place, the PL spectrum remains almost unchanged due to the small binding energy of the shallow donor, but the PL decay approaches the exponential law.⁸⁷ Figure 32 shows the PL spectrum at different delay times after the pulse excitation at 100 K. The UVL band decays exponentially with a characteristic time of about 10^{-4} s, revealing the BL band at about 2.9 eV which decays at a slower rate. Similar to the low-temperature case (Fig. 29), the shape and position of the GL band remain nearly unchanged up to about 10^{-5} s, but at longer delay times the GL band disappears, giving way to the YL band. At 100 K, the PL decay at 2.43 eV clearly contains two exponential components.¹¹³ The one with the characteristic time of 3.5×10^{-6} s is attributed to the GL band, and the other with the characteristic time of 1.5×10^{-3} s is attributed to the YL band (Fig. 32).

The effective lifetime, τ^* , defined in Sec. III B, is plotted as a function of photon energy in Fig. 32. Two branches of τ^* between 1.8 and 2.7 eV are related to overlapped GL and YL bands that have very different lifetimes.¹¹³ To a first approximation, the lifetimes are independent of the photon energy for all defect-related PL bands in the freestanding GaN template, including the RL band below 2.0 eV observed as a shoulder to the YL band and having the slowest decay. Figure 33 shows the PL lifetimes for the UVL, BL, GL, and YL bands at different temperatures. For transitions of electrons from the conduction band to the acceptors, the PL lifetime is inversely proportional to the free-electron concentration n (Sec. III B). The variation of the PL lifetime for the UVL, BL, and YL bands is consistent with Eq. (20) up to temperatures where the holes escape to the valence band from the acceptors, resulting in quenching of not only the SSPL inten-

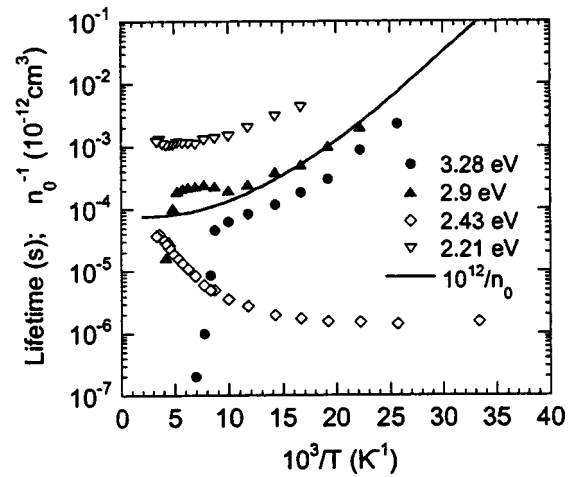


FIG. 33. PL lifetime (points) as a function of inverse temperature for the main PL bands in freestanding GaN: UVL band (at 3.28 eV), BL band (2.9 eV), GL band (2.43 eV), and YL band (2.21 eV). Variation of the inverse free-electron concentration (solid line) is also shown for comparison. Reprinted with permission from Reshchikov *et al.*, Physica B **340–342**, 448 (2003). Copyright (2003) by Elsevier.

sity but also the effective PL lifetime.⁸⁷ The obtained capture coefficients for the UVL, BL, and YL bands of about 2×10^{-12} , 4×10^{-13} , and 7×10^{-14} cm^3/s , respectively, are nearly temperature independent and agree with the values obtained for thin GaN films on sapphire (3.7×10^{-12} , 3.9×10^{-13} , and 6.2×10^{-14} cm^3/s , respectively).⁸⁷

In contrast to the UVL, BL, and YL bands, the PL lifetime for the GL band is temperature independent from 30 to 70 K and increases by 20 times at room temperature (Fig. 33). This type of the PL lifetime variation is completely different from the behavior described by Eq. (20) for the e-A transitions, although the decay of the GL band is exponential in the temperature range of 30–300 K. We attribute this unusual behavior to an internal transition associated with the defect.²²⁸

We propose that the acceptor responsible for the GL band has an excited state close to the conduction band. Depending on the temperature and concentration of free electrons in the conduction band, the plausible mechanisms of the GL-related recombination are (Fig. 34) (i) transitions from distant shallow donors (DAP-type), (ii) internal transitions from an excited state, and (iii) transitions from the conduction band directly to the ground state of the acceptor. At very low temperatures, there are almost no free electrons in the conduction band, and thus photogenerated electrons may primarily be captured by shallow donors. The contribution of the internal and e-A type transitions would be very small, and therefore the GL would be predominantly due to the DAP recombination. At elevated temperatures (30–70 K), the concentration of the free electrons increases from 10^{13} to almost 10^{16} cm^{-3} due to the thermal escape of electrons from the shallow donors to the conduction band. Consequently, the DAP channel is basically blocked, paving the way for internal transitions, as free electrons can easily saturate the excited state of the acceptor binding two holes. At even higher temperatures (70–300 K), electrons are able to escape from the excited state to the conduction band. Thus the increase of

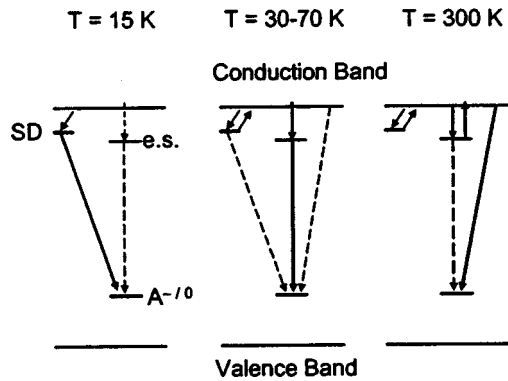


FIG. 34. Schematic of transitions responsible for the GL band in high-purity GaN. e.s. is the excited state of the acceptor, therefore the transition $e.s. \rightarrow A^0$ is of intracenter type. SD stands for the shallow donors, and the transitions involved are distant DAP transitions. The dashed lines correspond to less probable transitions, whereas the solid lines show the dominant transitions.

the PL lifetime for the GL band observed in this temperature range (Fig. 33) can be explained by the escape of electrons from the excited state located about 30–40 meV below the conduction band. Further, this escape at room temperature is so intense that the transitions from the conduction band directly to the ground state may dominate. Very large values of the electron-capture cross sections for transitions from the shallow donors and from the conduction band to the acceptor level responsible for the GL band in freestanding GaN have been reported.^{110,228} These values are consistent with the assignment of the GL band to the $V_{Ga}O_N$ complex in its 0/-state.¹¹² Note, however, that the existence of an excited state close to the conduction band is surprising for a neutral center which is the $(V_{Ga}O_N)^0$ complex when it binds two holes.

C. Ultraviolet (shallow DAP) band

The shallow DAP recombination in undoped GaN was studied in detail by Dingle and Ilegems.²²⁹ Those authors have observed PL peaks at 3.2571, 3.1672, and 3.0768 eV having the identical radiative lifetimes and assigned them to the zero-phonon line (ZPL) and LO phonon replicas, respectively, of transition from a shallow donor to a shallow acceptor. While the main candidates for the shallow donors are Si_{Ga} and O_N (with activation energies of 30 and 33 meV, respectively²³⁰), assignments of the shallow acceptor in undoped GaN are controversial, as discussed in Sec. IV C 3. The DAP hypothesis for this PL band has been fully confirmed by temperature-dependent PL studies and time-resolved PL.²²⁹ Dingle and Ilegems²²⁹ observed characteristic nonexponential decay of the PL intensity after pulse excitation, as well as narrowing of the PL band and shift to lower photon energies after ceasing light. These are the distinguishing features of the distant DAP recombination.⁷⁹

The DAP transitions involving shallow donors usually give way to the e-A transitions at elevated temperatures as free electrons thermally released from the shallow donor to the conduction band recombine with holes bound to the same acceptor. The shape of the e-A band is usually very similar to the one of the DAP band involving a shallow donor, because the shape of the defect-related PL band is largely determined

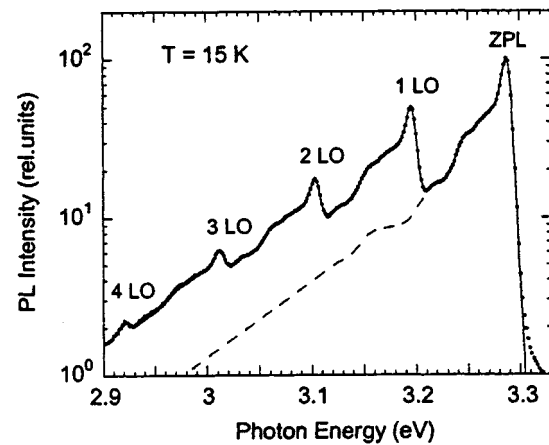


FIG. 35. UVL band in undoped GaN at 15 K. Points are from experiment. The dashed line is a modeled shape of the zero-phonon line (ZPL). The solid line is a fit accounting for LO phonon replicas having intensities of 0.4, 0.097, 0.022, and 0.004 with the shapes identical to the modeled shape of the ZPL. The ZPL and donor-bound-exciton peaks are located respectively at 3.286 and 3.475 eV in this undoped GaN layer grown by MBE on sapphire.

by the electron-phonon coupling for more localized carriers (hole bound to the acceptor), and the effect of the loosely bound electron on vibrational properties is negligible. Sometimes the DAP and e-A bands can be delineated.^{222,229,231} However, it is usually a challenging task to attribute the PL band to the DAP or e-A transition from the PL spectrum alone. For instance, the position of the PL peak may be affected by a strain in the epilayer grown on foreign substrates, concentration of the shallow donors and free electrons, and finally, by saturation of PL intensity from distant pairs in the particular excitation conditions employed. Only a comprehensive PL study encompassing different excitation intensities, temperatures, and time-resolved PL would allow delineation of the DAP and e-A emissions. The term “DAP band” universally adopted for the characteristic PL band with the main peak at about 3.27 eV in GaN is not good also because most of the PL bands in undoped GaN at low temperature arise from the DAP-type transitions due to the relatively large activation energy of shallow donors. For these reasons, we suggest the term “UVL band,” and where it is possible we require that the DAP- or e-A-type transitions are specified. Below, we review the experimental results associated with the UVL band in undoped GaN where the shallow acceptor is not clearly identified. When GaN is lightly doped with Mg, an enhancement of the UVL band is observed since Mg_{Ga} is the shallow acceptor. Although in some undoped GaN samples Mg_{Ga} may be present and responsible for the UVL band, in this section we will restrict our discussion to the nominally undoped GaN, while the UVL band in GaN doped with Mg is considered in detail in Sec. V B 1.

1. Steady-state PL

A typical shape of the UVL band in the case of the e-A transitions at low temperature in the MBE-grown GaN consists of a sharp peak at 3.286 eV followed by a number of LO phonon replicas, as shown in Fig. 35. Positions of the peaks are independent of the excitation intensity in the range

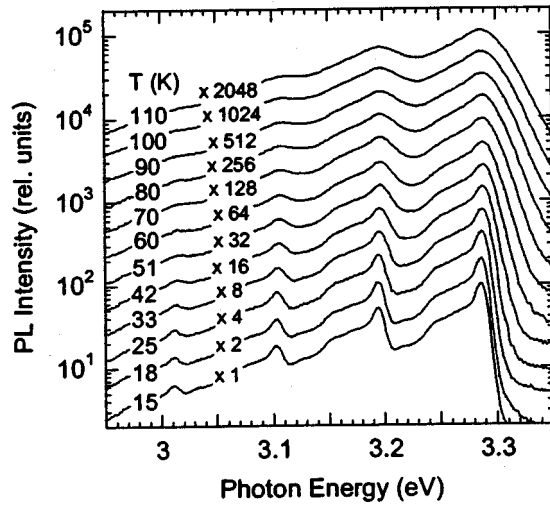


FIG. 36. Transformation of the UVL band (e-A related) in GaN with temperature.

of 10^{-2} – 100 W/cm² with the accuracy of 1 meV. Accounting for the residual strain in approximately 2- μ m-thick GaN layers grown by MBE in which all PL peaks are shifted by 4 meV to a higher energy compared to the positions in relaxed bulk GaN, we estimated the energy separation between the band gap in GaN and the ZPL in a set of more than 10 samples as 221 ± 3 meV at 15 K. This value can be considered as the low-temperature binding energy for the shallow acceptor involved in the UVL in undoped GaN.

A few LO phonon replicas at energy separations that are multiples of 91.7 ± 0.3 meV are clearly visible in Fig. 35. The intensities of the peaks are, in descending order, 1.0, 0.5, 0.17, 0.06, and 0.02 for the lines with $n=0, 1, 2, 3,$ and 4 , where n defines the number of LO phonons involved. We deconvolved the PL spectrum in Fig. 35 into a series of bands shifted by 91.7 meV with exactly the same shape but different intensities (the dashed curve in Fig. 35 shows a simulated single band). The relative intensities of the lines after deconvolution are 1.0, 0.4, 0.097, 0.022, and 0.004, which are close to the theoretical ratios between intensities of the phonon replicas if we use Eq. (24) with $S=0.4$, resulting in ratios of 1, 0.4, 0.08, 0.011, and 0.001. Note that each single band in this spectrum is broadened due to coupling with phonons other than LO phonons.

With increasing temperature from 15 to 110 K, the UVL band associated with the e-A transitions broadens (Fig. 36), although its integrated intensity remains nearly unchanged. At higher temperatures, the UVL band quenches and completely vanishes at room temperature. From the fit, with the aid of Eq. (6), to the experimental data for GaN layers grown by MBE on sapphire we obtained $E_A=170$ meV and $C_p=10^{-6}$ cm³/s. These values are nearly identical to those reported for the UVL band in undoped GaN grown by MOCVD.⁶⁷ The apparent discrepancy between the value of E_A obtained at 15 K from the position of the e-A peak (~ 220 meV) and the acceptor activation energy obtained from the quenching dependence (170 meV) at least in part can be attributed to the variation of the activation energy with temperature. This assumption is consistent with the fact

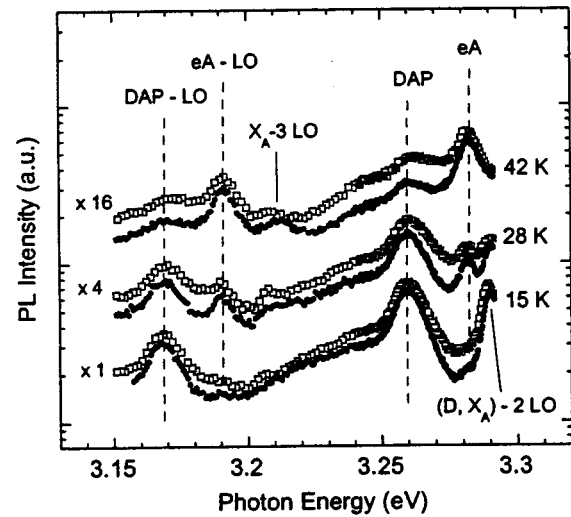


FIG. 37. PL spectrum of the UVL band at different eA temperatures in free-standing GaN (empty squares) and in the GaN overgrown on the free-standing GaN template by MBE (filled circles). Excitation density is 100 W/cm². Reprinted with permission from Reshchikov *et al.*, Appl. Phys. Lett. 79, 3779 (2001). Copyright (2001) by the American Institute of Physics.

that the position of the ZPL for the e-A emission was temperature independent (within an accuracy of ± 6 meV) in the range from 15 to 200 K while the band gap reduced by 25 meV in this temperature range. The larger value of E_A reported earlier for the UVL band in undoped GaN layers grown by MOCVD on sapphire substrate (198 meV) (Ref. 75) can be explained by neglecting the temperature dependence of the density of states in the valence band, N_V . Indeed, if we neglect the temperature dependence of the parameter Q_i in Eq. (6), the best fit would yield $E_A=195 \pm 5$ meV instead of 170 meV.

If the n -type GaN is nondegenerate, at sufficiently low temperatures the e-A emission gives way to the DAP emission involving the same acceptor because the free equilibrium electrons freeze-out, while the photogenerated electrons are captured much faster by shallow donors than by acceptors.⁶⁷ Conversely, an increase in temperature causes replacement of the DAP lines by slightly shifted e-A lines. A transformation of the DAP band into e-A band with increasing temperature in high-purity GaN is shown in Fig. 37. The e-A transitions begin to dominate at temperatures above 30 K when the concentration of the free electrons exceeds $\sim 10^{14}$ cm⁻³. Considering the separation between the DAP and e-A peaks in the low-excitation limit (at about 3.256 and 3.282 eV, respectively) and accounting for the average kinetic energy ($kT/2$) of free electrons (1.5 meV at 35 K) and the effective Coulomb interaction in DAP (about 7.5 meV for $N_D=2 \times 10^{16}$ cm⁻³), we estimated the ionization energy of the shallow donor as $E_D=32$ meV.²²² This value is very close to the binding energy of the O_N donor in GaN.²³⁰

Differentiating the DAP and e-A recombinations can be accomplished not only by recognizing their different energy positions and the distinct temperature dependence of their intensities in a PL experiment. In addition, such a delineation can be done by their different behavior with increasing excitation intensity or by analyzing the time-resolved PL data.

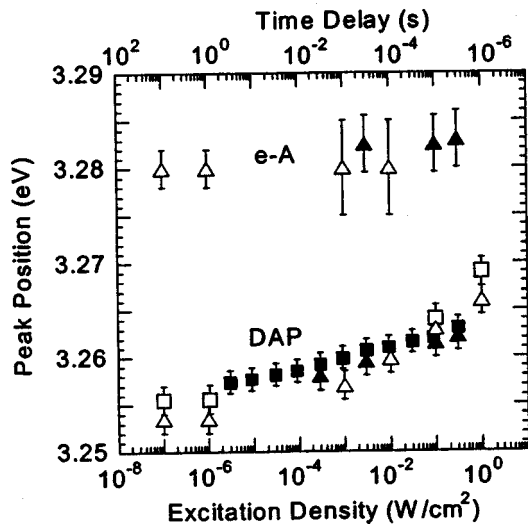


FIG. 38. Positions of the ZPL of the UVL band in undoped GaN as a function of excitation intensity in the steady-state PL (filled points, bottom scale) and time delay after excitation pulse (open points, top scale). Squares—30- μm -thick GaN layer on sapphire substrate, triangles—200- μm -thick freestanding GaN template, both grown by HVPE. The e-A line is detected at ~ 3.282 eV while the DAP line position varies from 3.253 to 3.269 eV depending on experimental conditions. Reprinted with permission from Reshchikov *et al.*, *Physica B* 340–342, 444 (2003). Copyright (2003) by Elsevier.

The above-mentioned differentiation is in part rooted in the statistical distribution of the DAP separations.^{79,86} For distant DAP the dependence of the emission energy $\hbar\omega$ on the pair separation R is given by⁷⁹

$$\hbar\omega = E_g - E_D - E_A + \frac{q^2}{\epsilon R}, \quad (29)$$

where E_g is the band gap, E_D and E_A are the donor and acceptor binding energies, respectively, ϵ is the low-frequency dielectric constant, and q is the electron charge. The last term represents the Coulomb interaction resulting from the interaction of ionized donors and acceptors. With increasing separation, the lifetime of radiative transitions becomes longer. Thus, close pairs would saturate at lower excitation intensities in experiments with variable excitation intensity and emit at shorter times in TRPL experiments. Consequently, the DAP band blue-shifts with increasing excitation intensity, and it narrows and shifts to the lower energy with time delay after excitation with a single pulse of light because the close pairs experience stronger Coulomb interaction and contribute at higher photon energies as compared to more distant pairs according to Eq. (29). Examples of the shifts of the UVL band with increasing excitation intensity and with time delay after pulse excitation are shown in Fig. 38. Similar shifts of the UVL band with excitation intensity have also been reported in Refs. 116 and 232. Additional information about the type of transition and parameters of the defects involved in the UVL band can be obtained from time-resolved PL, as discussed below.

2. Time-resolved PL

Transient behavior of the UVL band in undoped GaN has been studied extensively.^{87,113,114,142,188,228,229,233} In most

studies the observed decay of the UVL band at low temperatures has been nonexponential (usually in the microsecond range). The typical intensity decay curve for the UVL band is shown in Fig. 17 in comparison with the decays of other PL bands present in the same sample. The PL decay at 15 K has been fitted to Eq. (17) using the model of distant DAP transitions involving shallow donors and shallow acceptors. The value of W_{max} for the shallow acceptor, a parameter proportional to the capture cross section of the acceptor as discussed in Sec. III B, is of the order of 10^8 s^{-1} which is larger than for other radiative acceptors in undoped GaN.¹⁸⁸

The PL decay curve becomes nearly exponential with increasing temperature when the DAP transitions are replaced by the e-A transitions involving the same shallow acceptor.⁸⁷ The temperature dependencies of the emission lifetime for the UVL band, in comparison with the other bands in undoped n -type GaN grown by MOCVD and HVPE, are shown in Figs. 19 and 33, respectively. The effective lifetime of the UVL band has a weak temperature dependence between 50 and 110 K, but it sharply drops at $T > 110$ K due to the thermalization of holes from the shallow acceptor, in agreement with Eq. (22). The electron-capture coefficient C_n and the electron-capture cross section σ_n for the UVL band have been estimated as $(3.7 \pm 0.8) \times 10^{-12} \text{ cm}^3 \text{ s}^{-1}$ and $(2.8 \pm 0.6) \times 10^{-19} \text{ cm}^2$, respectively, with the aid of Eqs. (20) and (23).⁸⁷ The obtained relatively large values of C_n and σ_n for the shallow acceptor as compared to other radiative acceptors in undoped GaN can in part be due to a weaker localization of the bound hole. In majority of investigations, the decay of the UVL band in undoped GaN is reported to be relatively slow (in the microsecond range) and usually nonexponential at low temperatures. In contrast, Chetkine *et al.*¹⁴² reported a lifetime below 0.5 ns for the UVL band in undoped GaN grown by MOCVD. We should note that the shape of the UVL band in that particular investigation deviated substantially from the commonly observed one, necessitating the consideration that some exciton line or its LO phonon replica might be responsible for the very fast decay of the UVL line at about 3.26–3.29 eV in Ref. 142.

The UVL band transforms with delay time in a high-purity freestanding GaN template. The ZPL corresponding to the DAP transitions gradually shifts from 3.266 to 3.253 eV in a time interval from 10^{-6} to 10 s after pulsed excitation (Fig. 38). The shift is consistent with Eq. (29), according to which for short delay times the recombination in nearby pairs experiencing a stronger Coulomb interaction dominates. Besides the DAP peaks, the e-A emission is observed with the ZPL at about 3.282 eV followed by at least two LO phonon replicas.

Interestingly, both the DAP and e-A emission lines of the UVL band can be detected at delay times longer than 1 s after the excitation pulse, while beyond 10 s the UVL emission vanishes.^{113,114} These phenomena have been explained in Ref. 114 as follows: The DAP transitions easily persist up to 1–10-s delays because a substantial part of the acceptors holds photogenerated holes for a very long time (Fig. 31) due to large DAP separations in this sample. The relative contribution of the e-A transitions increases significantly in the

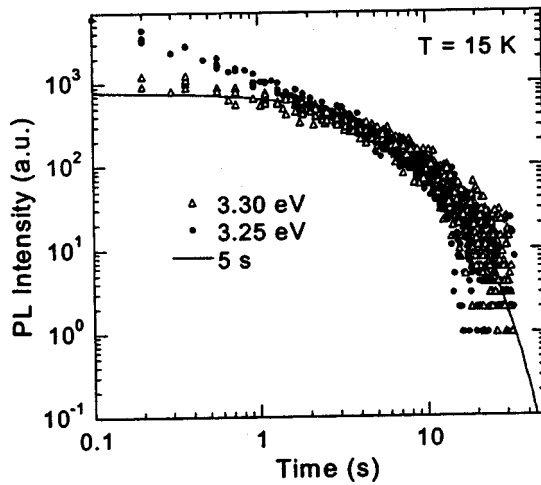


FIG. 39. PL decay for the DAP transitions (filled points) and e-A transitions (empty points) of the UVL band in freestanding GaN template. Reprinted with permission from Reshchikov *et al.*, *Physica B* 340–342, 444 (2003). Copyright (2003) by Elsevier.

time interval between 10^{-3} and 1 s. For longer delay times, the intensity of both DAP and e-A lines decays exponentially with a characteristic time of 5 s (Fig. 39). Such decay of the e-A emission can be explained by a low concentration of the equilibrium electrons in the conduction band. Indeed, by taking $n_0 = 10^{11} \text{ cm}^{-3}$ which corresponds to approximately 20 K for the studied sample,¹⁹⁶ and $C_n = 2 \times 10^{-12} \text{ cm}^3/\text{s}$,¹¹³ we obtain $\tau = 5 \text{ s}$ from Eq. (20). The fast exponential decay of the DAP peak at $t > 10 \text{ s}$ (Fig. 39) can be understood by considering that the e-A transitions deplete the holes from the shallow acceptor levels. Note that for the BL, YL, and RL bands, the deviation from the nonexponential PL decay due to the above-mentioned reason is expected at longer times, in accordance with the much lower electron-capture cross sections for the corresponding acceptors.^{113,114}

3. ODMR and identification of the shallow acceptor

Optically detected magnetic-resonance studies usually analyze the value and angular dependence of g factor of the defect-related signal, enabling in some cases identification of the defects involved in PL process. From the symmetry considerations, supported by calculations, Malyshev *et al.*¹⁰⁸ predicted that the ground-state g factor of an acceptor (unless it is very deep) in wurtzite GaN should be highly anisotropic, namely, $g_{\parallel} \neq 0$, $g_{\perp} = 0$, where g_{\parallel} and g_{\perp} represent the g factors for the magnetic-field vector aligned parallel and perpendicular to the c axis, respectively. However, until recently the experimentally found g factor for such acceptors as Mg and Zn in GaN was isotropic and close to g_0 . Note that in other semiconductors with similar structure such as CdS and 6H-SiC, the g factor of the shallow acceptor is indeed highly anisotropic.^{234–236} Malyshev *et al.*¹⁰⁸ assumed that unexpected isotropy is the result of spontaneous local strain fields due to the Jahn–Teller effect. Remarkably, Glaser *et al.*¹⁰⁹ have discovered a high anisotropy of the shallow acceptor in high-purity GaN by using the ODMR technique. They studied a 6- μm -thick Si-doped layer grown on a freestanding GaN template and observed a strong increase of the UVL

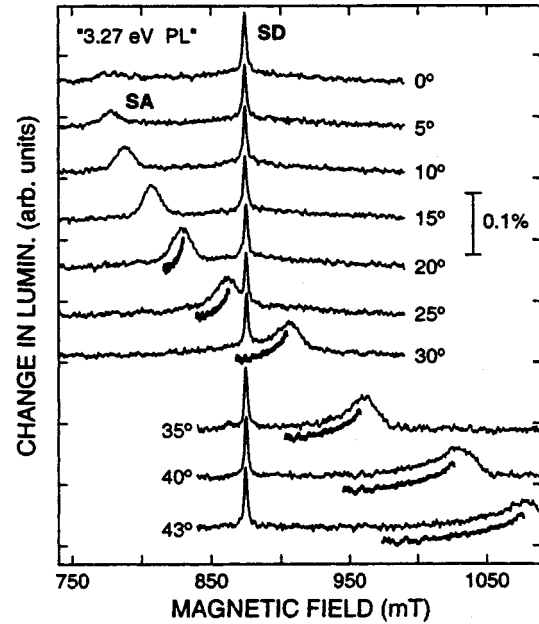


FIG. 40. ODMR spectra at 24 GHz detected on the UVL band (at 3.27 eV) for several orientations of the applied magnetic field in the (11-20) plane (0° refers to the c axis). The thick black curves (displaced vertically for clarity) are simulations of the low-field line shapes for resonance SA. Reprinted with permission from Glaser *et al.*, *Phys. Rev. B* 68, 195201 (2003). Copyright (2003) by the American Physical Society.

band compared to the unintentionally doped GaN. The UVL band has been attributed to DAP-type transitions involving a shallow donor (Si_{Ga} and possibly O_{N}) and shallow acceptor, identified as Si_{N} , although those authors could not rule out the possibility that unintentionally introduced carbon created shallow acceptors C_{N} in the deposited layer.¹⁰⁹

The ODMR spectrum contained two luminescence-increasing signals (Fig. 40). The first one, labeled as shallow donor (SD), was nearly isotropic with $g_{\parallel} = 1.952$ and $g_{\perp} = 1.949$ and has been assigned to shallow donors. The second one, labeled as shallow acceptor (SA), shifted rapidly with magnetic field (Fig. 40), i.e., with variation of the angle between the magnetic field and the c axis. The angular dependence of the g factor for resonance SA (Fig. 41) was fitted with the expression

$$g(\theta) = (g_{\parallel}^2 \cos^2 \theta + g_{\perp}^2 \sin^2 \theta)^{1/2}, \quad (30)$$

where g_{\parallel} and g_{\perp} are the g values with magnetic-field vector aligned parallel and perpendicular to the c axis, respectively. Good fits have been obtained with $g_{\parallel} = 2.193 \pm 0.001$ and $g_{\perp} = 0$,¹⁰⁹ in remarkable agreement with the theoretical prediction for the shallow acceptor in GaN.¹⁰⁸ Glaser *et al.*¹⁰⁹ suggested that the electric fields generated by high concentration of charged donors and acceptors in Mg-doped GaN and high density of dislocations may be responsible for the random distortions, leading to the previously observed nearly isotropic g factor in less pure samples (shown in Fig. 41 for comparison). Those authors have also attributed the asymmetric broadening of the SA signal at $\theta > 25^\circ$ to residual random strain fields and simulated the broadening in this assumption (Fig. 40).

Among the candidates for the shallow acceptor in undoped GaN, Mg_{Ga} , C_{N} , and Si_{N} are commonly regarded as

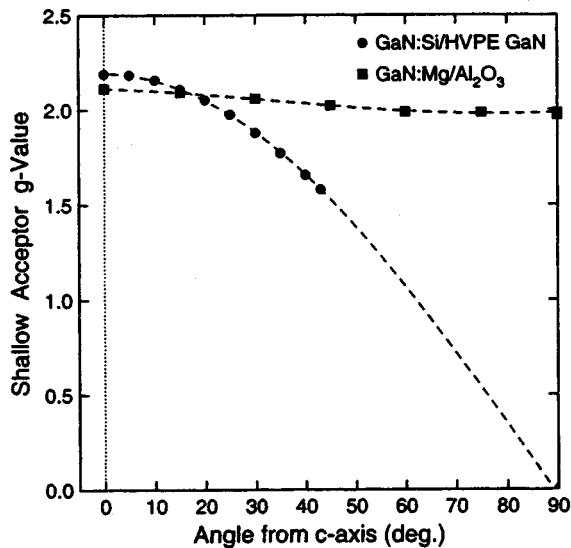


FIG. 41. g values of ODMR signal SA in homoepitaxial Si-doped GaN layer (circles) and those found previously for Mg shallow acceptors in Mg-doped GaN heteroepitaxial layers (squares) as a function of the angle (θ) between magnetic-field vector and the c axis. The dashed curves are fits to the data [see Eq. (30)]. Reprinted with permission from Glaser *et al.*, Phys. Rev. B **68**, 195201 (2003). Copyright (2003) by the American Physical Society.

most reasonable. The former impurity is clearly responsible for the shallow acceptor (and the UVL band) in GaN lightly or moderately doped with Mg. In nominally undoped GaN samples, Mg may be due to contamination of the reactor from previous growths using Mg. However, the undoped GaN sample studied by Glaser *et al.*¹⁰⁹ has been grown in a MOCVD reactor where Mg had never been introduced as a dopant source. The observation that the UVL band significantly increased after doping with Si apparently indicates that Si_N is also a shallow acceptor with possibly a high concentration. Jayapalan *et al.*²³¹ also observed an increase of the UVL intensity with Si doping and attributed it to the formation of the Si_N acceptor. As for carbon, there is no clear evidence that it forms a significant amount of the shallow acceptors C_N in undoped wurtzite GaN. Apparently there is no correlation between C doping and presence of the UVL band in wurtzite GaN.^{136–138,164} Note, however, that C_N easily incorporates in cubic GaN, where a good p -type conductivity had been reported with C doping (Sec. VI). At this stage we may conclude that the UVL in undoped wurtzite GaN is related to Si_N or C_N residual acceptors, unless the sample is contaminated with Mg.

D. Blue luminescence band

The BL band peaking at about 2.9 eV in GaN, similar to the notorious YL in this material, has attracted substantial attention of the semiconductor investigators for many years. This is in part due to the controversial assignment of its origin and important role that the related defect plays in GaN. The BL band is often observed in undoped, Mg- and Zn-doped GaN with very similar shape and position. The reported values of the energy position of the BL band vary from 2.7 to 3.0 eV. There is also evidence that in some samples the BL band, usually peaking at 3.0 eV, bleaches

under UV illumination. To avoid further confusion, we immediately clarify that the BL band in Mg-doped GaN has distinctive features, in particular, a large shift with excitation intensity, and is assigned to transitions from a deep donor to the Mg_Ga shallow acceptor (Sec. V B 3). The BL in Zn-doped GaN, having a characteristic fine structure in relatively pure samples, is attributed to transitions from the conduction band or shallow donors to the Zn-related acceptor (Sec. V A 1). In undoped GaN, the transitions are the same as in GaN:Zn, and apparently the acceptor is the same. Finally, the blue bands with a metastable behavior are related to different defects, as discussed in Sec. IX. Below the properties of the stable BL in undoped GaN are reviewed.

1. Steady-state PL

A broad BL band centered at 2.88–2.90 eV is often observed in the PL and CL spectra of undoped and Si-doped n -type GaN grown by MOCVD or HVPE.^{71,102,103,116,151,153,155,180–182,189,191,237–244} A BL band, similar in energy position and shape to that observed in undoped and Si-doped GaN, has also been observed in high-resistivity C-doped GaN.¹⁶⁴ In one investigation,¹³⁶ a slight deviation has been observed in that doping with C introduced a BL band peaking at approximately 3.03 eV (Sec. IV D 4). As shown below, the BL band in undoped or Si-doped GaN is due to transitions from the conduction band or a shallow donor to a relatively deep acceptor having an ionization energy of about 0.34–0.4 eV.

One of the fingerprints of the BL band in unintentionally doped GaN is the fine structure observed at low temperatures in high-quality GaN samples.^{116,160} The fine structure represents a set of sharp peaks associated with local and lattice phonons (Fig. 42). The set is identical among different samples. An analysis of the spectra from several samples has demonstrated^{116,160} that the fine structure is formed by a superposition of two series of sharp peaks. The energy separation between peaks in the first set is 36 ± 1 meV. This set is repeated at the energies of the LO phonon (Fig. 42). Observation of the fine structure enables one to determine the vibrational characteristics of the defect in its ground state. The first sharp peak at 3.098 eV is attributed to the ZPL (E_0) of the 2.9-eV band. Its replicas at the energy multiples of 36 ± 1 meV are attributed to transitions involving a local or pseudolocal vibrational mode of the acceptor. Repetition of this set in 91-meV intervals demonstrates that the coupling with both local and lattice phonons is relatively strong for the deep acceptor involved in the process. In the case of two vibrational modes, the intensity of the phonon replica corresponding to the emission of m local and n lattice phonons, W_{mn} , is given by⁹⁶

$$W_{mn} \propto \frac{S_1^m S_2^n}{m!n!}, \quad (31)$$

where S_1 and S_2 are the Huang–Rhys factors describing the coupling with two vibrational modes. An example of the PL band shape obtained by using Eq. (31) with $S_1=1.5$ for the local phonons and $S_2=2$ for the lattice LO phonons is shown in Fig. 42 by a solid curve.

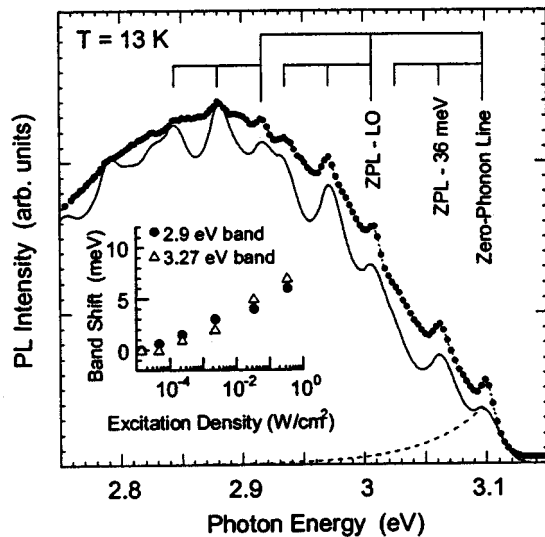


FIG. 42. PL spectrum of the BL band in undoped GaN sample at 13 K and excitation density of 2×10^{-4} W/cm². Two sets of sharp peaks with energy separations of 36 and 91 meV are seen. The zero-phonon line (ZPL) energy is 3.098 eV. The solid curve is the fit using Eq. (31) with $S_1=1.5$ and $S_2=2$ and simulated shape of the no-phonon transition (dashed curve). The inset shows the shift of the peaks with excitation intensity for the BL and shallow DAP bands. Reprinted with permission from Reshchikov *et al.*, J. Appl. Phys. 87, 3351 (2000). Copyright (2000) by the American Institute of Physics.

With increasing excitation power, a small shift to higher energies has been observed for both the sharp peaks and for the band as a whole.¹¹⁶ The shift averaged over several sharp peaks of the 2.9-eV band is shown in the inset of Fig. 42 in comparison with the shift for the ZPL of the UVL band. The observed small shift, as well as the similarity of the shifts of the BL and UVL bands, indicates that both bands arise from DAP-type transitions involving the same shallow donor.

The position of the acceptor level E_A can be estimated from the position of the ZPL with respect to the band edge. From the energy position of the donor-bound exciton line in the analyzed sample (3.480 eV), the gap width (E_g) at low temperature is estimated as 3.518 eV.¹¹⁶ Taking the ionization energy of the shallow donor E_D reduced by the Coulomb interaction as approximately 20 meV under low-excitation rate, and taking the ZPL at $E_0=3.098$ eV, the acceptor energy level is estimated as $E_A=E_g-E_D-E_0=0.40$ eV.¹¹⁶ This value is close to the thermal ionization energy (approximately 0.34 eV) obtained from the PL quenching analysis.⁶⁷ Note that in the temperature range where the PL quenching occurs (200–300 K), the value of E_A may differ from that derived at low temperatures. Note also that the activation energy of about 0.38 eV would be obtained from the Arrhenius plot of quenching at $T > 200$ K if one ignores the temperature dependence of the effective density of states in the valence band.⁶⁷

The temperature dependence of the intensity, position, and width of the BL band has been studied in Refs. 67, 116, and 160. The intensity of the BL band increases with increasing temperature from 10 to 40 K in the samples with high QE of this band (Fig. 15). This phenomenon is explained by redistribution of holes that are released from the exciton dissociation between acceptors.⁶⁷ Over the temperature range of

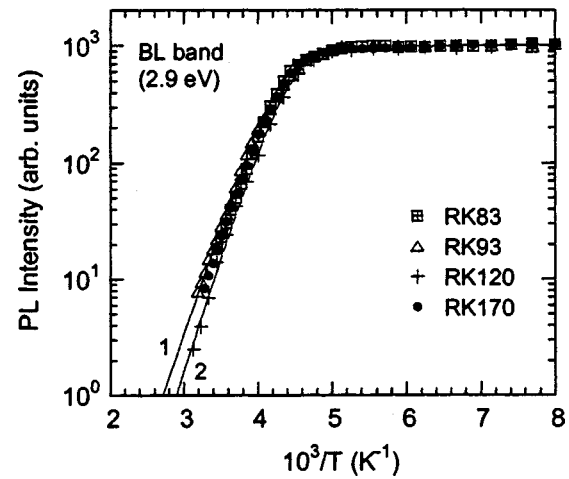


FIG. 43. Temperature-induced variation of the intensity of the BL band in MOCVD-grown GaN. The solid curves are the best fit for the samples RK93 (1) and RK120 (2) by using Eqs. (6)–(10). Reprinted with permission from Reshchikov and Korotkov, Phys. Rev. B 64, 115205 (2001). Copyright (2001) by the American Physical Society.

100–200 K the intensity of the BL band is nearly temperature independent. At higher temperatures, a thermal quenching is observed, as displayed in Fig. 43. Employing a fit to the experimental data for undoped GaN grown by MOCVD on sapphire (Fig. 43) with the aid of Eq. (6), Reshchikov and Korotkov⁶⁷ obtained $E_A=340 \pm 10$ meV and $C_p=(9 \pm 4) \times 10^{-7}$ cm³/s. In general, the quenching of PL band in *n*-type semiconductor does not necessarily indicate that holes are thermalized to the valence band. In an alternative model,²¹⁵ the bound holes do not escape to the valence band but non-radiatively recombine with free electrons in the conduction band. In the latter case, the activation energy is simply the energy separation between the adiabatic potential minimum of the excited state and the crossover point of the adiabatic potentials of the ground and excited states. However, the quenching of the BL band is clearly caused by the escape of holes from the acceptor to the valence band. Indeed, the observed increase in the intensity of the YL band in a temperature range corresponding to the quenching of the BL band (Fig. 15) strongly indicates that a redistribution of holes which are released to the valence band from the BL-related acceptor takes place.

The peak position of the BL band at about 2.88 eV at low temperatures remains almost unchanged or even shifts slightly to higher energies with increasing temperature from 13 to 380 K,¹⁶⁰ while the band gap decreases by about 100 meV in the same temperature range, as depicted in Fig. 44. Weak temperature dependence is typical for defects with strong electron-phonon coupling and may be quantitatively explained within the framework of the one-dimensional CC model discussed in Sec. III C. This model suggests, in particular, that the width of an emission band related to a deep point defect is determined by the strength of the electron-phonon coupling and by the energy of the zero vibrational state of the defect. The FWHM of the band in the case of a strong electron-phonon coupling is described by Eq. (26). From the best fit to the experimental data regarding the temperature variation of the bandwidth, which is shown in Fig.

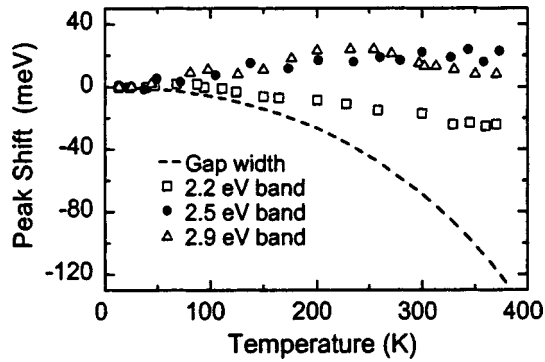


FIG. 44. Shift of the BL band maximum (triangles) with temperature. The shifts of the YL (2.2 eV) and GL3 (2.5 eV) bands in GaN grown by MOCVD are shown for comparison. Reprinted with permission from Reshchikov *et al.*, *Physica B* 273–274, 105 (1999). Copyright (1999) by Elsevier.

45, the energy of the effective vibrational mode for the excited state of the BL-related acceptor, $\hbar\omega_0^e$, has been estimated to be 43 meV.¹⁶⁰ Note that this is some averaged value, since the two-mode oscillation has been reduced to the effective one-dimensional oscillation in the fitting.

2. Time-resolved PL

Transient behavior of the BL band has been studied in undoped GaN grown by MOCVD (Refs. 87 and 188) and HVPE.^{114,228} At low temperatures the decay of the BL band is nonexponential (Fig. 17), in agreement with the model of the DAP transitions including shallow donors. From the fitting with the aid of Eqs. (16) and (17), the value of W_{\max} has been estimated as $\sim 10^7$ s⁻¹ for the acceptor involved in the transition.¹⁸⁸ The PL decay becomes nearly exponential with increasing temperature when the DAP transitions are replaced by the e-A transitions involving the same shallow acceptor.⁸⁷ The temperature dependences of the emission lifetime for the BL band in undoped *n*-type GaN grown by MOCVD (Ref. 87) and HVPE,¹¹⁴ are shown in Figs. 19 and 33. The effective lifetime of BL has weak temperature dependence between 50 and 200 K and sharply drops at $T > 200$ K due to escape of holes from the acceptor level to the

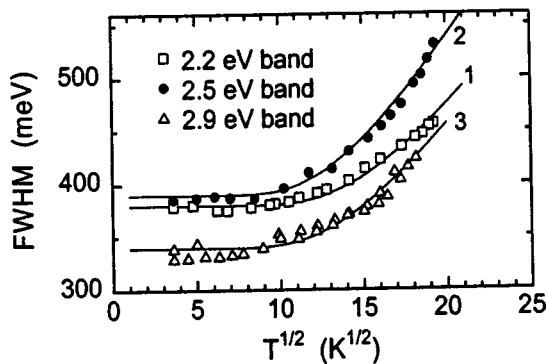


FIG. 45. Temperature dependence of FWHM of the BL band (triangles) in comparison with the dependences for the YL (2.2 eV) and GL3 (2.5 eV) bands in GaN grown by MOCVD. The solid curves are fit by Eq. (26) with the following parameters: $W(0)=380$ (1); 390 (2); 340 (3) meV. $\hbar\omega_0^e=52$ (1); 40 (2); 43 (3) meV. Reprinted with permission from Reshchikov *et al.*, *Physica B* 273–274, 105 (1999). Copyright (1999) by Elsevier.

valence band, in accordance with Eq. (22). The electron-capture coefficient C_n and the electron-capture cross section σ_n have been estimated for the BL-related acceptor as $(3.9 \pm 0.4) \times 10^{-13}$ cm³ s⁻¹ and $(2.1 \pm 0.2) \times 10^{-20}$ cm², respectively, by using Eqs. (20) and (23).^{87,114}

Evolution of the BL band with time after an excitation pulse at 15 K in GaN layer grown by MOCVD is shown in Fig. 18. There is no shift within an accuracy of 30 meV, in agreement with the assumption that the donor involved in the DAP transition is shallow. In pure enough GaN samples grown by HVPE, the BL band as well as the YL band could be observed long after the excitation is completely turned off.¹¹⁴ This observation is not surprising for such a pure GaN sample where according to Fig. 31 about half of the acceptors bind holes at least few seconds after pulsed excitation.

3. Spatially and depth-resolved cathodoluminescence

The spatial distribution of defects responsible for the BL band in undoped and Si-doped GaN has also been studied by CL in a scanning electron microscope (SEM).^{181,182} The SEM images showed round and hexagonal hillocks with sizes ranging from about 5 to 40 μm .¹⁸² The BL band was strong at hillocks and it almost completely vanished at the hillock boundary, whereas the YL band and the excitonic emission were distributed more uniformly.¹⁸² In another study,¹⁸¹ BL and YL decorated the grain boundaries with BL exhibiting a more homogeneous distribution than YL. The decoration of boundaries or hillocks indicates a nonuniform distribution or segregation of point defects in the GaN layer.

Depth-resolved CL has been used for depth profiling of BL and YL in undoped GaN.^{103,183} Fleischer *et al.*¹⁰³ observed an increase of the YL intensity and a decrease of the BL intensity in direction from the layer surface to the sapphire substrate. Herrera Zaldivar *et al.*¹⁸³ observed nonuniform in-depth distribution of YL and BL with the intensity increasing towards the surface and near the substrate-layer interface. Toth *et al.*¹⁸⁰ reported on the evolution of the CL intensity with electron irradiation time for YL, BL, and near-band-edge emission in undoped GaN. At 4 K, intensities of both the YL and BL bands decreased with the duration of the electron-beam exposure, whereas the UVL band and excitonic emission enhanced. Those authors attributed the observed phenomena to the electron-beam-induced diffusion of O and H and proposed that oxygen is involved in the defect responsible for the YL band and hydrogen is involved in the BL-related defect.¹⁸⁰ Note, however, that the accumulation of charge at the surface due to illumination or electron irradiation may also affect the evolution of the emission, as discussed in more detail in Sec. IX.

4. Origin of the BL band in undoped GaN

The BL band in undoped GaN is caused by transitions from the shallow donors (at low temperature) or conduction band (at elevated temperatures) to a relatively deep acceptor having an ionization energy of about 0.34–0.40 eV. Although this picture should be regarded as well established, we will critically review two alternative models. To explain PLE spectrum of the BL band, Yang *et al.*¹⁵³ attributed this band

to transitions from the resonant state of O_N located 0.25 eV above the conduction-band minimum to the $V_{Ga}O_N$ acceptor level located 0.8 eV above the valence band. We note that the resonant excitation of the BL band with above the band-gap photons is very unlikely due to the large absorption coefficient at 3.54–3.75 eV, and the peak in the PLE spectra observed in Ref. 153 (moving from 3.54 to 3.75 eV with variation of the emission energy from 2.75 to 2.91 eV) is apparently some feature of the scattered light. In another report, Kaufmann *et al.*¹⁷² suggested that the BL band in undoped or Si-doped GaN is due to transitions from a deep donor to the shallow acceptor. This model is unacceptable for undoped GaN where the overlap between the wave functions of a hole bound to the shallow acceptor and electron localized at a deep donor would be extremely small to explain the high intensity of the BL band in samples with concentrations of acceptors in the 10^{15}-cm^{-3} range.^{67,116}

Various proposals have been made as to the nature of the defect responsible for the BL band in undoped GaN. The BL band was attributed to a V_{Ga} -related complex,⁶⁷ in particular, to $V_{Ga}O_N$ (Refs. 153 and 242) and $V_{Ga}H_n$.¹⁸⁰ Although the band is often observed in Si-doped GaN, it is not enhanced by Si doping.⁷¹ This band should not be confused with the BL band in GaN heavily doped with Mg, to be discussed in Sec. V B 3, and with the band peaking at about 3.03 eV in C-doped GaN.¹³⁶ The clue for the origin of the acceptor can be found in the fact that the BL band with the aforementioned properties was observed only in GaN grown by MOCVD or HVPE but never in the layers grown by MBE. Therefore, it is unlikely that a native defect is involved. Moreover, we doubt that hydrogen is involved in the defect complex,¹⁸⁰ because the BL band has not been revealed in GaN layers grown by MBE with ammonia as the nitrogen source.

The most plausible explanation for the BL band in undoped GaN is contamination with Zn (see Sec. V A 1).²⁴⁵ Very large hole-capture cross section for this acceptor ($\sim 10^{-13}\text{ cm}^2$) explains why the BL is often observed in GaN samples with the Zn concentration of $\sim 10^{15}\text{ cm}^{-3}$ and even less.^{67,245} We may speculate that GaN can be contaminated with Zn from impure gases used in MOCVD and HVPE growth or from intentional Zn doping sometimes used in the buffer layer for improved growth.

E. Red luminescence band

The RL band with its emission in the range of $\sim 1.5\text{--}2.0$ eV is less studied and less common in undoped GaN as compared to the YL, BL, and UVL bands. The energy positions of the RL band differ in different reports, and it appears that several defects contribute to emission in this energy range. We have observed a few RL bands having very different properties. In this section, the RL band observed at room and cryogenic temperatures in GaN grown by HVPE and MBE is discussed, while Sec. IV F deals with specific red and green bands observed only in Ga-rich GaN grown by MBE at relatively low temperatures. The red band observed in the Mg-doped GaN is discussed in Sec. V B 4.

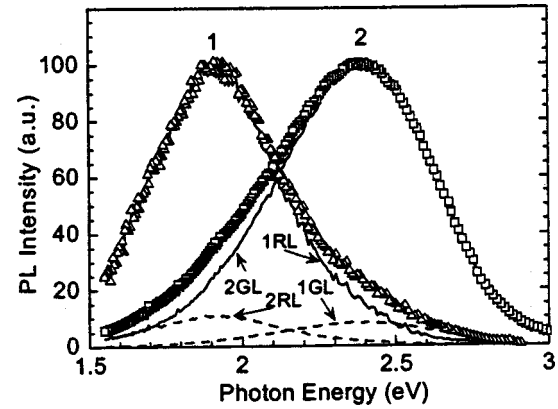


FIG. 46. Room-temperature PL spectrum of GaN layer grown by HVPE on sapphire (H966 for us) excited at $\hbar\omega_{\text{exc}}=3.41$ eV. The points are experimental data taken at $P_{\text{exc}}=1$ (1) and 0.001 W/cm^2 (2). The curves are self-consistent deconvolution of the experimental curves into two bands (a RL with a maximum at 1.92 eV and a GL with the maximum at 2.39 eV). Reprinted with permission from Reshchikov *et al.*, Mater. Res. Soc. Symp. Proc. 680, E5.6 (2001).

In GaN samples grown by HVPE, the RL band peaking at about 1.85 eV and having a FWHM of about 0.4 eV is observed if the YL band is sufficiently weak, as displayed in Fig. 13.^{114,246} In some HVPE-GaN samples, the RL band appears as a shoulder to the YL band and can be resolved only at very low excitation intensities (Fig. 46), because the RL band usually saturates at very low excitation intensities.⁹⁹ In the high-purity freestanding GaN templates, the RL band could be detected as a weak shoulder to the YL band (Fig. 22) and it is better resolved in the below-band-gap excitation case (Fig. 28). The effective lifetime of the RL is the longest among other defect-related PL bands in the visible part of the spectrum.^{189,228} For example, at 100 K the lifetime of RL is about 5 ms in a freestanding template (Fig. 32), resulting in the smallest electron-capture cross-section coefficient of $2 \times 10^{-14}\text{ cm}^3/\text{s}$.²²⁸ In sufficiently pure GaN, the RL band can be observed seconds after the excitation pulse,^{113,114} see Fig. 1 in Ref. 114 for the 200- μm -thick freestanding GaN template and 30- μm -thick GaN layer grown on sapphire. A very long lifetime of the RL band explains why it saturates at very low excitation intensities (Fig. 23). No energy shift of the RL band was detected with delay time,^{113,114,189} indicating that the RL band is due to transitions from a shallow donor (at low temperatures) or the conduction band (at elevated temperatures) to a deep acceptor level. The ODMR studies have also revealed that the RL band in GaN grown by HVPE is caused by transitions from the shallow donors to a deep-level defect at low temperatures.²⁴⁷ Owing to a nearly Gaussian shape of the RL band, we conclude that the electron-phonon coupling is very strong for the deep acceptor involved, and its ZPL should be near 2.2 eV. Therefore, the acceptor level is located at about 1.2–1.3 eV above the valence band. Deep energy position of the acceptor level is consistent with the PL intensity being independent of temperature.^{113,114,189,228} The above-analyzed RL band should not be confused with the very short-lived (the lifetime is 12 ns) broad band peaking at about 1.93 eV.²⁴⁸ The latter has been attributed to recombination of excitons bound to a neutral defect center.²⁴⁸

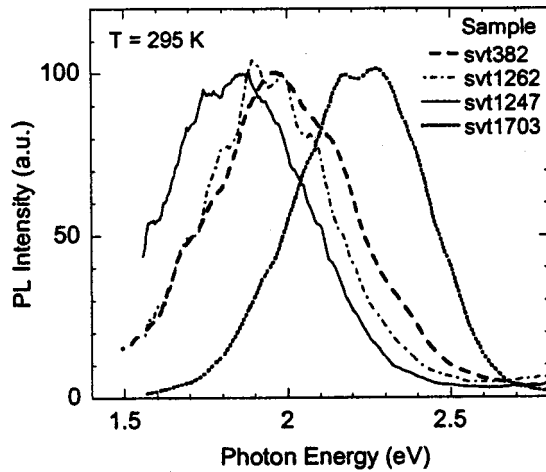


FIG. 47. Room-temperature PL spectra of GaN layers grown by MBE on sapphire. Oscillations with a period of 100–150 meV are caused by interference from the 1.5–2.5- μm -thick films. Sample svt1703 is a representative sample with a strong YL band in the PL spectrum.

In undoped GaN samples grown by MBE, we observed broad emission bands at 1.8–2.0 eV with their intensities being independent of temperature in the range from 15 to 300 K (Fig. 47). Similar to the RL in GaN grown by HVPE, these bands saturated at low excitation intensities due to a very long lifetime of the luminescence. It is not clear if this emission has the same origin as the RL band in GaN grown by HVPE, and even how many bands related to different defects contribute to the broad emission at photon energies below the YL band. We proposed that the point defect responsible for the YL (presumably containing V_{Ga}) may produce emission similar to the YL band but shifted if this defect is trapped by different kinds of extended defects.¹⁰⁰ Note that a broad emission in the red part of the spectrum (maximum at 1.66 eV) has also been observed in Ga-lean layers grown by MBE by Brillson *et al.*¹⁷⁹

The RL bands in the MBE- and HVPE-grown GaN and the GL band observed in high-quality HVPE-grown GaN, whose intensities are nearly independent of temperature from 15 to 300 K, should not be confused with the RL2 and GL2 bands in Ga-rich GaN to be discussed below.

F. Red and green luminescence bands in Ga-rich GaN grown by MBE

The YL band dominates the visible part of the PL spectrum in most of the GaN samples grown by MBE. However, with increasing III/V ratio the relative contribution of the YL band decreases, and other defect-related PL bands could then be detected in the PL spectrum.^{99,117} Extremely Ga-rich conditions can be easily obtained in MBE growth by using a rf plasma as a source of nitrogen with much reduced N flow and by reducing the growth temperature.²⁴⁹ The surface of the samples grown under such conditions is often covered with Ga droplets, and the samples are usually highly resistive,^{99,117} most likely due to self-compensation. The exciton emission is usually very weak in these samples, while two characteristic PL bands often dominate the visible part of the low-temperature PL spectrum in such samples: a red band peaking at about 1.8–1.9 eV and a green band with a

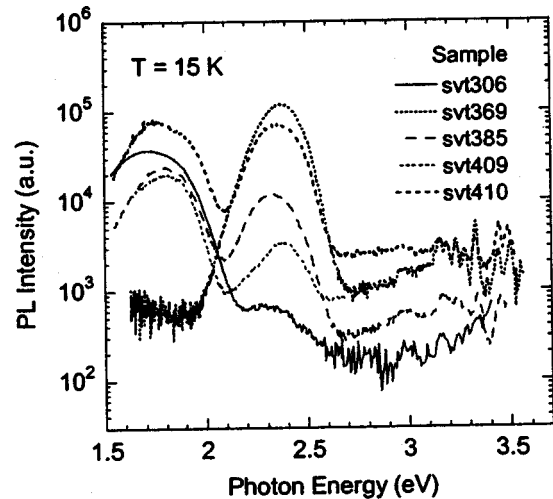


FIG. 48. PL spectra from Ga-rich GaN layers grown by MBE on sapphire. $T=15$ K.

maximum at about 2.35 eV, as illustrated in Fig. 48. To avoid any confusion with the GL and RL bands observed in GaN grown by HVPE (Secs. IV B and IV E), we label these bands as RL2 and GL2, respectively. We have studied the RL2 and GL2 bands in about 50 GaN samples grown by MBE in Ga-rich conditions. Most of the layers exhibiting these PL bands were deposited on sapphire, although the same emission bands were observed in the layers grown on SiC, ZnO, and LiGaO substrates, as well. Although the relative intensities of the RL2 and GL2 bands varied from sample to sample, as shown in Fig. 48, their energy position, shape, and properties were reproducible. The FWHM of these bands is about 240–340 meV, which is much smaller than the FWHM of the YL or GL bands in GaN grown by HVPE. The intensity, energy position, and shape of the GL2 and RL2 bands remained nearly unchanged after removal of the top 0.2–0.5- μm layer of GaN by wet chemical etching. This observation indicates that the associated point defects are bulk type, and they are more or less uniformly distributed in depth through the GaN film. Others, namely, Hofmann *et al.*²⁵⁰ and Skromme and Martinez,¹⁹⁹ apparently have studied the same bands in GaN. Below we review the main properties of the RL2 and GL2 bands. Preliminary investigations dealing with RL2 and GL2 bands have been the topic of Refs. 99 and 117.

1. Effect of excitation intensity

With increasing excitation intensity in the range of 10^{-4} –100 W/cm², the RL2 and GL2 bands do not shift within an accuracy of 5–10 meV, as displayed in Fig. 49. This is the first indication that those bands are not caused by DAP-type transitions. Moreover, since these bands dominate in the high-resistivity GaN samples (with $n_0 \approx 10^{15}$ cm⁻³ or less at room temperature), the equilibrium concentration of electrons at shallow donors is negligible, while the DAP transitions involving deep donors are usually characterized with very large shift of the PL band with the excitation intensity.⁸² Hofmann *et al.*²⁵⁰ also observed no shift of the red band with a maximum at 1.8 eV in GaN layers grown by MBE. However, those authors assumed that this band results from the

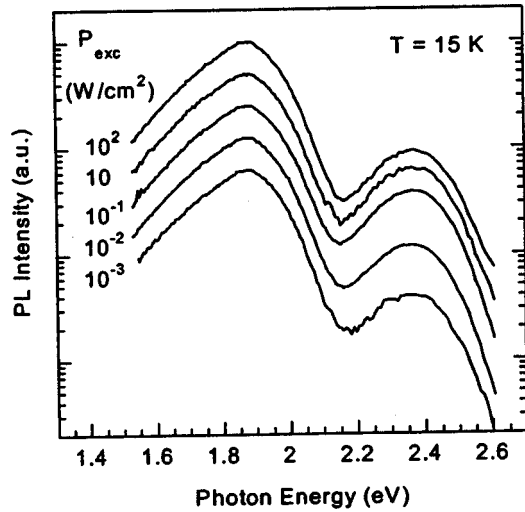


FIG. 49. Effect of excitation density, P_{exc} , on low-temperature PL spectrum of the Ga-rich GaN layer. Position and shape of the bands are independent of excitation density with accuracy of \pm (5–10) meV. The curves are shifted arbitrarily in the vertical direction (log scale).

DAP-type transitions involving deep donors and deep acceptors. The intensities of the RL2 and GL2 bands saturate at extremely low excitation intensities, which represent a deviation from the behavior of the majority of PL bands in GaN. Figure 50 shows the variation of the QE of these bands with excitation density. While the PL intensity of these bands is linear in the low-excitation regime up to $\sim 10^{-4}$ W/cm², at higher excitation densities the intensities of both PL bands saturate, and their QE gradually decreases. In contrast, the intensity of the exciton emission increases superlinearly, at least for $P_{exc} > 10^{-1}$ W/cm², giving rise to increasing QE, as shown in Fig. 50. The superlinear increase of the exciton emission is consistent with the high resistivity of the analyzed samples, where a bimolecular process is expected for the near-band-edge emission. As shown in Sec. IV F 3, very

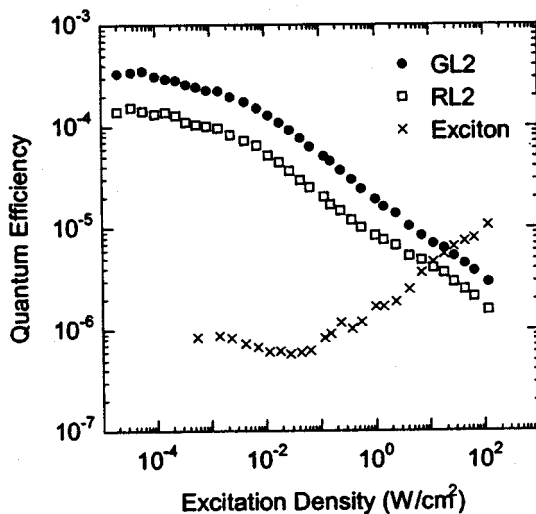


FIG. 50. Variation of quantum efficiency of the RL2, GL2, and exciton emission bands in the Ga-rich GaN layer with an excitation density at 15 K.

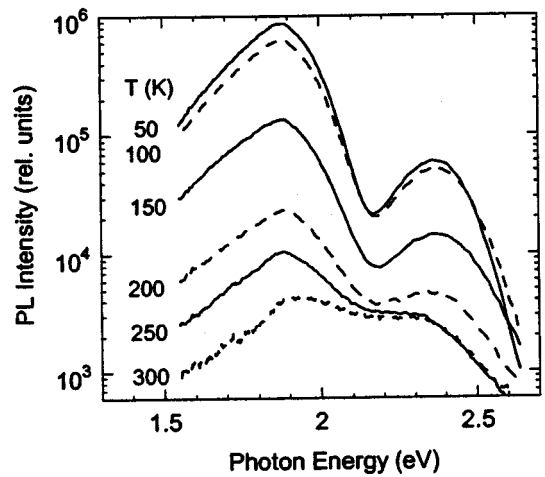


FIG. 51. PL spectra of the Ga-rich GaN layer (sample svt591) at different temperatures.

long lifetimes of the RL2 and GL2 are responsible for their saturation at relatively low excitation intensities.

2. Effect of temperature

The main difference of the RL2 and GL2 bands in Ga-rich GaN grown by low-temperature MBE from their color “twins” in GaN grown by HVPE lies in their behavior with temperature. Both the RL2 and GL2 bands quench at temperatures above 100 K, and nearly disappear at room temperature, as displayed in Fig. 51, whereas the intensities of the RL, YL, and GL bands in HVPE and MOCVD and N-rich-MBE GaN are nearly independent of temperature. An increase of intensity of the RL2 band in the temperature range of 10–60 K has been reported.^{117,250} Hofmann *et al.*²⁵⁰ assumed that the RL2 band is due to transitions from a deep donor to a deep acceptor, and thermal release of electrons from the shallow donors to the conduction band followed by their capture by deep donors enhanced the RL2 band. We proposed earlier that the enhancement of the RL2 band could indicate the presence of a potential barrier in the excited state of the defect,¹¹⁷ however, now we revise that proposal. Careful measurements *at very low excitation intensities* showed no increase in the intensity of the RL2 band in the temperature range of 10–60 K. The reason for the PL intensity increase reported in Ref. 117 was the fast variation of the RL2 lifetime at temperatures below 60 K (see Sec. IV F 3). The saturation of the RL2 band at 10 K begins at much lower excitation intensities as compared to that for 60 K. Therefore, an increase of the PL intensity with heating the sample from 10 to 60 K observed in Ref. 117 is artificial and caused by the choice of the excitation intensity which is not suitable. The GL2 band is independent of temperature between 15 and 100 K because its lifetime is nearly constant in this temperature range (Sec. IV F 3).

Above 100 K, the bands thermally quench, as depicted in Fig. 52.^{117,250} In several samples, the quenching activation energy E_A was estimated from a fit to the following expression:²⁵¹

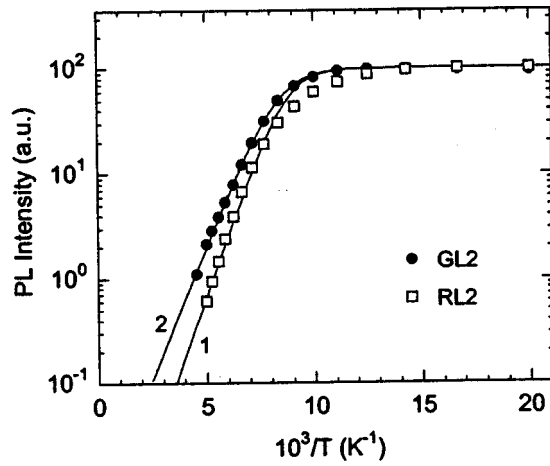


FIG. 52. PL intensity (in log scale) vs inverse temperature for the RL2 and GL2 bands. The solid lines are calculated curves using Eq. (32) with the activation energy (E_A) of 115 meV (1) and 100 meV (2) for the RL2 and GL2 bands, respectively.

$$I^{\text{PL}} = \frac{I^{\text{PL}}(0)}{1 + C \exp\left(-\frac{E_A}{kT}\right)}, \quad (32)$$

where C is a constant, and the values of 115 ± 10 meV for the RL2 band and 120 ± 20 meV for the GL2 band has been deduced.

The GL2 band shifted to a higher energy by about 10–30 meV with increasing temperature from 10 to 200 K, while the position of the RL2 band remained nearly unchanged in this temperature range, as displayed in Fig. 53. The temperature-induced shift, opposite to the shift of the band gap (which decreases by about 30 meV in this temperature range), is typical for defects with strong electron-phonon coupling⁸¹ and can be quantified by Eq. (28) if the local phonon energies are known.

The PL spectrum and the temperature-induced behavior of PL for defects with strong electron-phonon coupling can be described in terms of the CC model^{81,95} discussed in Sec.

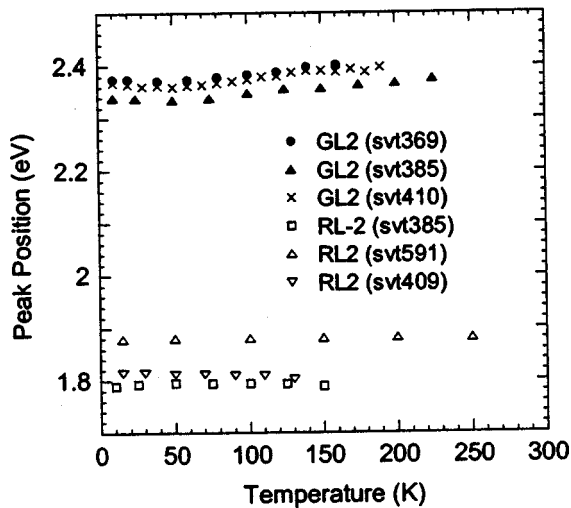


FIG. 53. Temperature dependence of the peak position of the RL2 and GL2 bands in Ga-rich GaN.

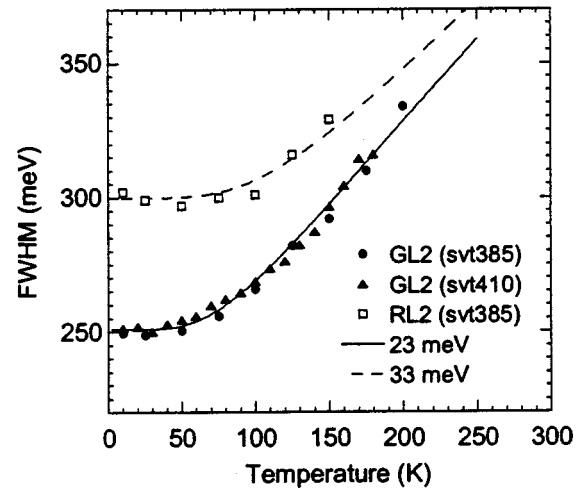


FIG. 54. Temperature dependence of the FWHM of the RL2 and GL2 bands in Ga-rich GaN. The curves are fit by Eq. (26) with the following parameters: $W(0)=250$ meV and $\hbar\omega_0^e=23$ meV (GL2); $W(0)=300$ meV and $\hbar\omega_0^e=33$ meV (RL2).

III C. In the simplest case, the electronic state interacts with a single localized vibrational mode of frequency ω_0 . The maximum of the PL band is observed at a photon energy equal to the difference between the adiabatic potentials for the ground and excited states as characterized by transition AB in Figs. 11 and 12. Due to the zero-level oscillations of the defect and large shift of the adiabatic potentials, the PL band has a relatively large width even at zero temperature. With increasing temperature, the higher phonon states of the excited state are occupied and the width of the PL band increases in accordance with Eq. (26).

The temperature-induced variations of the FWHM of the RL2 and GL2 bands are shown in Fig. 54. From the fit of the experimental data by Eq. (26), the energy of the averaged phonon mode in the excited state, $\hbar\omega_0^e$, is estimated to be 33 meV for the RL2 band and 23 meV for the GL2 band. The values of $\hbar\omega_0^e$ are much smaller than the LO phonon energy of 91 meV and are attributed to the local vibrational modes of the defects. Note also that these values are much smaller than those for other broad PL bands in undoped GaN.¹⁶⁰ We can approximately estimate the strength of the electron-phonon coupling by assuming for simplicity that the vibrational frequencies in the ground and excited states are the same.⁹⁵ Indeed, for $\hbar\omega_0^e=\hbar\omega_0^g=\hbar\omega_0$ and $S_{\text{ab}}=S_{\text{em}}=S$, one can find from Eq. (26), with parameters listed in the caption of Fig. 54, that $S \approx 20$ for both bands. This value indicates that the electron-phonon coupling for the studied defects is very strong ($S \gg 1$), a feature which is also confirmed by nearly Gaussian shape of the bands. More information can be extracted from the analysis of transient PL which is the topic of discussion below.

3. Time-resolved PL

The transient behavior of the GL2 and RL2 bands differs from those for the GL, YL, BL, and UVL bands discussed in Secs. IV A 5, IV B 3, IV C 2, and IV D 2. During time intervals between 2 and 500 μs , the RL2 and GL2 bands do not shift within the accuracy of ± 10 meV.²⁵² Both bands decay

exponentially, at least in the range between 20 and 400 μs ; at shorter times faster background largely contributes and distorts the spectrum. The absence of a noticeable shift with delay time and exponential decay indicate that the DAP nature of these bands is very unlikely. The characteristic lifetime for the GL2 band (about 0.25 ms) is invariant with increasing temperature from 15 to 100 K or excitation intensity from 10^{17} to 10^{19} electron-hole pairs per pulse per cubic centimeter. In contrast, the lifetime of RL2 band decreases almost two orders of magnitude (from 110 to 2 μs) with increasing temperature from 15 to 100 K, and it increases by about a factor of 1.5 when the excitation intensity is reduced by a factor of 100 at 15 K. Note that while the lifetime of the RL2 band substantially decreased in the temperature range of 15–100 K, its integrated intensity after each pulse remained nearly unchanged in this temperature range due to an increase in the peak intensity in the PL decay curve. This behavior is completely different from the transformation of the PL decay due to escape of a hole to the valence band when the peak intensity remains unchanged and only the lifetime varies with the activation energy corresponding to the ionization energy of the bound hole [see Eq. (22)]. Such a behavior indicates that the capture cross section for electrons on this center increases with increasing temperature since the capture cross section is inversely proportional to the PL lifetime.⁶⁷ Nearly exponential increase of the capture cross section is expected for repulsive multiply charged centers.²⁵³ We may expect the following temperature dependence of the PL lifetime $\tau(T)$ in this case:

$$\tau(T) = \tau_0 \left(\frac{T}{T_0} \right)^{2/3} \exp \left(\frac{T_0}{T} \right)^{1/3}, \quad (33)$$

where T_0 is the effective temperature characteristic of the material and the center.^{253,254} The experimental data were fitted by Eq. (33) in Ref. 252, and $kT_0 = 2.5$ eV has been obtained. A similar temperature dependence of the lifetime has been reported earlier for the capture of electrons by the doubly charged center Ag^{-2} in Ge.²⁵⁵

4. Resonant excitation of the GL2 and RL2 bands

The PLE spectra of the RL2 and GL2 bands are shown in Fig. 55.⁹⁹ The RL2 signal is very strong when it is excited with below the band-gap energy (note the very small thickness of the studied samples). The PLE spectrum can be deconvolved into two Gaussian-like bands (Fig. 55). This means that the adiabatic potential of the excited state of the associated defect has a complex shape and possibly contains two minima. Above 100 K, the resonantly excited RL2 band quenched with an activation energy of about 120–140 meV, very similar to the results obtained under the above-gap excitation.

In contrast to the RL2 and other bands in GaN (see Secs. IV A 6 and IV B 2), the GL2 band lacks the resonant excitation part in its PLE spectrum (or it cannot be distinguished from the noise level) at $\hbar\omega_{\text{exc}} < 3.2$ eV (Fig. 55).⁹⁹

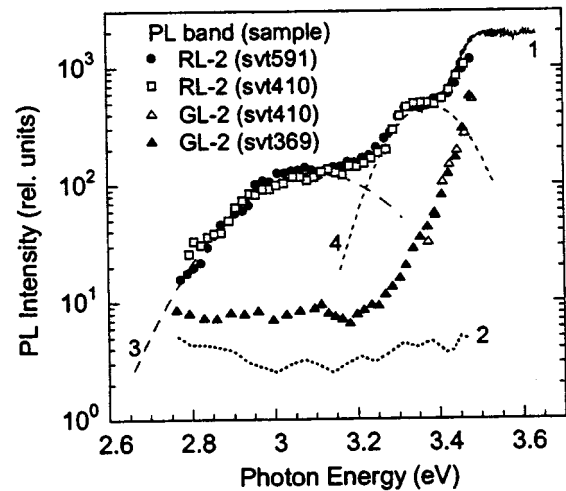


FIG. 55. PLE spectra at 15 K for the RL2 and GL2 bands in Ga-rich GaN. The points are experimental data. Curve 1 represents a part of the PLE spectrum for the RL2 band in the sample svt591 measured with excitation by Xe lamp. Curve 2 is the PLE spectrum of the sample svt369 at 295 K and represents the noise signal. Curves 3 and 4 are calculated Gaussians with maxima at 3.10 eV (3) and 3.38 eV (4) and FWHM of 372 meV (3), and 204 meV (4). Reprinted with permission from Reshchikov *et al.*, Mater. Res. Soc. Symp. Proc. 680, E5.6 (2001).

5. Origin and model of the GL2 and RL2 bands

An analysis of the peak position with excitation intensity and with delay time in transient PL may reveal whether the transition is of the DAP nature or not. In particular, DAPs involving deep donors are characterized by an enormous shift of the PL band with excitation intensity when the latter is varied in a wide range.⁸² The absence of noticeable shift of the RL2 and GL2 bands with excitation intensity or with delay time, and nearly exponential decay of the PL intensity in a wide time window, allows us to conclude that these transitions are not DAP type. The intense RL2 and GL2 bands, exhibiting slow exponential decay, cannot be attributed to transitions from the conduction band to the defect level or from the defect level to the valence band as well, since in high-resistivity GaN, free nonequilibrium carriers would be captured rapidly by other defects or form excitons on a time scale of the order of 10^{-10} s. The only remaining possibility is that RL2 and GL2 bands are due to internal transitions in some defects. Gaussian shape of the bands indicates that in both cases the carrier is strongly localized at the defect providing a strong electron-phonon coupling.

While discussing the type of possible transitions related to the studied defects, we should note that the observed values of activation energies for thermal quenching of the RL2 and GL2 bands (about 100–140 meV) are surprisingly small. Typically, the activation energies in thermal quenching correspond to escape of nonequilibrium holes (electrons) from the defect level to the valence (conduction) band (see Sec. III A 2). However, for defects with very strong electron-phonon coupling another mechanism of PL quenching is more plausible.²⁵⁶ This mechanism comprises nonradiative recombination of carriers at the defect site followed by emission of a large number of phonons. For defects with such a quenching mechanism, most of the recombination processes

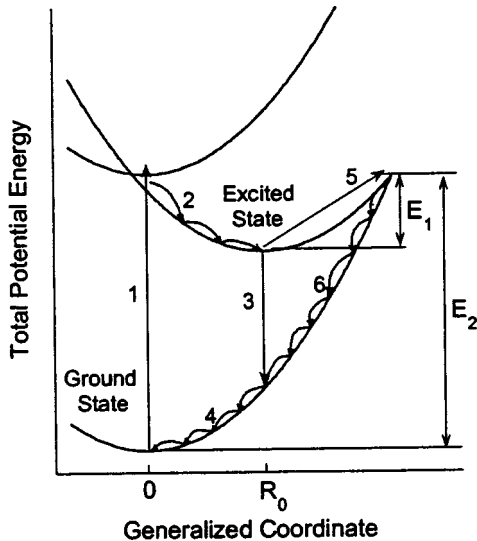


FIG. 56. An example of the CC diagram for the GL2 and RL2 bands in Ga-rich GaN. Transition 1 corresponds to excitation of the e-h pair; transition 2 corresponds to capture of carrier by defect in its excited state and relaxation of the lattice around the defect; PL involves emission of a photon (vertical transition 3) and relaxation of the lattice followed by emission of phonons (transition 4); thermal excitation of the defect up to crossover point (transition 5) results in nonradiative recombination with emission of many phonons (transitions 6 and 4). E_1 is the barrier height for the nonradiative recombination. Zero-phonon energy is $E_0 = E_2 - E_1$.

occur nonradiatively even at cryogenic temperatures, so that the defects act as killers of the PL efficiency. The ratio of the radiative to nonradiative processes, γ , at low temperatures may be roughly estimated utilizing the approximate expression $\gamma = E_1/E_2$ (see Fig. 56),²⁵⁶ which gives $\gamma < 7\%$ for the studied PL bands. Note that the radiative QE of the GL2 and RL2 bands varied from 0.05% to 0.5% in different samples we investigated. Therefore, the defects that are involved could be very efficient in reducing the PL emission in Ga-rich GaN.

We assume that defects responsible for the RL2 and GL2 bands are native defects or complexes related to excess Ga, presumably deep compensating acceptors. Indeed, these bands were observed only in high-resistivity Ga-rich samples where the YL band, attributed to the Ga vacancy-related acceptor, disappeared. Ga_N is a good candidate since it is predicted to be a double acceptor with a large outward relaxation around it and with the energy level close to the middle of the band gap (see Sec. II B). It is possible that the RL2 and/or GL2 band results from transitions from the excited state of this defect to the ground state. Alternatively some complex defects may be responsible for the PL bands discussed in this section.

Hofmann *et al.*²⁵⁰ apparently observed the RL2 band (and did not observe GL2 band) in the MBE-grown GaN contaminated with oxygen and carbon in the upper 10^{19}-cm^{-3} range and suggested that $V_\text{N}C_\text{N}$ donors and $V_\text{Ga}O_\text{N}$ or $V_\text{Ga}Si_\text{Ga}$ acceptors could be responsible for this band. Unfortunately, the conditions used during growth, such as Ga- or N-rich conditions, were not revealed. Skromme and Martinez¹⁹⁹ observed red (at 1.73 eV) and green (at 2.35 eV) bands after implanting Mg into GaN. We assume that these were the same RL2 and GL2 bands caused by

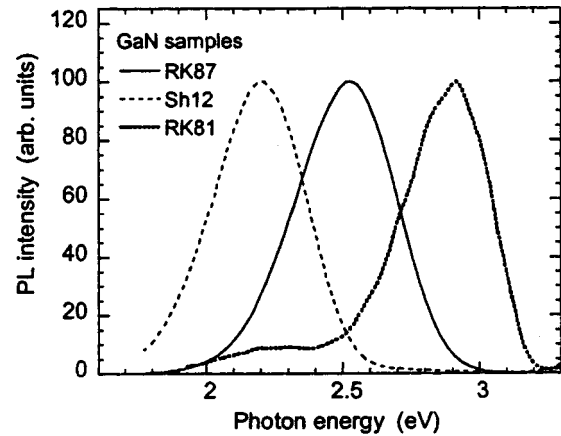


FIG. 57. PL spectra of undoped GaN samples grown by MOCVD on sapphire. $T = 200$ K.

implantation-induced native defects, rather than being directly related to the Mg impurity. Note that we observed the GL2 band in Mg-doped GaN grown by MBE in Ga-rich conditions, along with the broadened UVL band described in Sec. V B 3.

G. Other broad bands in undoped GaN

One of the less common PL features in undoped GaN is a rarely observed green PL band peaking at 2.5 eV.¹⁶⁰ Since the properties of this band are different from those of the GL band in high-purity GaN grown by HVPE and the GL2 band in Ga-rich GaN grown by MBE, we label it GL3. The spectrum of the GL3 band in comparison with the YL and BL bands is shown in Fig. 57. The quenching of this band at temperatures above 300 K with an activation energy of about 0.58 eV is attributed to thermalization of holes from the acceptor level to the valence band.¹⁶⁰ The GL3 band blue-shifted by about 10 meV with increasing excitation density from 10^{-4} to 10 W/cm², indicating that at low temperatures this band apparently involves transitions from a shallow donor to a deep acceptor. In contrast to the GL band in GaN grown by HVPE, the intensity of the GL3 band increased linearly with excitation intensity. From the temperature dependence of the peak position (Fig. 44) and FWHM (Fig. 45) of the GL3 band, the adiabatic parameters of the related deep defect have been evaluated.¹⁶⁰ In particular, the ZPL energy and the Huang-Rhys factor are 3.0 ± 0.05 eV and about 10 for this PL band.¹⁶⁰

In 1–2- μm -thick GaN layers grown by MBE on 5–10- μm -thick HVPE-GaN layers with underlying sapphire substrate, or on 200- μm -thick GaN templates, we sometimes observed a broad band peaking at about 2.6 eV, see Fig. 58. For its aquamarine color, we refer this band as the aquamarine luminescence (AL) band.²⁵⁷ The AL band was observed in several samples grown at relatively low temperatures under Ga-rich conditions. Often, the AL band appeared in the layers whose surfaces were covered with Ga droplets. However, removal of excess Ga from the surface did not affect the AL band intensity, indicating its bulk origin. At low temperatures, the AL band has a maximum at 2.55–2.56 eV and the FWHM of 380–400 meV. With increasing temperature,

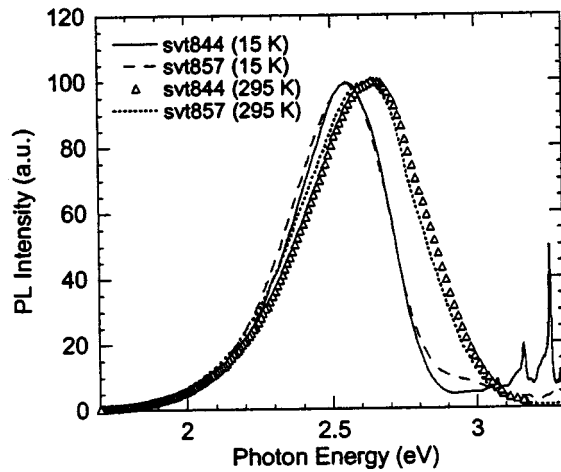


FIG. 58. Normalized AL band in GaN films grown by MBE on 10- μm HVPE layer (sample svt857) and on 200- μm HVPE freestanding template (sample svt844) at 15 and 295 K.

the AL band broadens, and its maximum gradually shifts to higher energies with a total shift of 80–90 meV up to room temperature (Fig. 58). Note that the band gap shrinks by about 65 meV in this temperature range. The AL band quenches at temperatures above 260 K with an activation energy of about 0.5 ± 0.1 eV. With increasing excitation density from 10^{-4} to 10 W/cm², the AL band shifted to higher energies by about 20 meV. The YL band could be detected in these samples only as a shoulder to the AL band at low excitation intensities. Although the shape and the peak position of the AL band are close to the characteristics of the GL band in a freestanding GaN template and the GL3 band in GaN layers grown by MOCVD, we distinguish these three bands for their different characteristics,²⁵⁷ as described above.

H. Characteristics and identification of radiative defects in undoped GaN

There have been numerous reports regarding the optical data on defects in undoped GaN, much of which are either incomplete and/or perhaps compromised by artifacts induced by experimental conditions such as high excitation intensity, bad thermal contact between the sample and the sample holder, lack of calibration of the spectral response, presence of other artifacts, etc. Consequently, we will quantify here only the bands measured under the same experimental conditions in our laboratory. The main characteristics of the PL bands in undoped GaN, such as the radiative efficiency, peak position, width, zero-phonon transition energy, typical lifetime, and activation energy, are given in Table III. Also tabulated are the estimated capture coefficients for electrons and holes by the radiative acceptors where the estimates are possible. The hole-capture coefficients have been evaluated from the temperature dependence of the defect-related PL intensity in its quenching region using Eqs. (6)–(10) while accounting for the QE and PL lifetime. The electron-capture coefficients have been evaluated from a TRPL study by using Eq. (20).

Most of the PL bands are attributed to unintentionally introduced or native acceptors. In particular, the UVL band is related to a shallow acceptor, the origin of which is still a topic of considerable debate. The shallow acceptor in question is Mg_{Ga} in Mg-doped or Mg-contaminated GaN, as will be shown in Sec. V B 1. However, in undoped GaN the acceptor in question may be Si_N or C_N. The deeper acceptor (about 0.34–0.4 eV above the valence band) is attributed to unintentionally introduced Zn impurity (see also Sec. V A 1). The YL and GL bands in high-quality GaN grown by HVPE are attributed to the two charge states ($2^-/-$ and $-/0$) of the V_{Ga}O_N acceptor. In less pure samples, V_{Ga}-containing defects bound to structural defects (e.g., dislocations) may contribute

TABLE III. Parameters of the PL bands in undoped GaN analyzed in our laboratory.

PL band	Growth method	Q.E. ^a (%)	Peak position (eV)		FWHM (eV)		ZPL (eV)	E_A (eV)	T_c^b (K)	W_{\max} (s ⁻¹)	Lifetime (μs)	C_n (cm ³ s ⁻¹)	C_p (cm ³ s ⁻¹)
T (K)			15	300	15	300				15	15	300 ^c	
UVL	MBE, MOCVD, HVPE	10	3.26				3.26	0.22	130	10^8	n.e. ^d	3	4×10^{-12} 1×10^{-6}
BL	MOCVD, HVPE	20	2.88	2.86	0.34	0.38	3.100	0.40	200	10^7	n.e.	10	4×10^{-13} 9×10^{-7}
YL	MBE, MOCVD	10	2.20–2.30	2.20–2.30	0.4–0.5	0.4–0.5	2.64	0.86	600	10^6	n.e.	400	7×10^{-14} 3×10^{-7}
YL	HVPE	2		2.22		0.58					n.e.	1500	1×10^{-13} 3.3×10^{-7}
GL	HVPE	2		2.48		0.53	2.9–3.0				n.e.	3.5	2×10^{-12} 1.5×10^{-7}
RL	HVPE	0.1		1.85		0.5	~ 2.2	~ 1.3			n.e.	5000	2×10^{-14}
RL	MBE	0.1		1.8–2.0		0.5	2.2–2.4	1.1–1.3					
RL2	MBE	1	1.79–1.88			0.3			100		110	2	
GL2	MBE	1	2.34–2.38			0.22–0.25			100		110	2	
GL3	MOCVD	5	2.51	2.53	0.39	0.48	~ 3.0	~ 0.5	280				
AL	MBE on HVPE	10	2.56	2.63	0.38–0.41	0.47–0.51	~ 2.9	~ 0.6	260		n.e.	20	$\sim 10^{-6}$

^aThe highest QE at low temperature.

^bCritical temperature above which the quenching takes place.

^cAt 300 K or at T_c , whichever is smaller.

^dn.e. = nonexponential

TABLE IV. Low-temperature parameters of the PL bands and related defects in doped GaN.

Dopant	PL band label	Maximum (eV)	ZPL (eV)	E_A (eV)	Selected Refs.
Zn	BL	2.88	3.100	0.40	199 and 267
	GL	2.6	2.85	0.65 ± 0.1	264
	YL	2.2	2.48	1.02 ± 0.05	264
	RL	1.8	2.08	1.42 ± 0.08	264
Mg	UVL	3.26	3.26	0.2	82, 199, and 312
	BL	2.7–3.0	~ 3.0	0.2;0.4	56, 82, and 308
	RL	1.7–1.8			309 and 354
C	BL	3.0–3.05			136 and 376
	RL	1.64	2.0 ± 0.2	1.5 ± 0.2	204
Be	UVL	3.38	3.38	0.1	203, 382, and 383
Ca	GL	2.5	2.8–2.9	0.6–0.7	202 and 387
Cd	BL	2.8	2.937	0.56	202 and 388
Mn	IR	1.27	1.6–1.8	1.8	396 and 393
Hg	GL	2.43	~ 2.7	0.8 ± 0.2	123
As	GL	2.6	2.952	0.56	202 and 397
P	BL	2.9	3.200	0.31	202 and 403

to the YL, as discussed in Sec. II E. Note that the role of C in the YL band remains questionable. We assume that the deeper acceptor, responsible for the RL band, is also a complex containing V_{Ga} . A variety of the RL band positions in GaN grown by MBE may reflect the influence of different structural defects on this acceptor. Although the data regarding the GL3 and AL bands are not exhaustive, it is clear from the already available studies that these bands are due to transitions from shallow donors (at low temperatures) or the conduction band (at elevated temperatures) to some deep acceptors. Two PL bands in Ga-rich GaN grown at low temperature by MBE, namely, RL2 and GL2 bands, have very special properties and have been tentatively assigned to internal transitions in some deep defects. Probably, the quenching of these defects is not followed by the release of carriers to the conduction or valence bands, but rather a manifestation of nonradiative recombination accompanied with emission of a large number of phonons. These defects might be native and related to excess of Ga (e.g., Ga_N or some complex). The exact microscopic origin of the defects in undoped GaN is not yet clear and would be a subject of future investigations.

The concentration of the dominant radiative acceptors in undoped GaN varies typically from 10^{15} cm^{-3} (in the freestanding templates) to about 10^{17} cm^{-3} (in thin layers on sapphire substrate). In the freestanding GaN templates from SAIT, the dominant acceptor is $V_{\text{Ga}}\text{O}_\text{N}$ complex at a density of about $(1-2) \times 10^{15} \text{ cm}^{-3}$. By using Eq. (15), we can to a first order estimate that these samples also contain about 10^{15} , mid- 10^{14} , and $\sim 10^{14} \text{ cm}^{-3}$ of acceptors responsible for the UVL, BL, and RL bands, respectively. Large capture coefficients for holes and small capture coefficients for electrons support the assignment of the majority of the broad PL bands in undoped GaN to acceptors. The hole-capture coefficients are consistent with the theoretical values for the multiply charged acceptors.⁶⁷ Similar values of the hole-capture coefficient (10^{-7} – $10^{-6} \text{ cm}^3/\text{s}$) have been obtained for the

$V_{\text{Ga}}\text{Te}_{\text{As}}$ acceptor responsible for the broad 1.2-eV band in n -type GaAs.⁹² Holes are captured very rapidly, in less than ~ 1 ns, by the acceptors, while the PL lifetime is quite long which ranges from microseconds to milliseconds. This ratio determines the balance of carriers in undoped n -type GaN: the lifetime of nonequilibrium holes is less than 1 ns, and the competition for these holes dictates the quantum efficiency for each recombination channel.

V. INTENTIONALLY INTRODUCED IMPURITIES AND NATIVE DEFECTS

In this section we discuss the luminescence data related to impurities and native defects that are intentionally introduced or created in GaN. The main characteristics for the luminescence bands and related impurities in GaN in terms of their peak position, measured or expected energy position of the zero-phonon transitions, and activation energy of the defects involved are summarized in Table IV.

A. Luminescence in Zn-doped GaN

Doping of GaN with Zn results in semi-insulating material with a room-temperature resistivity up to $10^{12} \Omega \text{ cm}$, which makes it attractive for high-power microwave devices which require high-resistivity buffer layers.²⁵⁸ Moreover, well before the conductive p -type GaN became available, green and blue LEDs were fabricated by using insulating GaN:Zn.^{259,260} Note, however, that in the early stages of GaN growth, doping with Zn often could not compensate unintentionally introduced shallow donors, so that GaN:Zn often remained degenerate n type.^{261,262}

Monemar *et al.*^{263,264} have established that Zn doping introduces four acceptorlike centers in GaN responsible for the broad red (RL), yellow (YL), green (GL), and blue luminescence (BL) bands peaking at about 1.8, 2.2, 2.6, and 2.9 eV, respectively. Among those four peaks, the one receiving the most attention is the BL band with a characteristically

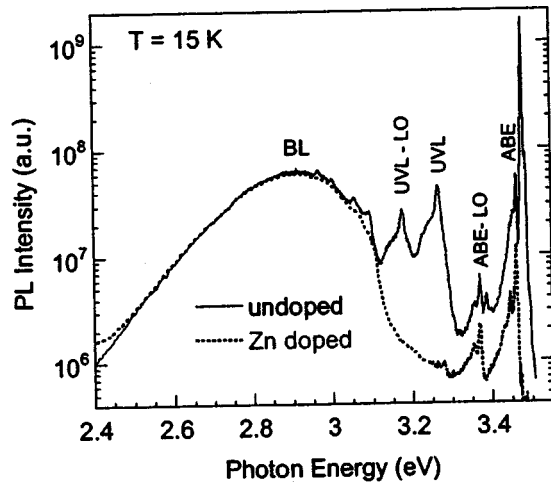


FIG. 59. Low-temperature PL spectrum of undoped and Zn-doped GaN layers grown by HVPE on sapphire. The intensity is normalized at maximum of the BL band.

very bright emission dominating the PL spectrum at moderate ($<10^{19} \text{ cm}^{-3}$) doping levels.^{261–263} As will be shown below, the BL band in Zn-doped GaN apparently has the same origin as the BL in undoped GaN grown by MOCVD and HVPE (see Sec. IV D). A word of caution is that this peak should not be confused with the BL band in Mg-doped GaN which is discussed in detail in Sec. V B 3.

1. Blue luminescence band

The BL band in Zn-doped GaN has been observed in degenerate *n*-type material,^{261–263} as well as in insulating layers.^{245,258,259,261,263,267} Ilegems *et al.*²⁶² reported that the BL band maximum shifted from 2.91 to about 2.81 eV with increasing Zn doping, presumably due to the presence of several defects. In another study, the energy position of the BL band was nearly independent of the doping level.²⁶¹ In moderately doped GaN samples ($[\text{Zn}] < 10^{19} \text{ cm}^{-3}$) the BL band always appeared at $2.88 \pm 0.04 \text{ eV}$ at low temperatures.^{199,261,263,265–267} Remarkably, the shape and energy position of the BL band in lightly Zn-doped GaN ($[\text{Zn}] < 10^{18} \text{ cm}^{-3}$) coincide with the parameters of the BL in undoped GaN (Fig. 59).^{199,245} Even the fine structure observed in the best-quality crystals, including the zero-phonon line at 3.100 eV,^{199,200,245} is identical to the phonon-related structure in undoped GaN described in Sec. IV D 1. This observation, as well as other arguments given below, strongly suggests that the BL in undoped and Zn-doped GaN have the same origin and caused most likely by Zn.

Another supporting evidence that the BL bands in undoped and Zn-doped GaN samples have the same origin follows from the analysis of the excitonic part of the PL spectrum (Fig. 60). It is well known that excitons can be bound to a Zn acceptor (which is responsible for the BL band), resulting in the acceptor-bound-exciton (ABE or A^0X) emission at about 3.46 eV, followed by strong LO phonon replicas.^{199,200,245,267–270} The exact energy position of the ABE line is sample dependent in strained layers grown on sapphire, whereas in strain-free GaN it is located at 3.455 eV and, in fact, represents a triplet.²⁶⁸ The Zn-related ABE has a

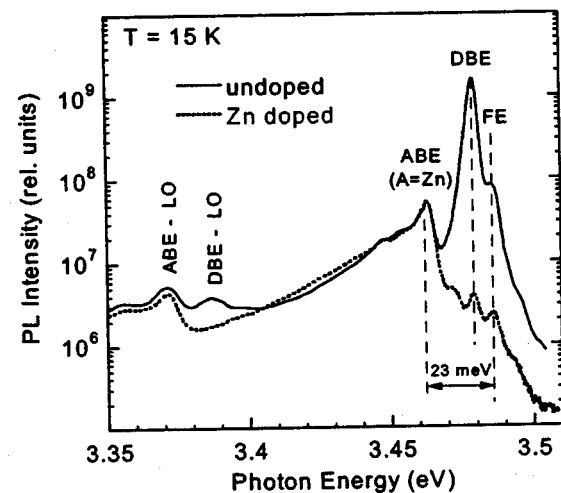


FIG. 60. Excitonic region of the low-temperature PL spectrum of undoped and Zn-doped GaN layers grown by HVPE on sapphire. The intensity is normalized at maximum of the ABE line.

localization energy of $23 \pm 1.5 \text{ meV}$ with respect to the free *A* exciton (Fig. 60).^{199,267,269} Scattered data for this value in the literature (from 19 to 34 meV) (Refs. 262 and 270) are probably related to broadening of the exciton lines in low-quality crystals. The Zn-related exciton lines, including phonon replicas, are very strong in the Zn-doped layer, and their shape and energy positions coincide with the corresponding lines in undoped GaN. Note that an observation of the strong Zn-related ABE lines in undoped GaN always correlates with the observation of the strong BL band in these samples.^{268,245} Although the BL band in Zn-doped GaN can be attributed with certainty to the same acceptor as that in undoped GaN (Sec. IV B), below we will present the main features of the BL in Zn-doped GaN because high concentration of defects and different positions of the Fermi level can affect the PL properties markedly.

a. Effect of temperature. The thermal quenching of the BL band in *undoped* GaN always takes place above 200 K with an activation energy of about 340–380 meV. In sharp contrast, a wide variety of the activation energies and temperature ranges of the quenching can be found for BL in GaN:Zn. In some Zn-doped samples, the BL band quenches above $\sim 200 \text{ K}$ with an activation energy of about 330 meV,^{261,262,267} yet activation energies of about 130 meV (deduced from the data for the sample Zn–V in Fig. 15 of Ref. 263) and 640 meV (Ref. 267) have been also reported. In some samples, the quenching of the BL band is negligible at room temperature^{263,265} and even at 500 K.²⁷¹

A significantly different temperature behavior of the BL band has been observed from two sides of the GaN:Zn layer ($[\text{Zn}] < 10^{18} \text{ cm}^{-3}$) grown on sapphire by HVPE.²⁶⁷ In contrast with the insulating nature of the main part of the 10- μm -thick GaN:Zn film (resistivity of $\sim 10^9 \Omega \text{ cm}$ at 300 K), the $\sim 0.2\text{-}\mu\text{m}$ -thick region close to the sapphire substrate was highly conductive ($\sim 3 \times 10^{-3} \Omega \text{ cm}$), with an estimated concentration of free electrons well above 10^{19} cm^{-3} .²⁷² Since the PL signal is collected from a depth of about 100–200 nm, the effect of Zn doping on GaN with large concentration of free electrons (backside) and high-resistivity GaN (front

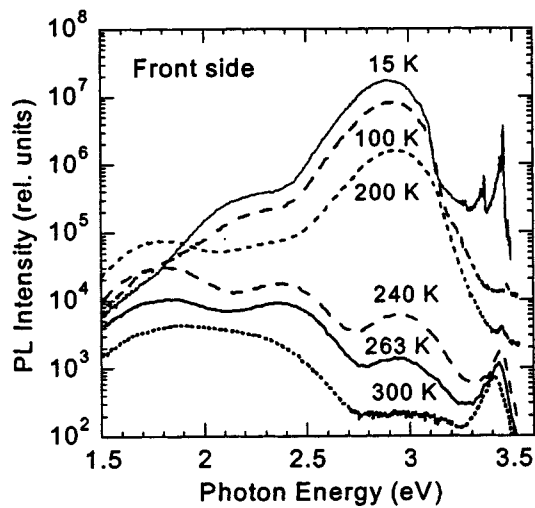


FIG. 61. PL spectra of high-resistivity Zn-doped GaN grown on sapphire (front side) at different temperatures. Excitation density is 0.1 W/cm^2 . Reprinted with permission from Reshchikov *et al.*, Mater. Res. Soc. Symp. Proc. 693, I2.10 (2002).

side) could be compared by exciting and collecting the PL signal from either the top surface or the interfacial region next to the substrate. A strong BL band dominated the PL spectrum from both sides of the sample, although the energy position of the BL band from the backside was shifted to higher energies, presumably due to high concentration of electrons in the degenerate near-interfacial layer. The dependencies of PL intensity on temperature are quite different for two sides of the GaN layer.²⁶⁷ The dramatic decrease of intensity of BL in semi-insulating GaN:Zn, top surface, between 200 and 260 K can be seen in comparison with the other PL bands in this sample (Fig. 61). After quenching of the BL band at $T > 200 \text{ K}$, the RL band peaking at 1.8 eV and the GL band peaking at 2.4 eV emerge. The large activation energy for quenching of BL (640 meV) when it is observed from the front side contrasts a small activation energy of 250 meV for quenching of the BL band associated with the backside. This is a very intriguing experimental observation that needs to be explained when sufficient data are available. We have tentatively attributed the rapid quenching to thermally activated transfer of the bound holes to some associated nonradiative defects, the exact mechanism and the origin of which are unclear.²⁶⁷

In spite of the shrinkage of the energy gap in GaN, the BL band with no substantial shift has been reported in some publications with increasing temperature up to 300 K.^{261,263,265} In other reports, even a shift to higher energies by about 50 meV has been reported.^{262,267} The invariance of the BL position with temperature is similar to the behavior of the BL band in undoped GaN (Fig. 44), whereas the shift to higher energies could be related to a high concentration of defects or presence of potential fluctuations in Zn-doped GaN. We will discuss possible reasons of the large shifts of the BL band with temperature in Sec. V A 1 b after presenting the effect of excitation intensity on this band.

b. Effect of excitation intensity. The intensity of the BL band increased linearly with the excitation intensity over a wide range,^{261,267} whereas the exciton emission increased lin-

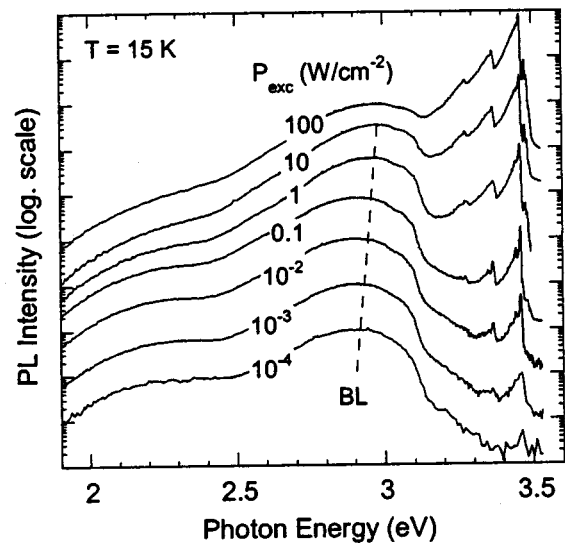


FIG. 62. Low-temperature PL spectra at different excitation intensities from high-resistivity GaN:Zn layer grown by HVPE on sapphire (front side).

early in the case of the degenerate GaN:Zn and increased superlinearly (with a power $3/2$) in the case of semi-insulating GaN:Zn (Fig. 62).²⁶⁷ This observation can be explained as follows: The intensity of the acceptor-related PL depends only on the concentration of photogenerated holes, whereas the exciton or near-band-edge emission intensity is proportional to product of photogenerated holes and free electrons.⁶⁷ In the degenerate *n*-type layer, the concentration of free electrons is independent of the excitation intensity up to sufficiently high excitation levels. In the insulating layer, however, the concentration of the free electrons increases with excitation for all excitation levels employed. A very broad near-band-edge emission peak extending well above the band gap also confirms a high concentration of free electrons in the interfacial layer.²⁶⁷

The shift of the BL in undoped GaN with excitation intensity is very small, similar to the shift of the UVL band attributed to the DAP transitions (Sec. IV D 1). In lightly Zn-doped GaN, a very similar shift has been established in the samples exhibiting the BL band with a characteristic fine structure.^{199,200} In some investigations, the excitation intensity was reported not to affect the energy position of the BL band in GaN:Zn.^{263,273} In contrast, others reported a substantial UV shift (about 50–70 meV) in the insulating GaN:Zn samples when the excitation intensity was varied by more than a factor of 10^4 .^{245,261} and the dynamics of the shift was sample dependent.²⁶⁷ It was suggested that pinning of Zn acceptors to dislocations and the effect of the latter on the energy levels of the acceptors cause the broadening and shift of the BL band in GaN:Zn.^{263,267} The results of annealing experiments using the Zn-implanted GaN could also be explained by assuming that Zn ions are gettered at dislocations.²⁷⁴ However, similar shifts of the BL band have also been observed in nearly dislocation-free bulk GaN.²⁷⁵ We suggest that the DAP-type recombination involving several donors and the same Zn acceptor may be responsible for the observed shifts. Indeed, in undoped GaN the Fermi level is close to the conduction band and the shallow donors are

mostly filled with electrons at low temperatures. The probability of the DAP transition decreases exponentially for deeper donors due to a smaller overlap of the electron and hole wave functions. Note also the relatively high concentration of shallow donors in undoped GaN. Therefore, the contribution to the BL band from deeper donors may be neglected in *n*-type conductive GaN. In contrast, the shallow donors may contribute much less due to their smaller occupancy in semi-insulating GaN:Zn. The transitions from deeper donors are slower and, hence, with increasing excitation density the intensity of transitions involving the deeper donors would begin to saturate at relatively lower excitation levels, causing a shift of the broad band with excitation intensity. Another manifestation of this effect is the shift of the PL band with the delay time, as discussed below.

c. Time-resolved PL. TRPL studies have revealed a nearly exponential decay of the BL band in GaN:Zn with a lifetime of about 300–400 ns,^{262,266} which is independent of Zn doping.²⁶² Slower decays have been observed in insulating GaN:Zn.^{245,261,267} Some of the experimental observations appear unusual and need further explanation. According to Eq. (20), the PL lifetime should be inversely proportional to the electron concentration in *n*-type GaN. In the semi-insulating material, however, the lifetime may be sensitive to the excitation intensity since the latter may affect the concentration of electrons in the conduction band. However, the decay of the BL in high-resistivity GaN:Zn did not change when the excitation intensity was varied by a factor of 10^5 .²⁶⁷ Moreover, similar lifetimes (300–400 ns) have been obtained for the conductive *n*-type GaN:Zn samples with the free-electron concentrations of $\sim 10^{18} \text{ cm}^{-3}$ (Ref. 266) and $(1\text{--}6) \times 10^{19} \text{ cm}^{-3}$.²⁶² Earlier, we suggested that BL in GaN:Zn involves transitions not from the conduction band but from the excited state of the Zn-related defect, which would result in a lifetime independent of carrier concentration. However, now it is firmly established that in undoped and lightly Zn-doped GaN the BL band is caused by transitions from the shallow donors (at low temperature) and from the conduction band (at elevated temperatures) to the Zn-related acceptor. Moreover, in different semi-insulating GaN:Zn samples the decay of the BL is not identical, as displayed in Fig. 63. In this figure we also show, for comparison, the decay of the BL band in undoped and Si-doped GaN samples with concentration of the shallow donors of 6×10^{17} and $3 \times 10^{18} \text{ cm}^{-3}$, respectively. The decays are nonexponential as it is expected for the DAP recombination at low temperatures. In *n*-type conductive material, the decay rate correlates with the concentration of shallow donors (see Sec. III B). In semi-insulating Zn-doped layers, the decay is distinctive for each sample because the distribution of the shallow and not very shallow donor states may be different in these samples.²⁴⁵ Similar to the TRPL results on the BL band in undoped GaN (Sec. IV D 2), the lifetime of BL in GaN:Zn decreases above $\sim 200 \text{ K}$ with an activation energy of about 300–400 meV,²⁴⁵ consistent with Eq. (22).

No shift in the BL band with delay time has been detected in degenerate GaN:Zn.²⁶² In contrast, Khan *et al.*²⁶⁵ observed a redshift of $\sim 20 \text{ meV}$ after $0.8 \mu\text{s}$, as well as two peaks in the TRPL spectrum. We also observed a redshift of

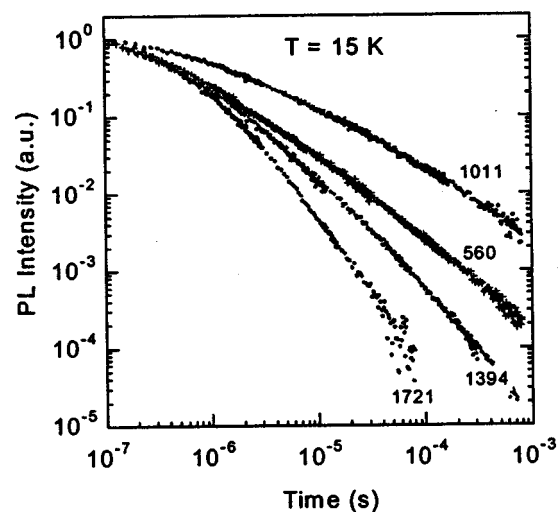


FIG. 63. PL intensity decay of the BL (at 2.9 eV) in undoped (1011), Si-doped (1721), and two Zn-doped (560 and 1394) GaN layers grown by HVPE on sapphire. Note the logarithmic scales. Reprinted with permission from Reshchikov *et al.*, Mater. Res. Soc. Symp. Proc. 693, 12.10 (2002).

up to 50 meV at $10 \mu\text{s}$ after the excitation pulse in semi-insulating GaN:Zn. These shifts are consistent with the model that several donors with ionization energies up to about 100 meV contribute to the PL decay in high-resistivity GaN:Zn. Note that the origin of the shift of the BL band with excitation intensity is different in Zn- and Mg-doped GaN, as discussed in Sec. V B 3.

d. Resonant excitation and vibrational properties. Monemar *et al.*²⁶⁴ investigated the BL band in Zn-doped GaN under resonant (below-band-gap) excitation. In the PLE spectrum related to the BL band, a steep increase of the optical cross section (about four orders of magnitude) has been observed at photon energies between 3.0 and 3.25 eV. This PLE spectrum has been attributed to transitions from the Zn-related acceptor to the conduction band.²⁶⁴ With the aid of an analysis of the absorption spectrum, Monemar *et al.*²⁶⁴ have also estimated the absolute value of the optical cross section for the BL band as approximately 10^{-16} cm^2 .

Although Monemar *et al.*^{263,264} identified the type of transitions in GaN:Zn and thoroughly examined the role of the electron-phonon coupling in these transitions, their quantitative results regarding the vibrational characteristics need to be revised in light of the recent data. It is well established that interaction with local ($\sim 36 \text{ meV}$) and lattice (91 meV) phonons is responsible for the characteristic fine structure of the BL band in undoped and Zn-doped GaN.^{116,199,200} The high-energy side of the BL band contains sharp peaks while the low-energy side is structureless (Fig. 42), similar to other classical cases of the electron-phonon coupling in semiconductors.²⁷⁶ The fine structure observed in Ref. 263 may actually be some sort of artifact rather than the result of the electron-phonon coupling for the following reasons: (i) The energy separation between peaks is $74 \pm 2 \text{ meV}$, which is different from the known phonon modes in GaN; (ii) the peaks at the low-energy side are better resolved than those at the high-energy side, which contradicts the common observations;^{116,276} (iii) the zero-phonon line is very broad

(>100 meV), which is contrary to the typical examples;^{116,276} and (iv) the fine structure is visible up to room temperature whereas it usually disappears at relatively low temperatures.

e. ODMR and defect identification. While PL studies are capable of revealing the type of transitions, and sometimes the type of defects involved (donors, acceptors, singly or multiply charged), the ODMR studies are able to establish the symmetry and microscopic origin of defects. The results of ODMR investigations involving the BL band in Zn-doped GaN have been reported in Refs. 277 and 278. In one of these studies Kunzer *et al.*²⁷⁷ detected two magnetic signals on the BL band in GaN:Zn. A weaker, nearly isotropic signal with $g \approx 1.95$ has been attributed to the effective-mass shallow donor. A stronger signal with $g_{\parallel}=1.997(2)$ and $g_{\perp}=1.992(2)$ has been attributed to Zn acceptor. Thus, transitions from the shallow donor to the Zn-related acceptor at low temperatures, as deduced earlier from the PL studies, have been confirmed by the ODMR study of Kunzer *et al.* Hai *et al.*²⁷⁸ also observed the above two signals associated with the BL band in GaN:Zn (with $g_{\parallel}=1.951$ and $=2.012$, respectively). However, they have also detected a signal (labeled as Ga-1) representing the characteristic fine structure of a single Ga atom. The axial symmetry C_{3v} of this center has been established from the angular dependence study. From these data, the Ga-1 center has been assigned to an axial complex of Ga_i with another defect, possibly Zn.²⁷⁸ Note that the spectral dependence of the ODMR signal Ga-1 is consistent with the position and shape of the BL band in these samples.

It may be concluded that the BL band in undoped and Zn-doped GaN is caused by transitions from the shallow donors or the conduction-band electrons to the acceptor level associated with Zn. However, the symmetry and exact microscopic structure of this acceptor remain unknown. Theoretical calculations predict that Zn_{Ga} is an acceptor in wurtzite GaN with an activation energy of 330–400 meV.^{37,38,279} This value is consistent with the position of the ZPL of the BL at about 3.1 eV.^{199,245,263} It is possible that the acceptor responsible for the BL band is just Zn_{Ga} , while the Ga-1 defect is indirectly involved in the recombination process, but not necessarily in all samples. Hydrostatic pressure experiments revealed that the shift of the BL band in Zn-doped GaN is similar to that of the GaN band gap with pressure.²⁷¹ This also confirms the model of transitions from the conduction-band or shallow donors to the Zn-related acceptor. Assignment of the BL in Zn-doped GaN to the e-A or shallow DAP transitions, and not to deep DAP transitions, contrasts the attribution of the BL band in Mg-doped GaN. The difference between these two models is discussed in more detail in Sec. V B 3.

2. Green, yellow, and red luminescence bands

Much less is known about other PL bands in GaN:Zn. The RL, YL, and GL bands, peaking at 1.8, 2.2, and 2.6 eV, respectively, appeared and sometimes dominated in heavily Zn-doped GaN.^{263,264} All three bands are broad due to strong electron-phonon coupling. Large shifts of the YL band with excitation intensity and temperature have been attributed to

the presence of several Zn-related centers with closely spaced energy levels but different saturation properties.²⁶³ These broad bands could be selectively excited by photons with energies below the band gap. From an analysis of the band shape, the RL, YL, and GL bands have been attributed to acceptors with estimated binding energies of 1.42 ± 0.08 , 1.02 ± 0.05 , and 0.65 ± 0.08 eV, respectively.^{263,264} Monemar *et al.*²⁶³ speculated that the RL, YL, and GL bands may originate from the three charge states of the Zn_N acceptor. Boulou *et al.*²⁸⁰ observed shifts of the BL, GL, and YL with excitation intensity in GaN:Zn, as well as nonexponential decay of these bands after pulsed excitation, and attributed these bands to distant DAP transitions. Linear polarization of the GL band in electroluminescence has been reported and attributed to superposition of polarized emission from Zn_{Ga} and Zn_N .²⁸¹ We observed also persistent luminescence effects for the GL band in semi-insulating GaN:Zn.

B. Luminescence in Mg-doped GaN

Magnesium is the most critical impurity in GaN because it is the only dopant that enables one to obtain reproducible *p*-type GaN. Although Mg_{Ga} is a shallow acceptor,^{282–284} the early attempts with Mg doping were not successful for most likely two reasons: (i) Hydrogen which is always present in MOCVD and HVPE growth passivates Mg by forming electrically and optically inactive complexes²⁸⁵ and (ii) heavily doped GaN is notorious for self-compensation.⁵⁶ Later it was determined that passivation with H during growth is, in fact, favorable for obtaining high-conductivity *p*-type GaN. Indeed, a lack of shift of the Fermi level towards the valence band due to H passivation facilitates incorporation of Mg, as discussed in Sec. II C.⁵⁹ Postgrowth treatments allow the conversion of the high-resistivity as-grown GaN:Mg into conductive *p* type. Hydrogenated Mg can be activated by annealing at temperatures above ~ 600 °C,^{286–290} by electron-beam irradiation,^{291,292} or even by UV illumination at temperatures above 500 °C.²⁹³ In contrast, self-compensation is a permanent effect and cannot be changed by annealing *per se*. In GaN:Mg grown by MOCVD, the concentration of free holes at room temperature reaches its maximum value at about 10^{18} cm⁻³ for a Mg concentration of about 3×10^{19} cm⁻³, and it decreases with further increase of Mg concentration (Fig. 64).²⁹⁴

It is not well established which levels are introduced by which defects in GaN as a result of Mg doping. The only firmly established fact is that Mg doping efficiently introduces the shallow acceptor Mg_{Ga} with an ionization energy of ~ 200 meV.^{287,288} Assumption that Mg doping introduces optically active deep acceptors^{141,286,295–302} has not been confirmed by experimental results which are presented below. Instead, one or more compensating deep donors are formed at high doping levels, affecting the optical properties of GaN:Mg.^{56,82,172,190,294,300,303,304} The origin of the compensating donors is still a topic of considerable debate.

A study of optical emission in Mg-doped GaN helps us to understand the material properties and defect formation in *p*-type GaN. It is well established that upon low and moderate doping with Mg, a strong enhancement of the UVL band,

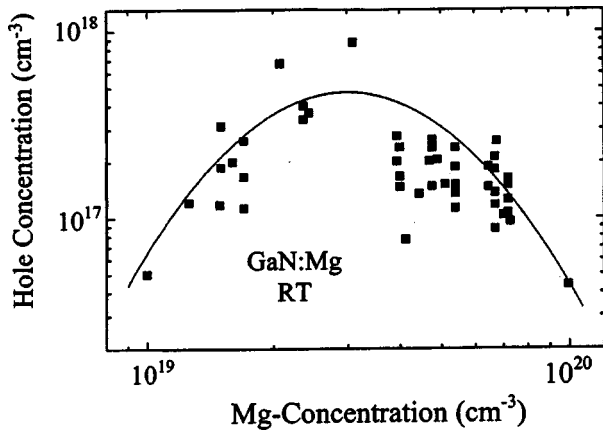


FIG. 64. Room-temperature concentration of free holes in Mg-doped GaN as determined from the Hall effect vs concentration of Mg obtained from SIMS measurements. The solid line is a guide to the eye. Reprinted with permission from Obloh *et al.*, *J. Cryst. Growth* **195**, 270 (1998). Copyright (1998) by Elsevier.

representing a relatively sharp peak at about 3.26 eV followed by a few LO phonon replicas, takes place.^{199,201,295,298,305–307} At a certain doping level, the peaks of the UVL band broaden, redshift,^{82,306,308} and apparently transform into a single structureless band peaking at about 3.2 eV.^{56,82,296,297,308,309} Further, at concentrations of Mg above 10^{19} cm^{-3} a broad BL band with a maximum at about 2.7–2.9 eV emerges and typically dominates the PL spectrum of heavily doped GaN.^{294,298,304,308} It was noted that, while the BL band emerges as the dominant transition, the hole concentration saturates and decreases with further Mg doping, suggesting a self-compensation process.²⁹⁴ Several investigators also noted that potential fluctuations may be substantial in heavily doped GaN and must be taken into account.^{82,299,306,310} Potential fluctuations appear in highly compensated or heavily doped semiconductors as a result of random distribution of charged impurities such as donors and acceptors.⁹¹ In an *n*-type material the potential fluctuations are usually screened by free electrons. However, in heavily Mg-doped GaN having almost no equilibrium holes, especially at low temperature, one may expect significant potential fluctuations. Existence of several types of deep donors may further complicate the analysis of the PL data.

Below we present an analysis of the Mg-doped GaN in some detail. Ironically, several mechanisms, such as DAP transitions, potential fluctuations, presence of several defect levels in the band gap, and polarization effect in macrodefects, may exhibit very similar behavior in the PL spectrum of GaN:Mg. In Sec. V B 6, we discuss possible transitions and assignment of the main PL bands in Mg-doped GaN.

1. Ultraviolet luminescence band in lightly Mg-doped GaN

The UVL band in Mg-doped GaN is very similar to the UVL band in undoped GaN. This property may indicate that different shallow acceptors, such as Mg_{Ga} and Si_{N} , manifest themselves similarly in GaN. However, the fine structure of the UVL band associated with transitions between pairs with fixed separation has been observed only in Mg-doped

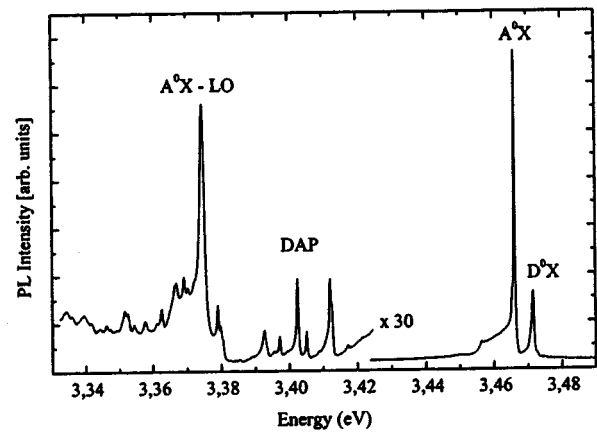


FIG. 65. Low-temperature (4.2 K) PL spectrum of a Mg-doped GaN sample. Reprinted with permission from R. Stepniewski *et al.*, *Phys. Status Solidi B* **210**, 373 (1998).

GaN.^{311,312} Those high-quality *p*-type GaN layers with low concentration of Mg ($\sim 10^{17} \text{ cm}^{-3}$) have been grown on bulk GaN platelets. The near-band-edge spectrum contained a donor-bound-exciton line D^0X at 3.472 eV, a strong acceptor-bound-exciton line A^0X at 3.467 eV, and a series of lines with FWHM of the order of 1 meV. The latter has been attributed to DAP transitions with different separations (Fig. 65). The energy positions of the DAP-related lines and their relative intensities remained unchanged versus Mg concentration. With increasing temperature, the A^0X line and its phonon replica diminished at about 32 K, while the DAP-related lines remained well resolved at least up to 39 K.³¹² The transition energy for each DAP emission depends on the pair separation due to the Coulomb interaction between ionized centers in the final state of the recombination process according to Eq. (29). The dependence of the DAP transition energies versus reciprocal DAP separation is a straight line, as shown in Fig. 66, which enables one to determine the static dielectric constant ($\epsilon=9.6$) and the sum of the isolated donor and acceptor binding energies (296 meV).³¹² The analysis of the pair spectra revealed that donors and acceptors involved in the DAP emission are located in different sublattices. It is tempting to identify them as Mg_{Ga} and O_{N} . With a well-determined binding energy of O_{N} (33 meV),²³⁰ the Mg_{Ga}

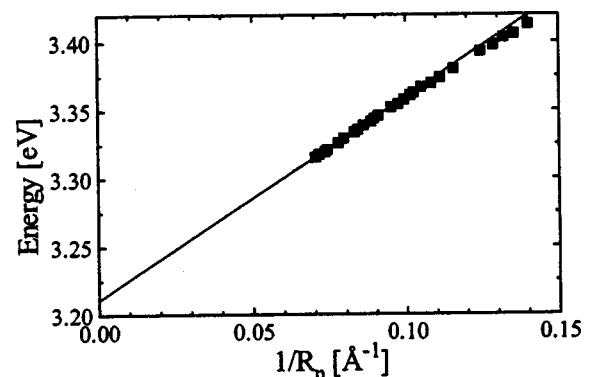


FIG. 66. Variation of the energy of the DAP transitions vs the reciprocal DAP separation for the Mg_{Ga} acceptor in GaN. Reprinted with permission from R. Stepniewski *et al.*, *Phys. Status Solidi B* **210**, 373 (1998).

binding energy of about 260 meV can be deduced. Note that even in the purest GaN crystals (which at present are free-standing templates grown by SAIT, Korea) with donor concentration of about $2 \times 10^{16} \text{ cm}^{-3}$, the average separation in DAP is about 200 Å. Therefore, the Coulomb shift of about 60 meV is expected (Fig. 66) for distant pairs forming a broad zero-phonon peak of the UVL band that is usually observed at about 3.26–2.27 eV in GaN. Note that the binding energy of Mg_{Ga} determined from the energy position of the e-A transition of the UVL band in lightly Mg-doped GaN (224 meV) (Ref. 199) is also affected by the Coulomb interaction between shallow acceptors and ionized donors in GaN:Mg.

The UVL band related to the Mg_{Ga} acceptor is the dominant PL band in lightly and moderately doped GaN:Mg with Mg concentrations below $\sim 10^{19} \text{ cm}^{-3}$.^{199,201,295,298,305–307,313} When the concentration of Mg becomes comparable to the concentration of residual shallow donors, usually $10^{17}–10^{18} \text{ cm}^{-3}$, Mg-doped GaN becomes semi-insulating. Substantial potential fluctuations may arise in such a material due to inhomogeneous distribution of charged defects and low concentration of free carriers.

2. Effect of potential fluctuations on PL

It is important to consider the effect of potential fluctuations on the properties of Mg-doped GaN while interpreting the experimental results. Potential fluctuations originating from the Poisson distribution of charged point defects play a very important role in the properties of compensated semiconductors.^{80,91} In Mg-doped GaN significant potential fluctuations are expected because the concentration of free carriers is usually too small to screen them. In the limit of a high degree of compensation, the amplitude γ and size r_s of a typical potential fluctuation can be expressed as⁹¹

$$\gamma = \frac{e^2}{4\pi\epsilon_0\epsilon} \frac{N_t^{2/3}}{p^{1/3}}, \quad (34)$$

$$r_s = N_t^{1/3} p^{-2/3}, \quad (35)$$

where $N_t = N_A + N_D$ is the combined concentration of acceptors and donors and, p is the concentration of free carriers. The other parameters have their usual meanings. As can be seen from Fig. 67, the typical fluctuation amplitude can be very large in Mg-doped GaN, commonly characterized with $N_t = 10^{19}–10^{20}$ and having concentration of free holes less than 10^{18} cm^{-3} at room temperature. With decreasing temperature, the potential fluctuation amplitude and size dramatically increase due to strong temperature dependence of the free hole concentration. Evidently the increase of the amplitude is limited by the band-gap energy because the screening increases with the Fermi level approaching the valence and conduction bands at the extreme points.

The effect of potential fluctuations on PL in compensated semiconductors has been studied within the framework of the above concept both theoretically⁸⁰ and experimentally.^{82,314–320} The energy of the emission has been simulated by the following expression:

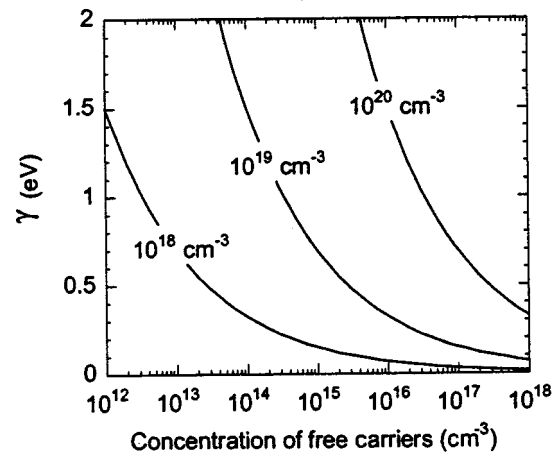


FIG. 67. Expected typical amplitude of potential fluctuations in p -type GaN:Mg with the combined concentration of donors and acceptors $N_t = 10^{18}, 10^{19}$, and 10^{20} cm^{-3} .

$$\hbar\omega = E_g - 2\gamma, \quad (36)$$

in the case of transitions from the conduction band to the valence band,^{80,319} or by

$$\hbar\omega = E_g - (E_D + E_A) - 2\gamma, \quad (37)$$

in the case of DAP transitions,^{314,315,317,318} where the parameter γ was estimated from Eq. (34). Equations (36) and (37) are obtained assuming that after excitation the photogenerated electrons and holes relax quickly to the potential minima and maxima of the conduction band and the valence band, respectively (Fig. 68). Then they recombine with the probability determined by the degree of overlap of the wave functions of the recombining carriers.^{80,319} In the case of the DAP recombination, the photogenerated carriers are first captured by donors and acceptors, resulting in an additional terms in Eq. (37). In both cases, the spatial separation of the recombining carriers results in diagonal transitions with reduced energy and slower dynamics. Increasing the excitation intensity flattens the potential fluctuations according to Eq. (34), and the PL bands shift to higher photon energies, approaching the shape and position ascribed to uncompensated semiconductor.^{80,82,316,319} It follows from the above arguments that Eqs. (36) and (37) can be used only when the wave function of at least one carrier is large enough, namely, comparable to the spatial size of potential fluctuations.

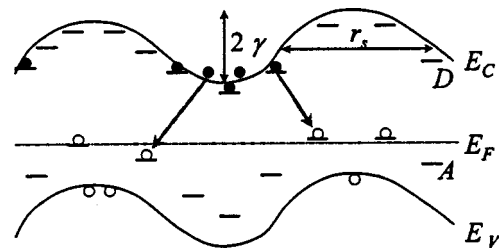


FIG. 68. Schematic representation of bands and defect levels in the presence of long-range potential fluctuations under conditions of PL. The arrows indicate diagonal transitions resulting in redshifted PL bands. Photogenerated electrons and holes are shown as filled and empty circles, respectively.

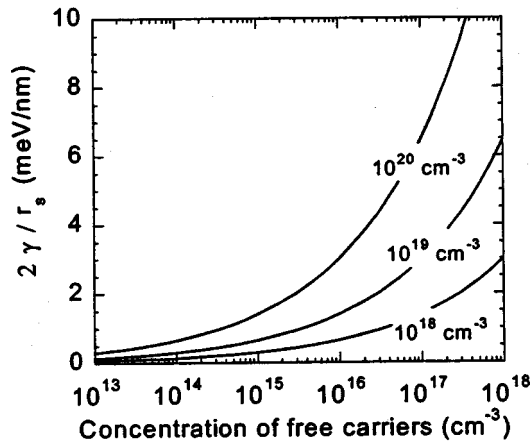


FIG. 69. Estimated average slope of potentials in compensated *p*-type GaN:Mg with the combined concentration of donors and acceptors $N_A = 10^{18}$, 10^{19} , and 10^{20} cm^{-3} .

In the case of giant potential fluctuations in GaN:Mg, a sizable portion of free carriers would be captured by donors and acceptors before they thermalize to the potential minima or maxima. The broadening and shift to lower photon energies at low excitation intensities would be governed by the ratio between the wave-function size and the slope of the potential at a particular point. The larger this ratio, the larger the broadening and the shift would be. The average slope of the potential, $2\gamma/r_s$, calculated from Eqs. (34) and (35) for typical concentration of defects and free carriers in GaN:Mg in PL experiments is shown in Fig. 69. Special attention must be paid to the following two features. (i) The potential slope is typically very small so that the wave-function size of the order of 1 nm or less can hardly cause any broadening and shift of the PL bands more than 10 meV due to potential fluctuations. (ii) The slope of the potential *increases* with increasing carrier concentration, i.e., with increasing excitation intensity. This means that with increasing excitation intensity, we would expect the shift of the PL bands not to higher but to lower photon energies, unless the wave-function and fluctuation sizes are comparable. However, in all reports on the BL in GaN:Mg, increasing excitation intensity resulted in shifts only to higher energies. The question then arises whether there are no potential fluctuations in GaN:Mg or the aforementioned concept is inapplicable. The concept of the long-range potential fluctuations, developed by Shklovskii and Efros⁹¹ is well validated, but in the case of wide-band-gap semiconductors with relatively deep defect levels it can only be used for a qualitative interpretation. It is most likely that the short-range potential fluctuations^{80,91} resulting in transitions between local minima and maxima play a more important role in the broadening and shifts of the PL bands in GaN:Mg. Moreover, the effects caused by potential fluctuations and the DAP nature of transitions are very similar, as will be discussed in more detail below.

It is very difficult to distinguish the DAP transitions and transitions between carriers (free or bound) that are localized by potential fluctuations. The electrons inside the potential valleys and holes inside potential hills are spatially localized, resembling point defects. Therefore, the signatures of PL in a

semiconductor with potential fluctuations may resemble that of the DAP transitions. In particular, the PL decay becomes slow and nonexponential in compensated semiconductors due to spatial localization of carriers.^{226,319} In the case of potential fluctuations the PL bands are blurred and shifted to lower energies for low excitation intensities because the transitions are diagonal, as shown in Fig. 68. In the case of DAP transitions the PL band also has the lowest energy at low excitation intensity when the most distant pairs essentially contribute to the PL spectrum. With increasing excitation intensity, the bands in a compensated semiconductor shift to higher photon energies due to screening of the potential fluctuations by photogenerated carriers. Similarly, the DAP bands shift to higher photon energies with increasing excitation intensity. However, in the DAP case the origin for the shift lies in the saturation of the PL emission from distant pairs. The distant pairs contribute at lower photon energies due to a weaker Coulomb interaction as compared to the close pairs that contribute at higher energies due to a stronger Coulomb interaction. The transitions between distant pairs are relatively slow due to a smaller overlap of the carriers' wave functions, which result in earlier saturation with increasing excitation intensity. In spite of the apparent similarity of PL behavior in the two aforementioned cases, there is an important difference. In the DAP transitions the undistorted positions of the defect levels correspond to the limit of low excitation intensity when the Coulomb interaction approaches zero. In the case of potential fluctuations, the undistorted positions of the defect levels correspond to the limit of high excitation intensity when the potential fluctuations vanish due to screening by photogenerated carriers. The DAP transitions in a compensated semiconductor may exhibit effects due to both potential fluctuations and the Coulomb interaction in which case the analysis becomes more complicated. Serendipitously, there is one particular case in which the role of potential fluctuations and the effect of the Coulomb interaction can be clearly separated. This is the case of the DAP transitions involving deep donors in GaN:Mg.

Deep donors and the Mg_{Ga} acceptor in GaN have high localization of the bound carriers (the Bohr radius is less than 1 nm for both). As a result, the transitions between such deep donors and the Mg_{Ga} acceptor become efficient only at high concentrations of the donors and acceptors (usually well above 10^{18} cm^{-3}) when the overlap between the carriers' wave functions becomes significant. The average separation in pairs, R_m , can be estimated as³²¹

$$R_m = (2\pi N_A)^{-1/3}, \quad (38)$$

which results in $R_m = 12\text{--}25$ Å for typical concentrations of Mg acceptor ($10^{19}\text{--}10^{20}$ cm^{-3}) in GaN:Mg. The potential drop over such distances due to the long-range potential fluctuations does not exceed 4–7 meV for typical excitation intensities below 10 W/cm^2 corresponding to a photogenerated free-carrier density of at most 10^{16} cm^{-3} . This is the upper limit of the contribution of the potential fluctuations to the broadening of the PL band. Note that the shifts related to the screening of the potential fluctuations would be even smaller since the transitions with smaller and higher energies

would have almost the same probability. In sharp contrast, the shifts due to Coulomb interaction in such pairs can be enormous.^{82,322} According to Eq. (29), the saturation of distant pairs, separated by about 25 Å, with excitation intensity and the resultant predominance of close pairs with a separation of less than 10 Å would cause shifts to higher energies by a figure exceeding 100 meV. The shift can be amplified by the presence of several deep-level defects, however, *a priori* it is not known which DAP transition would saturate first. In contrast to the deep DAP transitions, the PL bands related to the DAP transitions involving shallow donors in GaN can experience relatively large shifts due to potential fluctuations (since the wave function of the electron bound to the shallow donor is large) as compared to the shifts due to Coulomb interaction (limited by the ionization energy of the shallow donor).⁸²

3. UVL and BL bands in compensated and heavily Mg-doped GaN

In addition to the UVL band, which transforms into a structureless band at about 3.2 eV, the PL spectrum of the heavily Mg-doped GaN usually contains the BL band, the energy position of which is sensitive to the growth and experimental conditions. Less common are reports about the YL and RL bands in heavily Mg-doped GaN. The features of this type of material are considered in detail below.

a. Effects of growth conditions and annealing. The *p*-type GaN grown by MOCVD requires a postgrowth treatment for activating the Mg_{Ga} acceptor. The BL band appears in the PL spectrum of GaN:Mg only for high concentrations of Mg, typically above 10¹⁹ cm⁻³.^{56,304,308,323} Although the BL band shifts with excitation intensity by up to 0.2 eV (see Sec. V B 3 b), it should not be confused with a broad UVL band peaking at about 3.2 eV in heavily Mg-doped GaN samples, since these two bands often coexist.^{56,304,324}

Annealing at temperatures above 600 °C commonly converts the MOCVD-grown GaN:Mg from high-resistive to *p*-type conductivity. However, the effect of annealing on PL is not as straightforward as the conductivity. Early reports⁶ suggested that while the resistivity of GaN:Mg drastically drops after annealing temperature is increased above ~500 °C and remains unchanged for annealing temperatures between 700 and 1000 °C, the intensity of the BL band becomes very strong only after annealing at an optimal temperature (about 700 °C). Sheu *et al.*²⁹⁸ also reported on the substantial increase of the BL intensity after annealing at an optimal temperature, which in their case was 750 °C. Remarkably, annealing in NH₃ ambient at temperatures above 400 °C resulted in a significant decrease of the BL intensity and a drastic increase of the resistivity.⁶ The changes were reversible with a change in the annealing ambient gas from NH₃ to N₂. Nakamura and Fosol⁶ concluded that the BL band is related to Mg, while passivation of GaN:Mg with hydrogen is responsible for the decrease of its intensity when the annealing is performed in NH₃.

Annealing of moderately Mg-doped GaN grown by MOCVD in three different atmospheres [N₂, O₂, and H₂N₂(5:95)] revealed that the intensity of the UVL band, dominating the low-temperature CL spectrum in these

samples, drastically decreased after annealing in N₂ or O₂, but it slightly increased after annealing in the H₂N₂ atmosphere.³²⁵ In a control experiment aimed at the UVL band in Si-doped GaN, the intensity of that band remained nearly unchanged after annealing in all the aforementioned atmospheres. This observation led Gelhausen *et al.*³²⁵ to conclude that the shallow donors have different origin in Mg- and Si-doped GaN. While the Si doping introduces a stable Si_{Ga} donor, doping with Mg in hydrogen atmosphere may result in the formation of the V_N-H complex, assumed to be a shallow donor⁵⁹ that can dissociate during thermal annealing in a hydrogen-free atmosphere.³²⁵ Shahedipour and Wessels³⁰³ also observed a decrease of the UVL band intensity (up to a factor of 100) after annealing the Mg-doped GaN at 650 °C in a nitrogen ambient. The BL band markedly enhanced and replaced the UVL band after annealing. Interestingly, the sample grown in a hydrogen-free atmosphere (with only the nitrogen carrier gas) exhibited only the UVL band before as well as after thermal annealing in N₂. The authors of Ref. 303 explained their findings on the premise that H and V_NH are the shallow and deep donors in the Mg-doped GaN that are responsible for the UVL and BL, respectively. It was suggested that while isolated hydrogen is removed by annealing, the V_NH complex is formed. In criticism of that premise, we should note that isolated hydrogen is not expected to be a shallow donor in GaN, and diffusion of a hydrogen atom towards V_N is a highly unlikely process during thermal annealing.⁵⁹ It is possible also that it is not the hydrogen-free atmosphere but the N-rich conditions that prevent the appearance of the BL band that may be related to V_N or the V_N-related defects such as V_NMg_{Ga}.

In GaN:Mg grown by MBE, the postgrowth annealing is not necessary for obtaining conductive *p*-type GaN (Refs. 297 and 326) unless hydrogen is present in the growth chamber. Myoung *et al.*²⁹⁷ reported a broad emission band peaking at 3.18 eV in the MBE-grown GaN:Mg. With increasing measurement temperature, this PL band quenched and the BL band could be detected at room temperature. Leroux *et al.*³¹³ also observed the predominance of the UVL band in *p*-type GaN:Mg grown by MBE in contrast to the annealed GaN:Mg grown by MOCVD where the BL band dominated. In another investigation,³²⁴ the PL spectrum of the heavily Mg-doped MBE-grown GaN contained the UVL band but the BL band was barely resolved. This is in contrast with the MOCVD-grown GaN:Mg where the BL band dominated in the cases of heavy Mg doping.³²⁴ Alves *et al.*³²⁴ attributed the BL band to transitions from the V_N donor to the Mg_{Ga} acceptor and argued that in the MOCVD growth V_N is abundantly formed via the V_NH complex which dissociates after thermal annealing. The formation of the isolated V_N is less favorable; therefore, in hydrogen-free MBE growth the concentration of V_N is lower.

We observed both the BL and UVL bands in GaN:Mg grown by plasma-assisted MBE method. Typically the BL band dominates near the low-excitation limit, while the UVL band almost always dominates near the high excitation limit, as displayed in Fig. 70. At high excitation levels a relatively sharp line also appeared at about 3.45 eV which is attributed

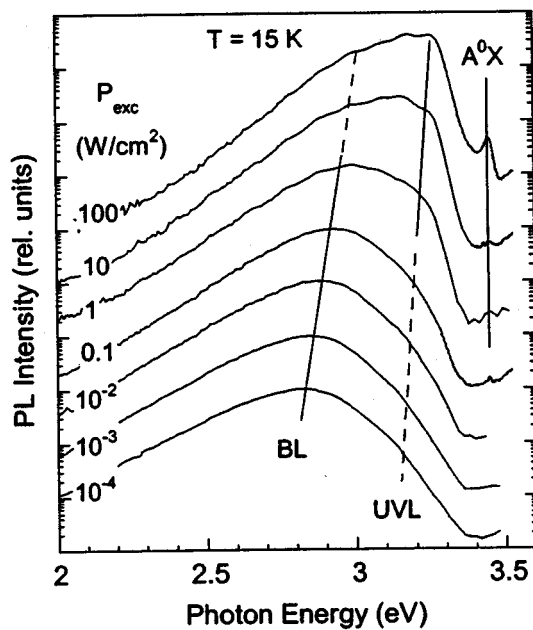


FIG. 70. Low-temperature PL spectrum of GaN:Mg grown by MBE at different excitation intensities. Note the gradual shift of the BL from 2.85 to ~ 2.95 eV with increasing excitation density up to 0.3 W/cm^2 above which the UVL band and the A^0X line at 3.45 eV emerge with roughly quadratic dependence of their intensities on the excitation density.

to recombination of excitons bound to neutral Mg_{Ga} acceptors. The effect of excitation intensity on the PL spectrum in Mg-doped GaN is discussed in detail below.

b. Effect of excitation intensity. In heavily Mg-doped GaN, large shifts of the PL bands with excitation intensity are commonly reported.^{56,82,294,297–299,304,306–309,322,327,328} Sometimes the moving band was clearly detected as a single band. However, often times one cannot exclude a superposition of several bands in a continuous shift.

The UVL band displaying the characteristic LO phonon replicas was found to redshift and broaden with decreasing excitation intensity. Dewsnip *et al.*³⁰⁶ reported that with increasing concentration of Mg from 3×10^{17} to $7 \times 10^{18} \text{ cm}^{-3}$ the extent of blueshift of the UVL band in GaN varied from 10 to 44 meV while the excitation intensity increased by a factor of 100. Figure 71 shows another example where the zero-phonon peak shifts from 3.27 to 3.22 eV with decreasing excitation intensity 2×10^4 times.⁸² From the characteristic shape, the UVL band is obviously caused by transitions from the shallow donors (or the conduction band) to the shallow acceptors. Since the shift due to Coulomb interaction in DAP cannot exceed the activation energy of the shallow donors,⁸⁰ we regard the large shift (about 50 meV) as a manifestation of potential fluctuations.⁸² In some GaN:Mg samples, the UVL band appears as a structureless broad band peaking at about 3.1–3.2 eV.^{56,82,296,297,303} Most probably, the origin of this band is the same as the UVL band with the characteristic LO phonon replicas,^{56,82,303} and the broadness is caused by potential fluctuations.⁸² Indeed, the shape of the band gradually transformed into the characteristic shape of the UVL band with LO phonon replicas as the excitation intensity increases.⁸² This effect is attributed to flattening of the potential fluctuations due to screening by

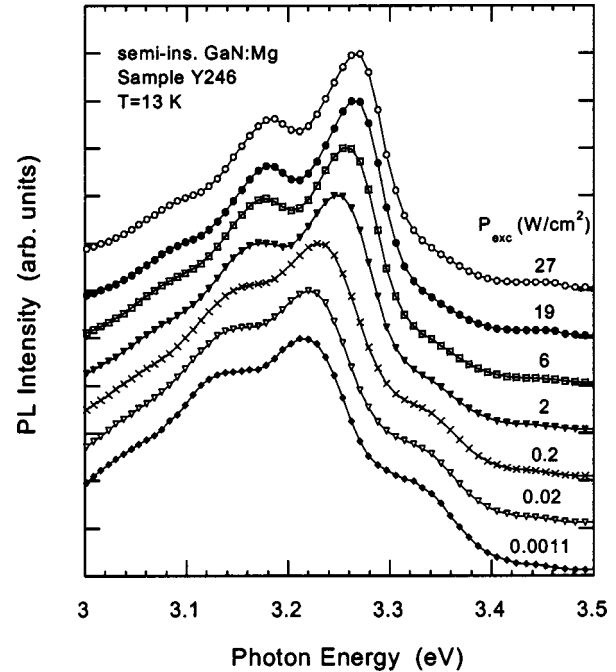


FIG. 71. Low-temperature PL spectra of semi-insulating GaN:Mg sample at different excitation intensities. Reprinted with permission from Reshchikov *et al.*, Phys. Rev. B 59, 13176 (1999). Copyright (1999) by the American Physical Society.

photogenerated carriers.

While the UVL band in GaN:Mg shifted notably with excitation intensity only in selected samples,⁸² the significant shift of the BL band, typically of the order of 0.1 eV, has been observed as its characteristic feature.^{56,82,294,296–300,304,307–310,322,323,329,330} Shifts as high as approximately 0.2 eV have been reported in investigations where the excitation intensity changed several orders of magnitude, as depicted in Fig. 72.^{82,304,310,322} While nearly all

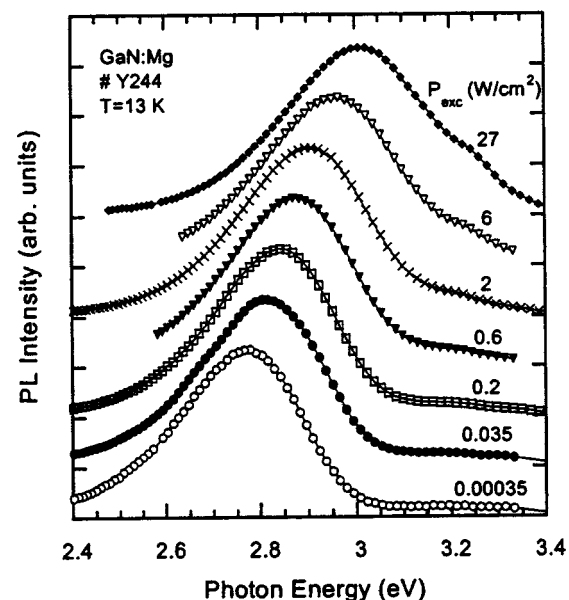


FIG. 72. Low-temperature PL spectra of semi-insulating GaN:Mg sample at different excitation intensities. Reprinted with permission from Reshchikov *et al.*, Phys. Rev. B 59, 13176 (1999). Copyright (1999) by the American Physical Society.

researchers who investigated the effect of the excitation intensity on the BL band attributed the BL band to transitions from a deep donor to the shallow Mg_{Ga} acceptor, a controversy still remains about that assignment for the giant shift. Most researchers propose that the Coulomb interaction in the DAP is responsible for the shift in the BL band,^{82,294,298,304,308,322,330} while others point to potential fluctuations as the main reason for the shift.^{299,310} As discussed in Sec. VB 2, the strong Coulomb interaction between the deep-level DAP in heavily doped GaN alone can explain the giant shifts of this band, whereas the potential fluctuations perhaps play only a secondary role which can be negligible. Note that a good quantitative agreement between the BL band position and the room-temperature hole concentration once obtained within the model of potential fluctuations³¹⁰ is apparently just a coincidence. In reality, the average size of the potential fluctuations in the analyzed GaN:Mg is about 100 nm at room temperature which dramatically increases as the temperature is reduced. The wave functions of the bound electron and hole are less than 1 nm, so that their overlap at distances exceeding 100 nm is completely negligible. The scatter in the reported BL band position, which has been attributed in Ref. 310 to different screening effects, is apparently related to the scatter in the concentration of defects that affects the average pair separation in DAP.

We can estimate the position of the energy level of the unperturbed deep donor responsible for the BL band in the following manner. The Coulomb interaction term in Eq. (29) for the DAP with an average distance of about 25 Å for the typical concentrations of Mg in mid- 10^{19} cm^{-3} can be estimated as ~ 0.1 eV. The energy of the ZPL for the broad BL band can be approximately estimated as ~ 3.0 eV from the band shape in the limit of low excitation intensities (see Fig. 72). Using $E_g = 3.5$ eV for the low-temperature band gap and $E_A = 0.2$ eV, we obtain $E_D = 0.4 \pm 0.1$ eV from Eq. (29).

A very interesting observation regarding the effect of excitation intensity on the BL and UVL structureless bands in *p*-type GaN:Mg, which has long been reported,⁵⁶ remains unexplained. Namely, the intensity of the BL band increased linearly with excitation intensity, whereas the increase of the UVL intensity was quadratic.⁵⁶ We also observed similar dependencies in a few GaN:Mg samples grown by MBE (see Fig. 70). From an analysis of the rate equations (within the concept presented in Sec. III A), we expect that in conductive *p*-type GaN:Mg the intensity of PL bands resulting from the transitions of electrons (free or bound) to the shallow Mg_{Ga} acceptor level should increase linearly with excitation intensity. Indeed, the concentration of holes bound to the Mg_{Ga} acceptor remains nearly constant in the nominal range of excitation intensities (and roughly equal concentration of the compensating donors), so that the intensity of the UVL and BL bands should be proportional to the concentration of the photogenerated electrons captured by the shallow and deep donors. Therefore, in *p*-type GaN:Mg, where the Fermi level is pinned to the shallow acceptor level, we expect a linear $I(P_{\text{exc}})$ dependence for both the BL and UVL bands. The above reasoning indicates that the observations in Ref. 56 may seem to contradict the Hall-effect results contained

therein, revealing the *p*-type conductivity. However, invoking the concept of long-range potential fluctuations can easily remove the discrepancy. The potential fluctuations divide the sample into areas where the Mg_{Ga} acceptor is filled with holes (in the hills) and empty of holes (in the valleys) in dark, as shown in Fig. 68. Photogenerated electrons that are captured by the shallow donors can escape to the conduction band since their activation energy is not too large (possibility of diagonal transitions leading to long carrier lifetimes enhances this probability). After multiple capture and thermal release, the electrons would be collected at the shallow donor states in the valleys where there are no equilibrium holes. Recombination of the electrons from the shallow donors with photogenerated holes at the shallow acceptors in these areas of the sample may be responsible for the quadratic $I(P_{\text{exc}})$ dependence of the UVL intensity. In contrast, electrons captured by deep donors cannot be thermally released (due to the larger activation energy and smaller size of the electron wave function), and therefore, the BL band will be observed mostly from the hills where the concentration of holes bound to the shallow acceptor is abundant even in dark. Thus, the BL intensity would increase linearly with the excitation intensity.

From an analysis of the PL spectra at different excitation intensities, it can be concluded that at least in some GaN:Mg samples more than two bands (the above-discussed BL and UVL) present in the photon range from 2.5 to 3.3 eV. Eckey *et al.*³⁰⁸ resolved three broad bands in this range. In the limit of low excitation intensity, these bands peaked at about 2.5, 2.8, and 3.0 eV, and all three bands substantially shifted with increasing excitation intensity, as displayed in Fig. 73. Those three bands have been attributed to transitions from the three distinct deep donors to the shallow Mg_{Ga} acceptor. A broad band peaking at about 3.3 eV was observed as a shoulder on the UVL band (see Fig. 71).⁸² Another broad band peaking at 3.0 eV was detected in GaN:Mg after electron irradiation.^{325,328} The band gradually shifted to higher photon energies and reached 3.2 eV upon increasing excitation intensity by a factor of 400. This 3.0-eV band has been attributed to transitions from a deep donor (apparently V_{N}) to the shallow Mg_{Ga} acceptor.³²⁵

c. Effect of temperature. With increasing temperature, the PL bands in Mg-doped GaN shift and quench. However, the temperature-related transformations are different for the BL band and the UVL band. The UVL band begins quenching at relatively low temperatures and by the time the room temperature is reached it either disappears under the tail of the BL band^{82,295,297,313} or transforms into a structureless band at about 3.2 eV with its intensity reduced by a factor of about 1000 as compared to that at low temperature.^{56,82} The activation energy of this quenching, ~ 200 meV, is similar to the values obtained for the UVL band in undoped and lightly doped *n*-type GaN.^{82,310,313} It may seem surprising that in the *p*-type GaN:Mg samples^{56,82,313} the UVL band quenches in a fashion similar to that in *n*-type GaN. Indeed, one would expect the abundance of holes at the shallow Mg_{Ga} acceptor sites at any temperature. Therefore, the thermal escape of small fraction of the bound holes would not affect the PL intensity of the UVL band up to room temperature. A pos-

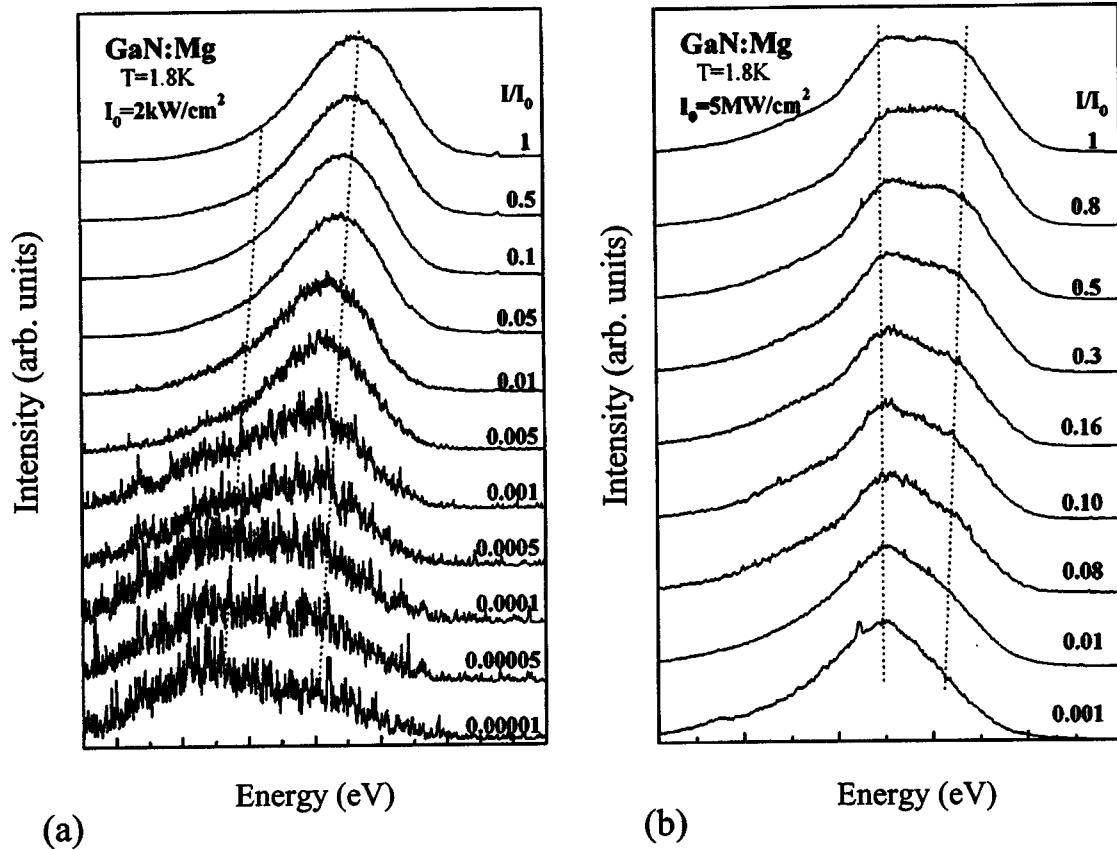


FIG. 73. Intensity dependence of the PL spectra in *p*-type GaN:Mg (a) measured with a cw-HeCd laser at up to 2 kW/cm², (b) measured with the third harmonic of a pulsed Nd:YAG (yttrium aluminum garnet) laser with pulse intensities up to 5 MW/cm². Reprinted with permission from Eckey *et al.*, J. Appl. Phys. **84**, 5828 (1998). Copyright (1998) by the American Institute of Physics.

sible explanation based on the concept of potential fluctuations has been suggested in Sec. V B 3 b. The UVL band dominates in the potential valleys, as shown in Fig. 68, where the Fermi level is higher than the shallow acceptor level. In this case, the Hall-effect measurements show a good *p*-type conductivity due to percolation of free holes between potential hills where they are abundant. A large redshift of the UVL band with increasing temperature that is observed in selected GaN:Mg samples can also be explained in terms of the potential fluctuation model. It has been suggested⁸² that thermal release of free carriers from the shallower short-range wells and their percolation into deeper valleys accounts for the large temperature shifts of the UVL band in GaN:Mg. In this model, the shift increases with decreasing excitation intensity,⁸⁰ which, in fact, has been observed not only in GaN:Mg (Ref. 82) but also in Ge (Ref. 331) and GaAs.³¹⁵

The BL band intensity quenches only by a factor of about 10 up to room temperature,^{56,82,322} and, therefore, it often dominates in the room-temperature PL spectrum of heavily Mg-doped GaN.^{6,56,82,295–298,310,313,323,325,332} The activation energy of 0.35 eV has been obtained from the Arrhenius plot in the temperature range between approximately 300 and 380 K and attributed to the thermal release of electrons from the deep donor to the conduction band.^{82,322} In other studies, the activation energies of 0.29,³²³ and 0.245,³¹⁰ and ~0.12 eV (Ref. 330) have been reported for quenching of the BL band in GaN:Mg. Note that the value of 0.12 eV in

Ref. 330 may be significantly underestimated since quenching was studied only up to 300 K, and the value in Ref. 310 could be affected by the green luminescence dominating at high temperatures in GaN:Mg samples codoped with Si.^{310,333} Note also that potential fluctuations can also affect the activation energy by reducing it due to possibility of diagonal transitions.⁸² The potential fluctuations could also resolve the following apparent paradox. While the UVL band quenches at low temperatures with an activation energy of about 0.2 eV, the BL band in the same samples quenches only above approximately 250 K with a much larger activation energy.^{56,82} Although both bands have their roots in the same shallow Mg_{Ga} acceptor, the BL band does not quench simultaneously with the UVL band because it dominates in the areas with high equilibrium concentration of bound holes (in potential hills). In contrast, the UVL band dominates in the high-resistivity areas (in potential valleys) where the shallow Mg_{Ga} acceptors bind only photogenerated holes.

The BL band markedly shifted to lower photon energies with increasing temperature,^{82,295,298,322} yet the shift was dependent on excitation intensity, as depicted in Fig. 74. Note that, in contrast to the UVL band, the shift of the BL band is larger at higher excitation intensities. This observation has been explained by the deep DAP character of the BL band.⁸² Emission from the closest pairs contributes more at the high-energy side of the band due to a stronger Coulomb interaction and dominates at high excitation intensity due to higher rate of closer transitions. The closer pair emission would

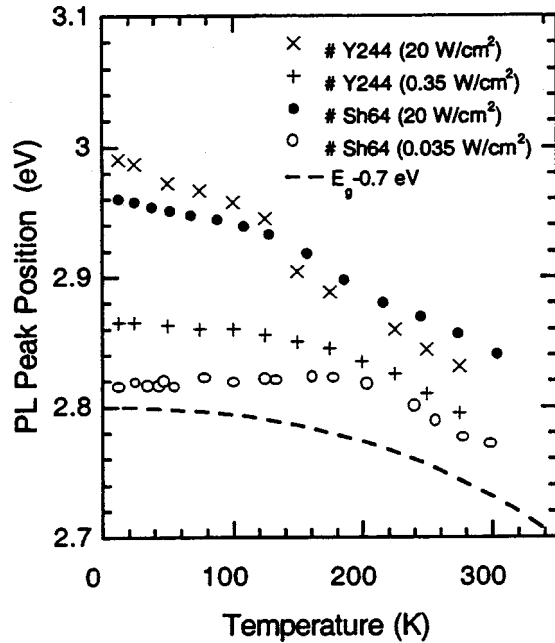


FIG. 74. Variation of the BL peak shifts with temperature at low and high excitation intensities. Variation of the band-gap width is also shown, shifted by 0.7 eV for convenience. Reprinted with permission from Reshchikov *et al.*, MRS Internet J. Nitride Semicond. Res. **4S1**, G11.8 (1999).

quench at lower temperatures since in the closest pairs the donor level is closer to the conduction band. However, for low excitation intensities the redshift is reduced since the emission from quite distant pairs with weak Coulomb interaction dominates in this case. A similar effect has previously been observed in Si codoped with donors and acceptors.³³⁴

d. Time-resolved PL. TRPL studies on the UVL and BL bands in GaN:Mg have been able to provide much needed insight into the transitions involved in these emission bands.^{190,301,335–339} In moderately Mg-doped GaN (with $p \approx 10^{17} \text{ cm}^{-3}$ at room temperature), the UVL band representing the characteristic peaks with the zero-phonon line at about 3.26 eV decayed nonexponentially after the excitation pulse.³³⁸ The UVL band shifted to lower energies by about 35 meV after 5 μs following the pulsed excitation. Strauf *et al.*³³⁸ attributed these observations to a manifestation of the DAP transitions involving a shallow donor and the shallow Mg_{Ga} acceptor. We believe that the observed shift is too large for the shallow DAP interpretation to be in effect and suggest instead that the potential fluctuations in these samples also contribute to the shifts and nonexponential recombination of the UVL band.

The decay of the BL band is in general relatively slow and nonexponential.^{82,190,301,335,336} The longer decay times have been observed at the low-energy tail of the BL band,^{190,301,336} consistent with the deep DAP model. Shaheedipour and Wessels³³⁵ explained the nonexponential decay of the BL band within the Thomas–Hopfield model of distant DAP transitions.⁷⁹ The fitting was reasonably good for the DAP transitions involving a deep donor and the shallow Mg_{Ga} acceptor, both with a Bohr radius of 5 Å.³³⁵ Even a stronger indication for the deep nature of the donor involved

in the BL band is a redshift of about 200 meV reported for the BL band with time delay,³³⁵ although that shift was also attributed to a superposition of several PL bands in another report.³⁰¹

From the time-resolved PL data at temperatures up to 380 K, Gurskii *et al.*³³⁷ concluded that a broad band at 3.05 eV, dominating at high temperatures and having nearly exponential decay with the characteristic time of about 200 ns, is caused by transitions from a deep donor to the valence band in *p*-type GaN:Mg. This is a reasonable analog of the e-A transitions dominating in *n*-type undoped GaN at high temperatures (see Sec. IV A 5).

Only in one work, very fast (on the subnanosecond scale) decays of the BL and UVL bands in *p*-type GaN:Mg have been reported.²⁹⁶ These results contrast with very slow decays on the microsecond scale for the BL (Refs. 190, 335, and 336) and were not confirmed by others. To explain the very fast radiative recombination, Smith *et al.*²⁹⁶ suggested that the UVL and BL bands involve transitions from the conduction band to the shallow and deep acceptor levels, respectively. This model and very fast decay of the BL band are inconsistent with most of the well-established features regarding this band in GaN:Mg. It is plausible that the fast decay of the BL band, reported in Ref. 296, is some artifact.

e. Effect of hydrostatic pressure. Additional data supporting the models of the BL and UVL bands in Mg-doped GaN have been obtained from the hydrostatic pressure studies with which one is able to delineate the localized and delocalized (shallow) electronic states.^{340,341} Transitions involving shallow donors are expected to follow the pressure dependence of the band gap. On the other hand, transitions involving deep donors tend to follow a weighted average of the various band extrema. For example, the pressure dependence of the PL bands originating from deep donors would be much weaker than the transitions involving shallow donors. A linear pressure coefficient of about 35 meV/GPa for the UVL band in GaN:Mg has been obtained which is very close to the pressure shift of the GaN band gap of about 40 meV/GPa.³⁴¹ The pressure coefficient for the BL band is much smaller, about 20–26 meV/GPa.^{340,341} This is consistent with the theoretical predictions for a deep donor in GaN.^{23,341,342} It is also smaller than that expected³⁴¹ and experimentally found pressure coefficient for a deep acceptor in undoped GaN which is 30 ± 2 meV/GPa.¹⁴⁹ Note also that even a larger pressure coefficient, similar to that of the GaN band gap, has been obtained for the deeper acceptor responsible for the BL band emission in Zn-doped GaN.²⁷¹ Thus, the results of the hydrostatic pressure studies favor the model that the donor involved in the BL band emission is deep with a localized wave function.

f. Effect of electron irradiation. Similar to thermal annealing, low-energy electron-beam irradiation (LEEBI) converts high-resistivity GaN:Mg into conductive *p*-type GaN.²⁹¹ After a LEEBI treatment, the intensity of the BL band has been reported to notably increase.⁶ Koide *et al.*³⁰⁰ studied the effect of the LEEBI treatment on the luminescence spectrum of GaN:Mg by using a very weak electron-beam current density of the order of 10^{-5} A/cm^2 and electron-beam energy in the range from 0.5 to 5 keV. They observed a decrease of the BL

band intensity by about 20% with electron exposure. Remarkably, the UVL band increased by about a factor of 2 after the LEEBI treatment of GaN:Mg samples. Koide *et al.*³⁰⁰ explained the changes by dissociation of the MgH and V_N H complexes under electron irradiation. Congruous with the assignments made in Ref. 303, these authors attributed the UVL and BL bands to transitions from the shallow donor, which was assumed to be H, and from a deep donor which was assumed to be V_N H, respectively, to the shallow Mg_{Ga} acceptor.

By contrast, Gelhausen *et al.*³²⁵ observed a drastic decrease of the UVL intensity under LEEBI treatment. The UVL band decreased under electron irradiation only in as-grown GaN:Mg sample and in a sample annealed in H_2N_2 ambient. The effect of electron irradiation was negligible in the GaN:Mg samples annealed in N_2 or O_2 ambient. The same was shown to hold for the Si-doped samples before and after annealing. Those authors assumed that the shallow donor responsible for the UVL band in GaN:Mg samples is the V_N H complex that can dissociate during LEEBI treatment. Besides the bleaching of the UVL band, Gelhausen *et al.*^{325,328} detected an emergence of a broad band at around 3.05 eV under electron irradiation. The broad band shifted from 3.0 to 3.2 eV with increasing excitation density (by a factor of 400). That broad band has been attributed to transitions from a deep donor, presumably V_N , to the shallow Mg_{Ga} acceptor.³²⁸ The LEEBI treatment also shifted the BL band to lower energies³²⁵ and activated a weak yellow luminescence band³²⁸ in these GaN:Mg samples.

g. Optically detected magnetic resonance. The ODMR spectra measured on the UVL and BL bands in GaN:Mg usually contain two lines: one with $g_{||} \approx 2.1$ attributed to Mg_{Ga} and another with $g_{||} \approx 1.95$ – 1.96 attributed to a compensating donor.^{141,277,309,343–345} The spectral distribution of both signals reproduces the shape of the BL band with a maximum at 2.9 eV observed in heavily doped GaN:Mg.¹⁴¹ The Mg-related signal is anisotropic. The values of $g_{||}$ and g_{\perp} which are typically in the range of 2.058–2.114 and 1.94–2.022, respectively, are sample dependent.^{277,309,343–346} Moreover, the difference $g_{||} - g_{\perp}$ decreases with decreasing detection energy across the broad BL band.^{309,346} The anisotropy of the g tensor, expected for the shallow acceptor in GaN,¹⁰⁸ is reduced by symmetry-lowering local distortions originating from structural defects or random distribution of charged impurities leading to potential fluctuations.^{309,346} Note that in early studies the above-mentioned small anisotropy of the g tensor of the Mg-related defect was inappropriately assigned to a so thought deep Mg-related level.^{141,344} The nearly isotropic signal with $g \approx 1.95$ – 1.96 has been attributed to the shallow effective-mass donor in GaN.^{141,309,345} Such an assignment is consistent with the attribution of the UVL band to transitions from the shallow donor to the shallow Mg_{Ga} acceptor. However, assignment of the donor-related signal to the shallow donor contradicts the above-described properties of the BL band ascribed to transitions from a deep donor to the shallow Mg_{Ga} acceptor. One possibility is that the ODMR signal from the deep donor is similar to that from the effective-mass shallow donor. Note that this signal in the heavily Mg-doped GaN exhibiting the BL band is much

broader than that in the lightly Mg-doped GaN where the UVL band dominates.³⁰⁹ Another possibility is that the spin-dependent capture of an electron from the shallow donor or possibly from the conduction band to a deep donor first takes place, followed by radiative transition from the deep donor to the shallow Mg_{Ga} acceptor. In the case the first process is detected by magnetic resonance the effective-mass resonance would be observed in the form of increasing BL signal.

h. DLTS, positron annihilation, and the infrared spectra. A DLTS study of undoped and Mg-doped GaN revealed a characteristic deep level at 0.62 eV below the conduction band.³⁴⁷ The concentration of this defect increased from $\sim 2 \times 10^{13}$ to $3 \times 10^{14} \text{ cm}^{-3}$ after moderate Mg doping of GaN that remained n type. Additionally, a defect level at ~ 0.4 eV below the conduction band with a concentration of about 10^{13} cm^{-3} appeared in one Mg-doped sample. The capture cross section is of the order of 10^{-14} cm^2 for both of the aforementioned deep levels.³⁴⁷

Positron annihilation studies have shown that the creation of V_{Ga} is suppressed by Mg doping.^{124,195,348} This result is consistent with theoretical predictions (Sec. II). When the Fermi level is close to the valence band during the growth, donors, such as V_N , V_N Mg, or V_N H, are more likely to incorporate in GaN, and not acceptors such as V_{Ga} . Positron annihilation experiments are able in principle to detect and distinguish V_{Ga} and V_N , as well as complex defects containing these vacancies. However, the detection of V_N in p -type GaN by positron annihilation is hampered even when this defect is abundant. The reason lies in a small difference in the positron lifetime in defect-free and V_N -containing GaN, as well as repulsion of positrons from the positively charged defects.¹²⁴ Nevertheless, Hautakangas *et al.*³⁴⁹ were able to detect a neutral V_N -related defect in p -type GaN grown by MOCVD. This should be contrasted with no vacancy-related defects having been observed in p -type GaN grown by MBE. The defect has been identified as the neutral V_N Mg $_{Ga}$ complex. Thermal annealing at 500–800 °C led to disappearance of this defect. A value of about 2.5 eV for the migration energy of V_N has been estimated by assuming that the V_N Mg $_{Ga}$ complex dissociates and V_N migrates to the surface during annealing. The absence of the V_N -related defects in p -type GaN:Mg grown by MBE has been attributed to better stability of the V_N Mg $_{Ga}$ complexes when the Fermi level is close to the midgap during the growth, a condition corresponding to the MOCVD but not MBE growth conditions.

Local vibrational modes of the Mg–H complex have been found in GaN:Mg at 3125 cm^{-1} .³⁵⁰ The hydrogen atom preferentially incorporates at an antibonding site of the nitrogen atom.^{47,351} Consequently, the vibrational frequency is primarily determined by the N–H vibrational mode. Thermal annealing converts the high-resistivity GaN to p -type conductivity and results in a sizable decrease of this local mode.³⁵⁰ A series of local modes in the range of about 2200 cm^{-1} was also detected in the Raman spectra of GaN:Mg and attributed to various defect complexes involving hydrogen.^{352,353}

4. Yellow and red luminescence bands

The YL band peaking at 2.2–2.3 eV usually vanishes with Mg doping, in agreement with its attribution to the V_{Ga} -containing defects (see Secs. IV A and IV B). However, the YL band sometimes persists in GaN:Mg when the sample remains n type^{298,354} or semi-insulating.⁶ The weak YL band appeared also after electron irradiation of p -type GaN:Mg.³²⁸ A relatively strong YL has been reported in p -type GaN grown by MBE.³⁵⁵ Note that the reports about the YL peak in p -type GaN are extremely rare and must be treated with caution.

The RL band having a maximum at about 1.7–1.8 eV is sometimes observed in heavily Mg-doped p -type GaN.^{309,354,356} The ODMR studies of this band indicate that the transition involves deep donors and the shallow Mg_{Ga} acceptor.³⁰⁹ Two signals, namely, an isotropic one with $g = 2.003$ (from deep donor) and an anisotropic one with $g_{\parallel} = 2.10$ and $g_{\perp} \approx 2$ (for the shallow Mg_{Ga} acceptor) have been detected for the RL band.³⁰⁹ The RL band has also been attributed to deep donor-deep acceptor transitions.^{172,354}

5. Luminescence in GaN:Mg codoped with shallow donors

Codoping of GaN:Mg with shallow donors has been considered as a means to increase the solubility of Mg and reduce its binding energy.³⁵⁷ Through codoping with oxygen the concentration of holes has been increased up to $2 \times 10^{18} \text{ cm}^{-3}$ while decreasing the resistivity of the GaN:Mg sample down to $0.2 \Omega \text{ cm}$.^{358,359} Incorporation of oxygen in GaN:Mg suppressed the BL band, and a broad GL emerged at 2.4–2.5 eV as a shoulder to the BL band.³⁵⁸ Similarly, a GL band appeared in GaN:Mg codoped with Si upon increasing the temperature up to room temperature.³³³ While the BL intensity increased linearly with excitation intensity, the GL intensity in O- and Si-codoped GaN:Mg increased superlinearly, as P_{exc}^n with $n = 1.4$ – 1.7 .³³³ The intensity of the GL band increased with increasing temperature from 200 to 260 K. In an effort to explain this unusual effect, Han *et al.*³³³ proposed that the GL band arises from transitions between a metastable deep donor and the shallow Mg_{Ga} acceptor. Those authors assumed that both oxygen and silicon would behave as DX centers in GaN, and their DX states form deep levels within the band gap. Kaufmann *et al.*¹⁷² also observed the BL band (at about 2.8 eV) and RL band (at about 1.8 eV) in GaN:Mg codoped with Si. The red band has been attributed to transitions from a deep donor to a deep acceptor.

6. Identification of defects in Mg-doped GaN

In spite of the plethora of activity, only two observations are well established, both from theoretical and experimental viewpoints regarding the defects in GaN:Mg: (i) Mg doping suppresses V_{Ga} -related defects which are common in n -type GaN and introduces compensating deep donors and (ii) a Mg atom replaces a Ga atom forming a shallow acceptor with an activation energy of about 0.2 eV.

As for the optical transitions contributing to the PL spectrum of GaN:Mg, only the following are undeniably established up to date: (i) In moderately Mg-doped GaN, transi-

tions from the shallow donor to the shallow Mg_{Ga} acceptor, which are responsible for the UVL band with the zero-phonon line at about 3.27 eV and the characteristic set of LO phonon replicas dominate, (ii) transitions from one or more deep donors to the shallow Mg_{Ga} acceptor in heavily Mg-doped GaN are responsible for the dominant BL band which shifts substantially with excitation intensity, (iii) the previously proposed model for the BL band as being due to transitions from the conduction band or from a shallow donor to a deep Mg-related defect^{141,286,295–300,302} must be rejected since it fails to explain very critical experimental observations, (iv) the BL bands in Mg- and Zn-doped or undoped GaN have different origins, and (v) potential fluctuations due to random distribution of charged defects play an important role in the PL properties of heavily Mg-doped GaN. Other deductions reported in the literature are more speculative. Nevertheless, we briefly review them below for the sake of completeness.

There are strong indications that the dominant shallow donor in Mg-doped GaN is hydrogen related, rather than Si_{Ga} or O_{N} as in the case of undoped n -type GaN.^{300,303,325} A proposal that the shallow donor is $V_{\text{N}}\text{H}$ complex^{59,325} appears much more likely than the assumption that isolated H is the shallow donor,^{300,303} since the latter contradicts the expectations grounded in the first-principles calculations.⁵⁹ As for the deep donors playing an important role in self-compensating the p -type GaN:Mg, the $V_{\text{N}}\text{Mg}_{\text{Ga}}$ complex,²⁹⁴ and hydrogenated V_{N} (Ref. 303) are the major candidates.

Vennéguès *et al.*³²⁹ have proposed that structural defects but not the point defects are responsible for the BL band in Mg-doped GaN. This supposition is based on the fact that high density (up to $\sim 10^{17} \text{ cm}^{-3}$) of pyramidal structural defects appears in heavily Mg-doped GaN.^{329,360–366} The pyramids represent Mg-rich inversion domains^{329,360,361} and therefore may form potential wells with carriers due to the polarization effect.^{329,366} However, the attribution of the BL band to diagonal transitions of free electrons from these quantum wells to the shallow Mg_{Ga} acceptors outside the pyramidal defect³²⁹ fails to explain the relatively constant position of the BL band (2.8 ± 0.1 eV at low temperatures and low excitation intensities) in various samples with a large scatter in the size of the pyramidal defects. Nonetheless, that accumulation of Mg at the pyramidal inversion domain boundaries can play a significant role in autocompensating Mg-doped GaN.³⁶⁶

C. Luminescence in GaN doped with other impurities

In Secs. V A and V B we considered the PL properties of GaN doped with Zn and Mg in some detail. Below we review the main contributions by shallow donors, acceptors, other than Zn and Mg, and isoelectronic impurities to the PL in GaN. Main contributions to the optical transitions in transition and rare-earth elements are briefly mentioned as well.

1. Doping with shallow donors

a. Silicon doping. Silicon is the major dopant for n -type GaN since the electron concentration can be controllably changed from $\sim 10^{17}$ to $2 \times 10^{19} \text{ cm}^{-3}$ by varying the flow

rate of SiH₄ in MOCVD growth.⁶ A similar case is applicable to MBE as well. The activation energy of Si_{Ga} donor is 30 meV.²³⁰ Typically, the YL band intensity increases with Si doping.^{6,71,131,172,208–210} However, at high doping levels the YL band intensity decreases.^{6,209} The initial enhancement of the YL band with Si doping can be explained by an inadvertent increase in the concentration of the V_{Ga}-related acceptors, such as V_{Ga}O_N and V_{Ga}Si_{Ga}, facilitated by the shift of the Fermi level to higher energies during growth (see Sec. II). Unlike O_N with features of a DX center (Sec. V C 1 b), Si_{Ga} behaves like a standard hydrogenic donor at high pressures.

Silicon is an amphoteric impurity, and it may appear as a shallow acceptor upon substituting a N atom. Although the first-principles calculations (Sec. II) predict that in thermodynamical equilibrium the formation of Si_N is less probable than Si_{Ga}, there are a few experimental observations supporting the existence of Si_N acceptors in GaN. Consequently, the intensity of the UVL band, which is attributed to transitions from the shallow donors to the shallow acceptors, increases with Si doping.^{109,231,367} In *n*-type GaN, the intensity of the DAP transitions depends only on the concentration of the acceptors involved (Sec. III). Therefore, the enhancement of the UVL band indicates that at least some shallow acceptors incorporate as a result of Si doping. Moreover, the increase of the shallow acceptor concentration with Si doping is confirmed by an increase of the emission intensity from the exciton bound to the shallow acceptor.²³¹ The Si_N acceptor binding energy of 224 meV has been estimated from the position of the ZPL of the UVL band in GaN:Si.²³¹ An ODMR study of Si-doped GaN has revealed a highly anisotropic resonance on the UVL band,¹⁰⁹ in concert with the theoretical predictions for an effective-mass shallow acceptor in wurtzitic GaN.¹⁰⁸

b. Oxygen doping. Oxygen is a shallow donor in GaN with an activation energy of 33 meV.²³⁰ However, with increasing concentration of O, the associated donor level moves closer to the conduction band, merging with it at $n_0 > 3 \times 10^{18} \text{ cm}^{-3}$. Further, the Fermi level increases with increasing donor concentration to the point that for concentrations of O exceeding 10^{19} cm^{-3} one may expect optical transitions blueshifted by 0.1 eV (the Burstein–Moss shift³⁶⁸). However, the band-gap renormalization³⁶⁹ effectively compensates this effect, and consequently, a very small shift is observed for optical transitions in degenerate GaN:O.³⁷⁰ Note that the solubility of O in GaN is approximately 10^{19} cm^{-3} , forcing the excess oxygen to form precipitates in surface microcavities.³⁷⁰

Sometimes oxygen is present in high concentrations in undoped GaN. For example, in bulk GaN grown under high pressures and at high temperatures the concentration of O is of the order of 10^{20} cm^{-3} .³⁷¹ The YL band is very strong in these bulk samples.³⁷² The correlation between the intensity of the YL band and concentration of O has been noted also by Slack *et al.*³⁷³ This is in agreement with the attribution of the YL band to the V_{Ga}O_N complex (Secs. IV A and IV B). Note that the concentration of both V_{Ga} and O_N increases with O doping (Sec. II). Oxygen in GaN shows characteristic features of the DX center. Namely, a strongly localized level associated with a distorted O configuration emerges from the

conduction band for hydrostatic pressures above 20 GPa.³⁷¹ The pressure dependence of the YL band energy position experiences a change of slope at these pressures,¹⁵⁰ thus confirming the attribution of the YL band to transitions from the O donor to a deep acceptor (presumably V_{Ga}O_N). No other PL bands related to O have been reported in the literature.

c. Selenium doping. Other dopants that have been attempted for achieving *n*-type conductivity are Se and Ge, both shallow donors when they replace nitrogen and gallium atoms, respectively. Free-electron concentrations of up to $1.7 \times 10^{18} \text{ cm}^{-3}$ (Ref. 213) and $6 \times 10^{19} \text{ cm}^{-3}$ (Ref. 214) have been reported with Se doping. The Ga-to-N ratio decreased about 15% with increasing concentration of Se. Although the authors of Ref. 213 attributed the change in Ga/N ratio to the formation of N_{Ga} defects, formation of V_{Ga} due to self-compensation is more likely in view of theoretical predictions (Sec. II B). The YL band intensity increased with Se doping.^{213,214} This is consistent with the YL band having V_{Ga}-related defect origin (see Sec. IV A 1). Yi and Wessels²¹⁴ suggested that the increase in electron concentration in GaN:Se as the cube root of the H₂Se partial pressure for $n_0 > 2 \times 10^{18} \text{ cm}^{-3}$ is due to compensation by a triply charged V_{Ga}. Note, however, that the results of this experiment do not prove that the compensating defect is the isolated triply charged V_{Ga} but not, for instance, the doubly charged V_{Ga}O_N. Indeed, the $N_A \propto N_D^{1/n}$ dependence, where *n* is the charge of the compensating defect,³⁷⁴ is valid only for a nondegenerate semiconductor, which may not hold for $n_0 > 2 \times 10^{18} \text{ cm}^{-3}$ in GaN.

d. Germanium doping. The electron concentration increased from approximately 10^{17} to approximately 10^{19} cm^{-3} when the flow rate of GeH₄ was varied by a factor of 100 in MOCVD growth.⁶ The intensity of both the excitonic emission and the YL band increased with Ge doping. Doping of GaN with Ge above approximately 10^{20} cm^{-3} leads to quenching of the YL band.²¹² Zhang *et al.*²¹² argued that this effect is due to reduction of the V_{Ga} concentration in heavily Ge-doped GaN.

2. Doping with acceptors

a. Carbon doping. Incorporation of C in GaN introduces mostly C_N acceptors (see Sec. II C 2) which compensate the residual shallow donors, resulting in semi-insulating GaN.^{205,375,376} However, as C doping is increased, the resistivity of GaN decreases, apparently due to the formation of compensating donors.³⁷⁵ Several deep-level defects have been detected in C-doped GaN by thermally stimulated current spectroscopy,³⁷⁵ photoionization spectroscopy,³⁷⁷ and deep-level optical spectroscopy.^{378,379} However, most of these defects are apparently not directly related to carbon.³⁷⁵

Several authors noted a correlation between the YL band intensity and C doping (see also Sec. IV A 10),^{98,135,136,139,140,204–206} although the properties of the YL band in undoped and C-doped GaN were apparently different.^{137,164} An enhancement of the YL band has also been observed in GaN after implantation with carbon.^{123,199,201} However, ion implantation certainly creates other defects, such as V_{Ga}, which would result in the YL band, along with many other possibly known and unknown

defects.

The intensity of the UVL band apparently also increased with C doping.²⁰⁶ However, in another report,³⁷⁶ a broad blue band peaking at 3.0 eV, instead of the UVL band, has been observed in the semi-insulating GaN:C. Seager *et al.*³⁷⁶ attributed this blue band to transitions from C_{Ga} donor to C_N acceptor. Polyakov *et al.*¹³⁶ also noted an enhancement of the blue band peaked at 3.05 eV in the GaN samples that were heavily contaminated with carbon.

Reuter *et al.*²⁰⁴ observed a broad red luminescence band with its maximum at 1.64 eV in C-doped GaN. This band could be excited resonantly, and its excitation spectrum involved one or two broad bands in the range from 2.1 to 2.9 eV. The energy position of the ZPL for this red band has been estimated at 2.0 ± 0.2 eV.²⁰⁴ When excited above the band gap, the red band was buried under the stronger 2.2-eV YL band.

b. Beryllium doping. Be is a potential *p*-type dopant, particularly since it is expected to introduce the shallowest acceptor level in wurtzite GaN (Sec. II). Although the theory predicts substantial self-compensation of Be by deep donors during growth, experimental approaches used to incorporate Be have been examined nonetheless. In particular, Yu *et al.*^{380,381} reported on an increase of the room-temperature hole concentration up to 2.6×10^{18} (Ref. 381) and even to $8 \times 10^{19} \text{ cm}^{-3}$ (Ref. 380) in Mg-doped GaN after implantation with Be.

Dewsnip *et al.*,²⁰³ Sánchez *et al.*,³⁸² and Ptak *et al.*³⁸³ observed the PL band that can be attributed to the shallow acceptor level introduced by Be_{Ga} acceptor in Be-doped GaN grown by MBE, as shown in Fig. 75. The band represents a set of peaks separated by the energy of LO phonon in GaN which is about 91 meV. The peak at 3.38 eV has been attributed to the zero-phonon transition from the shallow donor to the Be_{Ga} acceptor,^{203,382,383} while the peak at 3.397 eV is thought to be due to the zero-phonon transition from the conduction band to the Be_{Ga} acceptor.³⁸³ The ratio between the intensities of the ZPL and its phonon replicas is typical of the shallow acceptors with a small Huang–Rhys factor, similar to the case of the UVL band caused by the unidentified shallow acceptor in GaN described in Sec. IV C 1. The assignment of the 3.38- and 3.397-eV lines to the DAP and e-A transitions has been confirmed by an analysis of their behavior at different temperatures and excitation intensities.^{203,382,383} The 3.38-eV peak decayed nonexponentially and shifted to lower energies with time following a pulse excitation, as it is expected for the shallow DAP transitions.³⁸² From the energy position of the DAP and e-A peaks, the ionization energy of the Be_{Ga} acceptor can be estimated as 100 ± 10 meV, which is much lower than that of Mg_{Ga} .^{203,382,383}

In some investigations,^{199,384} though, the 3.38-eV peak was not observed in Be-doped GaN at all. Instead, the UVL band with the main peak at about 3.27 eV has been observed which is apparently related to residual shallow acceptor in GaN (Si_N , C_N , or Mg_{Ga} , as discussed in Sec. IV C). A tiny peak at 3.35 eV observed in Ref. 385, which was attributed to Be_{Ga} , should be regarded with a good deal of skepticism

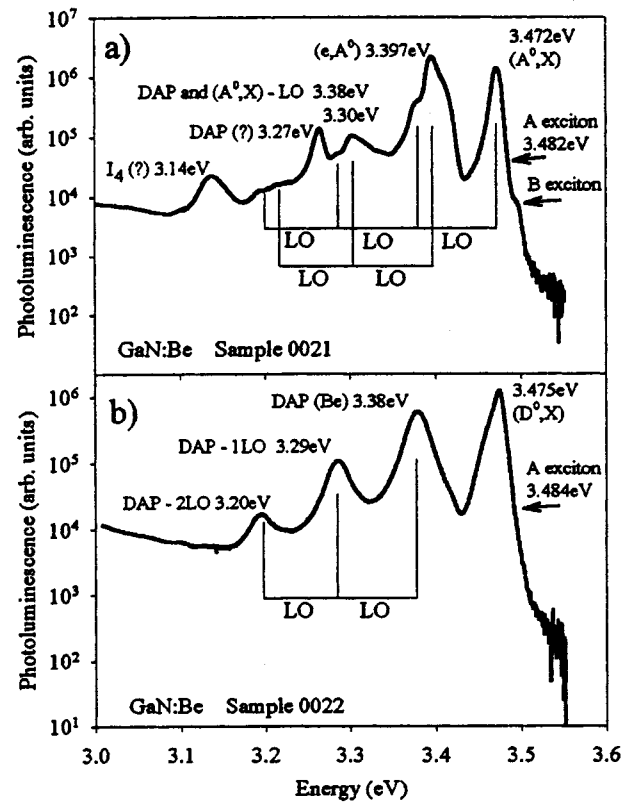


FIG. 75. Low-temperature PL from two Be-doped GaN grown by MBE. Reprinted with permission from Ptak *et al.*, Mater. Res. Soc. Symp. Proc. 639, G3.3 (2001).

as it might be noise or some artifact of measurement.

The enhancement of the YL band with its maximum at about 2.2 eV has been noted in GaN samples implanted with Be.^{123,199,201} It is quite likely that this transition is not related directly to Be but is caused by the implantation damage.^{199,201,386} In the samples doped with Be during growth, an enhancement of an emission in the visible part of the spectrum has also been reported.^{203,382} This emission represented a very broad band peaking at 2.4–2.5 eV and is thought to be related to some deep level or levels apparently caused by Be.

c. Calcium doping. Pankove and Hutchby,¹²³ Monteiro *et al.*,³⁸⁷ and Chen and Skromme²⁰² studied PL from GaN implanted with Ca. In two of these reports a strong green luminescence band with a maximum at about 2.5 eV appeared after the Ca implantation and subsequent annealing.^{123,387} It should be noted that Chen and Skromme²⁰² observed another green luminescence band with a maximum at 2.35 eV in GaN:Ca. However, those authors also noted that the 2.35 eV appeared in their semi-insulating GaN samples doped with Mg and Zn. Therefore, the 2.35-eV peak may not be related to Ca (see Sec. IV F on the 2.35-eV band). With increasing measurement temperature from 14 to 300 K, the green band shifted from about 2.52 to 2.59 eV.³⁸⁷ In another investigation, Monteiro *et al.*³⁸⁷ proposed that the 2.5-eV emission is due to transitions from a deep compensating donor located at about 0.6 eV below the conduction band to the Ca-related acceptor located at about 0.3 eV above the valence band. This assignment appears questionable because the deep DAP

transitions are characterized with enormous shifts of the band with excitation intensity⁸² or with time following a pulse excitation.³³⁵ Note that no shift of the green band with excitation intensity or time following pulse excitation was detected in Ca-doped GaN.³⁸⁷ We propose that the 2.5-eV band is related to transitions from the conduction band, or shallow donors at low temperatures, to the Ca_{Ga} acceptor. If so, the ionization energy of Ca_{Ga} can be estimated at about 0.6–0.7 eV. Indeed, the ZPL for the 2.5-eV band can be expected at 2.8–2.9 eV from the shape of this band at low temperature.

d. Cadmium doping. Cadmium at the Ga site (Cd_{Ga}) is an acceptor. The PL due to Cd has been studied in Refs. 123, 202, 266, 388, and 389. Simply, doping with Cd results in the emergence of a broad blue band peaking at 2.7–2.9 eV. Lagerstedt and Monemar³⁸⁸ observed the fine structure on the high-energy side of the band with the ZPL at 2.937 eV and a set of LO and apparently local phonon replicas. The fine structure, caused by electron-phonon coupling, is similar to that in the Zn-related BL band, shown in Fig. 42, although the energy position of the PL band in Cd-doped GaN is shifted to lower photon energies by about 0.1 eV.^{202,388} A lower photon energy of the Cd-related PL, as compared to Zn-related PL, is consistent with the theoretical predictions for the ionization energies of these two acceptors (Sec. II C 2). The ionization energy of Cd should be about 0.56–0.57 eV, provided that the assignment of the 2.937-eV peak in Ref. 388 is accurate.

At 77 K the time-decay of the Cd-related blue band is nonexponential in the microsecond range.²⁶⁶ No obvious variation in the shape and position of this band has been observed at different delay times following a pulse excitation. It is possible that the transitions from the conduction band to the Cd_{Ga} acceptor overlapped with transitions from the shallow donors to the same acceptor cause the nonexponential decay of PL.²⁶⁶

e. Manganese doping. Extrapolating the carrier-mediated magnetic interaction from dilute GaAs:Mn to GaN:Mn, Dietl *et al.*³⁹⁰ predicted high-temperature ferromagnetism in dilute $\text{Mn}_x\text{Ga}_{1-x}\text{N}$ with $x \approx 0.05$ in assumption that the free hole concentrations of the order of 10^{20} cm^{-3} can be achieved in such a material. This prediction paved the way for a plethora of activity for potential application of this material to spin-transport electronics (spintronics). However, in contrast with GaAs where Mn is a relatively shallow acceptor ($E_A \approx 0.1$ eV) which sets the stage for high concentration of free holes to be obtained at room temperature, the Mn level in GaN is almost in the middle of the band gap,^{391–394} and one cannot expect any detectable transport of holes bound to the Mn acceptor even at very high concentrations of Mn. Graf *et al.*^{393,394} have unambiguously demonstrated that in contrast with GaAs,³⁹⁵ holes bound to Mn in GaN:Mn are located in the *d* shell. The $\text{Mn}^{3+/2+}$ acceptor level is located at 1.8 eV above the valence band.^{393,394} Those authors also showed that the characteristic absorption spectrum with the ZPL at 1.42 eV, observed earlier by Korotkov *et al.*,^{391,392} results from an internal ${}^5E \rightarrow {}^5T$ transition in Mn^{3+} (configuration d^4). The transition of holes from Mn^{3+} to the valence band has also been seen in the absorption spectrum for photon

energies above 1.8 eV.^{393,394} Note that when the GaN:Mn sample is codoped with Si, an electron is captured by a Mn acceptor, transforming it into the Mn^{2+} (d^5) state.

Korotkov *et al.*³⁹⁶ observed a PL signal related to Mn acceptor. That band appeared as a broad structureless band with its maximum at 1.27 eV with a FWHM of about 0.26 eV. With increasing temperature from 13 to 300 K, the Mn peak position remained nearly unchanged. A transient PL study of this band revealed a very slow exponential decay of the PL intensity with a characteristic lifetime of about 8 ms.³⁹¹ A slow exponential decay of the PL is typical of internal transitions. Consequently, it is most likely that the 1.27-eV band is caused by transitions of holes from the excited states of Mn^{3+} , located close to the valence band, to its ground 5T level.

f. Other acceptors in GaN. In addition to the above-mentioned acceptors in GaN, Pankove and Hutchby¹²³ examined the effect of Hg implantation on the PL in GaN. Implantation of Hg resulted in a broad green band with a maximum at 2.43 eV. Assuming that this band is due to a transition from the conduction band or shallow donor to the Hg_{Ga} acceptor, the activation energy of the Hg_{Ga} acceptor can be estimated as 0.8 ± 0.2 eV based on the position and shape of this broad band.

Pankove and Hutchby¹²³ also implanted several other elements in GaN that might possibly act as acceptors, such as Cu, Ag, Au, Sr, Ba, Li, Na, K, Sc, Zr, Fe, Co, Ni, Dy, and Er. All of these elements resulted in broad PL bands with maxima ranging from 1.5 to 2.2 eV. In all cases deep levels are responsible for the observed PL. However, it is difficult to distinguish the emission bands associated with these elements from those arising from native defects formed by the implantation damage. In the case of transition metals or rare-earth elements, the emission in the red portion of the spectrum might also be caused by internal transitions in *d* or *f* shells (see Sec. V C 5).

3. Doping with isoelectronic impurities

Isoelectronic impurities, such as As_{N} and P_{N} , have been considered as promising candidates for the mixed anion nitride alloys such as $\text{GaAs}_x\text{N}_{1-x}$ and $\text{GaP}_x\text{N}_{1-x}$. However, formation of deep levels in these alloys, attributed to As_{N} and P_{N} , would induce discontinuous changes in the size of the band gap.⁴⁵

a. Arsenic doping. Arsenic introduces a broad blue band with its peak at about 2.6 eV in GaN.^{123,202,397–400} It is usually structureless, but a well-defined phonon-related fine structure has also been reported.²⁰² The intensity of the 2.6-eV band increases monotonically with increasing As doping,^{398,400} while the concentration of free electrons remains nearly unchanged.^{401,402} Several authors noted that the intensity of this band is nearly insensitive to temperature in the range of ~ 10 –300 K.^{397–399} An activation energy of ~ 50 meV has been estimated for quenching of the 2.6-eV band between 100 and 300 K.³⁹⁷ Note that the total decrease of the intensity in Ref. 397 was only a factor of 2; therefore, the small decrease might be related to the variation in the

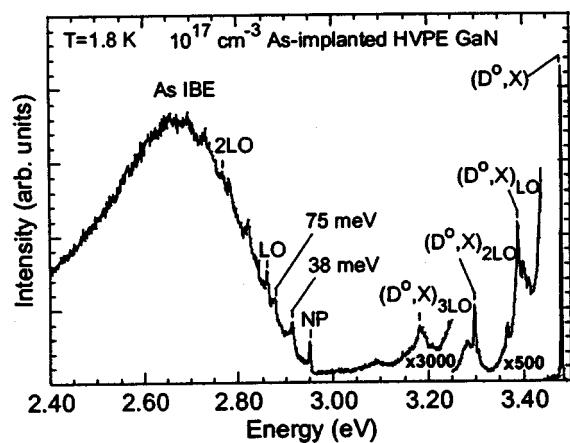


FIG. 76. Low-temperature PL spectrum of the As-implanted GaN, showing the no-phonon (NP) line and its phonon replicas. Reprinted with permission from Chen and Skromme, Mater. Res. Soc. Symp. Proc. 743, L11.35 (2003).

capture cross section,⁶⁷ and the real quenching of this band might take place above room temperature with yet an unknown activation energy.

A time-resolved PL study revealed that the decay of the 2.6-eV band is nearly exponential even at low temperatures with a characteristic time of about 0.1 μ s.^{397,399} The lifetime decreased from 92 to approximately 77 ns with increasing temperature from 8 to 100 K, and subsequently increased up to 148 ns with further increase of temperature up to 300 K.³⁹⁹ Such a behavior of the PL is typical for internal transitions rather than transitions involving the states in the conduction or valence bands.

Chen and Skromme²⁰² observed the fine structure on the high-energy side of the blue band related to As implantation, as depicted in Fig. 76. The ZPL was observed at 2.952 eV followed by two LO phonon replicas. Besides, the spectrum contained peaks separated from the ZPL by 38 and 75 meV that were attributed to other lattice phonon modes.²⁰² If the 2.6-eV band is due to the recombination of an exciton bound to the As-related defect, as it was suggested in Refs. 202, 397, and 399, its localization energy can be estimated as 535 meV which represents the energy difference between the zero-phonon line and free-exciton line.²⁰² However, if the transitions from the conduction band to the As-related defect were responsible for the 2.6-eV emission, the energy level of the As-related defect would be at about 560 meV above the valence band. A more detailed analysis, including comparison of the PL lifetime with concentration of free electrons at different temperatures, is warranted and would be able to provide the ultimate answer on identification of the 2.6-eV band in As-doped GaN.

b. Phosphorus doping. Implantation of P in GaN results in a broad blue-violet luminescence band peaking at about 2.9 eV.^{123,202,403,404} This band quenched above 100–150 K with an activation energy of about 168–180 meV.⁴⁰³ Chen and Skromme²⁰² observed the fine structure of the blue-violet band in GaN:P, as shown in Fig. 77. The ZPL at 3.200 eV is followed by two LO phonon replicas (91 meV) and a few other phonon replicas, separated by 39, 59, and 77 meV from the ZPL, that have been attributed to various lattice phonon

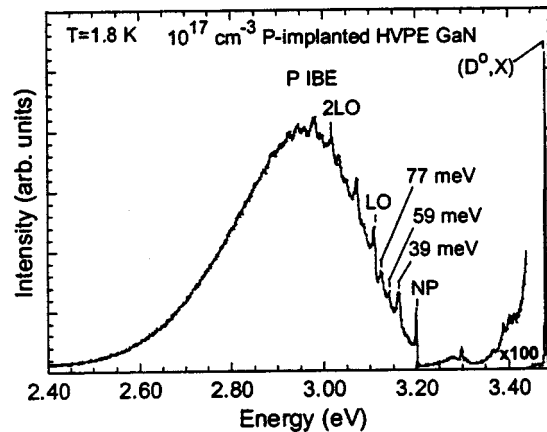


FIG. 77. Low-temperature PL spectrum of the P-implanted GaN, showing the no-phonon (NP) line and its phonon replicas. Reprinted with permission from Chen and Skromme, Mater. Res. Soc. Symp. Proc. 743, L11.35 (2003).

modes.²⁰² The energy separation of 287 meV between the ZPL and the free-exciton line yields the exciton localization energy, provided that the blue-violet band is due to the iso-electronic P_N bound exciton.²⁰²

4. Radiative defects introduced by irradiation

Native point defects, such as interstitials and vacancies, can be created by high-energy electron irradiation. However, a threshold energy, of the order of ~ 1 MeV, must be overcome to produce atomic displacements.¹⁷⁷ This forms the motivation for using 1–2.5-MeV electrons in studies of defects created by irradiation. To remove the additional crystal damage caused by irradiation the samples are subsequently annealed before conducting the intended studies.

The PL signal from defects created by electron irradiation has been a topic of investigation in a number of reports.^{31,184,185,405–408} Of particular interest, two infrared PL bands at about 0.85 and 0.95 eV emerge in the low-temperature PL spectrum after irradiation of GaN with 2.5-MeV electrons at doses above $\sim 10^{18}$ cm⁻² at room temperature.^{31,184,185,407,408} The former contains a sharp ZPL at 0.88 eV accompanied by a rich phonon structure. The latter is relatively broad and apparently structureless. Buyanova *et al.*⁴⁰⁸ proposed that the 0.88-eV emission is related to the internal transition between an excited and ground states of a deep defect, but the identity of the defect was not revealed. Relying on the thermal quenching of this PL band having an activation energy of ~ 30 meV, those authors concluded that the excited state is close to the conduction band and, therefore, the ground state is located 0.91 eV below the conduction band.

Paramagnetic-resonance studies of the PL signal led to the identification of the infrared bands. Four EPR signals labeled L1–L4 have been observed via ODMR experiments in these bands.^{31,405} The L1, L3, and L4 signals corresponding to the $S = \frac{1}{2}$ centers were detected in the 0.95-eV band, while the L2 signal corresponding to the $S = 1$ center matched the 0.88-eV band extremely well.⁴⁰⁵ A well-resolved hyperfine interaction structure observed for the L3 and L4 signals indicates that interstitial Ga atom (apparently by pairing with

some other defect) is responsible for the 0.95-eV band.⁴⁰⁵ *In situ* irradiation with 2.5-MeV electrons at 4.2 K resulted in the appearance of the 0.95-eV band while the 0.88-eV band became absent.³¹ Surprisingly, none of the L1–L4 signals was detectable by ODMR in this case, implying that none of the related defects had been created immediately following the 4-K *in situ* irradiation. Instead, the effective-mass donor and a new L5 signal were detected. The latter was unambiguously identified as the isolated Ga_i^{2+} .³¹ Upon a low-temperature annealing (below room temperature) the effective-mass donor and L5-related signals quenched, while the L1 and L2 signals emerged. This led Chow *et al.*³¹ to conclude that Ga_i^{2+} is formed by the low-temperature irradiation, but it easily migrates and eventually forms complexes with other defects at elevated temperatures. Therefore, both the 0.88- and 0.95-eV bands are considered related to some complexes involving Ga interstitials.

5. Transition and rare-earth elements

Optical properties of transition metals and rare-earth elements are mainly determined by internal transitions rather than by transitions between the host bands and the defect levels. The PL spectrum from transition and rare-earth elements usually contains a set of sharp lines corresponding to optical transitions between different states of the metal ion. The energy positions of these lines for a particular metal vary only weakly between different semiconductors. For this reason we confine the review of the PL from transition and rare-earth elements to a brief listing of the relevant references with only minimal comments.

a. Transition metals. Metals Zn, Cd, Hg, Cu, Ag, and Au are formally considered as transition metals. However, the *d* shells of these particular metals are normally filled completely. Consequently, these metals do not exhibit internal transitions in GaN (see Sec. IV B for Zn in GaN and Sec. IV D 2 for Cd- and Hg-doped GaN). A very common transition metal, Mn, and the PL transitions associated with it in the GaN host are reviewed in Sec. IV D 2 e. Among the other transition metals, the PL lines due to Fe, Cr, Ti, and V have been investigated. Generally, these transition metals are inadvertently incorporated into GaN as a result of contamination during the growth.

The ZPL due to the internal ${}^4T_1 \rightarrow {}^6A_1$ transition in *3d* shell of Fe^{3+} on Ga site (*3d*⁵) has been observed at 1.30 eV in GaN.^{152,409–412} Fe_{Ga} is an acceptor in GaN, and its $-/0$ level is located at 2.5 eV above the valence band.⁴¹³

The line at 1.193 eV has often been observed^{152,409,414–416} and assigned either to ${}^1E \rightarrow {}^3A_2$ transition of Ti^{2+} (*3d*²) (Ref. 416) or to ${}^3T_2 \rightarrow {}^3A_2$ transition of Cr^{4+} (*3d*²).⁴¹⁵ The line at 1.047 eV can be attributed to the ${}^4T_2 \rightarrow {}^4A_2$ transition of Co^{2+} on Ga site (*3d*⁷).⁴¹² The 0.931-eV line has been assigned to the *3d* shell transition ${}^3T_2 \rightarrow {}^3A_2$ of V^{3+} (*3d*²).⁴¹⁵ However, no correlation between vanadium doping and the 0.931-eV line has been noted.⁴¹⁷ Vanadium followed by annealing has been reported to give rise to a sharp and intense line at 0.820 eV.⁴¹⁷

b. Rare-earth elements. Rare-earth elements are incorporated into GaN to fabricate efficient light-emitting devices

whose wavelength is determined by internal transitions associated with the impurity while GaN acting as a host.⁴¹⁸ The luminescence properties of the partially filled *4f* shell associated with rare earths, which is electrically shielded from the surrounding host material, are to a first extent insensitive to the nature of the host. Blue,^{419–421} green,^{420,422–426} red,^{426–435} turquoise,⁴³⁶ yellow, and orange⁴³⁷ colors of luminescence from GaN doped with rare earth have been demonstrated. In GaN, Tm^{3+} is commonly used for blue, Er^{3+} for green and infrared, and Eu^{3+} or Pr^{3+} for red emission.

VI. DEFECT-RELATED LUMINESCENCE IN CUBIC GaN

The present review focuses mainly on wurtzite or hexagonal GaN, but we briefly review the defect-related PL in cubic GaN below for completeness. The discussion is deemed useful for understanding the physics of defects in GaN, both with hexagonal and cubic symmetries, since defects in these two lattice configurations are expected to have many common features. Moreover, optical transitions in wurtzite GaN are sometimes attributed to recombination in cubic inclusions, which necessitates some level of knowledge in this less studied polytype.

Zinc-blende (cubic) GaN is a metastable phase. It is usually obtained by MBE growth on cubic substrates. The band gap of cubic GaN is 3.300 ± 0.004 eV at low temperatures,^{438,439} which is about 200 meV smaller than that in hexagonal GaN. This material is attractive, in particular, due to high mobilities and controlled doping concentrations of free carriers already achieved in both *n* and *p* types.^{440,441}

A. Undoped material

1. Exciton emission

A line at 3.27 eV, which can be seen in Fig. 78, is attributed to an exciton bound to the shallow donor in cubic GaN.^{438,442–444} The position of this line is independent of the excitation intensity and follows the band gap with increasing temperature.^{438,444–447} With increasing temperature, this line is gradually replaced by the free-exciton emission, although these transitions have not been resolved as distinct lines.^{438,443,444,447} Utilizing temperature-induced quenching of the 3.27-eV line, Strauss *et al.*⁴⁴² have estimated the localization energy of the donor-bound exciton as 4 ± 2 meV. Assignment of the 3.27-eV line to the donor-bound exciton at low temperatures is in agreement with its very short lifetime of about 30 ps.^{442,448} Above 50 K, the free-exciton emission quenches with an activation energy of 22–26 meV, which is attributed to the binding energy of the free exciton.^{444,447}

2. Shallow DAP band

A line at about 3.16 eV (Fig. 78) observed in cubic GaN is assigned to the zero-phonon transition of the shallow DAP band.^{77,438,443,444,446,447,449–451} Up to two LO phonon replicas can be seen which are separated by about 86 meV from the zero-phonon line.⁴³⁸ A very small electron-phonon coupling, with a Huang–Rhys factor of about 0.02,⁴³⁸ is typical for the effective-mass acceptors, as seen in Fig. 78. The DAP emis-

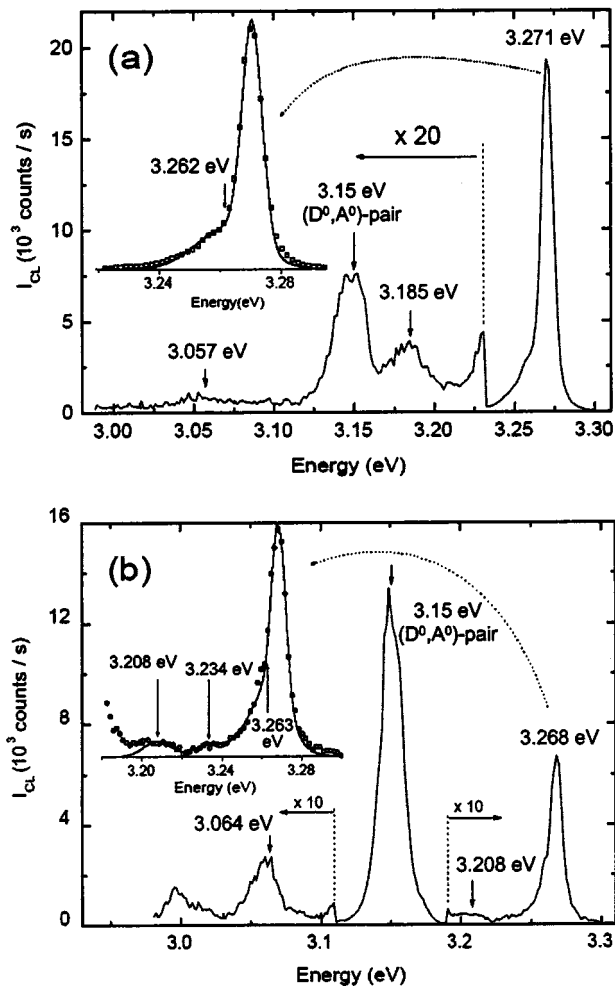


FIG. 78. CL spectra of a cubic GaN crystal at 5 K. (a) and (b) correspond to different points on the same crystal. The solid lines in the insets are fits to the data points, using Gaussians. The FWHM of the exciton line amounts to 8 meV (a) and 11 meV (b). Reprinted with permission from Menniger *et al.*, Phys. Rev. B 53, 1881 (1996). Copyright (1996) by the American Physical Society.

sion shifted markedly to higher photon energies both with excitation intensity^{438,443,445–447,451} and with temperature,^{438,445–447} demonstrating a behavior typical of the DAP-type transitions. As *et al.*⁴⁴⁴ observed transformation of the DAP transition into an e-A transition involving the same shallow acceptor and determined the activation energies of the shallow donor and acceptor in cubic GaN as 25 ± 5 and about 130 meV, respectively.

Two PL lines at 3.08 and 2.99 eV have been identified as the ZPL and LO phonon replica, respectively, of the DAP transition involving another deeper donor.⁴⁵² The electron-phonon coupling for this emission, with a Huang–Rhys factor of about 0.4, is stronger than that for the shallowest acceptor.⁴⁵² The 3.08-eV line should not be confused with the first LO phonon replica of the 3.16-eV line, appearing as a very weak peak in selected samples, as depicted in Fig. 78.^{438,452} Wu *et al.*⁴⁴⁶ also attributed the weak lines observed at 3.056 and 3.088 eV to a deeper acceptor in cubic GaN based, owing to their temperature and excitation intensity dependencies. Possibly the 3.08-eV line is caused by residual carbon, as discussed in Sec. VI B 1.

3. Deep defects

In addition to the common emission lines in cubic GaN, Xu *et al.*⁴⁴⁵ observed two relatively broad lines at 2.926 and 2.821 eV. These lines shifted by about 40 meV to higher energies with increasing excitation intensity by two orders of magnitude. With increasing temperature, the lines shifted to lower energies faster than the band gap decreased and quenched above ~ 100 K with an activation energy of about 18 meV. Xu *et al.*⁴⁴⁵ proposed that the 2.926- and 2.821-eV lines are caused by transitions between a shallow donor and two deep acceptor levels located at about 0.34 and 0.45 eV above the valence band.

Goldys *et al.*⁴⁵³ observed a broad red luminescence band peaking at about 1.9 eV in undoped cubic GaN. The red band shifted by 32 meV to higher energies with increasing excitation intensity by a factor of 10, demonstrating a behavior typical of DAP transitions.⁴⁵³ With increasing temperature, the red band quenched with an activation energy of 15 meV, although its intensity decreased by only $\sim 25\%$ up to room temperature.⁴⁵³ The decay of the red band is slow and non-exponential, in agreement with its assignment to DAP recombination.⁴⁵³

B. Doped material

1. Carbon doping

As *et al.*^{440,454,455} reported *p*-type doping of cubic GaN with carbon by plasma-assisted MBE on GaAs substrates. The reported hole concentration and hole mobilities were $6.1 \times 10^{18} \text{ cm}^{-3}$ and $23.5 \text{ cm}^2/\text{V s}$, respectively, in *c*-GaN.⁴⁴⁰ In samples with a hole concentration below approximately 10^{17} cm^{-3} the hole mobility exceeded $200 \text{ cm}^2/\text{V s}$.⁴⁴⁰

Doping with carbon results in a relatively narrow PL band at about 3.08 eV and a very broad band between 1.8 and 2.3 eV, as depicted in Fig. 79.⁴⁵⁶ The intensity of the 3.08-eV band monotonously increases with C doping (Fig. 79).⁴⁵⁵ In fact, the band consists of two lines separated by about 25 meV. The lower-energy component is attributed to the DAP transition and the higher-energy component to the e-A transition involving the same C_N acceptor with a binding energy of 215 meV.^{455,456} The donor, having a binding energy of 25 meV, is apparently the same as in undoped cubic GaN.⁴⁴⁴

As and co-workers^{440,454,456–458} also observed a broad red-yellow luminescence band with peaks at about 2.12 and 1.89 eV in C-doped GaN. As can be seen in Fig. 79, the intensity of this red-yellow band monotonously increases with C doping.⁴⁵⁷ Those authors assigned the double-peak band to transitions from a deep C-related donor which is located 1.185 eV below the conduction band to the shallow C acceptor and the valence band.^{454,456,458,459} Note, however, that there are no equilibrium holes in the valence band at 2 K. Therefore, transitions of photogenerated electrons from a deep donor to the valence band are highly unlikely. However, transitions from a deep donor to the shallow C_N acceptor are plausible for the heavily C-doped cubic GaN. This is in some ways similar to the assignment of the BL band in heavily Mg-doped GaN in hexagonal GaN discussed in Sec. V B 3. As *et al.*^{440,454} proposed that the deep donor is a $C_N C_i$ com-

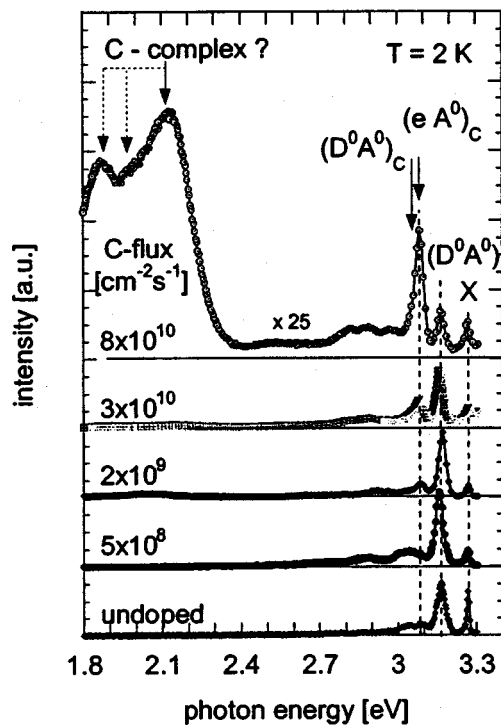


FIG. 79. PL spectra of C-doped cubic GaN layers grown with different fluxes of C. The topmost spectrum has been multiplied by a factor of 25. Reprinted with permission from As *et al.*, Mater. Res. Soc. Symp. Proc. 693, 12.3 (2002).

plex. Note that the energy level of this donor could be estimated from the high-energy cutoff of the yellow band where the ZPL is expected at about 2.3 eV, accounting for the Coulomb interaction in deep DAP which may be rather strong. Overall, an estimate of 1.1 ± 0.2 eV is a plausible figure. Experiments with varying excitation intensities can verify the proposed model and possibly improve the estimate of the donor energy level.

2. Magnesium doping

In contrast with C-doped cubic GaN where carbon incorporates with concentrations above 10^{20} cm^{-3} and the room-temperature hole concentration reaches 6×10^{18} cm^{-3} (Ref. 440), incorporation of Mg in cubic GaN saturates at about 5×10^{18} cm^{-3} and the room-temperature hole concentration does not exceed 10^{16} cm^{-3} (Ref. 460). With increasing Mg doping a blue band peaking at 2.8 eV and two barely resolved peaks at 3.04 and 3.07 eV emerge in the PL spectrum.⁴⁶⁰ The origin of the blue band may be similar to the BL band in hexagonal GaN (Sec. V B 3), although experiments with variation of temperature and excitation intensity as well as time-resolved PL study are needed for confirmation. Note that Xu *et al.*⁴⁶¹ observed the blue band in cubic GaN that noticeably shifted with the excitation intensity in much the same way as the BL band in hexagonal GaN.⁸² However, those authors attributed the oscillatory shape of the blue band to contributions from five transitions with different behavior on the intensity of excitation. One can argue that the oscillatory behavior could also be due to interference effects from the 1.5- μm -thick layer. The 3.04-

and 3.07-eV bands have been attributed to the DAP and e-A transitions, respectively, involving the same Mg_{Ga} acceptor with an activation energy of 0.23 eV.⁴⁶⁰

3. Silicon doping

As in the case of wurtzitic polytype, Si is a very efficient donor in cubic GaN. With increasing Si doping, it has been reported that the exciton emission peak shifted to lower energies with an accompanying increase in its width.^{462,463} For impurity concentrations near 10^{20} cm^{-3} , band-to-band transitions dominated in degenerate GaN:Si at low temperatures.⁴⁶³ The 3.15-eV band, assigned to DAP transitions involving an unidentified shallow acceptor, exhibited a shift to higher energies with increasing Si doping.^{441,463} That shift has been attributed to increased Coulomb interaction in donor-acceptor pairs with smaller separation.⁴⁴¹

VII. EXCITONS BOUND TO POINT DEFECTS

In this section a very brief review of the salient experimental results on exciton-related PL in wurtzitic GaN with an emphasis on excitons bound to shallow defects is presented. Excitonic transitions in GaN are very efficient. Excitons can be bound not only to shallow donors and acceptors but also to deep point defects and structural defects. The latter case is discussed in Sec. VIII.

A. Free excitons

Since the review is devoted to defects in GaN, and free excitons are not related to defects at all, the discussion in this section is mostly limited to the properties of free excitons that are imperative to understanding of PL from bound excitons.

The valence band in wurtzitic GaN is split into three subbands, A, B, and C, due to the crystal-field splitting and spin-orbit coupling. Free excitons may involve a hole from each of the subbands. Accordingly the free A, B, and C excitons are denoted as X_A , X_B , and X_C . The fine structure of the exciton spectrum includes the excited states ($n = 2, 3, \dots$). The fine structure is affected by crystal anisotropy, intersubband coupling, polar interactions with optical phonons (Fig. 80),⁴⁶⁴ as well as electron-hole exchange, and dipole-dipole interaction.^{464,465} In particular, the 1S state of the A exciton is split by the short-range exchange interaction into a dipole-forbidden Γ_6 state (with energy E_6) and a dipole-active Γ_5 state (with energy $E_5 = E_6 + \Delta_{56}$, where Δ_{56} is the energy of the electron-hole exchange interaction).⁴⁶⁵ The exciton fine structure depends on the geometrical configuration of the optical experiment (Fig. 81). When the exciton wave vector \vec{k} is parallel to the hexagonal axis c , both Γ_5 components are transverse Γ_{5T} states. On the other hand when $\vec{k} \perp c$, one of the components is a longitudinal Γ_{5L} state which is shifted to a higher energy $E_5 + \Delta_{LT}$ by the dipole-dipole interaction. Here Δ_{LT} denotes the longitudinal-transverse splitting of the exciton. The longitudinal exciton Γ_{5L} and the forbidden exciton Γ_6 have zero oscillator strength unless they are mixed with allowed states of the B exciton. Further, interaction of the transverse excitons Γ_{5T} with the radiation field results in the formation of lower,

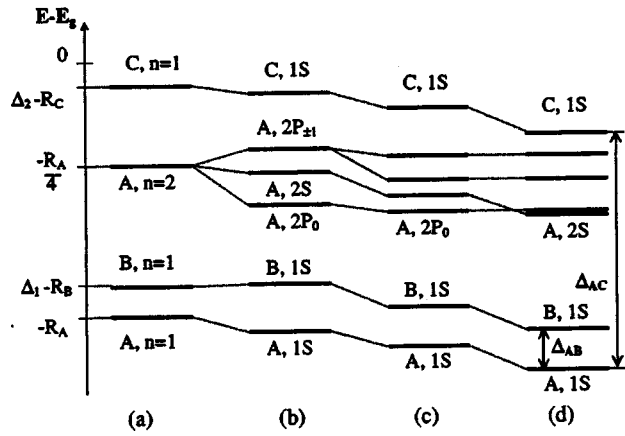


FIG. 80. A schematic of the exciton energy levels in wurtzite GaN in (a) an uncoupled hydrogenlike isotropic model, (b) including the effect of anisotropy, (c) including the effects both of anisotropy and intersubband coupling, and (d) including anisotropy, intersubband coupling, and polaron corrections. Reprinted with permission from Rodina *et al.*, Phys. Rev. B 64, 115204 (2001). Copyright (2001) by the American Physical Society.

Γ_{5T1} , and upper, Γ_{5T2} , transverse-polariton branches. Depending on the relaxation and scattering processes in the GaN layer and the excitation conditions, polaritons from both branches may contribute to the luminescence with energy peaks at about E_5 and $E_5 + \Delta_{LT}$.

Figure 82(a) presents the PL spectrum from the 80- μm -thick GaN layer in the commonly used configuration of PL experiment in which the wave vector of the emitted light \vec{k} is parallel to the crystalline c axis. Figure 82(b) shows the PL spectra taken in another configuration, namely, for the case where the emission \vec{k} vector is perpendicular to the c axis, and two polarizations of PL, determined by the orientation of the electric field \vec{E} , are distinguishable: σ polarization ($\vec{E} \perp c$) and π polarization ($\vec{E} \parallel c$). Free-exciton peaks at $\vec{E} \parallel c$ appear at lower energies than at $\vec{E} \perp c$. The small shifts in the amount of 0.53 ± 0.03 and 0.24 ± 0.08 meV for the A and B

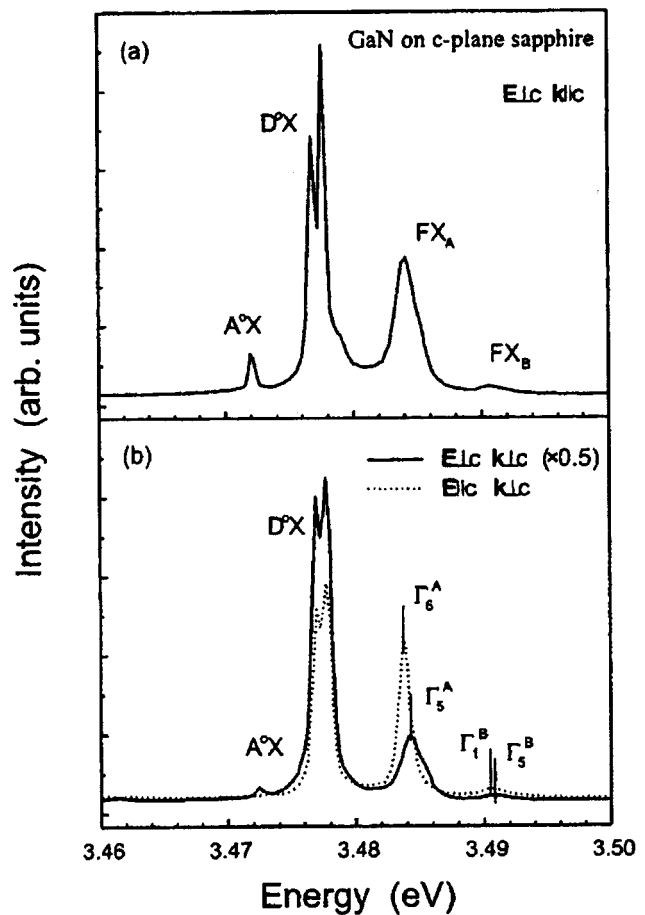


FIG. 82. PL spectra of the 80- μm -thick GaN layer for σ polarization (solid line) and π polarization (dotted line). The intensities of the donor-bound excitons (double peak at about 3.477 eV) and acceptor-bound excitons (at about 3.473 eV) are substantially lower in the π -polarized spectrum compared to the σ polarization because the bound A excitons are dipole-forbidden in the $\vec{E} \parallel c$ geometry. Note that due to biaxial compressive stress in GaN grown on sapphire all peaks in this sample are shifted to higher energy by 7 meV as compared to homoepitaxial GaN layers. Reprinted with permission from Paskov *et al.*, Phys. Status Solidi B 228, 467 (2001).

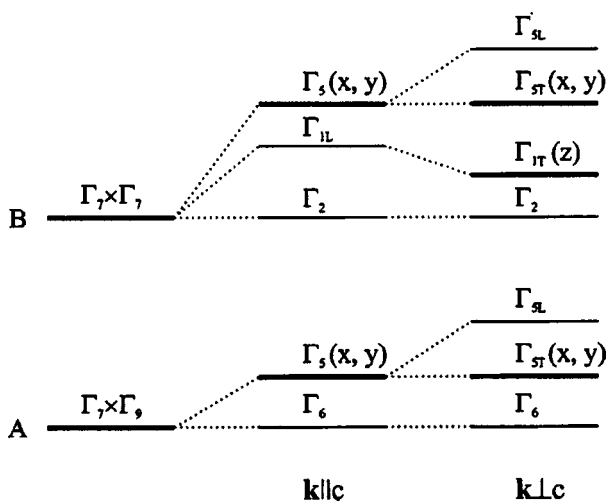


FIG. 81. Schematic diagram of the internal structure of X_A and X_B excitons in a wurtzite GaN. The allowed polarizations are given in parentheses. The thin lines correspond to dipole-forbidden states. Reprinted with permission from Paskov *et al.*, Phys. Rev. B 64, 115201 (2001). Copyright (2001) by the American Physical Society.

excitons, respectively, are due to the exchange interaction (Fig. 81).^{465,466} The observed splitting $\Delta_{56} = 0.53 \pm 0.03$ meV corresponds to the exchange interaction constant $\gamma = 0.58 \pm 0.05$ meV,⁴⁶⁵ in very good agreement with the value $\gamma = 0.6 \pm 0.1$ meV estimated from the polarized reflectance experiments.⁴⁶⁷ A much smaller value of 0.12 ± 0.1 meV for the Δ_{56} splitting has been reported in Ref. 464. Note that the width of free excitons is substantially larger than the estimated splittings, so that the accuracy may not be good enough. Reynolds *et al.*⁴⁶⁸ reported a much higher value of Δ_{56} (2.9 meV). However, apparently the peak assigned in Ref. 468 to Γ_6 state could, in fact, be the B exciton bound to a neutral shallow donor.⁴⁶⁵ The value of the longitudinal-transverse splitting, $\Delta_{LT} = 1.0 \pm 0.1$ meV, for the free A exciton has been estimated from magnetoluminescence data,⁴⁶⁴ as well as reflectance measurements.^{469,470}

The binding energy of the free A exciton has been estimated as 26.7 ± 0.3 meV from the temperature dependence of the X_A intensity.^{471,472} Alternatively, the ground-state binding energy of free exciton can be obtained at low temperatures from the difference between the $n=1$ and $n=2$ states: $E_{A,1S}$

$=\frac{4}{3}(E_{A,n=2}-E_{A,n=1})$. By this method, in nearly strain-free thick GaN layers, the free A exciton binding energy was estimated as 26.3 ± 0.3 meV.^{464,471} Within the limits of the experimental error, the binding energies of the B and C excitons are the same as for the A exciton.⁴⁶⁴ The obtained value of the free A exciton binding energy provides the band-gap value of about 3.503–3.504 eV for the strain-free GaN in the limit of low temperatures, in excellent agreement with an early estimate obtained in lower-quality samples.⁴⁷³ The Bohr radius of free excitons can be estimated from the binding energy of about 26 meV as about 30 Å.

The transition energies are dependent on the substrates employed due to the expansion-coefficient mismatch. Usually, thin GaN films grown on sapphire experience a biaxial compressive strain shifting the PL lines towards higher energies. In contrast, thin GaN films grown on SiC exhibit a biaxial tensile strain shifting the PL energies towards lower photon energies.^{471,474,475}

B. Bound excitons

In theory, excitons may be bound to neutral and ionized donors and acceptors, as well as to isoelectronic defects. Not all of the excitons may be observed in a given semiconductor for only some of them are stable. Since the bound excitons have much smaller kinetic energies than free excitons the spectral width of the bound-exciton transitions is generally narrower than those for the free excitons. The energy of the photon emitted through bound-exciton recombination is given by

$$\hbar\omega = E_g - E_x - E_{BX}, \quad (39)$$

where E_x is the free-exciton binding energy and E_{bx} is the additional energy of binding the free exciton to the defect. The same expression applies to excitons bound to neutral or charged impurities (if they are stable) as well with the last term naturally representing the additional energy of binding the free exciton to impurities. The radiative recombination lifetime of bound excitons increases with the binding energy E_{BX} .^{476,477} The emission lines corresponding to recombination of excitons bound to a neutral acceptor, a neutral donor, and an ionized donor are labeled A^0X , D^0X , and D^+X , respectively (or I_1 , I_2 , and I_3 , respectively, according to a nomenclature established for the hexagonal II-VI semiconductors many years earlier⁴⁷⁸). In excitons bound to neutral donors and acceptors, the like particles predominantly couple.⁴ The particle with the opposite sign is weakly bound by the attractive Coulomb potential of the two coupled particles. Since for shallow dopants all three particles involved are shallow, with a substantial wave-function overlap, other interactions do exist which may lead to additional excited configurations.³

The behavior of donor-bound excitons (DBEs) in magnetic field is dominated by the magnetic moment of the bound hole. Therefore, the magnetic properties of the principal state of the shallow DBE should reflect the properties of the Γ_0 top valence subband with the total momentum of hole $J=3/2$. The neutral acceptor-bound excitons (ABEs) should have a $J=0$ two-hole state derived from two Γ_0 holes. The

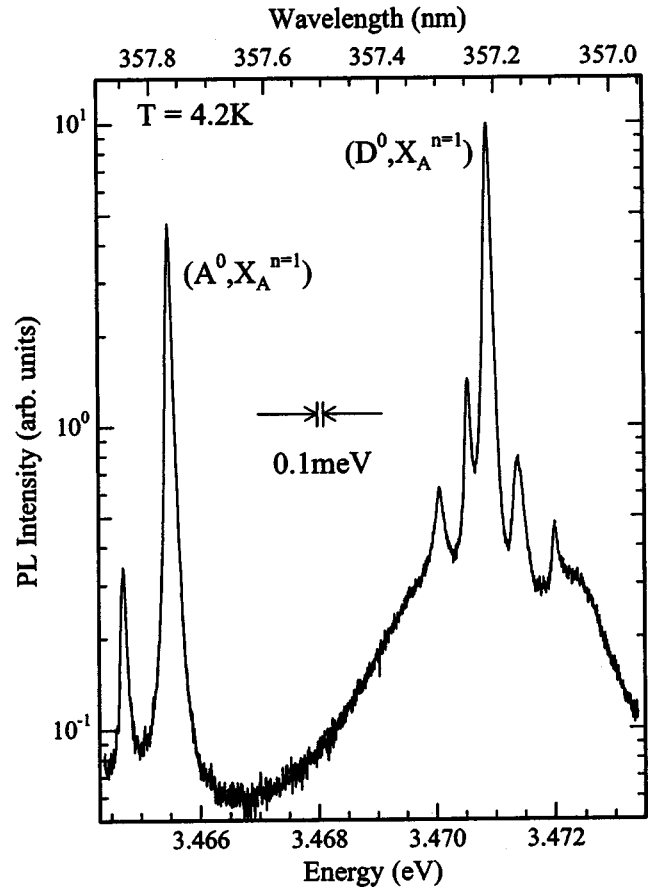


FIG. 83. A high-resolution PL spectrum of a homoepitaxial MOCVD-grown GaN. Reprinted with permission from Kornitzer *et al.*, Phys. Rev. B 60, 1471 (1999). Copyright (1999) by the American Physical Society.

additional electron in the ABE state then contributes its unpaired spin, so the ABE state would have $J=\frac{1}{2}$ (Ref. 3).

Excitons can also be bound to extended defects, such as dislocations or stacking faults, as discussed in Sec. VIII. Dislocations create strong local strain fields, causing effectively a one-dimensional electronic potential that may bind excitons.³ In addition, dislocations can getter point defects that in turn may bind excitons.

1. Excitons bound to shallow donors

Excitons bound to neutral donors (D^0X_A) are commonly responsible for the dominant PL line in n -type GaN grown by any technique on any substrate. In high-quality strain-free GaN samples with low concentration of defects, the D^0X_A emission at about 3.471 eV sometimes consists of two or more sharp lines (Fig. 83), tentatively attributed to different shallow donors.^{222,479–481} In addition to the principal D^0X_A emission, several excited states, satellite transitions, and phonon replicas related to the shallow donor-bound excitons have been reported.^{222,479,480,482,483} Figure 84 shows a typical low-temperature PL spectrum of a high-quality freestanding GaN template. The peak with the highest energy (the last peak in a triplet at about 3.50 eV in Fig. 84) is assigned to the $n=2$ excited state of the free A exciton.^{464,471,475,479,483,484} Two other components of the triplet are most probably related to the excited A exciton bound to a ground state of a

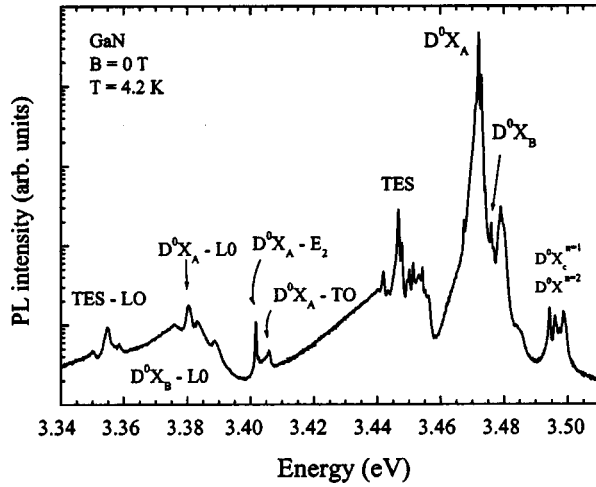


FIG. 84. Low-temperature PL spectrum of freestanding GaN template. Reprinted with permission from Wysmolek *et al.*, Phys. Status Solidi B 235, 36 (2003).

neutral donor ($D^0X_A^{n=2}$) and the donor-bound state of the C exciton (D^0X_C).^{464,479,483,484} A weak line at about 3.475 eV, between the main D^0X_A peak at 3.471 eV and the free-exciton line X_A at \sim 3.478 eV, is attributed to the donor-bound state of the B exciton (D^0X_B).^{222,464,479,480,482,483,485,486} Sometimes two or three peaks related to different shallow donors are resolved at this photon energy.^{222,480}

A series of lines observed between 3.44 and 3.46 eV (Figs. 84 and 85) is due to two-electron satellite (TES) transitions.^{222,479-484} The TES transitions occur when an exciton bound to a neutral donor (D^0X) recombines and leaves the donor in an excited state. The TES energy for a particular

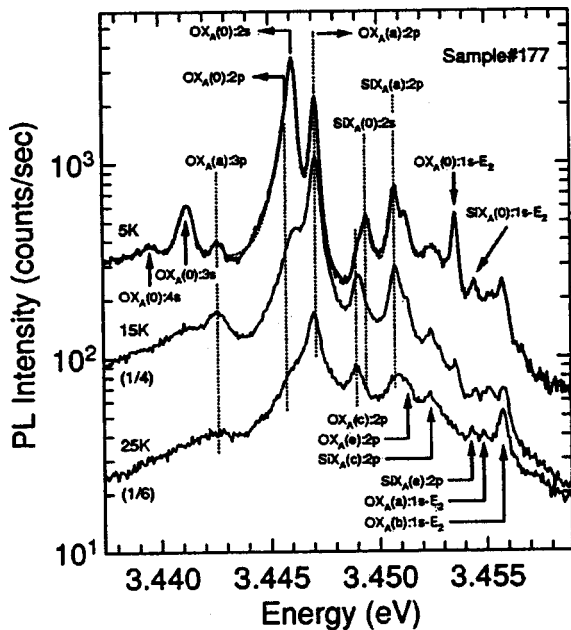


FIG. 85. PL spectra taken at 5, 15, and 25 K in the two-electron satellite region. The dotted line overlapping the 5-K spectrum represents the best fit. Emission-peak assignments apply to the indicated spectrum only except for emission peaks connected by a dotted line. The spectrum intensities measured at 15 and 25 K were divided by 4 and 6, respectively, to minimize overlapping. Reprinted with permission from Freitas, Jr. *et al.*, Phys. Rev. B 66, 233311 (2002). Copyright (2002) by the American Physical Society.

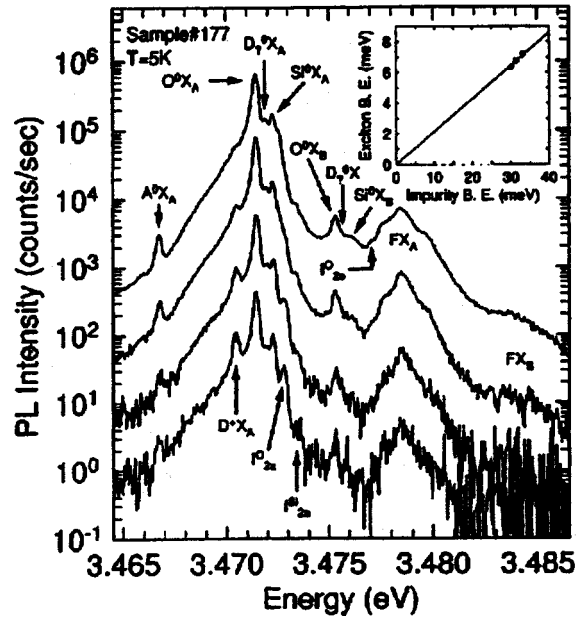


FIG. 86. Low-temperature PL spectra measured with the excitation power densities, from top to bottom, 61.1, 8.4, 0.80, and 0.08 W/cm². The inset represents the linear dependence of the excitons' binding energy with the neutral-donor binding energy. Reprinted with permission from Freitas, Jr. *et al.*, Phys. Rev. B 66, 233311 (2002). Copyright (2002) by the American Physical Society.

donor is smaller than the corresponding D^0X energy by the difference in the ground- and excited-state energies of the neutral donor. Freitas, Jr. *et al.*⁴⁸⁰ have proposed assignments of the TES lines, as shown in Fig. 85. The cumulative assignments are in excellent agreement with the binding energies of Si_{Ga} and O_N donors, 30.18 ± 0.1 and 33.2 ± 0.1 meV, respectively, obtained from magneto-optical studies.²³⁰ Independently, Wysmolek *et al.*⁴⁸¹ have suggested similar assignments of the TES lines based on a detailed analysis of the time-resolved, magneto-optical, and temperature-dependent data. In particular, the excited states of O_N for $n=2, 3, 4,$ and 5 have been resolved in the TES spectrum in magnetic field, and the lifetime of the O_N-bound exciton was estimated as 1.40 ± 0.05 ns.⁴⁸¹

Returning to the overall spectrum from a high-purity freestanding GaN, several phonon replicas of the main peaks have been observed below 3.41 eV, as displayed in Fig. 84. These include the E_2 (high) and TO phonon replicas of the principal D^0X_A transition at 3.402 and 3.406 eV, respectively, and LO phonon replicas of bound and free excitons below 3.39 eV.⁴⁸²

The high-resolution spectrum of the same freestanding GaN template at different excitation intensities is shown in Fig. 86. The assignment of the main D^0X_A peaks to O_N and Si_{Ga} in Fig. 86 is also supported by comparison of the PL spectra from undoped and Si-doped GaN.⁴⁸⁷ Beside the above-mentioned transitions, the spectra at low excitation intensities reveal the emission associated with the charged donor-bound-exciton D^+X_A at about 3.470 eV. Since Si_{Ga} is the shallowest neutral donor and, therefore, expected to be partially compensated, the D^+X_A can be attributed to recombination of excitons bound to Si_{Ga}⁺. Previously, several groups⁴⁸⁸⁻⁴⁹¹ proposed that the peak at about 3.466 eV is

related to a charged donor in GaN. However, compelling arguments, presented in Sec. VII B 2, support the assignment of this peak to exciton bound to a neutral acceptor.

With increasing measurement temperature, the donor-bound excitons thermally ionize which causes the related emission intensity to drop. That decrease in the PL intensity for the lines associated with the ground states of the DBE (including the principal transition and its TES) begins at temperatures just above 5 K.^{480,481} The thermal activation energy of this ionization process has been estimated as 4.5 ± 1 meV from quenching of the DBE emission.⁴⁹² However, this value is apparently underestimated due to the superposition of the PL line from free A excitons and the donor-bound B excitons. Korona⁴⁸⁶ reported an activation energy of 6 meV for the quenching of D^0X_A .

The ionization energies of the Si_{Ga} , Ge_{Ga} , and Sn_{Ga} donors have been estimated as 29, 30, and 33 meV, respectively, in GaN intentionally doped with these impurities.⁴⁹³ Note, however, that these results should be treated with caution since identification of transition reported in this work is not well founded due to a variety of effects. They include insufficient resolution, different residual strains in GaN layers grown on sapphire, and inconsistency with the well-established assignments of the excitonic transitions in undoped and Si-doped GaN. Yang *et al.*⁴⁹⁴ observed formation of a hydrogenic donor with a binding energy of 25 meV after electron irradiation and tentatively attributed it to V_{N} . The binding energy of the exciton bound to this donor was about 5 meV.

2. Excitons bound to acceptors

A transition due to an exciton bound to a neutral shallow acceptor is observed at about 3.466 eV in undoped strain-free GaN (Figs. 82, 83, and 86).^{222,479,480,483,486,495–497} In high-quality GaN, the ABE emission appears as a characteristic doublet (see Fig. 83),^{479,483,496,497} with a sample-independent intensity ratio between the two components.^{496,497} There are several arguments supporting the assignment of the 3.466-eV emission to the neutral shallow ABE. Firstly, its LO phonon coupling is strong, particularly as compared to the DBE case,^{312,479,483,498} a property noted earlier for shallow ABEs in CdS.⁴⁹⁸ Secondly, this line dominates in Mg-doped samples.^{3,199,307,312,313} Finally, its behavior in magnetic field is characteristic of the neutral ABE transitions^{312,496,497} to be discussed below.

In wurtzitic GaN the valence band is anisotropic, and a magnetic field \vec{B} applied along the c axis is expected to split the ground Γ_9 state, while for $\vec{B} \perp c$ no splitting should take place. As is shown below, not only the ground Γ_9 doublet but also the higher ground Γ_7 doublet can be observed in the PL spectrum. Transformation of the PL spectrum associated with A^0X_A under magnetic field applied at an angle $\Theta = 35^\circ$ to the c axis is shown in Fig. 87. Since for the ABE transition the holes are paired off,^{3,495,496} the initial state of the ABE reacts to the magnetic field as if it were a single weakly bound electron with $J = \frac{1}{2}$. By fitting the experimental results and assuming for generality that the effective g factor for A^0X_A is anisotropic, Stepniewski *et al.*⁴⁹⁶ obtained that the g factor

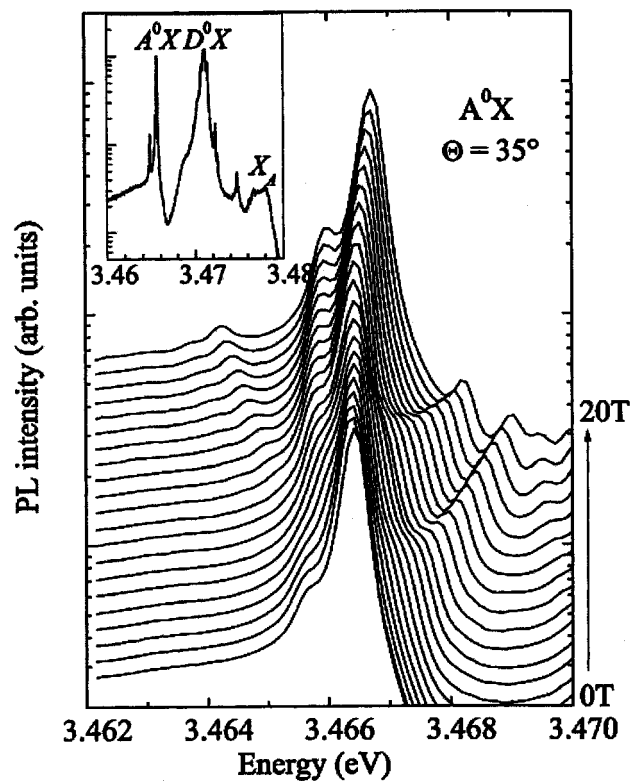


FIG. 87. PL spectra of the exciton bound to a neutral acceptor (A^0X_A) in GaN recorded at different values of magnetic field oriented at 35° to the c axis. The inset shows PL spectrum of GaN in the range of excitonic transitions. Reprinted with permission from Stepniewski *et al.*, Phys. Rev. Lett. 91, 226404 (2003). Copyright (2003) by the American Physical Society.

for A^0X_A varies from 1.914 to ~ 2.07 with increasing Θ from 0° to 90° . The anisotropy of the g factor in the ground state is attributed to an interaction with the excited states. The observed Zeeman splittings for different values of Θ and \vec{B} can be fitted well by assuming that the spin-orbit interaction for the hole bound to the neutral acceptor is significantly reduced (by more than a factor of 10) as compared to that for the free hole.⁴⁹⁶ The small separation between the Γ_7 and Γ_9 states of the A^0X_A complex (about 1 meV) makes its energy structure extremely sensitive to local axial fields in directions other than the c axis. Therefore, the effects of the spin-orbit interaction may not be delineated at all in the presence of local fields caused, for instance, by elevated concentration of impurities. Note that an alternative interpretation of the 3.466-eV line, which assigns it to charged DBE,^{488–491} conflicts with the observed behavior of this line in magnetic fields.

In homoepitaxial GaN layers, the following dynamics of the excitonic recombination is expected.⁴⁸⁶ At low temperatures the decay of free excitons is fast (~ 0.1 ns) due to the efficient capture of excitons by shallow donors. The radiative lifetime of D^0X and A^0X in GaN is about 1 ns, while the radiative lifetime of free excitons is expected to exceed 10 ns.⁴⁸⁶ With increasing temperature, excitons trapped by donors and acceptors delocalize, and the D^0X and A^0X lines quench in favor of the free-exciton emission. The quenching of the A^0X line can be fitted with Eq. (32) using $C \approx 10^4$ and $E_A = 14 \pm 3$ meV.⁴⁸⁶ The relatively high value of C reflects the

high probability of trapping of a free exciton by a neutral shallow acceptor in GaN. The activation energy is in agreement with a binding energy of 11 meV obtained as the difference between the energies of X_A and A^0X_A . The A^0X lifetime decreases above 15 K with the activation energy of 12 ± 3 meV,⁴⁸⁶ evidently due to thermally activated escape of the excitons from the shallow acceptors.

The chemical identity of shallow acceptors in undoped GaN is still not confirmed or defined with sufficient certainty. In Mg-doped GaN, Mg_{Ga} should be the shallow acceptor.^{270,307,312,499} The binding energy of the exciton bound to the Mg_{Ga} acceptor has been estimated as 11.4 meV in homoepitaxial GaN layers doped with Mg.³¹¹ A complicating factor in the identification of the ABE peak and obtaining its binding energy is the varying strain in different layers grown on heteroepitaxial material.²⁷⁰

Among the deeper acceptors in GaN, at least the Zn acceptor can bind excitons. The ABE line with a binding energy of 23–25 meV has been observed in undoped and Zn-doped GaN and attributed to excitons bound to Zn acceptors.^{199,245,267,268,500} Two or even three sharp lines have been resolved on the A^0X_A transition related to Zn.^{268,500} The energies of the triplet components are 3.4542, 3.4546, and 3.4556 eV in unstrained platelet bulk GaN samples.⁵⁰⁰ The same Zn acceptor is responsible for the BL band (with zero-phonon line at 3.100 eV) in undoped and Zn-doped GaN.^{199,245} The ABE with binding energy of about 21 meV observed in Refs. 3 and 501 can also be attributed to residual Zn acceptors.²⁶⁸ Strong electron-phonon coupling for these lines favors their attribution to the neutral acceptors in GaN, and the shape of the exciton emission is similar to that in Zn-doped GaN. Note that the bound-exciton peak with a binding energy of about 38 meV (the A^2X_A line in Ref. 501 and the ABE_3 line in Ref. 3) is apparently also related to excitons bound at the Zn acceptors since a peak with such an energy (at about 3.39 eV in unstrained GaN) always follows the Zn-related A^0X_A line (at about 3.455 eV) in undoped and Zn-doped GaN.^{199,245,267,268,500}

The transient behavior of excitons bound to Mg and Zn acceptors on GaN was studied by Korona *et al.*⁵⁰² In Fig. 88 the evolution of the PL spectrum with time delay is shown where the main peaks at 3.456 and 3.467 eV are assigned to excitons bound to Zn ($A_{Zn}X_A$) and Mg ($A_{Mg}X_A$) acceptors, respectively. The lifetimes of the $A_{Zn}X_A$ and $A_{Mg}X_A$ excitons were deduced to be 1.38 ± 0.03 and about 0.8 ns, respectively. The longer lifetime of the more strongly bound exciton is due to its more effective localization.⁵⁰³

3. Haynes rule in GaN

Haynes⁵⁰⁴ has established the following empirical rule for excitons in silicon. The energy required to free the bound exciton from a defect, E_{BX} , is proportional to the energy required to free the bound carrier from the same defect (E_D or E_A),

$$E_{ABX} = \alpha_A E_A \quad (40a)$$

for acceptors and

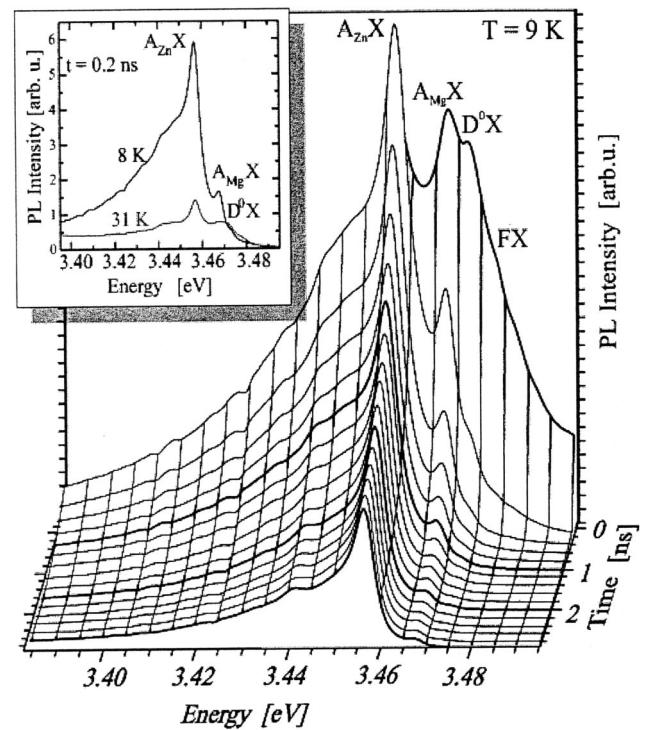


FIG. 88. Time-resolved PL spectrum of GaN:Zn at 9 K. Two lines of excitons bound to Mg acceptor ($A_{Mg}X$) and Zn acceptor ($A_{Zn}X$) are at 3.467 and 3.456 eV, respectively. Inset: comparison of time-integrated spectra of GaN:Zn at 8 and 31 K. Reprinted with permission from Korona *et al.*, Phys. Status Solidi B 235, 40 (2003).

$$E_{DBX} = \alpha_B E_D \quad (40b)$$

for donors. In Si, the proportionality constants α_A and α_B were nearly the same (~ 0.1) for donors and acceptors.⁵⁰⁴ In different SiC polytypes, a similar empirical rule has been established^{505,506} with the proportionality constants for donors and acceptors of ~ 0.2 and ~ 0.1 , respectively.⁵⁰⁶ Note that the data in Ref. 506 could better be fitted with the following set of empirical expressions

$$E_{ABX} = \alpha_A E_A + \beta_A, \quad (41a)$$

$$E_{DBX} = \alpha_B E_D + \beta_B, \quad (41b)$$

with $\alpha_A = 0.16$ and $\beta_A = -14.9$ meV for acceptors and $\alpha_B = 0.25$ and $\beta_B = -3.58$ meV for donors,⁵⁰⁶ or with the expressions

$$E_{ABX} = \alpha_A E_A^n, \quad (42a)$$

$$E_{DBX} = \alpha_D E_D^n, \quad (42b)$$

with $\alpha_A \approx 0.02$ and $\alpha_D \approx 0.06$ for acceptors and donors, respectively, and $n \approx 1.3$ for both. Similarly, Dean⁵⁰⁷ has found that the binding energies of excitons trapped by shallow and deep donors in GaP can be described by a modified Haynes rule [Eqs. (42)] with $\alpha \approx 0.01$ and $n = 1.63$. Note that for the shallow donors in GaP one would obtain $\alpha \approx 0.1$ for $n = 1$, similar to the value in Si.

For the bound donors and acceptors in GaN, the Haynes rule is also applicable, as shown in Fig. 89. The experimental data can be fitted with Eqs. (40). For shallow donors, α_D

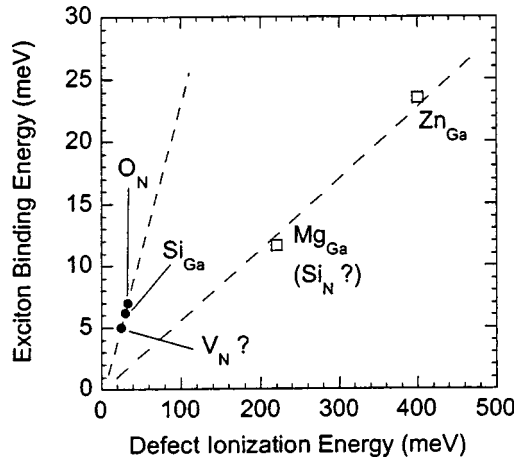


FIG. 89. Dependence of the ionization energies of donors and acceptors on binding energies of the related bound excitons in GaN. The dashed lines show the slope of 0.21 for donors and 0.057 for acceptors.

$\alpha = 0.21 \pm 0.01$, similar to the previous reports.^{480,492,494} However, for acceptors we find $\alpha_A = 0.057 \pm 0.003$. This result substantially differs from the previous estimates ($\alpha_A \approx 0.1$).^{492,508} It should be noted that the exciton binding energies and ionization energies reported in Refs. 492 and 508 for Mg and Zn should be treated with caution. Here, we used the refined data: $E_{ABX} = 11.6$ meV for the shallow acceptor (Mg_{Ga} or Si_N)^{479,486,495,502} and $E_{ABX} = 23.5$ for the Zn acceptor.^{199,267,500} The ionization energies for these acceptors have been estimated as ~ 220 and 400 meV, respectively, from the position of the zero-phonon e-A transition at low temperature.^{116,199,245} The above-deduced values of α agree remarkably well with the theoretical predictions. Chang and McGill⁵⁰⁹ have calculated in spherical approximation that $\alpha_A \approx 0.06$ for the effective-mass acceptors and $\alpha_D \approx 0.14$ for the effective-mass donors in Eqs. (40) in the case of a semiconductor with $m_e/m_h \approx 0.1$, which is what was assumed for GaN.^{93,284}

VIII. UNUSUAL LUMINESCENCE LINES IN GaN

Along with the well-identified lines related to excitons and shallow defects (see Secs. IV C and VII), numerous PL lines with unusual properties have been reported in GaN.^{190,283,510–545} The aggravating factor is that the origin of these lines spans the range from simply being unknown to controversial. For example, the commonly observed line at 3.42 eV (Refs. 512–521 and 537–545) has been attributed to recombination between electrons bound to oxygen donors and free holes,^{512,513} DAP-type transitions involving a very shallow unidentified acceptor,⁵¹⁴ and excitons bound to structural defects,^{515–520,537,538,540,543,544} in particular, to stacking faults^{517,519} and *c*-axis screw dislocations,⁵²⁰ or surface-related defects.^{537,538,540} To emphasize the resemblance between the properties of the unusual lines in GaN and the *Y* lines in II–VI compounds (Sec. VIII C), we labeled the unusual lines in GaN as *Y_i*, with *i* starting from 1 ascending with descending the peak energy of the transition in question, as tabulated in Table V.^{537,538} Below, we review the characteristics of the *Y_i* lines in GaN. Some preliminary results have already been presented in Refs. 537–541. The *Y_i* lines should not be confused with the widely observed lines at ~ 3.31 and 3.36 eV, which are apparently related to oil contamination (Sec. VIII B).

A. *Y_i* lines

Among the several hundred undoped GaN samples investigated, the *Y_i* lines having varying contribution to the low-temperature PL spectrum (Fig. 90) have been detected in some one hundred samples grown in our laboratory. No correlation between the growth method or the substrate used and the *Y* lines is apparent. Some 20 samples grown by MBE have been selected for a detailed investigation of the *Y_i* lines. The positions of the most frequently observed *Y_i* lines are quite repeatable in a large set of GaN samples, as depicted in

TABLE V. Classification and typical characteristics of the *Y_i* lines in GaN. Reprinted with permission from Reshchikov *et al.*, Physica B 340–342, 440 (2003). Copyright (2003) by Elsevier.

Group label	Sub group label	Nominal position (eV)	Huang –Rhys factor	Comments, properties	Tentative identification
<i>Y₁</i>	<i>Y₁'</i>	3.45	0.02	Observed only in N-Polar films with high density of inversion domains	Exciton bound to inversion domain interface
	<i>Y₁''</i>	3.46			
<i>Y₂</i>	<i>Y₂'</i>	3.41	0.05	Disappears after etching. Shifts with excitation intensity in some samples	Exciton bound to structural defect at the surface
	<i>Y₂''</i>	3.42			
<i>Y₃</i>	<i>Y₃'</i>	3.37	<0.2	Observed only in two samples	Exciton bound to structural defect.
	<i>Y₃''</i>	3.38			
<i>Y₄</i>	<i>Y₄'</i>	3.350	0.01	Evolves with UV exposure. Memory effect at 15 K. Intensity depends on history of the surface	Exciton bound to structural defect at the surface
	<i>Y₄''</i>	3.362			
<i>Y₅</i>		3.34		Observed in six samples	Exciton bound to structural defect?
<i>Y₆</i>		3.32	~ 0.1	Evolves with UV exposure. Memory effect at 15 K. Intensity depends on history of the surface. In all samples shifts much with excitation intensity	Surface donor-acceptor pair
<i>Y₇</i>	<i>Y₇'</i>	3.21	0.06	The most common <i>Y_i</i> peak. Not affected by etching or UV exposure	Exciton bound to structural defect
	<i>Y₇''</i>	3.23			
<i>Y₈</i>		3.08	~ 0.2	Observed only in one sample	?
<i>Y₉</i>		2.86	<0.3	Observed only in one sample	?
<i>Y₁₀</i>		2.80		Observed in four samples	?
<i>Y₁₁</i>		2.68		Observed only in one sample	?

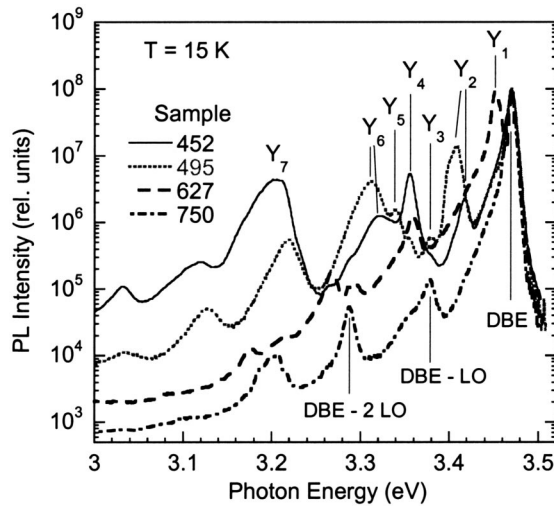


FIG. 90. Low-temperature PL spectra from different GaN layers grown on sapphire by MBE. The spectra are normalized at maximum and shifted along the energy axis (from 1 to 7 meV) so that the DBE peak position is the same for all samples (3.470 eV). Reprinted with permission from Reshchikov *et al.*, J. Appl. Phys. 94, 5623 (2003). Copyright (2003) by the American Institute of Physics.

Fig. 91. In particular, the Y_2 , Y_4 , Y_6 , and Y_7 lines appeared at following energies in relation to the DBE peak: 53 ± 3 meV (Y_2); 115 ± 1 meV (Y_4); 156 ± 5 meV (Y_6); and 262 ± 3 meV (Y_7).⁵³⁷

The appearance of particular Y_i lines correlated with the polarity of the samples, which was established using a variety of methods such as wet chemical etching, atomic force microscopy (AFM), investigation of surface morphology, transmission electron microscopy (TEM), and x-ray diffraction (XRD).⁵⁴⁶ For instance, the Y_2 , Y_4 , Y_6 , and Y_7 lines have usually been detected in Ga-polar films whereas the Y_1 line dominated in N-polar films. The Y_i lines could not really be assigned to inclusions of the cubic phase of GaN because the position, shape, and behavior of these lines with respect to temperature and excitation intensity are very different from

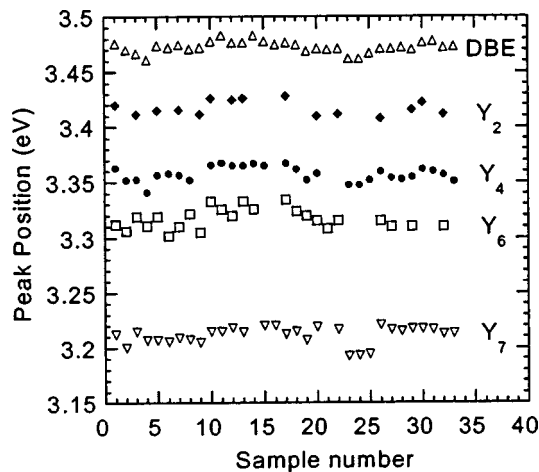


FIG. 91. Positions of the DBE and Y_i peaks in different samples. The samples, including etched ones, are numbered 1,2,3..., on this figure. For example, numbers 23, 24, and 25 correspond to the same sample 605: as-grown, etched in phosphoric acid, and PEC etched, respectively. Note that $Y_2=Y'_2$, $Y_4=Y'_4$, and $Y_7=Y'_7$ on this figure when the doublets are resolved.

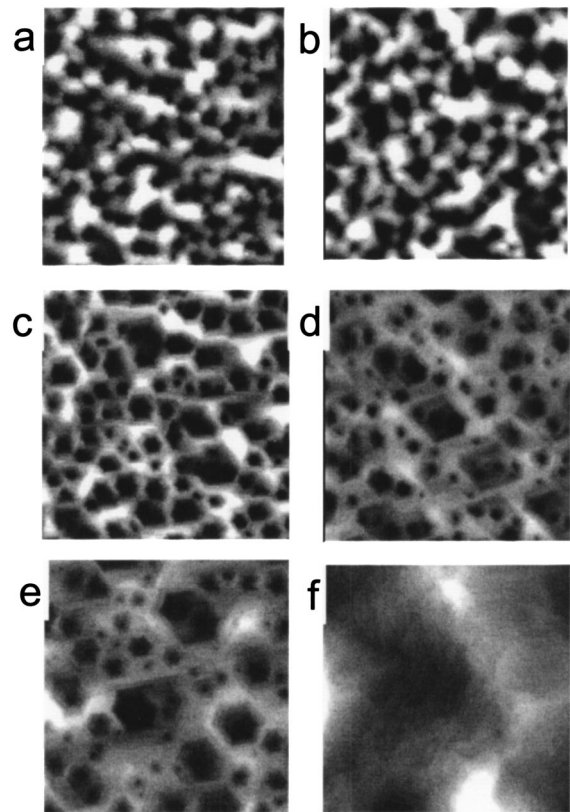


FIG. 92. $1 \times 1\text{-}\mu\text{m}$ AFM images of the GaN sample 426. (a)—as-grown; (b)—after etching in boiled aqua regia for 5 min; (c), (d), (e), (f)—after etching in H_3PO_4 at 160°C for 5 s, 15 s, 1 min, and 30 min, respectively. The vertical scale is 30 nm for all images. Density of the etch pits is about 10^{10} cm^{-2} in (c) and (d). Note that the depth of the pits did not increase with increasing etching time, remaining under 30 nm, and we could not detect any reduction of the layer thickness even after 1 h or longer etching time.

the features observed in cubic GaN (Sec. VI). To make certain that these lines are not caused by contamination of the sample surface, we cleaned the selected samples in a variety of ways which included boiling in aqua regia ($\text{HNO}_3:\text{HCl} = 1:3$) and etching in hot phosphoric acid. Below, the effects of sample treatments and experimental conditions on the Y_i lines in GaN are briefly reviewed. More details can be found in Refs. 537 and 547.

1. Effects of sample treatments and experimental conditions on the Y_i lines

a. Effect of hot wet chemical etching. Columnar or bubble-like surfaces of the Ga-polar films remained unchanged after etching in boiled aqua regia, whereas the surface became relatively flat with hexagonal-shaped pits after etching in hot H_3PO_4 or molten KOH, as depicted in Fig. 92. Cleaning of the sample in aqua regia did not affect the Y_i lines, while etching in H_3PO_4 slightly decreased the intensities of the Y_4 and Y_7 peaks and substantially reduced the intensities of the Y_2 and Y_6 peaks, as exhibited in Fig. 93 (see also Fig. 3 in Ref. 540).

On the other hand, the N-polar GaN layers are much less resistant to etching so that in 10 s of etching in H_3PO_4 at 100°C the substantial part of the layers can be removed.⁵⁴⁷ Note that MBE-grown N-polar GaN samples contained very high density of inversion domains, of the order of 10^{11} cm^{-2}

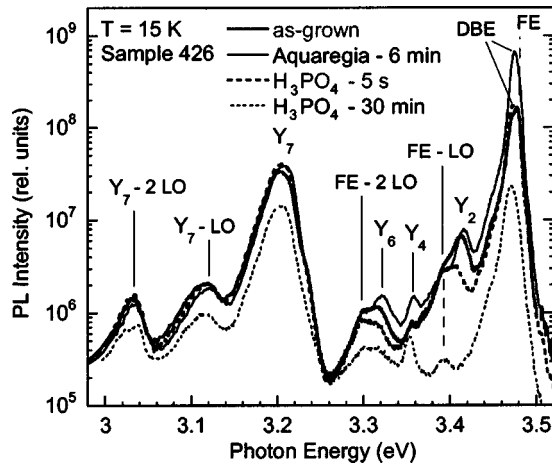


FIG. 93. Effect of etching of Ga-polar GaN in boiled aqua regia for 6 min and in H_3PO_4 at 160°C for 5 s and 30 min. $P_{\text{exc}}=100\text{ W/cm}^2$. See the surface morphologies for this sample in Fig. 92.

(Ref. 539), which means that contributions from the Ga-polar regions to the PL spectrum could not be ruled out. The Y_1 peak dominating the PL spectrum in N-polar films increased markedly after etching (Fig. 94).

b. Effect of photoelectrochemical etching. Photoelectrochemical (PEC) etching results in the formation of whiskers due to selective etching of GaN between dislocation sites.^{548,549} After the PEC etching, the intensity of the DBE, free exciton (FE), and Y_2 lines decreased and the intensity of the Y_4 and Y_7 lines increased.⁵⁴⁷

c. Evolution of PL and memory effect. The Y_4 and Y_6 peaks in Ga-polar films evolved with duration of the UV laser exposure while the rest of the peaks, including the DBE peak, remained unchanged, as exhibited in Fig. 95. After 2 h of UV exposure the intensity of the Y_4 and Y_6 peaks increased several times in selected samples without a complete saturation of the effect, as shown in Fig. 96. The effect was irreversible at low temperatures.^{537,547}

d. Effect of excitation intensity. The PL intensity of most of the Y_i lines increased approximately linearly with increas-

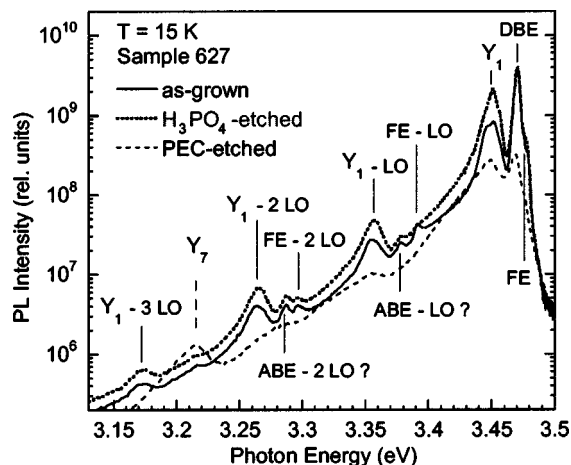


FIG. 94. Low-temperature PL spectrum of the N-polar GaN layer grown by MBE on sapphire substrate, $P_{\text{exc}}=300\text{ W/cm}^2$. A piece of the sample was etched in H_3PO_4 at 100°C for 10 s and another piece of the sample was etched by PEC method.

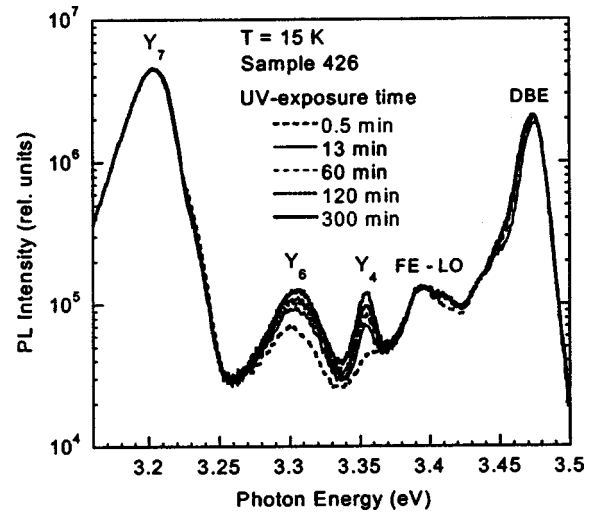


FIG. 95. Transformation of PL spectrum with time of exposure by HeCd laser at 15 K . $P_{\text{exc}}=200\text{ W/cm}^2$. The sample was etched in H_3PO_4 at 160°C for 1 min and subsequently exposed to air for 20 days. Reprinted with permission from Reshchikov *et al.*, Mater. Res. Soc. Symp. Proc. 743, L11.3 (2003).

ing excitation density from 10^{-4} to 300 W/cm^2 , in much the same manner as that for the FE and DBE peaks (Figs. 97 and 98). In terms of the transition energy, the Y_3 , Y_4 , Y_5 , and Y_7 lines did not shift with the excitation intensity while the Y_6 line shifted to higher photon energies by up to 20 meV (Figs. 97 and 98).^{544,547} Figure 99 summarizes the peak shifts involved with excitation intensity for representative samples.

e. Effect of temperature. With increasing temperature, all the Y_i peaks quenched with activation energies in the range between 10 and 30 meV at temperatures below 100 K. Typical transformation of the PL spectrum in Ga-polar film is shown in Fig. 100. The Y_1 , Y_2 , Y_4 , and Y_7 lines revealed two components.^{537,544,547} The low-energy components (Y'_1 at 3.21 eV, Y'_4 at 3.350 eV, Y'_2 at 3.400 eV, and Y'_1 at about 3.45 eV) quenched first, giving way to the high-energy components (Y''_1 at 3.23 eV, Y''_4 at 3.362 eV, Y''_2 at 3.407 eV, and Y''_1 at 3.46 eV) which quenched at higher temperatures (Fig. 100). The quenching of these lines could be fitted using Eq. (32) with $E_A=18$ and 42 meV for the Y'_4 and Y''_4 components and $E_A=15\pm 5$ and 120 ± 20 meV for the Y'_7 and Y''_7 compo-

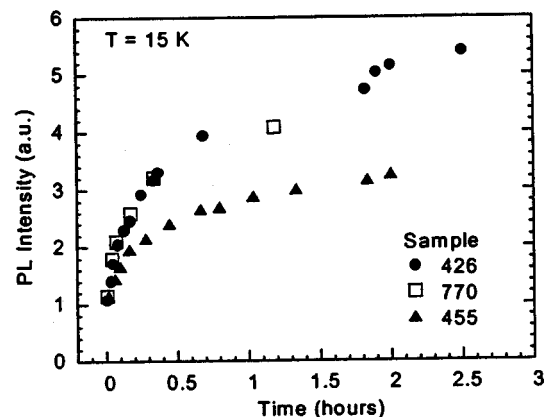


FIG. 96. Evolution of PL intensity at 3.36 eV with time of HeCd laser exposure. $T=15\text{ K}$. $P_{\text{exc}}=200\text{ W/cm}^2$.

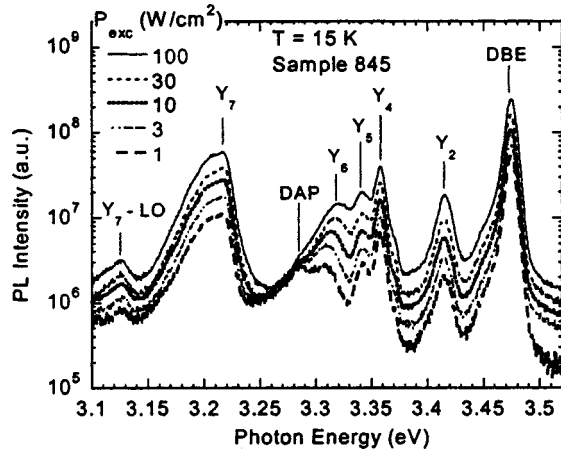


FIG. 97. Low-temperature PL spectrum of Ga-polar GaN layer grown by MBE on top of the HVPE-grown 10- μ m-thick GaN on sapphire substrate. Excitation density was attenuated from 100 to 1 W/cm² by neutral density filters. The spectra are shifted arbitrary along the vertical axis for better viewing. Reprinted with permission from Reshchikov *et al.*, Mater. Res. Soc. Symp. Proc. 693, I6.28 (2002).

nents, respectively. Activation energies of the other Y_i lines did not exceed 30 meV at temperatures up to 120 K, and these lines could be barely detected at higher temperatures.⁵⁴⁷

The temperature dependencies of the energy positions of the Y_i lines are shown in Fig. 101 in comparison with the shift of the FE line. All the Y_i lines shift in agreement with the temperature shrinkage of the GaN band gap,⁴⁷³ supporting the assumption that the Y_i lines originate from GaN.

2. Characteristics of the Y_i lines

a. The 3.45-eV line (Y_1). The 3.45-eV peak, labeled as Y_1 , appeared only in the N-polar films containing a high density of inversion domains ($\sim 10^{11}$ cm⁻²) and relatively low density of dislocations ($\sim 10^9$ cm⁻²).^{550,551} Schuck *et al.*⁵¹⁰ related this peak to the inversion domain boundaries. A very small Huang-Rhys factor⁵⁵² for the Y_1 peak (about 0.02)

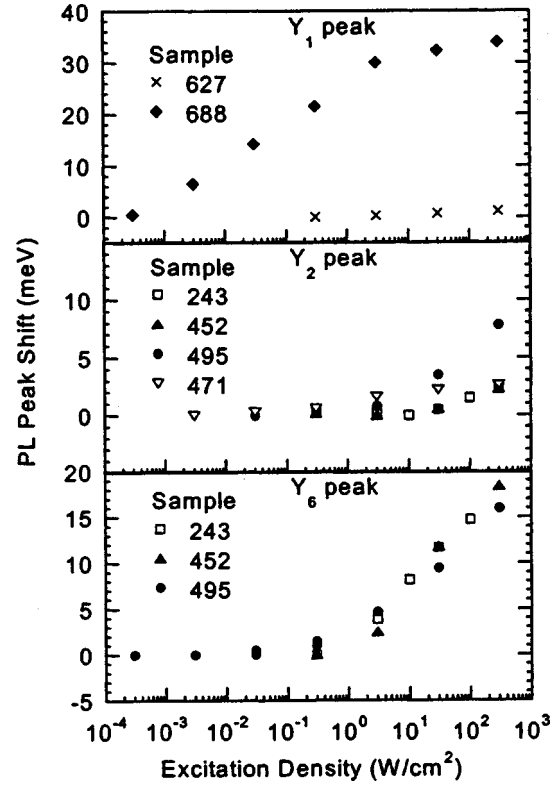


FIG. 99. Dependence of the PL peak shift on excitation density at 15 K.

supports the assignment of the Y_1 line to excitons bound to inversion domain boundaries.⁵³⁷ Narrow Ga-polar domains in N-polar media might create high and narrow potential humps near the surface due to essentially different band bending near the surface in Ga- and N-polar films.⁵⁵³ However, this remains to be confirmed before it can be treated with sufficient level of confidence. The exact potential profile may be sample dependent, explaining the slightly differ-

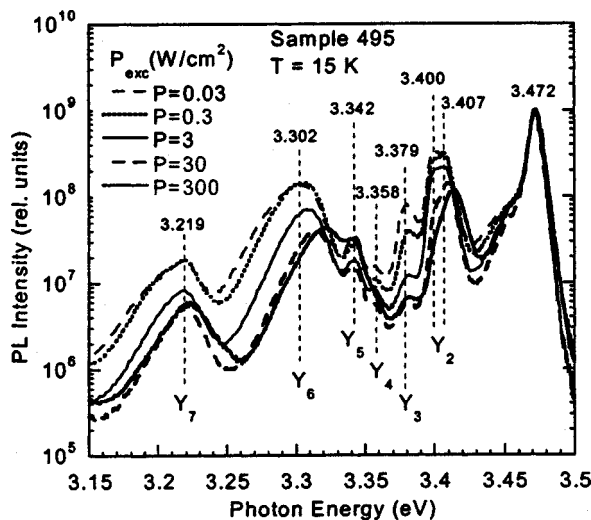


FIG. 98. Low-temperature PL spectrum of N-polar GaN layer grown by MBE on sapphire substrate. The spectra are normalized at maximum. Reprinted with permission from Reshchikov *et al.*, Mater. Res. Soc. Symp. Proc. 743, L11.3 (2003).

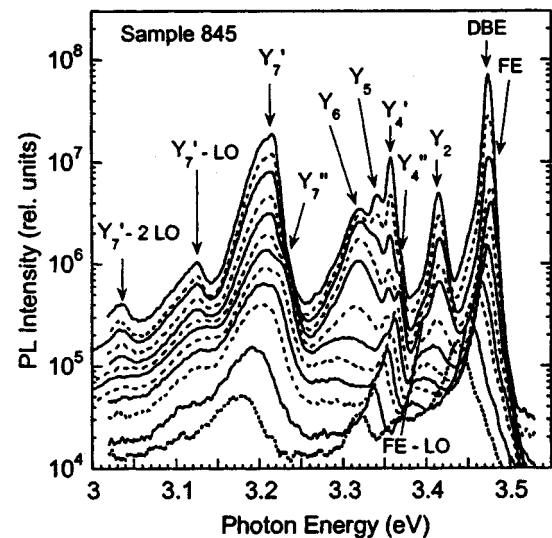


FIG. 100. Temperature dependence of PL spectrum at $P_{exc} = 100$ W/cm² for as-grown Ga-polar GaN layer by MBE on top of the HVPE-grown 10- μ m-thick GaN on sapphire substrate. Temperatures are 15, 35, 60, 100, 140, 195 K (solid curves), 25, 50, 80, 120, 160 K (dashed curves), and 240 K (dotted curve). Reprinted with permission from Reshchikov *et al.*, Mater. Res. Soc. Symp. Proc. 693, I6.28 (2002).

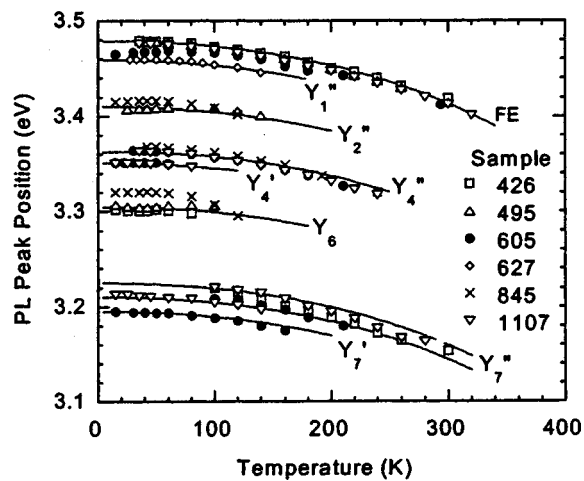


FIG. 101. Temperature dependence of positions of the FE (DBE) and Y_i peaks in GaN samples. For the sample 605 the DBE and FE peaks were unresolved and the position of their common maximum is plotted. The solid curves show the shift of the GaN band gap (Ref. 473) corrected to the following positions of lines at $T=0$: 3.479 eV (FE); 3.459 eV (Y_1'); 3.410 eV (Y_2'); 3.351 eV (Y_4'); 3.363 eV (Y_4''); 3.305 eV (Y_6); 3.195 eV, 3.210, and 3.225 eV (Y_7' and Y_7''). Reprinted with permission from Reshchikov *et al.*, J. Appl. Phys. **94**, 5623 (2003). Copyright (2003) by the American Institute of Physics.

ent positions of the Y_1 peak in different samples and the significant shift of the Y_1' component with excitation intensity.⁵⁴⁷

b. The 3.42-eV line (Y_2). The exact position of this line is sample dependent, typically spaced from the DBE line by 40–65 meV.^{512,516} In some investigations a doublet structure of the 3.42-eV line has also been observed.^{515,518,520} Further, Chen *et al.*⁵⁴⁴ resolved up to five peaks in the range from 3.40 to 3.44 eV. The relative intensity of the 3.42-eV peak increased after annealing, especially in water vapor atmosphere.⁵³⁵ The cumulative consensus is that the 3.42-eV line is related to structural defects.^{313,515–520,544}

The 3.42-eV or Y_2 line appeared in some 70 as-grown GaN layers (typically with Ga polarity) deposited on sapphire or SiC by MBE in our laboratory. A doublet nature of the Y_2 line (Fig. 98) was observed only in N-polar samples having a high density of inversion domains. The Y_2 line was never found in the samples with flat surfaces where only the Y_4 and Y_7 peaks were sometimes detected.

The Y_2 peak disappeared or drastically decreased after etching in hot phosphoric acid (Fig. 93) which removed the rough portion of the columnarlike layer without essentially changing the thickness of the higher-quality GaN layer, and after PEC etching which etched away the good-quality GaN leaving dislocation sites intact as pillars. The Huang–Rhys factor of this emission was estimated as 0.05. We assign the Y_2 line to excitons bound to some surface defects rather than to dislocations in bulk GaN.^{537,547}

c. The 3.38-eV line (Y_3). The 3.38-eV line, labeled as Y_3 , appeared only in two samples: 495 (N polar) and 770 (Ga polar). In contrast with the FE and DBE lines and their LO phonon replicas, the intensity of the Y_3 line saturated with excitation intensity (Fig. 98). No shift was detected in a wide range of excitation intensities. With increasing temperature,

the Y_3 line quenched and disappeared above 50 K due to a large contribution of the Y_2 , Y_4 and FE emissions at this photon energy. A peak at about 3.38 eV, along with other peaks similar to our Y_2 , Y_4 , and Y_7 peaks, was observed in the CL spectrum of GaN grown by MBE on sapphire.⁵¹⁷ An intense peak at ~ 3.38 eV, observed in bulk GaN platelets,⁵⁴⁴ might also have the same origin as the Y_3 line. Due to the absence of any shift of the Y_3 peak with excitation intensity (reported also in Ref. 544), we rule out the DAP nature for this line and assign it instead to excitons bound to some unknown defects.⁵⁴⁷

d. The 3.35-eV line (Y_4). The 3.35-eV or Y_4 line is associated with GaN and should not be confused with the oil-related 3.36-eV line (Sec. VIII B). We assume that the line at 3.35–3.36 eV observed in Refs. 517, 536, and 543 has the same origin as the Y_4 line in our studies.^{537–541,547} A strong PL peak at 3.35–3.36 eV has been observed in *M*-plane GaN containing a high concentration of stacking faults.^{511,545} While the assignment of this peak to excitons bound to stacking faults in these samples is convincing, this conclusion should not be extended to the Y_4 line in GaN grown on *c*-plane sapphire because the TEM investigation has not revealed stacking faults in the samples which exhibited a high intensity of the Y_4 line.^{541,554,547}

The Y_4 line appeared only in Ga- and N-polar samples exhibiting a strong Y_7 peak.^{537,547,554} This line never shifted nor saturated with excitation intensity. We assign the Y_4 line to an exciton bound to some point defects trapped by the edge threading dislocations.^{547,554} Slow photoinduced charging of the edge dislocations near the surface may cause its evolution with UV exposure. The excitonic nature of the Y_4 line is supported by a very small FWHM (8–10 meV in representative samples) and a very small Huang–Rhys factor (0.01). The LO phonon replica of this peak can be clearly seen at an energy distance of about 90 meV in the samples with well-defined Y_4 peak.^{540,547,554}

e. The 3.34-eV line (Y_5). The line with its maximum at about 3.34 eV (the Y_5 line) was observed in six samples: 495, 688, 692 (N-polar films) and 243, 463, 845 (Ga-polar films). The Y_5 line was relatively sharp in all the aforementioned samples. It did not shift or saturate with increasing excitation intensity, as can be seen in Fig. 98. With increasing temperature, this line quenched in a manner similar to the other Y_i lines. Therefore, we assign the Y_5 line to exciton bound to some unidentified defect.^{537,547}

f. The 3.32-eV line (Y_6). The 3.32-eV or Y_6 line must not be confused with the oil-related 3.31-eV line, because the properties of these two lines are very different (see Sec. VIII B). The Y_6 line was detected in some 40 GaN layers grown by MBE on sapphire and SiC, both Ga and N polar. However, the Y_6 line never appeared in GaN films with very flat surfaces.^{547,554} Unlike other Y_i lines, the Y_6 line always shifted in energy significantly with excitation intensity and is relatively broad in all the studied samples. With increasing temperature, we observed a small shift of the Y_6 line to higher energies at low excitation intensities (see Fig. 8 in Ref. 537) and a shift to lower energies at high excitation intensities (Fig. 100). This observation, together with the strong shift of the peak with increasing excitation intensity, is

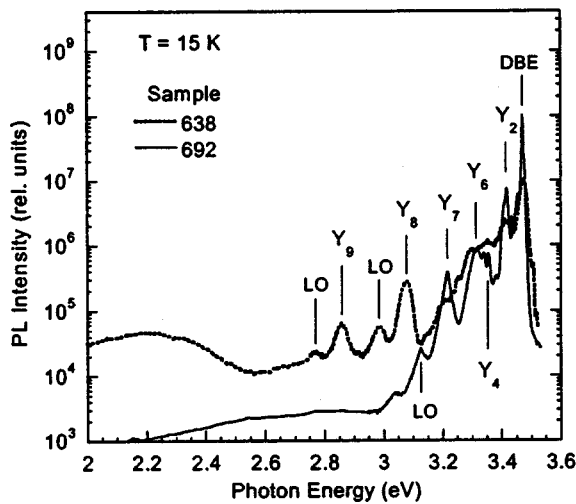


FIG. 102. Low-temperature PL spectrum from GaN layers grown by MBE on sapphire substrate.

a hallmark of the DAP-type transition.⁸² With increasing temperature, the Y_6 line quenched (Fig. 100) with an activation energy of about 30 meV. We assume that this is the binding energy of the donor involved in the DAP.⁵³⁷

We propose that the shallow donor and acceptor responsible for the Y_6 line are located on the GaN surface^{537,547} where the binding energies for donors and acceptors are reduced.^{555,556} Previously, the surface-related shallow DAP band has been identified in CdS at photon energies higher than the bulk shallow DAP band.⁵⁵⁷

g. The 3.21-eV line (Y_7). The 3.21-eV line, denoted as Y_7 , with the characteristic LO phonon replicas has been observed in several investigations.^{513,516,517,521,536–538,541,544} We observed the Y_7 line in some 70 layers grown by MBE on sapphire and SiC substrates. In fact, it consists of two components separated by 15 ± 3 meV with the low-energy component Y_7' being dominant at low temperatures.^{537,547} The transformation of the Y_7 line with temperature is very similar among all our samples and the ones used in Ref. 544. The suggestion of the excitonic origin of the Y_7 line is supported by a linear increase and absence of the peak shift with increasing excitation intensity, and a very small Huang–Rhys factor (about 0.06). A set of combined PL and TEM studies showed that the Y_7 line may be strong in GaN containing only the edge threading dislocations.⁵⁵⁴ On the other hand, the Y_7 line may be completely absent in the layers with comparable densities of the dislocations.^{541,547} We therefore suggest that the Y_7 line arises from recombination of an exciton bound to some point defect that is in turn trapped by the stress field of the threading-edge dislocation.

h. The 3.08-, 2.85-, 2.80- and 2.66-eV lines (Y_8 – Y_{11}). In a large set of GaN samples we could find samples representing unusual PL lines. Two such lines, labeled Y_8 and Y_9 , were observed in small areas of only one nonuniform GaN sample (sample 638) at high excitation intensities, as exhibited in Fig. 102. Both the Y_8 line with the ZPL at 3.078 eV and the Y_9 line with the ZPL at 2.858 eV were accompanied by LO phonon replicas that are 90–92 meV apart from the main

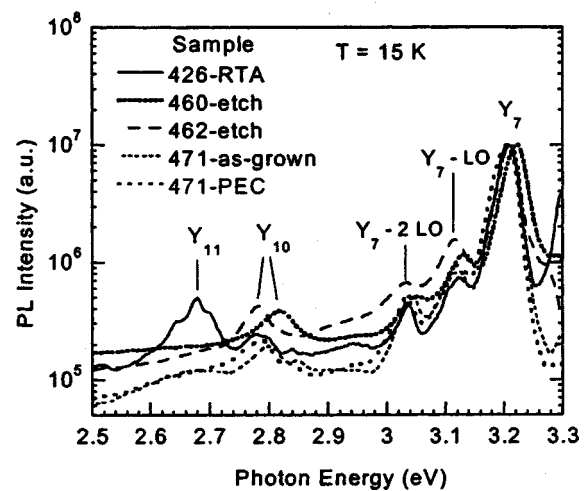


FIG. 103. Low-temperature PL spectrum of Ga-polar GaN layers grown by MBE on sapphire substrate subjected to different treatments [rapid thermal annealing (RTA), etching in hot H_3PO_4 and PEC etching].

peaks. Since the Y_8 and Y_9 peaks emerged at high excitation intensities and had a rather sharp shape, we tentatively attribute them to strongly localized excitons.⁵⁴⁷

Even deeper PL peaks emerged at high excitation intensities in the Ga-polar samples 426, 460, 462, and 471 (Fig. 103) when the contribution of the YL band decreased substantially due to a large lifetime of this band.⁸⁷ The energy position of the peak, denoted as Y_{10} , varied from 2.78 to 2.82 eV in different samples. The deepest PL peak, of apparently excitonic origin, denoted as Y_{11} was detected at 2.68 eV in sample 426 (Fig. 103). With increasing temperature, the Y_{11} peak quenched with a small activation energy in the same manner as the other Y_i peaks.⁵⁴⁷

3. Y_i lines and structural defects

The PL properties of the samples containing the Y_i lines and a few control samples (free from the Y_i lines) were compared to the structural properties of the samples by using the AFM, XRD, and TEM methods typically used for crystal characterization.

a. Atomic force microscopy. Comparison of the AFM images of samples exhibiting the Y_i lines and the control samples showed that there is no clear correlation between the surface morphology and appearance of the Y_i lines.⁵⁴⁷ In particular, the surface morphology of the control sample 750 was nearly identical to that of sample 426 (Fig. 92) before and also after etching in hot H_3PO_4 . Interestingly, the Ga-polar layers with very flat surfaces, such as samples 605 and 1107, did not contain any Y_i lines in their PL spectrum except for the sharp Y_4 and Y_7 lines. Remarkably, the Y_2 line, dominating in many samples with bubblelike or columnar surface structure disappeared after hot wet chemical etching (either in H_3PO_4 or KOH) when the surface became flat, albeit with etch pits.

b. X-ray diffraction. Information about crystalline structure can be gained from an analysis of XRD rocking curves measured regarding different crystal directions. In two reports,^{558,559} an apparent correlation between the crystal quality, established by XRD, and the intensity and energy

TABLE VI. Comparison of dislocation densities (from TEM data) and relative intensities of the Y_i and DBE lines (from PL spectrum) in GaN layers grown by MBE on sapphire substrate

Sample	Density of dislocations and inversion domains (IDs) (cm^{-2})				PL intensity (rel. units)								Surface (from AFM)
	screw	mixed	edge	ID	DBE	Y_1	Y_2	Y_4	Y_5	Y_6	Y_7	QE (%)	
750	$<1 \times 10^7$	8×10^7	2.5×10^9		1×10^{10}	$<10^6$ (?)	6	Rough
1541	$<7 \times 10^7$	7×10^7	7×10^{10}		2×10^7	1×10^5	0.03	Flat
618	1×10^8	5×10^8	4×10^8	1×10^{11}	1.7×10^8	8×10^7	0.3	Rough
605	$<1 \times 10^7$	3×10^7	1×10^{10}		1.3×10^8	4.4×10^6	1.8×10^6	0.15	Flat
463	$<1 \times 10^7$	2×10^7	1×10^{10}	4×10^8	3×10^9	...	1.6×10^8	6.3×10^7	3×10^7	5×10^7	5×10^7	3.3	Rough

position of the 3.42-eV peak has been reported. We compared the peak positions and relative intensities of the Y_i peaks with the FWHM of the (0002) GaN diffraction peak in a large set of GaN layers grown by MBE on sapphire and could not find any clear correlation for any of the Y_i peaks with that parameter.^{537,541,547} Note that in a large set of control GaN samples not containing the Y_i peaks, the FWHM of the (0002) diffraction peak also varied substantially in the range from 1 to 50 arc min.^{537,541,547} The broadening of the (0002) diffraction peak has been reported to relate to the density of screw dislocations.^{386,560} The lack of a clear correlation between the appearance of the Y_i peaks and the FWHM of the (0002) GaN diffraction peak^{537,541} indicates that none of the Y_i peaks is directly related to screw or mixed dislocations, which contradicts the assumption of Shreter *et al.*⁵²⁰ regarding the possible origin of the 3.42-eV peak in GaN. These suggestions that we put forward are also supported by TEM studies, as will be shown below.

c. Transmission electron microscopy. Cross-sectional TEM images have been obtained for the selected samples representing the Y_i lines as well as for a few control samples lacking these lines.^{538,541,547,554} An analysis of the TEM images allowed us to independently estimate the density of threading-edge, screw, and mixed dislocations in addition to the density of columnar (with a diameter of 5–20 nm) inversion domains in the selected samples having a large variation in the density of structural defects (Table VI). Note that the densities of edge and screw dislocations, obtained by TEM and XRD methods, are consistent.⁵⁴¹ The densities were compared with the relative intensities of the Y_i lines in the same samples (see Fig. 104 and Table VI). Similarity in the structural properties of the samples 463 and 605 (Table VI) indicates that the Y_2 and Y_6 lines are not related to the structural defects inside the crystal (densities of different dislocations and the crystal quality are about the same in these two samples while the Y_2 and Y_6 lines appear only in one sample) but related instead to the surface.^{537,538,541,547} No other correlations could be determined between the structural defects and Y_i lines in these five selected samples.^{541,547} We are also highly skeptical that stacking faults are responsible for any Y_i line. Although the apparent correlation between the presence of the Y_2 line and high concentration of stacking faults in GaN has been reported,^{561,562} we could not detect any stacking fault in cross-sectional TEM images of the GaN

samples exhibiting the Y_i lines.^{547,554} Note also that a brief etching of the GaN layer in hot H_3PO_4 smoothens the surface and completely quenches the Y_2 line.

B. Oil-related 3.31- and 3.36-eV lines

In numerous investigations involving PL in GaN, the artificial oil-related lines with their characteristic properties, presented below, were inadvertently attributed to emission from GaN.^{190,283,323,522–534} The energy position of these lines falls into the range of 3.358–3.370 and 3.298–3.313 eV. These lines have often been detected in undoped GaN where no emission typical for GaN was observed^{522–528} or in *p*-type GaN where the near-band-edge emission was absent or very weak.^{190,283,323,529} A few clearly observed phonon replicas of the 3.31-eV line (separated by about 70 meV which is smaller than the LO phonon energy in GaN by about 20 meV) have been recorded.^{522–525,529} At low temperatures, the 3.36-eV line is stronger and sharper than the 3.31-eV line. With increasing temperature, the 3.36-eV line quenches faster than the 3.31-eV line,^{323,522–524,526,529,530} and the activation energy of quenching does not exceed 30 meV.^{523,526,534} Increasing the measurement temperature re-

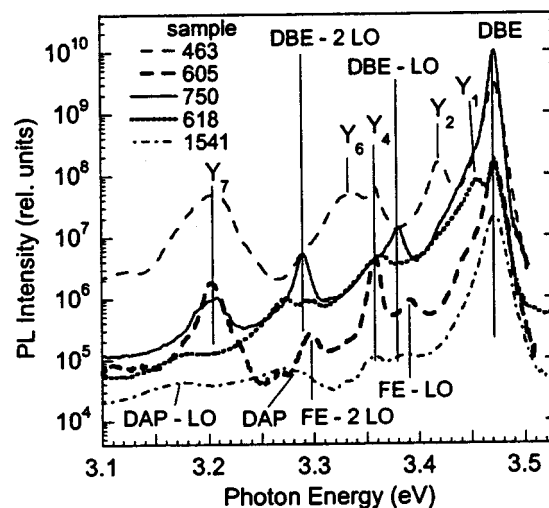


FIG. 104. Low-temperature (15 K) PL spectra of five GaN layers grown by MBE on sapphire. All the spectra are measured under identical conditions. Excitation density is 30 W/cm^2 . The spectra have been shifted by up to 10 meV to compensate different strain-related shifts and align the DAP peaks. See characteristics of these samples in Table VI. Reprinted with permission from Reshchikov *et al.*, Mater Res. Soc. Symp. Proc. 798, Y5.66 (2004).

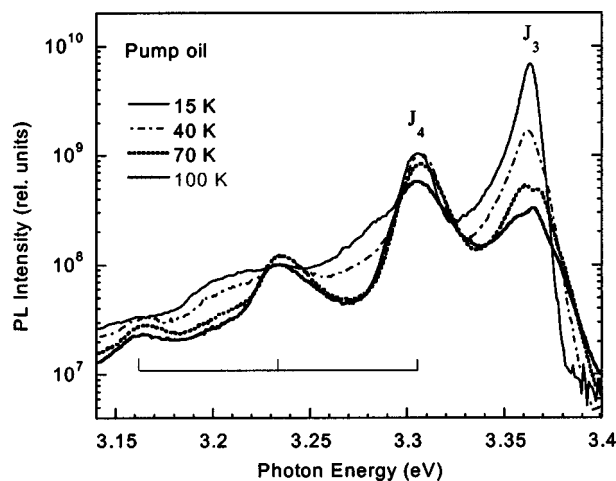


FIG. 105. PL spectra of oil from mechanical pump. Phonon replicas of the J_4 peaks are separated by 70 meV.

veals the complex nature of the 3.36-eV line.^{522,524,527,529,532} No shift in the position of the 3.36-eV line was observed under hydrostatic pressure up to 4.4 GPa, while the band gap of GaN should increase by about 190 meV.⁵²³ The lines could be excited with photon energies below the band gap of GaN.^{529,530} The lines were most commonly attributed to the cubic phase inclusions formed as a result of stacking faults^{526,530} or to excitons localized at extended defects in GaN.^{522,523,529,531}

We have shown^{537,540} that these lines with specific *properties* appear only in the samples contaminated with small amount of oil. Among the sources of these parasitic lines, one can name the oil-based thermal compound for affixing the samples to the sample holder (see Fig. 1 in Ref. 540) and contamination of the cryostat chamber by pump oil (Fig. 105). The oil-related emission is extremely strong, with the QE being about 30%. Consequently, fairly small contamination with oil would make these lines visible when the intensity of the PL from GaN is weak in this energy region. To eliminate these sorts of artifacts in our experiments, we used an oil-free pump system and chose to clip the samples to the holder without any glue or paste at the expense of losing good contact with the cold finger that is why the minimum measurement temperature in our studies is limited to 15 K. Note that the properties of the Y_4 , Y_5 , and Y_6 lines that fall in the same spectral region are completely different from those of the oil-related lines.

C. Identification of the Y_i lines

Unusual luminescence lines have been originally discovered in Si (Ref. 563) and ZnSe.⁵⁶⁴ Since then numerous papers have been published on PL lines with similar properties in ZnSe,⁵⁶⁵ CdTe,⁵⁶⁶ ZnTe (Refs. 565–567) (Y and Z lines), and in silicon (D lines).^{568–570} These lines have commonly been attributed to excitons bound to extended structural defects,^{570,571} although Higgs *et al.*⁵⁶⁹ also suggested that these lines could originate from excitons bound to point defects trapped in the strain fields of dislocations. In the light

of the previous reports and discussions, it is reasonable to assume that most of the Y_i lines in GaN could also be related to extended structural defects in some way.

The Y_i peaks in GaN quench with rather small activation energies, much smaller than the binding energy of the shallowest known acceptors in GaN. The small activation energy can be accounted for by assuming that the Y_i peaks arise from recombination of excitons bound to some structural defects. Due to the strain field the defect may create local potential, which can strongly bind a hole, and in turn attract a loosely bound electron to form a bound exciton.³ Different localization of the electron and the hole would explain two activation energies in the temperature quenching of Y_i lines (in particular, 15 and 120 meV for the Y_7 line). The doublet nature of some peaks (Y_2 , Y_4 , and Y_7) can be attributed to neutral and charged excitons,⁵³⁷ as it was suggested earlier for the 364-nm line in GaN.⁵²⁰ Alternatively, one component could be attributed to the contribution from the surface while the other to the bulk regions of the sample, which may be more appropriate for the Y_1 doublet with the component separation depending on the excitation intensity.

Considering the detailed TEM and PL studies,^{538,541,547,554} it is doubtful that any of the Y_i peaks is caused by annihilation of an exciton bound *directly* to any dislocation, cubic phase, or a stacking fault in GaN. However, it is very likely that the Y_i lines are related to some point defects gettered by dislocations. The fact that no unusual deep-level PL band is observed in the samples with strong Y_i lines may indicate that these point defects are non-radiative even though they can bind excitons. The above assignment is also able to explain why the presence of one type or another structural defect or just a rough surface results in the appearance of the Y_i lines in GaN in only some cases.

IX. UNSTABLE LUMINESCENCE FROM DEFECTS

Under continuous illumination conditions, PL in semiconductors sometimes bleaches or enhances with time. The process is normally reversible after a moderate thermal annealing or a lapse of time. The metastable behavior of PL is often attributed to a metastable nature of bulk defects responsible for PL. However, it is well known that surface states can trap charge carriers. Moreover, slow variations of the PL intensity can sometimes be attributed to changes in the band bending due to charging or discharging processes on the semiconductor surface. Furthermore, recombination-enhanced defect reactions^{572,573} can also cause unstable luminescence,^{574,575} and, in particular, degradation of PL.^{576–578} Below, we review what is known about unstable PL in GaN and provide preliminary analysis and assignment as to the origin of the observed phenomena.

A. Unstable luminescence bands

In a few studies a broad blue luminescence band centered at about 3.0 eV has been observed that exhibited a strong fatigue effect.^{579–583} A broad blue band with a similar fatigue behavior has also been reported to appear after brief etching of the Ga-polar surface of the MBE-grown GaN by

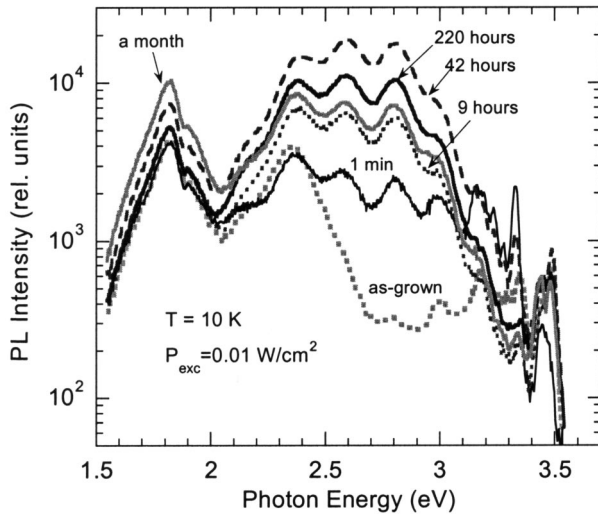


FIG. 106. PL spectrum of a high-resistive MBE-grown GaN sample. The sample was etched in 160 °C H_3PO_4 for 2 mins and then repeatedly exposed to air at room temperature for various times. Two broad bands with maxima at about 1.8 and 2.4 eV are related to point defects in bulk layer. Broad blue band emerging after etching is attributed to the surface states. The multiple peaks with separation of about 0.2 eV are due to interference effect.

hot phosphoric acid or molten KOH. The bleaching blue band has been attributed to radiative recombination on the GaN surface.^{584,585} Recently, we have discovered that even in as-grown samples grown by MOCVD an unstable blue band sometimes appears.⁵⁸⁶ The characteristic features of the latter band are the phonon-related fine structure and the metastability remaining for several days after annealing at room temperature. After a comprehensive study of the latter band, we are inclined to conclude that its origin is different from that appearing in the MBE-grown GaN layers subject to a wet etching treatment. The bleaching of the blue band in MOCVD-grown layers was accompanied by an enhancement of the YL band, similar to the PL behavior reported in Refs. 579–583.

In addition to the blue band, the unstable behavior has also been reported for the YL band,^{579–581,583,587,588} UVL band at about 3.2 eV,⁵⁸⁹ and excitonic emission in undoped GaN.^{583,590} Note that the Y_4 and Y_6 lines discussed in Sec. VIII also exhibit unstable behavior.

1. Blue band from the etched GaN surface

Although most recombination processes involving surface states are believed to be nonradiative, optically active recombination centers related to surfaces have been previously reported in InP ,⁵⁹¹ porous silicon,^{592,593} and in GaN grown by MBE and HVPE.^{584,585} In our experiments, after a brief etching of the GaN surface in hot phosphoric acid, a broad band appeared at low temperatures in the blue part of the PL spectrum. Its intensity gradually increased with exposure time of the sample to air after etching, as shown in Fig. 106.

With increasing excitation density from 10^{-2} to 100 W/cm^2 , the blue band gradually shifted to higher energies by about 100 meV, while its shape and width remained unchanged.⁵⁸⁴ At high excitation intensities the blue band

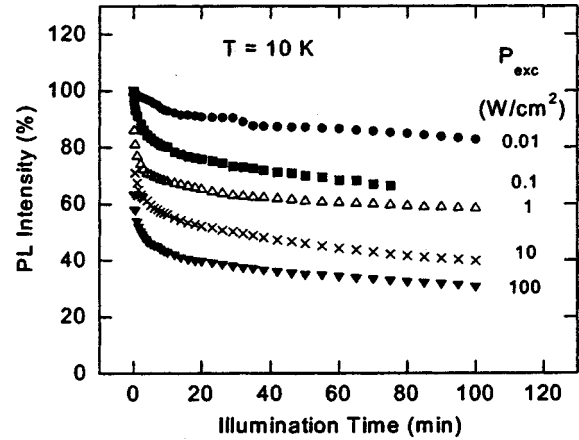


FIG. 107. Variation of the blue band intensity with time (recorded at 2.8 eV). The intensity at “zero time” is normalized to 100% for all excitation densities. The bleaching with time has fast and slow components. The latter is nearly independent of the excitation density. Reprinted with permission from Reshchikov *et al.*, Appl. Phys. Lett. 78, 177 (2001). Copyright (2001) by the American Institute of Physics.

intensity saturated, whereas the intensity of the exciton emission at about 3.47 eV increased superlinearly in the high-resistivity layers grown by MBE.

The blue luminescence bleached with UV exposure time, as shown in Fig. 107. It should be noted that the intensity of the exciton emission and other PL bands in the studied samples did not vary with UV exposure time under the same conditions. This rules out the possibility that bleaching is caused by heating of the sample by the laser beam. The effect of bleaching was irreversible at low temperatures. However, the PL intensity could be restored after annealing at 200 K for 30 min.⁵⁸⁴ Two activation energies (12 and 100 meV) have been determined from the temperature dependence of the intensity of this blue band.

It is well known that exposure of GaN to oxygen or air results in the formation or modification of the surface states that affect the electrical and optical properties of GaN.^{590,594,595} We proposed^{584,585} that oxidation of the GaN surface in air creates surface states in the lower part of the gap, and radiative recombination involving these states is responsible for the broad blue band in the etched and air exposed GaN layers.

2. Blue and yellow unstable bands

In several investigations, GaN layers grown by MOCVD on sapphire exhibited metastable BL and YL bands in the low-temperature PL spectrum.^{579–583} The YL band peaked at about 2.2–2.25 eV, and the BL band had a maximum at about $3.0 \pm 0.05 \text{ eV}$ (Refs. 579, 580, and 582) or at $2.9 \pm 0.05 \text{ eV}$.^{581,583} In all these investigations the BL band bleached under UV illumination and this process was accompanied with enhancement of the YL band. The memory effect at low temperatures lasted for many hours,⁵⁸⁰ whereas the PL band intensities completely recovered after a short annealing process at room temperature.^{579,582,583} Dhar and Ghosh⁵⁸² and Kim *et al.*⁵⁸³ noted a correlation between the metastable effect and high electrical resistivity of GaN films. Brown *et al.*⁵⁸⁰ noted that reactive-ion etching of GaN in

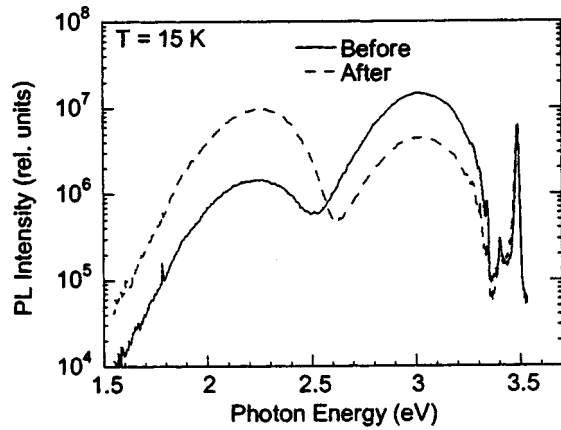


FIG. 108. Low-temperature PL spectrum of undoped GaN before and after UV illumination during 150 min with $P_{\text{exc}}=0.3 \text{ W/cm}^2$. Excitation density during the PL scan is 0.003 W/cm^2 .

different plasmas enhanced the metastable effect to varying degrees. Most of the authors attributed the observed transformation of PL with UV illumination to manifestation of a metastable point defect^{579,580,582} and believed that the same defect is responsible for both bands.^{579,580} Ryan *et al.*⁵⁸¹ ruled out a direct connection between the defects responsible for the BL and YL bands since, in their experiments, there was no correlation between the variations of these two bands.

Chang *et al.*^{587,588} observed an enhancement of the YL band at room temperature after UV irradiation,⁵⁸⁷ or after electron-beam irradiation.⁵⁸⁸ The intensity of the YL band returned to its initial value after a few hours at room temperature and much sooner at elevated temperatures. The thermal activation energy, deduced from the temperature dependence of the restoration time, was reported to be 1.34 eV. Only the YL band showed the unstable behavior in these studies. Chang *et al.*^{587,588} proposed that the UV or electron-beam irradiation affected the number or charge state of the deep defects responsible for the YL band.

A decrease of the near-band-edge emission intensity at room temperature in undoped GaN has also been reported.^{589,596} In one case, the decrease was accompanied by the emergence of UV emission with a maximum at about 3.2 eV.⁵⁸⁹ The effect of UV irradiation on the YL band and near-band-edge emissions at room temperature is also discussed in Sec. IX B 2.

In a few GaN samples grown by MOCVD we also observed unstable behavior of the BL and YL bands (Fig. 108),⁵⁸⁶ similar to that described in Refs. 579–583. Note that the samples were as grown and not subject to any surface treatment.⁵⁹⁷ After a 150 min of irradiation with 0.3 W/cm^2 of the He–Cd laser emitting at 3.81 eV, the BL intensity decreased by more than three times, the YL intensity increased by more than a factor of 10, and the exciton emission enhanced by a factor of about 1.4 (Fig. 109). The total radiative efficiency varied only about 10% during the irradiation, indicating that nonradiative recombination is hardly involved in the competition between the recombination channels. The rate of change in the PL intensity was about the same for the YL and BL bands, and it was proportional to the excitation

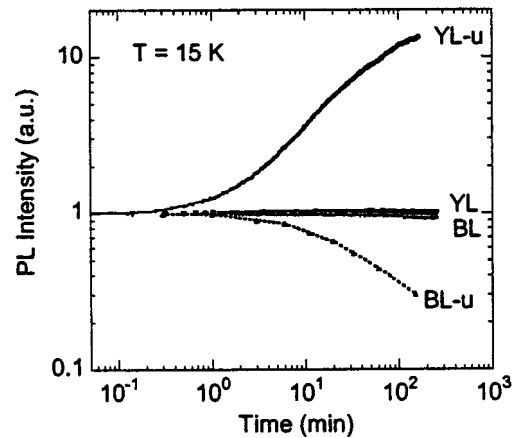


FIG. 109. Evolution of PL intensity at 15 K with UV exposure time for unstable YL and BL bands (YL-u and BL-u, respectively) and stable PL bands (YL and BL) in undoped GaN layers. $P_{\text{exc}}=0.3 \text{ W/cm}^2$.

intensity, at least in the range from 0.3 to 300 W/cm^2 . Remarkably, after heating the sample up to room temperature, the YL band in the UV-exposed areas remained much stronger than in the adjacent areas for several days. At room temperature the UV illumination with high intensity did not cause any significant changes in the PL intensity and no memory effect could be observed.

The BL band peaked at 3.05 eV, and its high-energy side exhibited a fine structure. The sharp peak at 3.342 eV is assumed to be the ZPL of this band. The next sharp peak was separated in energy by 36 meV from the ZPL and believed to be the local phonon mode of the defect responsible for the BL band. The second phonon replica could be seen as a weak peak at 3.27 eV. With increasing excitation intensity from 0.003 to 30 W/cm^2 , the BL band did not shift, neither as a whole (within an accuracy of $\pm 10 \text{ meV}$) nor its ZPL (within an accuracy of $\pm 1 \text{ meV}$). With increasing temperature, the BL band quenched above 75 K with an activation energy of about 150 meV, as displayed in Fig. 110. At temperatures above 150 K, the “unstable BL band” completely vanished, giving way to the “stable BL band” peaking at 2.90 eV. The

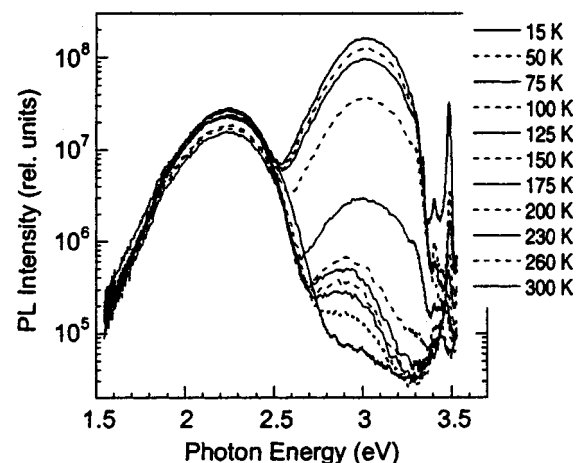


FIG. 110. Variation of PL spectrum with temperature for the GaN layer exhibiting unstable BL and YL bands. Excitation density is 10^{-3} W/cm^2 (at such low-excitation density the bleaching caused by UV exposure was negligible). The spectra were taken without high-intensity UV exposure.

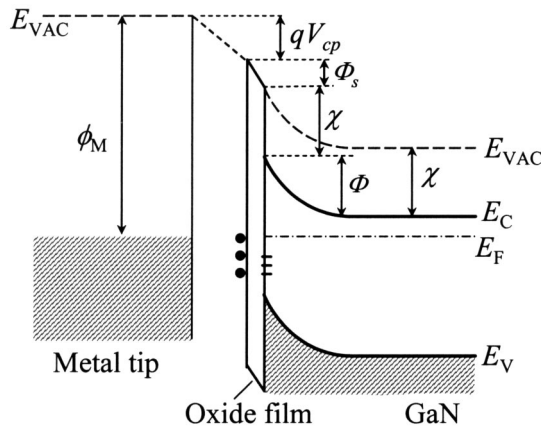


FIG. 111. Schematic diagram showing the band bending and the vacuum level (E_{VAC}) near the surface of GaN in vicinity of the metal tip.

stable BL band quenched above 200 K, and its characteristics were the same as those for the commonly observed BL band in undoped GaN grown by MOCVD (see Sec. IV D). The intensity of the YL band remained nearly unchanged up to room temperature, in agreement with its typical behavior in undoped GaN (Sec. IV A).

B. Manifestation of surface states in photoluminescence

The semiconductor surface significantly affects the electrical and optical properties of the material and related devices. The states inside the band gap are formed on the GaN surface due to Ga or N termination, reconstruction, structural and point defects, adsorbates, oxidation, etc. The surface of the air-exposed undoped GaN grown on *c*-plane sapphire shows an upward band bending, reported as 0.4, 0.75, and 1.0 ± 0.2 eV in various studies.^{598–601} It has been reported that a thin (~ 9 Å) Ga_2O_3 layer,⁶⁰² as well as chemisorbed oxygen atoms (up to one monolayer),^{598,603} cover the GaN surface. The band bending has been reported to be larger on the Ga-polar surface due to the spontaneous polarization effect.⁵⁵³ The surface states may affect the PL signal directly by varying the radiative or nonradiative recombination rate via the surface states or indirectly via varying the band bending. Below, we discuss how the surface states on GaN may affect the band bending in GaN and lead to a metastable behavior of the measured characteristics.

1. Band bending at the surface of GaN

The absolute value of the surface band bending can be measured by the Kelvin probe method.⁶⁰⁴ The band bending near GaN surface, or the potential barrier height in dark, Φ_d , can be found as

$$\Phi_d = \phi_M - qV_{cp} - \Phi_s - \chi + E_F, \quad (43)$$

where V_{cp} is the contact potential between the tip and GaN surface, ϕ_M is the tip metal work function ($\phi_M = 5.1$ eV for Au), χ is the electron affinity of the semiconductor, and E_F is the Fermi level, measured with respect to the conduction-band minimum, E_C , as depicted schematically in Fig. 111. The parameter Φ_s includes potential drop across the oxide

film arising from a possible distribution of charge in it, surface dipole due to adsorbate species, and microscopic dipole at the surface which is determined by the specific arrangement of the atoms near the surface.⁶⁰⁴ Based on the findings of Bermudez,⁵⁹⁸ Wu *et al.*,⁵⁹⁹ and Nienhaus *et al.*,⁶⁰⁵ we assume $\chi = 3.3 \pm 0.3$ eV for GaN. The variation in values of χ reported in the literature may be due to different microscopic surface dipoles, different degrees of oxidation, and presence of different adsorbed species in the experimentally studied GaN.

The upward band bending at the surface of *n*-type GaN with uncompensated concentration of shallow donors N_D can be characterized by the barrier height Φ_d , density of the negatively charged surface states n_s , and associated depletion region width W . The relationship of these parameters can be described by the expression⁶⁰⁶

$$W = \sqrt{\frac{2\Phi_d \epsilon \epsilon_0}{q^2 N_D}} = \frac{n_s}{N_D}. \quad (44)$$

The origin of n_s is in part the acceptorlike surface states below the Fermi level and in part uncompensated negative charge of ions adsorbed on the surface. We have obtained that in a large set of GaN samples with different concentrations of electrons the barrier height at the surface is of the order of 1 eV.⁶⁰⁰ Consequently, the depletion region width is about 100–30 nm for the concentrations of shallow donors in the range of 10^{17} – 10^{18} cm^{-3} , respectively, and the density of the negative charge at the surface is in low 10^{12} cm^{-3} according to Eq. (44). Note, however, that the value of Φ_d obtained from the Kelvin probe measurements may be overestimated by the unknown value of Φ_s [see Eq. (43)]. Some insight into the value of Φ_d can be gained independently from the dependence of photovoltage on light intensity.

When the sample is exposed to light, the band bending changes (photovoltage effect) due to charging or discharging of the semiconductor surface states, states inside the oxide layer, and finally, due to photoassisted desorption of atoms or molecules from the surface.⁶⁰⁴ Under UV illumination, the electron-hole pairs are generated mostly in the top 0.1–0.3- μm -thick layer of GaN sample [the effective absorption depth in GaN is about 80 nm for the photon energies of 3.7–3.8 eV (Ref. 167)]. Since the depletion region width in a typical undoped GaN is comparable to the effective absorption depth, a substantial part of the photogenerated holes is swept towards the surface by the strong near-surface electric field and rapidly (in $\sim 10^{-10}$ – 10^{-8} s) captured by the surface states. On the other hand, the photogenerated electrons are rapidly swept towards the bulk, increasing the concentration of free electrons in the bulk, likely in close vicinity of the surface barrier since the diffusion length is relatively small in GaN. The holes captured by the surface states reduce the negative charge on the surface and, consequently, reduce the depletion region width.

After the light is switched off, restoration of the band bending depends on temperature and specifics of the surface states and adsorbates. At room temperature and in air ambient the complete restoration of the dark value of the band bending lasts from 1 h to a few days depending on the details of preparation of the sample surface.⁶⁰¹ The main mechanism

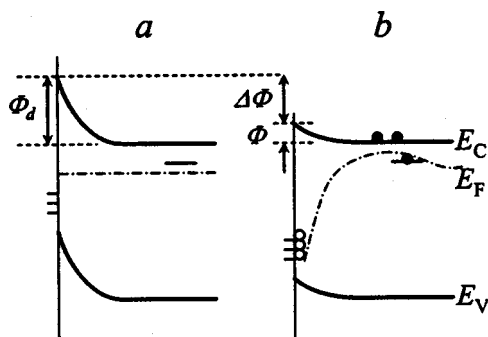


FIG. 112. Schematic diagram showing the band bending near the surface of GaN in dark (a) and after UV light pulse (b). Electrons are shown with solid circles and holes—with empty circles. The Fermi level E_F is shown as the same for electrons and holes in nonequilibrium case (b) in assumption that recombination in bulk is much faster than recombination over the barrier, and concentration of traps in the depletion region is much less than density of the surface states.

of the restoration is believed to be a thermionic transfer of free electrons over the surface barrier to the surface states.^{600,601} At cryogenic temperatures this mechanism evidently can be ignored. Therefore, at low temperatures we may expect significant flattening of the band bending under UV illumination that would stay for an indefinitely long time after the excitation light is switched off. Moreover, the excess concentration of the photogenerated electrons may accumulate at some distance from the surface, whereas the photogenerated holes bound to the surface states can avoid recombination for an indefinitely long time. The Fermi level would significantly depart from its equilibrium position (as shown in Fig. 112), and a metastable gradient of the charge near the surface would remain for an indefinitely long time at low temperatures.

2. Effect of UV illumination on PL

The PL intensity from GaN often changes with time under UV irradiation when the sample is in air ambient at room temperature. We have analyzed the effect of UV illumination with a He-Cd laser (3.81 eV and 0.3 W/cm²) on the PL intensity in a set of 30 undoped GaN layers grown by MBE, including samples grown under Ga- and N-rich conditions inclusive of Ga- and N-polar samples. The room-temperature PL spectrum of the undoped GaN samples contained a near-band-edge emission band at about 3.40–3.42 eV and the YL band. Typically the intensity of both the near-band-edge emission and the YL band decreased with time, although exceptions to this rule have been reported.⁵⁹⁴ In most cases only a partial restoration of the PL intensity was observed after the sample was kept in dark for a few hours at room temperature. The PL intensity restored to its original value sometimes only after two weeks.

The above-mentioned decrease of the PL intensity cannot be explained by flattening of the band bending due to filling the surface states with photogenerated holes because the reduction of the band bending and depletion width would have the opposite effect, namely an increase of the PL intensity. Besides, the photovoltage signal in the case of the employed excitation intensity saturated in the selected samples

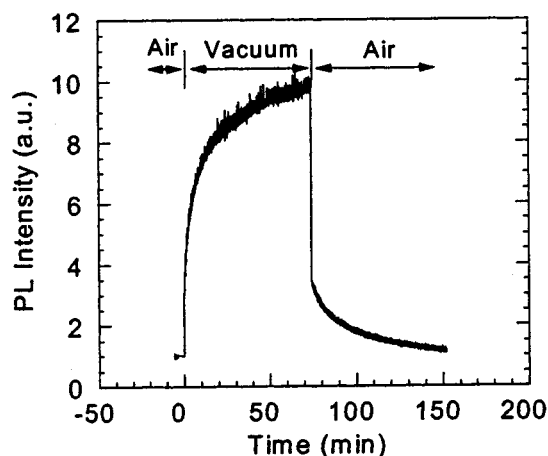


FIG. 113. Evolution of the YL intensity at room temperature in changing ambient for the MBE-grown GaN layer.

much faster (in a few seconds) than the slow quenching of the PL intensity. The saturation of the photovoltage also means that the equilibrium is reached between the filling of the surface states with photogenerated holes and thermionic transfer of free electrons situated in the bulk over the barrier to the surface states. Therefore, the slow variations in the PL intensity cannot be attributed to passivation of the surface states by photogenerated carriers. As a possible mechanism, we suggest that photoinduced desorption of oxygen or water vapor from the surface is responsible for the slow changes of the PL intensity (usually degradation) under UV irradiation in air ambient. To verify the validity of this assumption, we carried out PL experiments in different ambients at room temperature.^{594,595,607}

3. Effect of ambient on intensity and shape of PL bands

In a majority of our samples regardless of how they were grown, an enhancement in the PL intensity under UV illumination was observed as the sample chamber was evacuated. Figure 113 shows an example of strong enhancement of the YL band in vacuum for a GaN layer grown by MBE. Switching off the excitation light for several minutes did not change the emission intensity upon reexcitation, or the change was small. However, allowing air into the chamber returned the emission signal to its original level prior to evacuation. The amount of rise of the PL signal upon evacuation was found to be nearly proportional to the UV illumination intensity for excitation densities below 0.01 W/cm².⁶⁰⁷ Evacuation of air affected PL in different samples to different degrees.⁵⁹⁴ Along with the increase of PL intensity, a large decrease of the photoreflectance amplitude has been observed upon evacuation of air.⁵⁹⁰ Behn *et al.*⁵⁹⁰ attributed the changes in the photoreflectance and PL intensity to a UV-light-induced desorption of oxygen from the sample surface.

In order to ascertain whether oxygen or, e.g., water vapor in air plays a dominant role in the evolution of PL, we exposed the surface of GaN to various gases.^{594,595} The results for the near-band-edge PL are presented in Fig. 114. It can be seen that the oxygen ambient produces an effect similar to air, i.e., a prolonged decay of the PL signal as com-

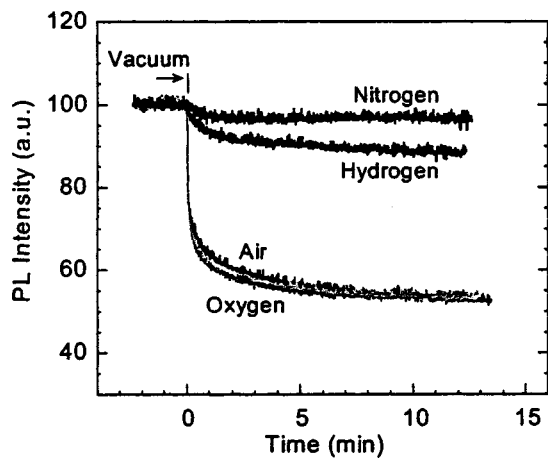


FIG. 114. Evolution of the near-band-edge emission intensity at room temperature under different ambient conditions for the MBE-grown GaN. Reprinted with permission from Reshchikov *et al.*, Mater Res. Soc. Symp. Proc. 743, L11.2 (2003).

pared to its value in vacuum. However, exposure to nitrogen or hydrogen leads to a much smaller decrease in the signal. Exposure to different gases followed by evacuation was repeated several times for one sample, and the effect was reproducible. The clear distinction between the transient changes in the PL emission in vacuum and oxygen as compared to other ambient (nitrogen and hydrogen) and similarity of the changes in air and oxygen ambients indicate that oxygen adsorption is responsible for the degradation of the optical quality of the GaN surface.

The observed degradation of the PL intensity and photo-reflectance in air or oxygen ambient can be attributed to either nonradiative recombination at the oxygen-induced surface states or to an increase of the band bending due to adsorption of oxygen.^{590,594,595} The latter mechanism is especially plausible for explaining the oxygen-induced changes of the PL spectrum.⁵⁹⁴ Note that generally the oxygen ambient affects the intensity of the YL and near-band-edge emission differently. If oxygen introduced only nonradiative surface states, the varying ratio between the radiative and nonradiative recombinations would not distort the PL spectrum. The redshift of the YL band observed in a few samples⁵⁹⁴ can also be explained by an increase of the surface band bending in air or oxygen ambient. The surface depletion resulting from this band bending may lead to diagonal (spatially indirect) transitions of free electrons or electrons bound to the shallow donors to the deep-level states located closer to the surface. The redshift would be greater for a larger band bending. In contrast, the shift of the exciton emission cannot be large because increasing the near-surface electric field would break up excitons rather than separate an electron and a hole significantly. A remarkable observation, discerned from the experiments with varying irradiation intensity, is that evacuation without UV irradiation does not remove the oxygen-related states,⁶⁰⁷ only that the UV light supplies the necessary energy to activate desorption of oxygen.

Degradation of the PL intensity under UV illumination in air ambient apparently cannot be attributed to oxygen de-

sorption. The PL intensity usually decreases under UV illumination, in contrast to the intensity increase during the photoassisted oxygen desorption in vacuum. Possibly some nonradiative recombination centers are created under UV illumination in air ambient due to surface reconstruction or recombination-enhanced defect reactions.^{572,573} However, the variety of PL behavior upon air or gas evacuation or upon UV illumination in air ambient⁵⁹⁴ cannot be explained by a single mechanism. Apparently, more than one effect are responsible for variations observed from sample to sample.

4. Effect of passivation on PL

Martinez *et al.*⁶⁰⁸ observed a dramatic increase in the room-temperature PL intensity (a factor of 4–6) when the GaN samples were treated with aqueous and alcoholic solutions of inorganic sulfides, such as ammonium or sodium sulfide [(NH₄)₂S_x and Na₂S]. The sulfide treated surfaces remained passivated for at least seven months in air. It is remarkable that the YL intensity did not change after the treatment. The effect of nonsulfide-based chemicals was also tested in these experiments. In general, acidic solutions increased the PL intensity (by up to a factor of 2.5), whereas bases and H₂O₂ slightly decreased it. Martinez *et al.*⁶⁰⁸ explained the stability of the sulfide passivation by the formation of a strong N–S bond instead of the weak N–O bond. Under UV illumination the PL intensity from the passivated GaN surface decreased in some cases, apparently due to photochemical reactions, and remained stable in others. The passivation effect could be easily removed by a short rinse in de-ionized (DI) water. In contrast, the surface which was pretreated with an oxide etch before passivation was much more resistant to DI water cleaning.⁶⁰⁸

Konenkova⁶⁰⁹ has also demonstrated that sulfidizing of the GaN surface improves the PL intensity. The most pronounced increase of the exciton emission intensity (by a factor of 3.6) compared with the intensity of untreated GaN was observed after treatment in a saturated solution of Na₂S in isopropyl alcohol. Song *et al.*⁶¹⁰ reported an increase by more than 100 times in the room-temperature exciton emission intensity after passivation of *n*-type GaN with CH₃CSNH₂ solution. Note that along with the enhancement of the PL intensity, the electrical properties of GaN significantly improved after passivation.^{608,610} In particular, the specific contact resistance decreased from 2.4×10^{-2} to $3.1 \times 10^{-6} \Omega \text{ cm}^2$,⁶¹⁰ and the Schottky barrier height increased from 1.18 to 1.63 eV (Ref. 608) after sulfide passivation.

In *p*-type Mg-doped GaN, no measurable improvement in the PL efficiency after sulfide passivation was observed by Martinez *et al.*,⁶⁰⁸ and about a twofold decrease of the BL intensity was reported by Lin *et al.*⁶¹¹ The observed decrease was attributed to a reduction of the concentration of V_N near the surface, which could be replaced by sulfur.⁶¹¹

The aforementioned examples of the effect of sulfide passivation on the PL intensity in GaN clearly show that the surface states play an important role in electrical and optical properties of GaN just like any other semiconductor.

X. SUMMARY

Point defects affect optical and electrical properties of GaN to a greater extent than perhaps recognized. Luminescence methods are particularly advantageous for detection and revealing the nature of point defects, however, great efforts must be extended to identify numerous defects in GaN. Even in unintentionally doped GaN a plethora of luminescence bands is discovered that are attributed to residual impurities, native defects, complexes, and structural defects. In this review, we provide a comprehensive analysis of the behavior of numerous luminescence bands associated with defects in GaN. Special attention was given to the notorious luminescence bands such as the yellow band in undoped GaN, and the blue band observed in undoped, Zn-, and Mg-doped GaN. It should be noted that the previous assignments as to the origin of most of the luminescence bands in GaN were very preliminary and often based largely on speculations without much basis or on controversial theoretical predictions rather than on convincing experimental evidence. By analyzing a large body of published literature, combined with “hands on experience” in this field we have attempted to shed light on the identity and properties of many point defects in GaN. Typical concentrations of uncontrolled acceptors, responsible for spontaneous emission in the visible part of the spectrum in undoped GaN, are of the order of 10^{15} cm^{-3} , even in the purest available material. In doped GaN the situation is not much clearer because the doping universally results in the creation of yet unknown compensating defects. Among the defects in *p*-type GaN that are explored the most, properties of luminescence bands due to Mg doping are established with high degree of certainty. The importance of potential fluctuations, which are unavoidable in heavily Mg-doped GaN, has been treated in detail. A class of luminescence lines in GaN, most probably related in some way or another to structural defects, has been discussed in detail. The stability of several luminescence bands with time and ambient conditions has also been examined.

ACKNOWLEDGMENTS

This work was funded by AFOSR (Dr. G. L. Witt and Dr. T. Steiner), NSF (Dr. L. Hess and Dr. U. Varshney), and ONR (Dr. C. E. C. Wood), and was motivated to a large extent by the Wood-Witt program. Due to space limitation we thank our close collaborators and those who provided their papers: Dr. D. Huang, Dr. F. Yun, Dr. P. Visconti, Dr. J. Jasinski, Dr. R. J. Molnar, Dr. C. G. Van de Walle, Dr. J. E. Northrup, Dr. R. Y. Korotkov, Dr. Z. Liliental-Weber, Dr. B. W. Wessels, Dr. F. Shahedipour, Dr. S. S. Park, Dr. K. Y. Lee, Dr. V. Dmitriev, Dr. D. C. Reynolds, Dr. C. W. Litton, Dr. D. C. Look, Dr. Z. Fang, Dr. D. K. Johnstone, Dr. Y. T. Moon, Dr. K. Saarinen, Dr. J. Freitas, Jr., Dr. E. Glaser, and Dr. A. J. Steckl, and graduate students S. Sabuktigin and Lei He.

¹B. Monemar, in *Optical Properties of GaN*, Semiconductors and Semimetals Vol. 50 (Academic, San Diego, 1998), pp. 305–368.

²B. Monemar, *J. Mater. Sci.: Mater. Electron.* **10**, 227 (1999).

³B. Monemar, *J. Phys.: Condens. Matter* **13**, 7011 (2001).

⁴B. Monemar *et al.*, *Mater. Sci. Eng., B* **93**, 112 (2002).

⁵S. Strite and H. Morkoç, *J. Vac. Sci. Technol. B* **10**, 1237 (1992).

⁶S. Nakamura and G. Fosol, *The Blue Laser Diode* (Springer, Berlin, 1998).

⁷H. Morkoç, *Nitride Semiconductors and Devices* (Springer, Heidelberg, 1999).

⁸In *Properties, Processing, and Applications of Gallium Nitride and Related Semiconductors*, edited by J. H. Edgar, S. Strite, I. Akasaki, H. Amano, and C. Wetzel (INSPEC, UK, 1999).

⁹S. J. Pearton, J. C. Zolper, R. J. Shul, and F. Ren, *J. Appl. Phys.* **86**, 1 (1999).

¹⁰S. C. Jain, M. Willander, J. Narayan, and R. Van Overstraeten, *J. Appl. Phys.* **87**, 965 (2000).

¹¹A. K. Viswanath, *Growth and Optical Properties of GaN*, Semiconductors and Semimetals Vol. 73, edited by R. Willardson, and H. S. Nalwa (Academic, San Diego, 2001), pp. 63–150.

¹²H. Morkoç, *Mater. Sci. Eng., R.* **33**, 135 (2001).

¹³J. K. Sheu and G. C. Chi, *J. Phys.: Condens. Matter* **14**, 657 (2002).

¹⁴D. W. Jenkins and J. D. Dow, *Phys. Rev. B* **39**, 3317 (1989).

¹⁵J. Neugebauer and C. G. Van de Walle, *Phys. Rev. B* **50**, 8067 (1994).

¹⁶J. Neugebauer and C. G. Van de Walle, *Appl. Phys. Lett.* **68**, 1829 (1996).

¹⁷J. Neugebauer and C. G. Van de Walle, *Appl. Phys. Lett.* **69**, 503 (1996).

¹⁸P. Boguslawski, E. L. Briggs, and J. Bernholc, *Phys. Rev. B* **51**, 17255 (1995).

¹⁹P. Boguslawski, E. L. Briggs, and J. Bernholc, *Appl. Phys. Lett.* **69**, 233 (1996).

²⁰P. Boguslawski and J. Bernholc, *Phys. Rev. B* **56**, 9496 (1997).

²¹S. Limpijumnong and C. G. Van de Walle, *Phys. Rev. B* **69**, 035207 (2004).

²²T. Mattila and R. M. Nieminen, *Phys. Rev. B* **55**, 9571 (1997).

²³I. Gorczyca, A. Svane, and N. E. Christensen, *Phys. Rev. B* **60**, 8147 (1999).

²⁴J. Neugebauer and C. G. Van de Walle, in *Festkörperprobleme/Advances in Solid State Physics*, edited by R. Helbig (Vieweg, Braunschweig, 1996), Vol. 35, p. 25.

²⁵S. B. Zhang and J. E. Northrup, *Phys. Rev. Lett.* **67**, 2339 (1991).

²⁶C. G. Van de Walle and J. Neugebauer, *J. Appl. Phys.* **95**, 3851 (2004).

²⁷G. A. Baraff and M. Schlüter, *Phys. Rev. Lett.* **55**, 1327 (1985).

²⁸I. Gorczyca, N. E. Christensen, and A. Svane, *Phys. Rev. B* **66**, 075210 (2002).

²⁹C. H. Park and D. J. Chadi, *Phys. Rev. B* **55**, 12995 (1997).

³⁰J. Neugebauer and C. G. Van de Walle, *J. Appl. Phys.* **85**, 3003 (1999).

³¹K. H. Chow, G. D. Watkins, A. Usui, and M. Mizuta, *Phys. Rev. Lett.* **85**, 2761 (2000).

³²T. Mattila, A. P. Seitsonen, and R. Nieminen, *Phys. Rev. B* **54**, 1474 (1996).

³³D. J. Chadi and K. J. Chang, *Phys. Rev. Lett.* **60**, 2183 (1988).

³⁴J. Dabrowski and M. Scheffler, *Phys. Rev. Lett.* **60**, 2183 (1988).

³⁵H. Wang and A.-B. Chen, *J. Appl. Phys.* **87**, 7859 (2000).

³⁶A. F. Wright, *J. Appl. Phys.* **92**, 2575 (2002).

³⁷F. Mireles and S. E. Ulloa, *Phys. Rev. B* **58**, 3879 (1998).

³⁸H. Wang and A.-B. Chen, *Phys. Rev. B* **63**, 125212 (2001).

³⁹B. Pödör, *Semicond. Sci. Technol.* **11**, 827 (1996).

⁴⁰C. G. Van de Walle, S. Limpijumnong, and J. Neugebauer, *Phys. Rev. B* **63**, 245205 (2001).

⁴¹C. D. Latham, R. M. Nieminen, C. J. Fall, R. Jones, S. Öberg, and P. R. Briddon, *Phys. Rev. B* **67**, 205206 (2003).

⁴²S. Limpijumnong, C. G. Van de Walle, and J. Neugebauer, *Mater. Res. Soc. Symp. Proc.* **639**, G4.3 (2001).

⁴³L. E. Ramos, J. Furthmüller, L. M. R. Scolfaro, J. R. Leite, and F. Bechstedt, *Phys. Rev. B* **66**, 075209 (2002).

⁴⁴L. Bellaiche, S.-H. Wei, and A. Zunger, *Phys. Rev. B* **56**, 10233 (1997).

⁴⁵T. Mattila and A. Zunger, *Phys. Rev. B* **58**, 1367 (1998).

⁴⁶C. G. Van de Walle and J. Neugebauer, *Appl. Phys. Lett.* **76**, 1009 (2000).

⁴⁷J. Neugebauer and C. G. Van de Walle, *Phys. Rev. Lett.* **75**, 4452 (1995).

⁴⁸A. F. Wright, C. H. Seager, S. H. Myers, D. D. Koleske, and A. A. Allerman, *J. Appl. Phys.* **94**, 2311 (2003).

⁴⁹C. G. Van de Walle, *Phys. Status Solidi B* **235**, 89 (2003).

⁵⁰N. S. Averkiev, A. A. Gutkin, E. B. Osipov, M. A. Reshchikov, and V. R. Sosnovskii, *Defect Diffus. Forum* **103–105**, 31 (1993).

⁵¹H. Xu and U. Lindelfelt, *J. Appl. Phys.* **68**, 4077 (1990).

⁵²C. W. Myles and O. F. Sankey, *Phys. Rev. B* **29**, 6810 (1984).

⁵³C. G. Van de Walle, J. Neugebauer, C. Stampel, M. D. McCluskey, and N. M. Johnson, *Acta Phys. Pol. A* **96**, 613 (1999).

⁵⁴I. Gorczyca, A. Svane, and N. E. Christensen, *Phys. Rev. B* **61**, 7494 (2000).

⁵⁵J. Z. Li, J. Y. Lin, H. X. Jiang, A. Salvador, A. Botchkarev, and H.

- Morkoç, Appl. Phys. Lett. **69**, 1474 (1996).
- ⁵⁶U. Kaufmann, M. Kunzer, M. Maier, H. Obloh, A. Ramakrishnan, B. Santic, and P. Schlöter, Appl. Phys. Lett. **72**, 1326 (1998).
- ⁵⁷C. D. Latham, R. Jones, S. Öberg, R. M. Nieminen, and P. R. Briddon, Phys. Rev. B **68**, 205209 (2003).
- ⁵⁸S.-G. Lee and K. J. Chang, Semicond. Sci. Technol. **14**, 138 (1999).
- ⁵⁹C. G. Van de Walle, Phys. Rev. B **56**, R10020 (1997).
- ⁶⁰B. Szűcs, A. Gali, Z. Hajnal, P. Deák, and C. G. Van de Walle, Phys. Rev. B **68**, 085202 (2003).
- ⁶¹J. Elsner *et al.*, Phys. Rev. Lett. **79**, 3672 (1997).
- ⁶²A. F. Wright and U. Grossner, Appl. Phys. Lett. **73**, 2751 (1998).
- ⁶³S. M. Lee, M. A. Belkhir, X. Y. Zhu, Y. H. Lee, Y. G. Hwang, and T. Frauenheim, Phys. Rev. B **61**, 16033 (2000).
- ⁶⁴J. E. Northrup, Phys. Rev. B **66**, 045204 (2002).
- ⁶⁵K. Leung, A. F. Wright, and E. B. Stechel, Appl. Phys. Lett. **74**, 2495 (1999).
- ⁶⁶P. J. Hansen *et al.*, Appl. Phys. Lett. **72**, 2247 (1998).
- ⁶⁷M. A. Reshchikov and R. Y. Korotkov, Phys. Rev. B **64**, 115205 (2001).
- ⁶⁸J. Elsner, R. Jones, M. I. Heggie, P. K. Sitch, M. Haugk, Th. Frauenheim, S. Öberg, and P. R. Briddon, Phys. Rev. B **58**, 12571 (1998).
- ⁶⁹L. W. Tu, Y. C. Lee, D. Stocker, and E. F. Schubert, Phys. Rev. B **58**, 10696 (1998).
- ⁷⁰A. Göldner *et al.*, Mater. Res. Soc. Symp. Proc. **482**, 637 (1998).
- ⁷¹E. F. Schubert, I. D. Goepfert, and J. M. Redwing, Appl. Phys. Lett. **71**, 3224 (1997).
- ⁷²I.-H. Lee, J. J. Lee, P. Kung, F. J. Sanchez, and M. Razeghi, Appl. Phys. Lett. **74**, 102 (1999).
- ⁷³R. Singh, R. J. Molnar, M. S. Ünü, and T. D. Moustakas, Appl. Phys. Lett. **64**, 336 (1994).
- ⁷⁴W. Grieshaber, E. F. Schubert, I. D. Goepfert, R. F. Karlicek, Jr., M. J. Schurman, and C. Tran, J. Appl. Phys. **80**, 4615 (1996).
- ⁷⁵D. A. Turnbull, X. Li, S. Q. Gu, E. E. Reuter, J. J. Coleman, and S. G. Bishop, J. Appl. Phys. **80**, 4609 (1996).
- ⁷⁶D. M. Hofmann *et al.*, Phys. Rev. B **52**, 16702 (1995).
- ⁷⁷J. Krüger, D. Corlatan, C. Kisielowski, Y. Kim, R. Klockenbrink, G. S. Sudhir, M. Rubin, and E. Weber, Mater. Sci. Forum **258–263**, 1191 (1997).
- ⁷⁸O. Brandt, J. Ringling, K. H. Ploog, H.-J. Wünsche, and F. Henneberger, Phys. Rev. B **58**, R15977 (1998).
- ⁷⁹D. G. Thomas, J. J. Hopfield, and W. M. Augustyniak, Phys. Rev. **140**, A202 (1965).
- ⁸⁰A. P. Levanyuk and V. V. Osipov, Usp. Fiz. Nauk **133**, 427 (1981) [Sov. Phys. Usp. **24**, 187 (1981)].
- ⁸¹S. Shinoya, T. Koda, K. Era, and H. Fujiwara, J. Phys. Soc. Jpn. **19**, 1157 (1964).
- ⁸²M. A. Reshchikov, G.-C. Yi, and B. W. Wessels, Phys. Rev. B **59**, 13176 (1999).
- ⁸³P. W. Mason, A. Dörnen, V. Haerle, F. Scholz, and G. D. Watkins, Mater. Res. Soc. Symp. Proc. **449**, 793 (1997).
- ⁸⁴F. Binet, J. Y. Duboz, J. Off, and F. Scholz, Phys. Rev. B **60**, 4715 (1999).
- ⁸⁵The temperature should be low enough that the considered PL bands do not quench, and the excitation should be chosen below the saturation region.
- ⁸⁶F. E. Williams, J. Phys. Chem. Solids **12**, 265 (1960); Phys. Status Solidi **25**, 493 (1968).
- ⁸⁷R. Y. Korotkov, M. A. Reshchikov, and B. W. Wessels, Physica B **325**, 1 (2003).
- ⁸⁸W. A. Barry and G. D. Watkins, Phys. Rev. B **54**, 7789 (1996).
- ⁸⁹A. G. Milnes, *Deep Impurities in Semiconductors* (Wiley, New York, 1973), p. 6.
- ⁹⁰F. C. Rong, W. A. Barry, J. F. Donegan, and G. D. Watkins, Phys. Rev. B **54**, 7779 (1996).
- ⁹¹B. I. Shklovskii and A. L. Efros, *Electronic Properties of Doped Semiconductors* (Springer, Berlin, 1984), pp. 53–73 and 253–313.
- ⁹²V. I. Vovnenko, K. D. Glinchuk, K. Lukat, and A. V. Prokhorovich, Fiz. Tekh. Poluprovodn. (S.-Peterburg) **14**, 1003 (1980) [Sov. Phys. Semicond. **14**, 596 (1980)].
- ⁹³W. J. Moore, J. A. Freitas, Jr., and R. J. Molnar, Phys. Rev. B **56**, 12073 (1997).
- ⁹⁴K. Huang and A. Rhys, Proc. R. Soc. London, Ser. A **204**, 406 (1950).
- ⁹⁵C. C. Klick and J. H. Schulman, Solid State Phys. **5**, 97 (1957).
- ⁹⁶K. K. Rebane, *Impurity Spectra of Solids* (Plenum, New York, 1970).
- ⁹⁷A. M. Stoneham, *Theory of Defects in Solids* (Clarendon, Oxford, 1975).
- ⁹⁸T. Ogino and M. Aoki, Jpn. J. Appl. Phys. **19**, 2395 (1980).
- ⁹⁹M. A. Reshchikov, R. J. Molnar, and H. Morkoç, Mater. Res. Soc. Symp. Proc. **680**, E5.6 (2001).
- ¹⁰⁰M. A. Reshchikov, H. Morkoç, S. S. Park, and K. Y. Lee, Mater. Res. Soc. Symp. Proc. **693**, 16.19 (2002).
- ¹⁰¹J. Cazaux, J. Appl. Phys. **59**, 1418 (1986).
- ¹⁰²X. Li and J. J. Coleman, Appl. Phys. Lett. **70**, 438 (1997).
- ¹⁰³K. Fleischer, M. Toth, M. R. Phillips, J. Zou, G. Li, and S. J. Chua, Appl. Phys. Lett. **74**, 1114 (1999).
- ¹⁰⁴M. Toth and M. R. Phillips, Scanning **20**, 425 (1998).
- ¹⁰⁵K. Knobloch, P. Perlin, J. Krueger, E. R. Weber, and C. Kisielowski, MRS Internet J. Nitride Semicond. Res. **3**, 4 (1998).
- ¹⁰⁶G. E. Pake and T. L. Estle, *The Physical Properties of Electron Paramagnetic Resonance* (Benjamin, Reading, MA, 1973).
- ¹⁰⁷E. R. Weber, H. Ennen, U. Kaufmann, J. Windscheif, J. Schneider, and T. Wosinski, J. Appl. Phys. **53**, 6140 (1982).
- ¹⁰⁸A. V. Malyshev, I. A. Merkulov, and A. V. Rodina, Fiz. Tverd. Tela (S.-Peterburg) **40**, 1002 (1998) [Phys. Solid State **40**, 917 (1998)].
- ¹⁰⁹E. R. Glaser, J. A. Freitas, Jr., B. V. Shanabrook, and D. D. Koleske, Phys. Rev. B **68**, 195201 (2003).
- ¹¹⁰M. A. Reshchikov, H. Morkoç, S. S. Park, and K. Y. Lee, Appl. Phys. Lett. **78**, 2882 (2001).
- ¹¹¹M. A. Reshchikov, H. Morkoç, S. S. Park, and K. Y. Lee, Appl. Phys. Lett. **78**, 3041 (2001).
- ¹¹²M. A. Reshchikov, H. Morkoç, S. S. Park, and K. Y. Lee, Appl. Phys. Lett. **81**, 4970 (2002).
- ¹¹³M. A. Reshchikov, M. Zafar Iqbal, H. Morkoç, S. S. Park, and K. Y. Lee, Appl. Phys. Lett. **83**, 266 (2003).
- ¹¹⁴M. A. Reshchikov, M. Zafar Iqbal, S. S. Park, K. Y. Lee, D. Tsvetkov, V. Dmitriev, and H. Morkoç, Physica B **340–342**, 444 (2003).
- ¹¹⁵R. Dingle and M. Ilegems, Solid State Commun. **9**, 175 (1971).
- ¹¹⁶M. A. Reshchikov, F. Shahedipour, R. Y. Korotkov, M. P. Ulmer, and B. W. Wessels, J. Appl. Phys. **87**, 3351 (2000).
- ¹¹⁷M. A. Reshchikov, M. H. Zhang, J. Cui, P. Visconti, F. Yun, and H. Morkoç, Mater. Res. Soc. Symp. Proc. **639**, G6.7 (2001).
- ¹¹⁸S. Christiansen *et al.*, MRS Internet J. Nitride Semicond. Res. **1**, 19 (1996).
- ¹¹⁹J. S. Colton, P. Y. Yu, K. L. Teo, E. R. Weber, P. Perlin, I. Grzegory, and K. Uchida, Appl. Phys. Lett. **75**, 3273 (1999).
- ¹²⁰J. S. Colton, P. Y. Yu, K. L. Teo, P. Perlin, E. R. Weber, I. Grzegory, and K. Uchida, Physica B **273–274**, 75 (1999).
- ¹²¹D. C. Reynolds, D. C. Look, B. Jogai, J. E. Van Nostrand, R. Jones, and J. Jenny, Solid State Commun. **106**, 701 (1998).
- ¹²²J. Kang, Y. Shen, and Z. Wang, Mater. Sci. Eng., B **91–92**, 303 (2002).
- ¹²³J. I. Pankove and J. A. Hutchby, J. Appl. Phys. **47**, 5387 (1976).
- ¹²⁴L. V. Jorgensen, A. C. Kruseman, H. Schut, A. Van Veen, M. Fanciulli, and T. D. Moustakas, Mater. Res. Soc. Symp. Proc. **449**, 853 (1997).
- ¹²⁵K. Saarinen *et al.*, Phys. Rev. Lett. **79**, 3030 (1997).
- ¹²⁶K. Saarinen *et al.*, Physica B **273–274**, 33 (1999).
- ¹²⁷J. Oila *et al.*, Phys. Rev. B **63**, 045205 (2001).
- ¹²⁸A. Uedono *et al.*, J. Appl. Phys. **90**, 181 (2001).
- ¹²⁹K. Saarinen, T. Suski, I. Grzegory, and D. C. Look, Physica B **308–310**, 77 (2001).
- ¹³⁰K. Saarinen, V. Ranki, T. Suski, M. Bockowski, and I. Grzegory, J. Cryst. Growth **246**, 281 (2002).
- ¹³¹P. Laukkanen *et al.*, J. Appl. Phys. **92**, 786 (2002).
- ¹³²J. Oila, K. Saarinen, A. E. Wickenden, D. D. Koleske, R. L. Henry, and M. E. Twigg, Appl. Phys. Lett. **82**, 1021 (2003).
- ¹³³J. Oila *et al.*, Appl. Phys. Lett. **82**, 3433 (2003).
- ¹³⁴X. Zhang, P. Kung, D. Walker, A. Saxler, and M. Razeghi, Mater. Res. Soc. Symp. Proc. **395**, 625 (1996).
- ¹³⁵R. Niebuhr, K. Bachem, K. Bombrowski, M. Maier, W. Plierschen, and U. Kaufmann, J. Electron. Mater. **24**, 1531 (1995).
- ¹³⁶A. Y. Polyakov, M. Shin, J. A. Freitas, Jr., M. Skowronski, D. W. Greve, and R. G. Wilson, J. Appl. Phys. **80**, 6349 (1996).
- ¹³⁷R. Zhang and T. F. Kuech, Appl. Phys. Lett. **72**, 1611 (1998).
- ¹³⁸R. Armitage, Q. Yang, H. Feick, S. Y. Tzeng, J. Lim, and E. R. Weber, Mater. Res. Soc. Symp. Proc. **743**, L10.7 (2003).
- ¹³⁹S. O. Kucheyev, M. Toth, M. R. Phillips, J. S. Williams, C. Jagadish, and G. Li, J. Appl. Phys. **91**, 5867 (2002).
- ¹⁴⁰E. Silkowski, Y. K. Yeo, R. L. Hengehold, M. A. Khan, T. Lei, K. Evans, and C. Cerny, Mater. Res. Soc. Symp. Proc. **395**, 813 (1996).
- ¹⁴¹E. R. Glaser *et al.*, Phys. Rev. B **51**, 13326 (1995).
- ¹⁴²D. G. Chichikine *et al.*, J. Appl. Phys. **81**, 2197 (1997).
- ¹⁴³M. Godlewski *et al.*, Mater. Sci. Forum **258–263**, 1149 (1997).

- ¹⁴⁴F. K. Koschnick, K. Michael, J.-M. Spaeth, B. Beaumont, and P. Gibart, *Appl. Phys. Lett.* **76**, 1828 (2000).
- ¹⁴⁵P. Muret, A. Phillippe, E. Monroy, E. Munoz, B. Beaumont, F. Omnès, and P. Gibart, *J. Appl. Phys.* **91**, 2998 (2002).
- ¹⁴⁶E. Calleja *et al.*, *Phys. Rev. B* **55**, 4689 (1997).
- ¹⁴⁷M. Ramsteiner, J. Menniger, O. Brandt, H. Yang, and K. H. Ploog, *Appl. Phys. Lett.* **69**, 1276 (1996).
- ¹⁴⁸S. Tripathy, R. K. Soni, H. Asahi, and S. Gonda, *Physica B* **275**, 301 (2000).
- ¹⁴⁹T. Suski *et al.*, *Appl. Phys. Lett.* **67**, 2188 (1995).
- ¹⁵⁰P. Perlin *et al.*, *Phys. Rev. Lett.* **75**, 296 (1995).
- ¹⁵¹C. Trager-Cowan, K. P. O'Donnell, S. E. Hooper, and C. T. Foxon, *Appl. Phys. Lett.* **68**, 355 (1996).
- ¹⁵²A. Hoffmann *et al.*, *Solid-State Electron.* **41**, 275 (1997).
- ¹⁵³H. C. Yang, T. Y. Lin, and Y. F. Chen, *Phys. Rev. B* **62**, 12593 (2000).
- ¹⁵⁴L. W. Tu, Y. C. Lee, S. J. Chen, I. Lo, D. Stocker, and E. F. Schubert, *Appl. Phys. Lett.* **73**, 2802 (1998).
- ¹⁵⁵D. Basak, M. Lachab, T. Nakanishi, and S. Sakai, *Appl. Phys. Lett.* **75**, 3710 (1999).
- ¹⁵⁶I. Shalish, L. Kronik, G. Segal, Y. Shapira, M. Eizenberg, and J. Salzman, *Appl. Phys. Lett.* **77**, 987 (2000).
- ¹⁵⁷I. Shalish, L. Kronik, G. Segal, Y. Rosenwaks, Y. Shapira, U. Tisch, and J. Salzman, *Phys. Rev. B* **59**, 9748 (1999).
- ¹⁵⁸G. Li, S. J. Chua, S. J. Xu, W. Wang, P. Li, B. Beaumont, and P. Gibart, *Appl. Phys. Lett.* **74**, 2821 (1999).
- ¹⁵⁹X. Li, P. W. Bohn, and J. J. Coleman, *Appl. Phys. Lett.* **75**, 4049 (1999).
- ¹⁶⁰M. A. Reshchikov, F. Shahedipour, R. Y. Korotkov, M. P. Ulmer, and B. W. Wessels, *Physica B* **273–274**, 105 (1999).
- ¹⁶¹R. Seitz, C. Gaspar, T. Monteiro, E. Pereira, M. Leroux, B. Beaumont, and P. Gibart, *MRS Internet J. Nitride Semicond. Res.* **2**, 36 (1997).
- ¹⁶²K. Kuriyama, H. Kondo, and M. Okada, *Solid State Commun.* **119**, 559 (2001).
- ¹⁶³A. P. Young and L. J. Brillson, *Appl. Phys. Lett.* **77**, 699 (2000).
- ¹⁶⁴R. Armitage, W. Hong, Q. Yang, H. Feick, J. Gebauer, E. R. Weber, S. Hautakangas, and K. Saarinen, *Appl. Phys. Lett.* **82**, 3457 (2003).
- ¹⁶⁵V. Guénaud, E. Deleporte, M. Voos, C. Delalande, B. Beaumont, M. Leroux, P. Gibart, and J. P. Faurie, *MRS Internet J. Nitride Semicond. Res.* **2**, 10 (1997).
- ¹⁶⁶H. Haag, B. Hönerlage, O. Briot, and R. L. Aulombard, *Phys. Rev. B* **60**, 11624 (1999).
- ¹⁶⁷G. Yu, G. Wang, H. Ishikawa, M. Umeno, T. Soga, T. Egawa, J. Watanabe, and T. Jimbo, *Appl. Phys. Lett.* **70**, 3209 (1997); J. F. Muth, J. H. Lee, I. K. Shmagin, R. M. Kolbas, H. C. Casey, Jr., B. P. Keller, U. K. Mishra, and S. P. DenBaars, *ibid.* **71**, 2572 (1997).
- ¹⁶⁸Z. Z. Bandić, P. M. Bridger, E. C. Piquette, and T. C. McGill, *Appl. Phys. Lett.* **72**, 3166 (1998).
- ¹⁶⁹P. M. Bridger, Z. Z. Bandić, E. C. Piquette, and T. C. McGill, *Appl. Phys. Lett.* **73**, 3438 (1998).
- ¹⁷⁰L. Chernyak *et al.*, *Appl. Phys. Lett.* **77**, 2695 (2000).
- ¹⁷¹N. Yamamoto *et al.*, *J. Appl. Phys.* **94**, 4315 (2003).
- ¹⁷²U. Kaufmann, M. Kunzer, H. Obloh, M. Maier, Ch. Manz, A. Ramakrishnan, and B. Santic, *Phys. Rev. B* **59**, 5561 (1999).
- ¹⁷³J. Chadi, in *Proceedings of the 22nd International Conference on the Physics of Semiconductors*, Vancouver, Canada, 16–19 August 1994, edited by D. J. Lockwood (World Scientific, Singapore, 1995), p. 2311.
- ¹⁷⁴W. Shan, T. J. Schmidt, R. J. Hauenstein, J. J. Song, and B. Goldenberg, *Appl. Phys. Lett.* **66**, 3492 (1995).
- ¹⁷⁵S. Kim, I. P. Herman, J. A. Tuchman, K. Doverspike, L. B. Rowland, and D. K. Gaskill, *Appl. Phys. Lett.* **67**, 380 (1995).
- ¹⁷⁶K. Michael, U. Rogulis, F. K. Koschnick, Th. Tröster, J.-M. Spaeth, B. Beaumont, and P. Gibart, *Physica B* **308–310**, 85 (2001).
- ¹⁷⁷D. C. Look, *Phys. Status Solidi B* **228**, 293 (2001).
- ¹⁷⁸K. Saarinen, T. Suski, I. Grzegory, and D. C. Look, *Phys. Rev. B* **64**, 233201 (2001).
- ¹⁷⁹L. J. Brillson *et al.*, *Physica B* **273–274**, 70 (1999).
- ¹⁸⁰M. Toth, K. Fleischer, and M. R. Phillips, *Phys. Rev. B* **59**, 1575 (1999).
- ¹⁸¹A. Cremades, J. Piqueras, C. Xavier, T. Monteiro, E. Pereira, B. K. Meyer, D. M. Hofmann, and S. Fischer, *Mater. Sci. Eng., B* **42**, 230 (1996).
- ¹⁸²M. Herrera Zaldivar, P. Fernandez, and J. Piqueras, *J. Appl. Phys.* **83**, 462 (1998).
- ¹⁸³M. Herrera Zaldivar, P. Fernandez, and J. Piqueras, *J. Appl. Phys.* **83**, 2796 (1998).
- ¹⁸⁴I. A. Buyanova, Mt. Wagner, W. M. Chen, B. Monemar, J. L. Lindström, H. Amano, and I. Akasaki, *Appl. Phys. Lett.* **73**, 2968 (1998).
- ¹⁸⁵M. Linde, S. J. Uffring, G. D. Watkins, V. Härle, and F. Scholz, *Phys. Rev. B* **55**, R10177 (1997).
- ¹⁸⁶Y. Hayashi, T. Soga, M. Umeno, and T. Jimbo, *Physica B* **304**, 12 (2001).
- ¹⁸⁷Q. Yang, H. Feick, R. Armitage, and E. R. Weber, *Mater. Res. Soc. Symp. Proc.* **693**, I11.36 (2002).
- ¹⁸⁸R. Y. Korotkov, M. A. Reshchikov, and B. W. Wessels, *Physica B* **273**, 80 (1999).
- ¹⁸⁹C. Diaz-Guerra, J. Piqueras, and A. Cavallini, *Appl. Phys. Lett.* **82**, 2050 (2003).
- ¹⁹⁰Y.-H. Kwon, S. K. Shee, G. H. Park, S. J. Hwang, and J. J. Song, *Appl. Phys. Lett.* **76**, 840 (2000).
- ¹⁹¹Z. Chine, B. Piriou, M. Oueslati, T. Boufaden, and B. El. Jani, *J. Lumin.* **82**, 81 (1999).
- ¹⁹²T. Monteiro *et al.*, *J. Lumin.* **72–74**, 696 (1997).
- ¹⁹³B. K. Ridley, *J. Phys.: Condens. Matter* **10**, L461 (1998).
- ¹⁹⁴K. Saarinen, P. Hautojärvi, and C. Corbel, in *Identification of Defects in Semiconductors*, edited by M. Stavola (Academic, New York, 1998), p. 209.
- ¹⁹⁵K. Saarinen, P. Seppälä, J. Oila, P. Hautojärvi, C. Corbel, O. Briot, and R. L. Aulombard, *Appl. Phys. Lett.* **73**, 3253 (1998).
- ¹⁹⁶D. Huang *et al.*, *Solid-State Electron.* **45**, 711 (2001).
- ¹⁹⁷D. C. Look and J. R. Sizelove, *Appl. Phys. Lett.* **79**, 1133 (2001).
- ¹⁹⁸E. R. Glaser, T. A. Kennedy, H. C. Crookham, J. A. Freitas, Jr., M. Asif Khan, D. T. Olson, and J. N. Kuznia, *Appl. Phys. Lett.* **63**, 2673 (1993).
- ¹⁹⁹B. J. Skromme and G. L. Martinez, *Mater. Res. Soc. Symp. Proc.* **551**, W9.8 (2000).
- ²⁰⁰B. J. Skromme, G. L. Martinez, A. Sukhanov, L. Krasnobaev, and D. B. Poker, in *State-of-the-Art Program on Compound Semiconductors XXXIII*, edited A. G. Baca and P. C. Chang (Electrochemical Society, Pennington, NJ, 2000), PV Vol. 2000-18, p. 120.
- ²⁰¹B. J. Skromme, G. L. Martinez, L. Krasnobaev, and D. B. Poker, *Mater. Res. Soc. Symp. Proc.* **639**, G11.39 (2001).
- ²⁰²L. Chen and B. J. Skromme, *Mater. Res. Soc. Symp. Proc.* **743**, L11.35 (2003).
- ²⁰³G. J. Dewsnip *et al.*, *Semicond. Sci. Technol.* **13**, 500 (1998).
- ²⁰⁴E. E. Reuter, R. Zhang, T. F. Kuech, and S. G. Bishop, *MRS Internet J. Nitride Semicond. Res.* **4S1**, G3.67 (1999).
- ²⁰⁵H. Tang, J. B. Webb, J. A. Bardwell, S. Raymond, J. Salzman, and C. Uzan-Saguy, *Appl. Phys. Lett.* **78**, 757 (2001).
- ²⁰⁶U. Birkle, M. Fehrer, V. Kirchner, S. Einfeldt, D. Hommel, S. Strauf, P. Michler, and J. Gutowski, *MRS Internet J. Nitride Semicond. Res.* **4S1**, G5.6 (1999).
- ²⁰⁷L. Dai, J. C. Zhang, Y. Chen, G. Z. Ran, and G. G. Qin, *Physica B* **322**, 51 (2002).
- ²⁰⁸I.-H. Lee, I.-H. Choi, C. R. Lee, and S. K. Noh, *Appl. Phys. Lett.* **71**, 1359 (1997).
- ²⁰⁹I.-H. Lee, I.-H. Choi, C.-R. Lee, S.-J. Son, J.-Y. Leem, and S. K. Noh, *J. Cryst. Growth* **182**, 314 (1997).
- ²¹⁰S. Li, C. Mo, L. Wang, C. Xiong, X. Peng, F. Jiang, Z. Deng, and D. Gong, *J. Lumin.* **93**, 321 (2001).
- ²¹¹R. Seitz, C. Gaspar, T. Monteiro, E. Pereira, M. Leroux, B. Beaumont, and P. Gibart, *J. Cryst. Growth* **189/190**, 546 (1998).
- ²¹²X. Zhang, P. Kung, A. Saxler, D. Walker, T. C. Wang, and M. Razeghi, *Appl. Phys. Lett.* **67**, 1745 (1995).
- ²¹³H. M. Chen, Y. F. Chen, M. C. Lee, and M. S. Feng, *Phys. Rev. B* **56**, 6942 (1997).
- ²¹⁴G.-C. Yi and B. W. Wessels, *Appl. Phys. Lett.* **69**, 3028 (1996).
- ²¹⁵E. W. Williams, *Phys. Rev.* **168**, 922 (1968).
- ²¹⁶Z. Liliental-Weber, J. Jasinski, and J. Washburn, *J. Cryst. Growth* **246**, 259 (2002).
- ²¹⁷D. C. Look, C. E. Stutz, R. J. Molnar, K. Saarinen, and Z. Liliental-Weber, *Solid State Commun.* **117**, 571 (2001).
- ²¹⁸Z.-Q. Fang, D. C. Look, J. Jasinski, M. Benamara, Z. Liliental-Weber, and R. J. Molnar, *Appl. Phys. Lett.* **78**, 332 (2001).
- ²¹⁹A. Saxler *et al.*, *Mater. Res. Soc. Symp. Proc.* **639**, G7.2 (2001).
- ²²⁰P. Visconti, K. M. Jones, M. A. Reshchikov, F. Yun, R. Cingolani, H. Morkoç, S. S. Park, and K. Y. Lee, *Appl. Phys. Lett.* **77**, 3743 (2000).
- ²²¹J. Jasinski *et al.*, *Appl. Phys. Lett.* **78**, 2297 (2001).
- ²²²M. A. Reshchikov, D. Huang, F. Yun, L. He, H. Morkoç, D. C. Reynolds, S. S. Park, and K. Y. Lee, *Appl. Phys. Lett.* **79**, 3779 (2001).
- ²²³J. A. Freitas, Jr., W. J. Moore, B. V. Shanabrook, G. C. B. Braga, S. K. Lee, S. S. Park, J. Y. Han, and D. D. Koleske, *J. Cryst. Growth* **246**, 307 (2002).

- ²²⁴M. A. Reshchikov, F. Yun, D. Huang, L. He, H. Morkoç, S. S. Park, and K. Y. Lee, *Mater. Res. Soc. Symp. Proc.* **722**, K1.4 (2002).
- ²²⁵G. A. Baraff and M. Schluter, *Phys. Rev. Lett.* **55**, 2340 (1985).
- ²²⁶I. Kuskovsky, G. F. Neumark, V. N. Bondarev, and P. V. Vikhitsu, *Phys. Rev. Lett.* **80**, 2413 (1998).
- ²²⁷A. M. Gilinsky and K. S. Zhuravlev, *Appl. Phys. Lett.* **79**, 3455 (2001).
- ²²⁸M. A. Reshchikov, S. S. Park, K. Y. Lee, and H. Morkoç, *Physica B* **340–342**, 448 (2003).
- ²²⁹R. Dingle and M. Ilegems, *Solid State Commun.* **9**, 175 (1971).
- ²³⁰W. J. Moore, J. A. Freitas, Jr., S. K. Lee, S. S. Park, and J. Y. Han, *Phys. Rev. B* **65**, 081201 (2002).
- ²³¹J. Jayapalan, B. J. Skromme, R. P. Vaudo, and V. M. Phanse, *Appl. Phys. Lett.* **73**, 1188 (1998).
- ²³²P. W. Yu, C. S. Park, and S. T. Kim, *J. Appl. Phys.* **89**, 1692 (2001).
- ²³³H. Teisseyre *et al.*, *Phys. Status Solidi B* **198**, 235 (1996).
- ²³⁴U. Kaufmann, M. Kunzer, C. Merz, I. Akasaki, and H. Amano, in *Gallium Nitride and Related Materials*, MRS Symposia Proceedings No. 395, edited by R. D. Dupuis, J. A. Edmond, F. A. Ponce, and S. Nakamura (Materials Research Society, Pittsburgh, 1996), p. 633, and references therein.
- ²³⁵J. L. Patel, J. E. Nicholls, and J. J. Davies, *J. Phys. C* **14**, 139 (1981).
- ²³⁶L. S. Dang, K. M. Lee, G. D. Watkins, and W. J. Choyke, *Phys. Rev. Lett.* **45**, 390 (1980).
- ²³⁷A. Y. Polyakov, N. B. Smirnov, A. S. Usikov, A. V. Govorkov, and B. V. Pushnyi, *Solid-State Electron.* **42**, 1959 (1998).
- ²³⁸R. Niebuhr, K. H. Bachem, U. Kaufmann, M. Maier, C. Merz, B. Santic, P. Schlotter, and H. Jürgensen, *J. Electron. Mater.* **26**, 1127 (1997).
- ²³⁹J. C. Carrano, P. A. Grudowski, C. J. Eiting, R. D. Dupuis, and J. C. Campbell, *Appl. Phys. Lett.* **70**, 1992 (1997).
- ²⁴⁰M. Herrera Zaldivar, P. Fernandez, J. Piqueras, and J. Solis, *J. Appl. Phys.* **85**, 1120 (1999).
- ²⁴¹C.-C. Tsai, C.-S. Chang, and T.-Y. Chen, *Appl. Phys. Lett.* **80**, 3718 (2002).
- ²⁴²H. C. Yang, T. Y. Lin, and Y. F. Chen, *Phys. Rev. B* **62**, 12593 (2000).
- ²⁴³M. R. Phillips, H. Telg, S. O. Kucheyev, O. Gelhausen, and M. Toth, *Microsc. Microanal.* **9**, 144 (2003).
- ²⁴⁴A. S. Zubrilov, Yu. V. Mel'nik, D. V. Tsvetkov, V. E. Bugrov, A. E. Nikolaev, S. I. Stepanov, and V. A. Dmitriev, *Semiconductors* **31**, 523 (1997).
- ²⁴⁵M. A. Reshchikov, D. Huang, H. Morkoç, and R. J. Molnar, *Mater. Res. Soc. Symp. Proc.* **743**, L11.1 (2003).
- ²⁴⁶W. Götz, L. T. Romano, B. S. Krusor, N. M. Johnson, and R. J. Molnar, *Appl. Phys. Lett.* **69**, 242 (1996).
- ²⁴⁷C. Bozdog *et al.*, *Phys. Rev. B* **59**, 12479 (1999).
- ²⁴⁸E. M. Goldys, M. Godlewski, T. Paskova, G. Pozina, and B. Monemar, *MRS Internet J. Nitride Semicond. Res.* **6**, 1 (2001).
- ²⁴⁹C. Adelman, J. Brault, D. Jalabert, P. Gentile, H. Mariette, G. Mula, and B. Daudin, *J. Appl. Phys.* **91**, 9638 (2002).
- ²⁵⁰D. M. Hofmann *et al.*, *Phys. Status Solidi A* **180**, 261 (2000).
- ²⁵¹This expression is similar to Eq. (6), however, the factor C is assumed to be temperature independent because, as will be shown below, the quenching is most probably not related to escape of holes to the valence band.
- ²⁵²M. A. Reshchikov and H. Morkoç, *Mater. Res. Soc. Symp. Proc.* **831**, E3.8 (2005).
- ²⁵³V. L. Bonch-Bruevich, *Fiz. Tverd. Tela (Leningrad)* **11**, 182 (1959); V. L. Bonch-Bruevich and E. G. Landsberg, *Phys. Status Solidi* **29**, 9 (1968).
- ²⁵⁴V. N. Abakumov, V. Karpus, V. I. Perel, and I. N. Yassievich, *Fiz. Tekh. Poluprovodn. (S.-Peterburg)* **22**, 262 (1988).
- ²⁵⁵I. G. Aksyanov, V. G. Ivanov, S. K. Novoselov, M. A. Reshchikov, and Y. S. Smetannikova, *Fiz. Tekh. Poluprovodn. (S.-Peterburg)* **21**, 2018 (1987) [*Sov. Phys. Semicond.* **21**, 1223 (1987)].
- ²⁵⁶W. Hayes and A. M. Stoneham, *Defects and Defect Processes in Nonmetallic Solids* (Wiley, New York, 1985), pp. 202–209.
- ²⁵⁷M. A. Reshchikov, L. He, R. J. Molnar, S. S. Park, K. Y. Lee, and H. Morkoç, *Mater. Res. Soc. Symp. Proc.* **831**, E9.8 (2005).
- ²⁵⁸N. I. Kuznetsov, A. E. Nikolaev, A. S. Zubrilov, Y. V. Melnik, and V. A. Dmitriev, *Appl. Phys. Lett.* **75**, 3138 (1999).
- ²⁵⁹J. I. Pankove, E. A. Miller, and J. E. Berkeyheiser, *J. Lumin.* **5**, 84 (1972).
- ²⁶⁰J. I. Pankove, E. A. Miller, Richman, and J. E. Berkeyheiser, *J. Lumin.* **4**, 63 (1971).
- ²⁶¹J. I. Pankove, J. E. Berkeyheiser, and E. A. Miller, *J. Appl. Phys.* **45**, 1280 (1973).
- ²⁶²M. Ilegems, R. Dingle, and R. A. Logan, *J. Appl. Phys.* **43**, 3797 (1972).
- ²⁶³B. Monemar, O. Lagerstedt, and H. P. Gislason, *J. Appl. Phys.* **51**, 625 (1980).
- ²⁶⁴B. Monemar, H. P. Gislason, and O. Lagerstedt, *J. Appl. Phys.* **51**, 640 (1980).
- ²⁶⁵M. R. H. Khan, N. Sawaki, and I. Akasaki, *Semicond. Sci. Technol.* **7**, 472 (1992).
- ²⁶⁶P. Bergman, G. Ying, B. Monemar, and P. O. Holtz, *J. Appl. Phys.* **61**, 4589 (1987).
- ²⁶⁷M. A. Reshchikov, D. Huang, H. Morkoç, and R. J. Molnar, *Mater. Res. Soc. Symp. Proc.* **693**, I2.10 (2002).
- ²⁶⁸B. J. Skromme, K. Palle, C. D. Poweleit, H. Yamane, M. Aoki, and F. J. DiSalvo, *J. Cryst. Growth* **246**, 299 (2002).
- ²⁶⁹K. P. Korona, R. Doradzinski, M. Palczewska, M. Pietras, M. Kaminska, and J. Kuhl, *Phys. Status Solidi B* **235**, 40 (2003).
- ²⁷⁰C. Merz, M. Kunzer, U. Kaufmann, I. Akasaki, and H. Amano, *Semicond. Sci. Technol.* **11**, 712 (1996).
- ²⁷¹H. Teisseyre, P. Perlin, T. Suski, I. Grzegory, J. Jun, and S. Porowski, *J. Phys. Chem. Solids* **56**, 353 (1995).
- ²⁷²D. C. Look and R. J. Molnar, *Appl. Phys. Lett.* **70**, 3377 (1997).
- ²⁷³L. A. Marasina, A. N. Pikhtin, I. G. Pinchugin, and A. V. Solomonov, *Phys. Status Solidi A* **38**, 753 (1976).
- ²⁷⁴T. Suski *et al.*, *J. Appl. Phys.* **84**, 1155 (1998).
- ²⁷⁵T. Suski and P. Perlin (private communication).
- ²⁷⁶R. Dingle, *Phys. Rev. Lett.* **23**, 579 (1969).
- ²⁷⁷M. Kunzer, J. Baur, U. Kaufmann, J. Schneider, H. Amano, and I. Akasaki, *Solid-State Electron.* **41**, 189 (1997).
- ²⁷⁸P. N. Hai, W. M. Chen, I. A. Buyanova, B. Monemar, H. Amano, and I. Akasaki, *Phys. Rev. B* **62**, R10607 (2000).
- ²⁷⁹F. Bernardini, V. Fiorentini, and R. M. Nieminen, in *Proceedings of the 23rd International Conference on the Physics of Semiconductors*, Berlin, July 21–26, 1996, edited by M. Scheffler and R. Zimmerman (World Scientific, Singapore, 1996), p. 2881.
- ²⁸⁰M. Boulou, G. Jacob, and D. Bois, *Rev. Phys. Appl.* **13**, 555 (1978).
- ²⁸¹V. V. Rossin, V. G. Sidorov, A. D. Shagalov, and Y. K. Shalabutov, *Fiz. Tekh. Poluprovodn. (S.-Peterburg)* **15**, 1021 (1981).
- ²⁸²I. Akasaki and H. Amano, *J. Electrochem. Soc.* **141**, 2266 (1994).
- ²⁸³W. Götz, N. M. Johnson, J. Walker, D. P. Bour, and R. A. Street, *Appl. Phys. Lett.* **68**, 667 (1996).
- ²⁸⁴P. Kozodoy, H. Xing, S. P. DenBaars, U. K. Mishra, A. Saxler, R. Perrin, S. Elhamri, and W. C. Mitchel, *J. Appl. Phys.* **87**, 1832 (2000).
- ²⁸⁵S. Nakamura, N. Iwasa, M. Senoh, and T. Mukai, *Jpn. J. Appl. Phys., Part 1* **31**, 1258 (1992).
- ²⁸⁶S. Nakamura, M. Senoh, T. Mukai, and N. Iwasa, *Jpn. J. Appl. Phys., Part 2* **31**, L139 (1992).
- ²⁸⁷H. Harima, T. Inoue, S. Nakashima, M. Ishida, and M. Taneya, *Appl. Phys. Lett.* **75**, 1383 (1999).
- ²⁸⁸S. M. Myers, A. F. Wright, G. A. Petersen, W. R. Wampler, C. H. Seager, M. H. Crawford, and J. Han, *J. Appl. Phys.* **89**, 3195 (2001).
- ²⁸⁹O. Ambacher, H. Angerer, R. Dimitrov, W. Rieger, M. Stutzmann, G. Dollinger, and A. Bergmaier, *Phys. Status Solidi A* **159**, 105 (1997).
- ²⁹⁰E. Litwin-Staszewska *et al.*, *J. Appl. Phys.* **89**, 7960 (2001).
- ²⁹¹H. Amano, M. Kito, K. Hiramatsu, and I. Akasaki, *Jpn. J. Appl. Phys., Part 2* **28**, L2112 (1989).
- ²⁹²S. M. Myers, C. H. Seager, A. F. Wright, B. L. Vaandrager, and J. S. Nelson, *J. Appl. Phys.* **92**, 6630 (2002).
- ²⁹³Y. Kamiura, Y. Yamashita, and S. Nakamura, *Physica B* **273–274**, 54 (1999).
- ²⁹⁴H. Obloh, K. H. Bachem, U. Kaufmann, M. Kunzer, M. Maier, A. Ramakrishnan, and P. Schlotter, *J. Cryst. Growth* **195**, 270 (1998).
- ²⁹⁵A. K. Vismanath, E.-J. Shin, J. I. Lee, S. Yu, D. Kim, B. Kim, Y. Choi, and C.-H. Hong, *J. Appl. Phys.* **83**, 2272 (1998).
- ²⁹⁶M. Smith *et al.*, *Appl. Phys. Lett.* **68**, 1883 (1996).
- ²⁹⁷J. M. Myoung, K. H. Shim, C. Kim, O. Gluschenkov, K. Kim, S. Kim, D. A. Turnbull, and S. G. Bishop, *Appl. Phys. Lett.* **69**, 2722 (1996).
- ²⁹⁸J. K. Sheu, Y. K. Su, G. C. Chi, B. J. Pong, C. Y. Chen, C. N. Huang, and W. C. Chen, *J. Appl. Phys.* **84**, 4590 (1998).
- ²⁹⁹E. Oh, H. Park, and Y. Park, *Appl. Phys. Lett.* **72**, 70 (1998).
- ³⁰⁰Y. Koide, D. E. Walker, Jr., B. D. White, L. J. Brillson, M. Murakami, S. Kamiyama, H. Amano, and I. Akasaki, *J. Appl. Phys.* **92**, 3657 (2002).
- ³⁰¹R. Seitz, C. Gaspar, T. Monteiro, E. Pereira, M. Leroux, B. Beamont, and P. Gibart, *Mater. Sci. Forum* **258–263**, 1155 (1997).
- ³⁰²C. Lee, J.-E. Kim, H. Y. Park, S. T. Kim, and H. Lim, *J. Phys.: Condens. Matter* **10**, 11103 (1998).
- ³⁰³F. Shahedipour and B. W. Wessels, *Appl. Phys. Lett.* **76**, 3011 (2000).

- ³⁰⁴ S. Hess, R. A. Taylor, J. F. Ryan, N. J. Cain, V. Roberts, and J. Roberts, *Phys. Status Solidi B* **210**, 465 (1998).
- ³⁰⁵ H. Amano, M. Kitoh, K. Hiramatsu, and I. Akasaki, *J. Electrochem. Soc.* **137**, 1639 (1990).
- ³⁰⁶ D. J. Dewsnip *et al.*, *Semicond. Sci. Technol.* **13**, 927 (1998).
- ³⁰⁷ M. Leroux, B. Beaumont, N. Grandjean, P. Lorenzini, S. Haffouz, P. Venegues, J. Massies, and P. Gibart, *Mater. Sci. Eng., B* **50**, 97 (1997).
- ³⁰⁸ L. Eckey *et al.*, *J. Appl. Phys.* **84**, 5828 (1998).
- ³⁰⁹ E. R. Glaser *et al.*, *Phys. Rev. B* **65**, 085312 (2002).
- ³¹⁰ B. Han, J. M. Gregie, and B. W. Wessels, *Phys. Rev. B* **68**, 045205 (2003).
- ³¹¹ R. Stepniowski and A. Wyszynski, *Acta Phys. Pol. A* **90**, 681 (1996).
- ³¹² R. Stepniowski *et al.*, *Phys. Status Solidi B* **210**, 373 (1998).
- ³¹³ M. Leroux, N. Grandjean, B. Beaumont, G. Nataf, F. Semond, J. Massies, and P. Gibart, *J. Appl. Phys.* **86**, 3721 (1999).
- ³¹⁴ H. P. Gislason, B. H. Yang, and M. Linnarsson, *Phys. Rev. B* **47**, 9418 (1993).
- ³¹⁵ P. W. Yu, *J. Appl. Phys.* **48**, 5043 (1977).
- ³¹⁶ P. Bäume, J. Gutowski, D. Wiesmann, R. Heitz, A. Hoffmann, E. Kurtz, D. Hommel, and G. Landwehr, *Appl. Phys. Lett.* **67**, 1914 (1995).
- ³¹⁷ M. Behringer, P. Bäume, J. Gutowski, and D. Hommel, *Phys. Rev. B* **57**, 12869 (1998).
- ³¹⁸ C. Kothandaraman, G. F. Neumark, and R. M. Park, *J. Cryst. Growth* **159**, 298 (1996).
- ³¹⁹ Zh. I. Alferov, V. M. Andreev, D. Z. Garbuzov, and M. K. Trukan, *Fiz. Tekh. Poluprovodn. (S.-Peterburg)* **6**, 2015 (1972) [*Sov. Phys. Semicond.* **6**, 1718 (1972)].
- ³²⁰ P. W. Yu and Y. S. Park, *J. Appl. Phys.* **50**, 1097 (1979).
- ³²¹ F. Williams, *Phys. Status Solidi* **25**, 493 (1968).
- ³²² M. A. Reshchikov, G.-C. Yi, and B. W. Wessels, *MRS Internet J. Nitride Semicond. Res.* **4S1**, G11.8 (1999).
- ³²³ B. Z. Qu *et al.*, *J. Vac. Sci. Technol. A* **21**, 838 (2003).
- ³²⁴ H. Alves, M. Böhm, A. Hofstaetter, H. Amano, S. Einfeldt, D. Hommel, D. M. Hofmann, and B. K. Meyer, *Physica B* **308-310**, 38 (2001).
- ³²⁵ O. Gelhausen, M. R. Phillips, E. M. Goldys, T. Paskova, B. Monemar, M. Strassburg, and A. Hoffmann, *Mater. Res. Soc. Symp. Proc.* **798**, Y5.20 (2004).
- ³²⁶ M. E. Lin, G. Xue, G. L. Zhou, J. E. Greene, and H. Morkoç, *Appl. Phys. Lett.* **63**, 932 (1993).
- ³²⁷ C.-K. Shu *et al.*, *Jpn. J. Appl. Phys., Part 2* **40**, L306 (2001).
- ³²⁸ O. Gelhausen, H. N. Klein, M. R. Phillips, and E. M. Goldys, *Appl. Phys. Lett.* **83**, 3293 (2003).
- ³²⁹ P. Venegues *et al.*, *Mater. Sci. Eng., B* **93**, 224 (2002).
- ³³⁰ L. S. Wang, W. K. Fong, C. Surya, K. W. Cheah, W. H. Zheng, and Z. G. Wang, *Solid-State Electron.* **45**, 1153 (2001).
- ³³¹ V. P. Dobrego and I. S. Shlimak, *Phys. Status Solidi* **33**, 805 (1969).
- ³³² S.-W. Kim, J.-M. Lee, C. Huh, N.-M. Park, H.-S. Kim, I.-H. Lee, and S.-J. Park, *Appl. Phys. Lett.* **76**, 3079 (2000).
- ³³³ B. Han, J. M. Gregie, M. P. Ulmer, and B. W. Wessels, *Mater. Res. Soc. Symp. Proc.* **743**, L5.8 (2003).
- ³³⁴ A. S. Kaminskii and Y. E. Pokrovskii, *Fiz. Tekh. Poluprovodn. (S.-Peterburg)* **3**, 1766 (1969) [*Sov. Phys. Semicond.* **3**, 1496 (1970)].
- ³³⁵ F. Shahedipour and B. W. Wessels, *MRS Internet J. Nitride Semicond. Res.* **6**, 12 (2001).
- ³³⁶ M. Godlewski, T. Suski, I. Grzegory, S. Porowski, J. P. Bergman, W. M. Chen, and B. Monemar, *Physica B* **273-274**, 39 (1999).
- ³³⁷ A. L. Gurskii *et al.*, *Phys. Status Solidi B* **228**, 361 (2001).
- ³³⁸ S. Strauf, S. M. Ulrich, P. Michler, J. Gutowski, T. Böttcher, S. Figge, S. Einfeldt, and D. Hommel, *Phys. Status Solidi B* **228**, 379 (2001).
- ³³⁹ V. Yu. Nekrasov, L. V. Belyakov, O. M. Sreseli, and N. N. Zinov'ev, *Fiz. Tekh. Poluprovodn. (S.-Peterburg)* **33**, 1428 (1999) [*Semiconductors* **33**, 1284 (1999)].
- ³⁴⁰ S. Ves, U. D. Venkateswaran, I. Loa, K. Syassen, F. Shahedipour, and B. W. Wessels, *Appl. Phys. Lett.* **77**, 2536 (2000).
- ³⁴¹ H. Teisseyre *et al.*, *Phys. Rev. B* **62**, 10151 (2000).
- ³⁴² C. Wetzel, W. Walukiewicz, E. E. Haller, J. W. Ager, I. Grzegory, S. Porowski, and T. Suski, *Phys. Rev. B* **53**, 1322 (1996).
- ³⁴³ D. M. Hofmann *et al.*, *Physica B* **273-274**, 43 (1999).
- ³⁴⁴ E. R. Glaser, T. A. Kennedy, J. A. Freitas, Jr., B. V. Shanabrook, A. E. Wickenden, D. D. Koleske, R. L. Henry, and H. Obloh, *Physica B* **273-274**, 58 (1999).
- ³⁴⁵ E. R. Glaser *et al.*, *Mater. Sci. Eng., B* **93**, 39 (2002).
- ³⁴⁶ H. Alves, F. Leiter, D. Pfisterer, D. M. Hofmann, B. K. Meyer, S. Einfeldt, H. Heinke, and D. Hommel, *Phys. Status Solidi C* **0**, 1770 (2003).
- ³⁴⁷ P. Hacke, H. Nakayama, T. Detchprohm, K. Hiramatsu, and N. Sawaki, *Appl. Phys. Lett.* **68**, 1362 (1996).
- ³⁴⁸ K. Saarinen, J. Nissilä, P. Hautojärvi, J. Likonen, T. Suski, I. Grzegory, B. Lucznik, and S. Porowski, *Appl. Phys. Lett.* **75**, 2441 (1999).
- ³⁴⁹ S. Hautakangas, J. Oila, M. Alatalo, K. Saarinen, L. Liskay, D. Seghier, and H. P. Gislason, *Phys. Rev. Lett.* **90**, 137402 (2003).
- ³⁵⁰ W. Götz, N. M. Johnson, D. P. Bour, M. D. McCluskey, and E. E. Haller, *Appl. Phys. Lett.* **69**, 3725 (1996).
- ³⁵¹ B. Clerjaud, D. Côte, A. Lebki, C. Naud, J. M. Baranowski, K. Pakula, D. Wasik, and T. Suski, *Phys. Rev. B* **61**, 8238 (2000).
- ³⁵² A. Hoffmann, A. Kaschner, and C. Thomsen, *Phys. Status Solidi C* **0**, 1783 (2003), and references therein.
- ³⁵³ A. Kaschner *et al.*, *Appl. Phys. Lett.* **74**, 3281 (1999).
- ³⁵⁴ M. W. Bayer *et al.*, *Phys. Rev. B* **63**, 125203 (2001).
- ³⁵⁵ G. Salviati *et al.*, *MRS Internet J. Nitride Semicond. Res.* **5S1**, W11.50 (2000).
- ³⁵⁶ M. W. Bayerl, M. S. Brandt, T. Suski, I. Grzegory, S. Porowski, and M. Stutzmann, *Physica B* **273-274**, 120 (1999).
- ³⁵⁷ H. Katayama-Yoshida, T. Nishimatsu, T. Yamamoto, and N. Orita, *Phys. Status Solidi B* **210**, 429 (1998).
- ³⁵⁸ R. K. Korotkov, J. M. Gregie, and B. W. Wessels, *Mater. Res. Soc. Symp. Proc.* **639**, G6.39 (2001).
- ³⁵⁹ R. K. Korotkov, J. M. Gregie, and B. W. Wessels, *Appl. Phys. Lett.* **78**, 222 (2001).
- ³⁶⁰ P. Venegues, M. Benaissa, B. Beaumont, E. Feltin, P. De Mierry, S. Dalmaso, M. Leroux, and P. Gibart, *Appl. Phys. Lett.* **77**, 880 (2000).
- ³⁶¹ M. Benaissa, P. Venegues, B. Beaumont, E. Feltin and P. Gibart, *Appl. Phys. Lett.* **77**, 2115 (2000).
- ³⁶² M. Hansen, L. F. Chen, S. H. Lim, S. P. DenBaars, and J. S. Speck, *Appl. Phys. Lett.* **80**, 2469 (2002).
- ³⁶³ Z. Liliental-Weber, J. Jasinski, M. Benamara, I. Grzegory, S. Porowski, D. J. H. Lampert, C. J. Eiting, and R. D. Dupuis, *Phys. Status Solidi B* **228**, 345 (2001).
- ³⁶⁴ Z. Liliental-Weber, M. Benamara, I. Grzegory, and S. Porowski, *Phys. Rev. Lett.* **83**, 2370 (1999).
- ³⁶⁵ S. Figge, R. Kröger, T. Böttcher, P. L. Ryder, and D. Hommel, *Appl. Phys. Lett.* **81**, 4748 (2002).
- ³⁶⁶ P. Venegues *et al.*, *Phys. Rev. B* **68**, 235214 (2003).
- ³⁶⁷ M. R. H. Khan, Y. Ohshita, N. Sawaki, and I. Akasaki, *Solid State Commun.* **57**, 405 (1986).
- ³⁶⁸ E. Burstein, *Phys. Rev.* **93**, 632 (1954).
- ³⁶⁹ H. Haug and S. W. Koch, *Phys. Rev. A* **39**, 1887 (1989).
- ³⁷⁰ R. Y. Korotkov, F. Niu, J. M. Gregie, and B. W. Wessels, *Physica B* **308-310**, 26 (2001).
- ³⁷¹ C. Wetzel *et al.*, *Phys. Rev. Lett.* **78**, 3923 (1997).
- ³⁷² A. Gassmann *et al.*, *J. Appl. Phys.* **80**, 2195 (1996).
- ³⁷³ G. A. Slack, L. J. Schowalter, D. Morelli, and J. A. Freitas, Jr., *J. Cryst. Growth* **246**, 287 (2002).
- ³⁷⁴ W. Walukiewicz, *Appl. Phys. Lett.* **54**, 2094 (1989).
- ³⁷⁵ Z.-Q. Fang, D. C. Look, R. Armitage, Q. Yang, and E. R. Weber, *Mater. Res. Soc. Symp. Proc.* **798**, Y5.27 (2004).
- ³⁷⁶ C. H. Seager, A. F. Wright, J. Yu, and W. Götz, *J. Appl. Phys.* **92**, 6553 (2002).
- ³⁷⁷ P. B. Klein, S. C. Binari, K. Ikossi, A. E. Wickenden, D. D. Koleske, and R. L. Henry, *Appl. Phys. Lett.* **79**, 3527 (2001).
- ³⁷⁸ A. Armstrong, A. R. Arehart, S. A. Ringel, B. Moran, S. P. DenBaars, U. K. Mishra, and J. S. Speck, *Mater. Res. Soc. Symp. Proc.* **798**, Y5.38 (2004).
- ³⁷⁹ A. Armstrong, A. R. Arehart, B. Moran, S. P. DenBaars, U. K. Mishra, J. S. Speck, and S. A. Ringel, *Appl. Phys. Lett.* **84**, 374 (2004).
- ³⁸⁰ C.-C. Yu, C. F. Chu, J. Y. Tsai, C. F. Lin, and S. C. Wang, *J. Appl. Phys.* **92**, 1881 (2002).
- ³⁸¹ C.-C. Yu, C. F. Chu, J. Y. Tsai, and S. C. Wang, *Mater. Sci. Eng., B* **82**, 82 (2001).
- ³⁸² F. J. Sánchez *et al.*, *Semicond. Sci. Technol.* **13**, 1130 (1998).
- ³⁸³ A. J. Ptak *et al.*, *Mater. Res. Soc. Symp. Proc.* **639**, G3.3 (2001).
- ³⁸⁴ A. Salvador, W. Kim, Ö. Aktas, A. Botchkarev, Z. Fan, and H. Morkoç, *Appl. Phys. Lett.* **69**, 2692 (1996).
- ³⁸⁵ C. Ronning, E. P. Carlson, D. B. Thomson, and R. F. Davis, *Appl. Phys. Lett.* **73**, 1622 (1998).
- ³⁸⁶ H. Heinke, V. Kirchner, S. Einfeldt, and D. Hommel, *Appl. Phys. Lett.* **77**, 2145 (2000).
- ³⁸⁷ T. Monteiro, C. Boemare, M. J. Soares, E. Alves, and C. Liu, *Physica B* **308-310**, 42 (2001).

- ³⁸⁸O. Lagerstedt and B. Monemar, *J. Appl. Phys.* **45**, 2266 (1974).
- ³⁸⁹M. Ilegems, R. Dingle, and R. A. Logan, *J. Appl. Phys.* **43**, 3797 (1972).
- ³⁹⁰T. Dietl, H. Ohno, F. Matsukura, J. Cibert, and D. Ferrand, *Science* **287**, 1019 (2000).
- ³⁹¹R. Y. Korotkov, J. M. Gregie, and B. W. Wessels, *Physica B* **308–310**, 30 (2001).
- ³⁹²R. Y. Korotkov, J. M. Gregie, and B. W. Wessels, *Appl. Phys. Lett.* **80**, 1731 (2002).
- ³⁹³T. Graf, M. Gjukic, M. S. Brandt, M. Stutzmann, and O. Ambacher, *Appl. Phys. Lett.* **81**, 5159 (2002).
- ³⁹⁴T. Graf, M. Gjukic, M. Hermann, M. S. Brandt, M. Stutzmann, L. Görgens, J. B. Phillip, and O. Ambacher, *J. Appl. Phys.* **93**, 9697 (2003).
- ³⁹⁵N. S. Averkiev, A. A. Gutkin, N. M. Kolchanova, and M. A. Reshchikov, *Fiz. Tekh. Poluprovodn. (S.-Peterburg)* **18**, 1629 (1984) [*Sov. Phys. Semicond.* **18**, 1019 (1984)].
- ³⁹⁶R. Y. Korotkov, J. M. Gregie, and B. W. Wessels, *Mater. Res. Soc. Symp. Proc.* **639**, G3.7 (2001).
- ³⁹⁷X. Li, S. Kim, E. E. Reuter, S. G. Bishop, and J. J. Coleman, *Appl. Phys. Lett.* **72**, 1990 (1998).
- ³⁹⁸A. J. Winsor, S. V. Novikov, C. S. Davis, T. S. Cheng, C. T. Foxon, and I. Harrison, *Appl. Phys. Lett.* **77**, 2506 (2000).
- ³⁹⁹B. Gil, A. Morel, T. Talierecio, P. Lefebvre, C. T. Foxon, I. Harrison, A. J. Winsor, and S. V. Novikov, *Appl. Phys. Lett.* **79**, 69 (2001).
- ⁴⁰⁰S. V. Novikov *et al.*, *Phys. Status Solidi B* **228**, 227 (2001).
- ⁴⁰¹L. J. Guido, P. Mitev, M. Gerasimova, and B. Gaffey, *Appl. Phys. Lett.* **72**, 2005 (1998).
- ⁴⁰²S. R. Jin *et al.*, *J. Cryst. Growth* **212**, 56 (2000).
- ⁴⁰³H. Y. Huang, C. H. Chuang, C. K. Shu, Y. C. Pan, W. H. Lee, W. K. Chen, W. H. Chen, and M. C. Lee, *Appl. Phys. Lett.* **80**, 3349 (2002).
- ⁴⁰⁴W. M. Jadwisieniczak and H. J. Lozykowski, *Mater. Res. Soc. Symp. Proc.* **482**, 1033 (1998).
- ⁴⁰⁵C. Bozdog *et al.*, *Phys. Rev. B* **59**, 12479 (1999).
- ⁴⁰⁶K. H. Chow and G. D. Watkins, *Phys. Rev. Lett.* **81**, 2084 (1998).
- ⁴⁰⁷W. M. Chen, I. A. Buyanova, M. Wagner, B. Monemar, J. L. Lindström, H. Amano, and I. Akasaki, *Phys. Rev. B* **58**, R13351 (1998).
- ⁴⁰⁸I. A. Buyanova, Mt. Wagner, W. M. Chen, J. L. Lindström, B. Monemar, H. Amano, and I. Akasaki, *MRS Internet J. Nitride Semicond. Res.* **3**, 18 (1998).
- ⁴⁰⁹J. Baur *et al.*, *Appl. Phys. Lett.* **64**, 857 (1994).
- ⁴¹⁰R. Heitz, P. Thurian, I. Loa, L. Eckey, A. Hoffmann, K. Pressel, B. K. Meyer, and E. N. Mokhov, *Appl. Phys. Lett.* **67**, 2822 (1995).
- ⁴¹¹K. Maier, M. Kunzer, U. Kaufmann, J. Schneider, B. Monemar, I. Akasaki, and H. Amano, *Mater. Sci. Forum* **143–147**, 93 (1994).
- ⁴¹²K. Pressel, S. Nilsson, R. Heitz, A. Hoffmann, and B. K. Meyer, *J. Appl. Phys.* **79**, 3214 (1996).
- ⁴¹³J. Baur, K. Maier, M. Kunzer, U. Kaufmann, and J. Schneider, *Appl. Phys. Lett.* **65**, 2211 (1994).
- ⁴¹⁴C. Wetzel, D. Volm, B. K. Meyer, K. Pressel, S. Nilsson, E. N. Mokhov, and P. G. Baranov, *Appl. Phys. Lett.* **65**, 1033 (1994).
- ⁴¹⁵J. Baur, U. Kaufmann, M. Kunzer, J. Schneider, H. Amano, I. Akasaki, T. Detchprom, and K. Hiramatsu, *Appl. Phys. Lett.* **67**, 1140 (1995).
- ⁴¹⁶R. Heitz *et al.*, *Phys. Rev. B* **52**, 16508 (1995).
- ⁴¹⁷U. Kaufmann, A. Dörnen, V. Härle, H. Bolay, F. Scholz, and G. Pensl, *Appl. Phys. Lett.* **68**, 203 (1996).
- ⁴¹⁸A. J. Steckl, J. Heikenfeld, D. S. Lee, and M. J. Garter, *Mater. Sci. Eng., B* **81**, 97 (2001).
- ⁴¹⁹A. J. Steckl, M. Garter, D. S. Lee, J. Heikenfeld, and R. Birkhahn, *Appl. Phys. Lett.* **75**, 2184 (1999).
- ⁴²⁰D. S. Lee and A. J. Steckl, *Appl. Phys. Lett.* **81**, 2331 (2002).
- ⁴²¹D. S. Lee and A. J. Steckl, *Appl. Phys. Lett.* **82**, 55 (2003).
- ⁴²²A. J. Steckl and R. Birkhahn, *Appl. Phys. Lett.* **73**, 1700 (1998).
- ⁴²³R. Birkhahn and A. J. Steckl, *Appl. Phys. Lett.* **73**, 2143 (1998).
- ⁴²⁴M. J. Garter, J. Scofield, R. Birkhahn, and A. J. Steckl, *Appl. Phys. Lett.* **74**, 182 (1999).
- ⁴²⁵A. J. Steckl, M. Garter, R. Birkhahn, and J. Scofield, *Appl. Phys. Lett.* **73**, 2450 (1998).
- ⁴²⁶L. C. Chao, B. K. Lee, C. J. Chi, J. Chyr, and A. J. Steckl, *J. Vac. Sci. Technol. B* **17**, 2791 (1999).
- ⁴²⁷S. Morishima, T. Maruyama, M. Tanaka, Y. Masumoto, and K. Akimoto, *Phys. Status Solidi A* **176**, 113 (1999).
- ⁴²⁸R. Birkhahn, M. Garter, and A. J. Steckl, *Appl. Phys. Lett.* **74**, 2161 (1999).
- ⁴²⁹J. Heikenfeld, M. J. Garter, D. S. Lee, R. Birkhahn, and A. J. Steckl, *Appl. Phys. Lett.* **75**, 1189 (1999).
- ⁴³⁰Z. Li, H. Bang, G. Piao, J. Sawahata, and K. Akimoto, *J. Cryst. Growth* **240**, 382 (2002).
- ⁴³¹H. J. Lozykowski, W. M. Jadwisieniczak, and I. Brown, *J. Appl. Phys.* **88**, 210 (2000).
- ⁴³²T. Monteiro, C. Boemare, M. J. Soares, R. A. Sa Ferreira, L. D. Carlos, K. Lorenz, R. Vianden, and E. Alves, *Physica B* **308–310**, 22 (2001).
- ⁴³³H. J. Lozykowski, W. M. Jadwisieniczak, J. Han, and I. Brown, *Appl. Phys. Lett.* **77**, 767 (2000).
- ⁴³⁴L. C. Chao and A. J. Steckl, *Appl. Phys. Lett.* **74**, 2364 (1999).
- ⁴³⁵J. M. Zavada, R. A. Mair, C. J. Ellis, J. Y. Lin, H. X. Jiang, R. G. Wilson, P. A. Grudowski, and R. D. Dupuis, *Appl. Phys. Lett.* **75**, 790 (1999).
- ⁴³⁶A. J. Steckl and J. M. Zavada, *MRS Bull.* **24**, 33 (1999).
- ⁴³⁷D. S. Lee, J. Heikenfeld, R. Birkhahn, M. J. Garter, B. K. Lee, and A. J. Steckl, *Appl. Phys. Lett.* **76**, 1525 (2000).
- ⁴³⁸J. Menniger, U. Jahn, O. Brandt, H. Yang, and K. Ploog, *Phys. Rev. B* **53**, 1881 (1996).
- ⁴³⁹G. Ramírez-Flores, H. Navarro-Contreas, A. Lastras-Martínez, R. C. Powell, and J. E. Greene, *Phys. Rev. B* **50**, 8433 (1994).
- ⁴⁴⁰D. J. As, D. G. Pacheco-Salazar, S. Potthast, and K. Lichka, *Mater. Res. Soc. Symp. Proc.* **798**, Y8.2 (2004).
- ⁴⁴¹D. J. As *et al.*, *MRS Internet J. Nitride Semicond. Res.* **5S1**, W3.81 (2000).
- ⁴⁴²U. Strauss *et al.*, *Semicond. Sci. Technol.* **12**, 637 (1997).
- ⁴⁴³A. V. Andrianov, D. E. Lacklison, J. W. Orton, T. S. Cheng, C. T. Foxon, K. P. O'Donnell, and J. F. H. Nicholls, *Semicond. Sci. Technol.* **12**, 59 (1997).
- ⁴⁴⁴D. J. As, F. Schmilgus, C. Wang, B. Schöttker, D. Schikora, and K. Lischka, *Appl. Phys. Lett.* **70**, 1311 (1997).
- ⁴⁴⁵D. Xu *et al.*, *Appl. Phys. Lett.* **76**, 3025 (2000).
- ⁴⁴⁶J. Wu, H. Yaguchi, K. Onabe, R. Ito, and Y. Shiraki, *Appl. Phys. Lett.* **71**, 2067 (1997).
- ⁴⁴⁷Z. X. Liu, A. R. Goni, K. Syassen, H. Siegle, C. Thomsen, B. Schöttker, D. J. As, and D. Schikora, *J. Appl. Phys.* **86**, 929 (1999).
- ⁴⁴⁸R. Klann, O. Brandt, H. Yang, H. T. Grahm, K. Ploog, and A. Trampert, *Phys. Rev. B* **52**, 11615 (1995).
- ⁴⁴⁹S. Strite, J. Ruan, Z. Li, A. Salvador, H. Chen, D. J. Smith, W. J. Choyke, and H. Morkoç, *J. Vac. Sci. Technol. B* **9**, 1924 (1991).
- ⁴⁵⁰B. Daudin *et al.*, *J. Appl. Phys.* **84**, 2295 (1998).
- ⁴⁵¹T. Kurobe, Y. Sekiguchi, J. Suda, M. Yoshimoto, and H. Matsunami, *Appl. Phys. Lett.* **73**, 2305 (1998).
- ⁴⁵²J. Menniger, U. Jahn, O. Brandt, H. Yang, and K. Ploog, *Appl. Phys. Lett.* **69**, 836 (1996).
- ⁴⁵³E. M. Goldys, M. Godlewski, R. Langer, A. Barski, P. Bergman, and B. Monemar, *Phys. Rev. B* **60**, 5464 (1999).
- ⁴⁵⁴D. J. As, U. Köhler, and K. Lischka, *Mater. Res. Soc. Symp. Proc.* **693**, I2.3 (2002).
- ⁴⁵⁵D. J. As, U. Köhler, M. Lübbbers, J. Mimkes, and K. Lischka, *Phys. Status Solidi A* **188**, 699 (2001).
- ⁴⁵⁶U. Köhler, M. Lübbbers, J. Mimkes, and D. J. As, *Phys. Status Solidi B* **308–310**, 126 (2001).
- ⁴⁵⁷J. R. L. Fernandez *et al.*, *Microelectron. J.* **35**, 73 (2004).
- ⁴⁵⁸D. J. As and U. Köhler, *J. Phys.: Condens. Matter* **13**, 8923 (2001).
- ⁴⁵⁹D. J. As, *Defect Diffus. Forum* **206–207**, 87 (2002).
- ⁴⁶⁰D. J. As, *Phys. Status Solidi B* **210**, 445 (1998).
- ⁴⁶¹D. Xu, H. Yang, D. G. Zhao, S. F. Li, and R. H. Wu, *J. Appl. Phys.* **87**, 2064 (2000).
- ⁴⁶²Z. Q. Li *et al.*, *Appl. Phys. Lett.* **76**, 3765 (2000).
- ⁴⁶³C. Moysés Araújo *et al.*, *Microelectron. J.* **33**, 365 (2002).
- ⁴⁶⁴A. V. Rodina, M. Dietrich, A. Göldner, L. Eckey, A. Hoffmann, Al. L. Efros, M. Rosen, and B. K. Meyer, *Phys. Rev. B* **64**, 115204 (2001).
- ⁴⁶⁵P. P. Paskov, T. Paskova, P. O. Holtz, and B. Monemar, *Phys. Rev. B* **64**, 115201 (2001).
- ⁴⁶⁶P. P. Paskov, T. Paskova, P. O. Holtz, and B. Monemar, *Phys. Status Solidi B* **228**, 467 (2001).
- ⁴⁶⁷M. Julier, J. Campo, B. Gil, J. P. Lascaray, and S. Nakamura, *Phys. Rev. B* **57**, R6791 (1998).
- ⁴⁶⁸D. C. Reynolds, D. C. Look, B. Jogai, A. W. Saxler, S. S. Park, and J. Y. Hahn, *Appl. Phys. Lett.* **77**, 2879 (2000).
- ⁴⁶⁹A. Hoffmann, *Adv. Solid State Phys.* **36**, 33 (1996).
- ⁴⁷⁰R. Stepniewski *et al.*, *Phys. Rev. B* **56**, 15151 (1997).
- ⁴⁷¹D. Volm *et al.*, *Phys. Rev. B* **53**, 16543 (1996).
- ⁴⁷²D. Kovalev, B. Averboukh, D. Volm, B. K. Meyer, H. Amano, and I. Akasaki, *Phys. Rev. B* **54**, 2518 (1996).
- ⁴⁷³B. Monemar, *Phys. Rev. B* **10**, 676 (1974).

- ⁴⁷⁴B. Gil, O. Briot, and R. L. Aulombard, *Phys. Rev. B* **52**, 17028 (1995).
- ⁴⁷⁵A. A. Yamaguchi, Y. Mochizuki, H. Sunakawa, and A. Usui, *J. Appl. Phys.* **83**, 4542 (1998).
- ⁴⁷⁶E. I. Rashba and G. E. Gurgenishvili, *Sov. Phys. Solid State* **4**, 759 (1962).
- ⁴⁷⁷S. Permogorov, A. N. Reznitskii, S. Yu. Verbin, and V. A. Bonch-Bruевич, *Pis'ma Zh. Eksp. Teor. Fiz.* **38**, 22 (1983).
- ⁴⁷⁸J. J. Hopfield and D. G. Thomas, *Phys. Rev.* **122**, 35 (1961).
- ⁴⁷⁹K. Kornitzer *et al.*, *Phys. Rev. B* **60**, 1471 (1999).
- ⁴⁸⁰J. A. Freitas, Jr., W. J. Moore, B. V. Shanabrook, G. C. B. Braga, S. K. Lee, S. S. Park, and J. Y. Han, *Phys. Rev. B* **66**, 233311 (2002).
- ⁴⁸¹A. Wyszomolek *et al.*, *Phys. Rev. B* **66**, 245317 (2002).
- ⁴⁸²A. Wyszomolek, M. Potemski, R. Stepniewski, J. M. Baranowski, D. C. Look, S. K. Lee, and J. Y. Han, *Phys. Status Solidi B* **235**, 36 (2003).
- ⁴⁸³K. Kornitzer *et al.*, *Phys. Rev. B* **60**, 1471 (1999).
- ⁴⁸⁴B. J. Skromme, J. Jayapalan, R. P. Vaudo, and V. M. Phanse, *Appl. Phys. Lett.* **74**, 2358 (1999).
- ⁴⁸⁵K. Pakula *et al.*, *Solid State Commun.* **97**, 919 (1996).
- ⁴⁸⁶K. P. Korona, *Phys. Rev. B* **65**, 235312 (2002).
- ⁴⁸⁷J. A. Freitas, Jr., W. J. Moore, B. V. Shanabrook, G. C. B. Braga, S. K. Lee, S. S. Park, J. Y. Han, and D. D. Koleske, *J. Cryst. Growth* **246**, 307 (2002).
- ⁴⁸⁸D. C. Reynolds, D. C. Look, B. Jogai, V. M. Phanse, and R. P. Vaudo, *Solid State Commun.* **103**, 533 (1997).
- ⁴⁸⁹U. Kaufmann, C. Merz, B. Santic, R. Nieguhr, H. Obloh, and K. H. Bachem, *Mater. Sci. Eng., B* **50**, 109 (1997); B. Santic, C. Merz, U. Kaufmann, R. Niebuhr, H. Obloh, and K. Bachem, *Appl. Phys. Lett.* **71**, 1837 (1997).
- ⁴⁹⁰A. K. Vismanah, J. I. Lee, D. Kim, C. R. Lee, and J. Y. Leam, *Phys. Rev. B* **58**, 16333 (1998).
- ⁴⁹¹R. A. Mair, J. Li, S. K. Duan, J. Y. Lin, and H. X. Jiang, *Appl. Phys. Lett.* **74**, 513 (1999).
- ⁴⁹²B. K. Meyer, *Mater. Res. Soc. Symp. Proc.* **449**, 497 (1997).
- ⁴⁹³A. Shikanai, H. Fukahori, Y. Kawakami, K. Hazu, T. Sota, T. Mitani, T. Mukai, and S. Fujita, *Phys. Status Solidi B* **235**, 26 (2003).
- ⁴⁹⁴Q. Yang, H. Feick, and E. R. Weber, *Appl. Phys. Lett.* **82**, 3002 (2003).
- ⁴⁹⁵B. Monemar, W. M. Chen, P. P. Paskov, T. Paskova, G. Pozina, and J. P. Bergman, *Phys. Status Solidi B* **228**, 489 (2001).
- ⁴⁹⁶R. Stepniewski *et al.*, *Phys. Rev. Lett.* **91**, 226404 (2003).
- ⁴⁹⁷A. Wyszomolek *et al.*, *Phys. Status Solidi B* **216**, 11 (1999).
- ⁴⁹⁸D. G. Thomas and J. J. Hopfield, *Phys. Rev.* **128**, 2135 (1965).
- ⁴⁹⁹B. Monemar, J. P. Bergman, I. G. Ivanov, J. M. Baranowski, K. Pakula, I. Grzegory, and S. Porowski, *Mater. Sci. Forum* **264–268**, 1275 (1998).
- ⁵⁰⁰B. J. Skromme, K. C. Palle, C. D. Poweleit, H. Yamane, M. Aoki, and F. J. DiSalvo, *Appl. Phys. Lett.* **81**, 3765 (2002).
- ⁵⁰¹V. Kirilyuk, P. R. Hageman, P. C. M. Christianen, P. K. Larsen, and M. Zielinski, *Appl. Phys. Lett.* **79**, 4109 (2001); V. Kirilyuk, P. R. Hageman, P. C. M. Christianen, W. H. M. Corbeek, M. Zielinski, L. Macht, J. L. Weyher, and P. K. Larsen, *Phys. Status Solidi A* **188**, 473 (2001).
- ⁵⁰²K. P. Korona, R. Doradzinski, M. Palczewska, M. Pietras, M. Kaminska, and J. Kuhl, *Phys. Status Solidi B* **235**, 40 (2003).
- ⁵⁰³K. P. Korona *et al.*, *Phys. Status Solidi B* **235**, 31 (2003).
- ⁵⁰⁴J. R. Haynes, *Phys. Rev. Lett.* **4**, 361 (1960).
- ⁵⁰⁵M. Ikeda, H. Matsunami, and T. Tanaka, *Phys. Rev. B* **22**, 2842 (1980).
- ⁵⁰⁶A. Henry, C. Hallin, I. G. Ivanov, J. P. Bergman, O. Kordina, U. Lindelfelt, and E. Janzen, *Phys. Rev. B* **53**, 13503 (1996).
- ⁵⁰⁷P. J. Dean, *Physica B & C* **117–118**, 140 (1983).
- ⁵⁰⁸H. Y. An, O. H. Cha, J. H. Kim, G. M. Yang, K. Y. Lim, E. K. Suh, and H. J. Lee, *J. Appl. Phys.* **85**, 2888 (1999).
- ⁵⁰⁹Y. C. Chang and T. C. McGill, *Solid State Commun.* **30**, 187 (1979).
- ⁵¹⁰P. J. Schuck, M. D. Mason, R. D. Grober, O. Ambacher, A. P. Lima, C. Miskys, R. Dimitrov, and M. Stutzmann, *Appl. Phys. Lett.* **79**, 952 (2001).
- ⁵¹¹Y. J. Sun, O. Brandt, U. Jahn, T. Y. Liu, A. Trampert, S. Cronenberg, S. Dhar, and K. H. Ploog, *J. Appl. Phys.* **92**, 5714 (2002).
- ⁵¹²B. C. Chung and M. Gershenson, *J. Appl. Phys.* **72**, 651 (1992).
- ⁵¹³K. Kornitzer, M. Mayer, M. Mundbrod, K. Thonke, A. Pelzmann, M. Kamp, and R. Sauer, *Mater. Sci. Forum* **258–263**, 1113 (1997).
- ⁵¹⁴B. G. Ren, J. W. Orton, T. S. Cheng, D. J. Dewsnip, D. E. Lacklison, C. T. Foxon, C. H. Malloy, and X. Chen, *MRS Internet J. Nitride Semicond. Res.* **1**, 22 (1996).
- ⁵¹⁵S. Fischer *et al.*, *J. Cryst. Growth* **189–190**, 556 (1998).
- ⁵¹⁶E. Calleja, M. A. Sánchez-García, F. J. Sánchez, F. Calle, F. B. Naranjo, E. Munoz, U. Jahn, and K. Ploog, *Phys. Rev. B* **62**, 16826, (2000).
- ⁵¹⁷G. Salviati *et al.*, *Phys. Status Solidi A* **171**, 325 (1999).
- ⁵¹⁸K. W. Mah, E. McGlynn, J. Castro, J. G. Lunney, J. P. Mosnier, D. O'Mahony, and M. O. Henry, *J. Cryst. Growth* **222**, 497 (2001).
- ⁵¹⁹Y. T. Rebane, Y. G. Shreter, and M. Albrecht, *Phys. Status Solidi A* **164**, 141 (1997).
- ⁵²⁰Y. G. Shreter *et al.*, *Mater. Res. Soc. Symp. Proc.* **449**, 683 (1997).
- ⁵²¹F. Calle, F. J. Sanchez, J. M. G. Tiero, M. A. Sanchez-Garcia, E. Calleja, and R. Beresford, *Semicond. Sci. Technol.* **12**, 1396 (1997).
- ⁵²²M. Cazzanelli, D. Cole, J. F. Donegan, J. G. Lunney, P. G. Middleton, K. P. O'Donnell, C. Vinegoni, and L. Pavesi, *Appl. Phys. Lett.* **73**, 3390 (1998).
- ⁵²³C. Wetzel, S. Fisher, J. Krüger, E. E. Haller, R. J. Molnar, T. D. Moustakas, E. N. Mokhov, and P. G. Baranov, *Appl. Phys. Lett.* **68**, 2556 (1996).
- ⁵²⁴C. H. Hong, D. Pavlidis, S. W. Brown, and S. C. Rand, *J. Appl. Phys.* **77**, 1705 (1995).
- ⁵²⁵Z. Chen *et al.*, *J. Appl. Phys.* **93**, 316 (2003).
- ⁵²⁶K. W. Mah, J.-P. Mosnier, E. McGlynn, M. O. Henry, D. O'Mahony, and J. G. Lunney, *Appl. Phys. Lett.* **80**, 3301 (2002).
- ⁵²⁷P. G. Middleton, K. P. O'Donnell, C. Trager-Cowan, D. Cole, M. Cazzanelli, and J. Lunney, *Mater. Sci. Eng., B* **59**, 133 (1999).
- ⁵²⁸Y. Shon, Y. H. Kwon, T. W. Kang, X. Fan, D. Fu, and Y. Kim, *J. Cryst. Growth* **245**, 193 (2002).
- ⁵²⁹G. Martinez-Criado, A. Cros, A. Cantareo, R. Dimitrov, O. Ambacher, and M. Stutzmann, *J. Appl. Phys.* **88**, 3470 (2000).
- ⁵³⁰W. Rieger, R. Dimitrov, D. Brunner, E. Rohrer, O. Ambacher, and M. Stutzmann, *Phys. Rev. B* **54**, 17596 (1996).
- ⁵³¹B. K. Meyer *et al.*, *Mater. Res. Soc. Symp. Proc.* **378**, 521 (1995).
- ⁵³²L. Eckey *et al.*, *Mater. Res. Soc. Symp. Proc.* **395**, 589 (1996); L. Eckey *et al.*, *Appl. Phys. Lett.* **68**, 415 (1996).
- ⁵³³F. A. Ponce, D. P. Pour, W. Götz, and P. J. Wright, *Appl. Phys. Lett.* **68**, 57 (1996).
- ⁵³⁴R. Dai, S. Fu, J. Xie, G. Fan, G. Hu, H. Schrey, and C. Klingshirn, *J. Phys. C* **15**, 393 (1982).
- ⁵³⁵A. Bell, I. Harrison, D. Korakakis, E. C. Larkins, J. M. Hayes, M. Kuball, N. Grandjean, and J. Massies, *J. Appl. Phys.* **89**, 1070 (2001).
- ⁵³⁶N. Grandjean, M. Leroux, M. Lügt, and J. Massies, *Appl. Phys. Lett.* **71**, 240 (1997).
- ⁵³⁷M. A. Reshchikov *et al.*, *J. Appl. Phys.* **94**, 5623 (2003).
- ⁵³⁸M. A. Reshchikov, J. Jasinski, Z. Liliental-Weber, D. Huang, L. He, P. Visconti, and H. Morkoç, *Physica B* **340–342**, 440 (2003).
- ⁵³⁹M. A. Reshchikov, D. Huang, F. Yun, H. Morkoç, R. J. Molnar, and C. W. Litton, *Mater. Res. Soc. Symp. Proc.* **693**, I6.28 (2002).
- ⁵⁴⁰M. A. Reshchikov, D. Huang, and H. Morkoç, *Mater. Res. Soc. Symp. Proc.* **743**, L11.3 (2003).
- ⁵⁴¹M. A. Reshchikov, J. Jasinski, F. Yun, L. He, Z. Liliental-Weber, and H. Morkoç, *Mater. Res. Soc. Symp. Proc.* **798**, Y5.66 (2004).
- ⁵⁴²S. J. Xu, H. J. Wang, S. H. Cheung, Q. Li, X. Q. Dai, M. H. Xie, and S. Y. Tong, *Appl. Phys. Lett.* **83**, 3477 (2003).
- ⁵⁴³K. Palle, L. Chen, H. X. Liu, B. J. Skromme, H. Yamane, M. Aoki, C. B. Hoffmann, and F. J. DiSalvo, *Mater. Res. Soc. Symp. Proc.* **743**, L3.36 (2003).
- ⁵⁴⁴L. Chen *et al.*, *Mater. Res. Soc. Symp. Proc.* **798**, Y5.55 (2004).
- ⁵⁴⁵M. A. Reshchikov, A. Teke, H. P. Maruska, D. W. Hill, and H. Morkoç, *Mater. Res. Soc. Symp. Proc.* **798**, Y5.53 (2004).
- ⁵⁴⁶D. Huang, P. Visconti, K. M. Jones, M. A. Reshchikov, F. Yun, A. A. Baski, T. King, and H. Morkoç, *Appl. Phys. Lett.* **78**, 4145 (2001).
- ⁵⁴⁷M. A. Reshchikov, *Progress in Condensed Matter Research* (Nova Science Publishers, Inc., New York, to be published).
- ⁵⁴⁸P. Visconti, M. A. Reshchikov, K. M. Jones, D. F. Wang, R. Cingolani, H. Morkoç, R. J. Molnar, and D. J. Smith, *J. Vac. Sci. Technol. B* **19**, 1328 (2001).
- ⁵⁴⁹C. Yotsey, L. T. Romano, and I. Adesida, *Appl. Phys. Lett.* **73**, 797 (1998).
- ⁵⁵⁰M. A. Reshchikov, D. Huang, F. Yun, P. Visconti, T. King, H. Morkoç, J. Jasinski, and Z. Liliental-Weber, *Mater. Res. Soc. Symp. Proc.* **693**, I10.3 (2002).
- ⁵⁵¹D. Huang *et al.*, *Phys. Status Solidi A* **188**, 571 (2001).
- ⁵⁵²The Huang–Rhys factor is determined here as the ratio of intensities between the first phonon replica and the zero-phonon line, see, K. Huang and A. Rhys, *Proc. R. Soc. London, Ser. A* **204**, 406 (1950).
- ⁵⁵³U. Karrer, O. Ambacher, and M. Stutzmann, *Appl. Phys. Lett.* **77**, 2012 (2000).
- ⁵⁵⁴M. A. Reshchikov, D. Huang, L. He, H. Morkoç, J. Jasinski, Z. Liliental-

- Weber, S. S. Park, and K. Y. Lee, (unpublished).
- ⁵⁵⁵ J. D. Levine, *Phys. Rev.* **140**, A586 (1965).
- ⁵⁵⁶ D. Schechter, *Phys. Rev. Lett.* **19**, 692 (1967).
- ⁵⁵⁷ V. V. Travnikov, *Opt. Spectrosc.* **67**, 377 (1989).
- ⁵⁵⁸ Q. K. Xue, Q. Z. Xue, S. Kuwano, K. Nakayama, T. Sakurai, I. S. T. Tsong, X. G. Qui, and Y. Segawa, *J. Cryst. Growth* **229**, 41 (2001).
- ⁵⁵⁹ S. T. Kim, Y. J. Lee, S. H. Chung, and D. C. Moon, *Semicond. Sci. Technol.* **14**, 156 (1999).
- ⁵⁶⁰ T. Metzger *et al.*, *Philos. Mag. A* **77**, 1013 (1998).
- ⁵⁶¹ T. F. Huang, A. Marshall, S. Spruytte, and J. S. Harris, Jr., *J. Cryst. Growth* **200**, 362 (1999).
- ⁵⁶² M. Albrecht *et al.*, *Mater. Res. Soc. Symp. Proc.* **468**, 293 (1997).
- ⁵⁶³ N. A. Drozdov, A. A. Partin, and V. D. Tkachev, *Pis'ma Zh. Eksp. Teor. Fiz.* **23**, 651 (1976) [*JETP Lett.* **23**, 597 (1976)].
- ⁵⁶⁴ P. J. Dean, *Inst. Phys. Conf. Ser.* **46**, 100 (1979).
- ⁵⁶⁵ P. J. Dean, *Phys. Status Solidi A* **81**, 625 (1984).
- ⁵⁶⁶ A. Naumov, K. Wolf, T. Reisinger, H. Stanzl, and W. Gebhardt, *J. Appl. Phys.* **73**, 2581 (1993).
- ⁵⁶⁷ A. V. Kvit *et al.*, *Fiz. Tverd. Tela (S.-Peterburg)* **40**, 1010 (1998) [*Phys. Solid State* **40**, 924 (1998)].
- ⁵⁶⁸ R. Sauer, Ch. Kisielowski-Kammerich, and H. Alexander, *Phys. Rev. Lett.* **57**, 1472 (1986).
- ⁵⁶⁹ V. Higgs, E. C. Lightowers, and P. Kightley, *Mater. Res. Soc. Symp. Proc.* **163**, 57 (1990).
- ⁵⁷⁰ Yu. Shreter, Yu. T. Rebane, and A. R. Peaker, *Phys. Status Solidi A* **138**, 681 (1993).
- ⁵⁷¹ P. J. Dean, G. M. Williams, and G. Blackmore, *J. Phys. D* **17**, 2291 (1984).
- ⁵⁷² L. C. Kimerling, *Solid-State Electron.* **21**, 1391 (1978).
- ⁵⁷³ P. J. Dean and L. C. Kimerling, *Adv. Phys.* **26**, 1 (1977).
- ⁵⁷⁴ R. M. Feenstra and T. C. McGill, *Phys. Rev. Lett.* **47**, 925 (1981).
- ⁵⁷⁵ Y. Koshka, *Phys. Rev. B* **69**, 035205 (2004).
- ⁵⁷⁶ P. W. Hutchinso, P. S. Dobson, B. Wakefield, and S. O'Hara, *Solid-State Electron.* **21**, 1413 (1978).
- ⁵⁷⁷ P. D. Dapkus and C. H. Henry, *J. Appl. Phys.* **47**, 4061 (1976).
- ⁵⁷⁸ D. Shvydka, C. Verzella, V. G. Karpov, and A. D. Compaan, *J. Appl. Phys.* **94**, 3901 (2003).
- ⁵⁷⁹ S. J. Xu, G. Li, S. J. Chua, X. C. Wang, and W. Wang, *Appl. Phys. Lett.* **72**, 2451 (1998).
- ⁵⁸⁰ S. A. Brown, R. J. Reeves, and C. S. Haase, R. Cheung, C. Kirchner, and M. Kamp, *Appl. Phys. Lett.* **75**, 3285 (1999).
- ⁵⁸¹ B. J. Ryan, M. O. Henry, E. McGlynn, and J. Fryar, *Physica B* **340–342**, 452 (2003).
- ⁵⁸² S. Dhar and S. Ghosh, *Appl. Phys. Lett.* **80**, 4519 (2002).
- ⁵⁸³ B. Kim, I. Kuskovsky, I. P. Herman, D. Li, and G. F. Neumark, *J. Appl. Phys.* **86**, 2034 (1999).
- ⁵⁸⁴ M. A. Reshchikov, P. Visconti, and H. Morkoç, *Appl. Phys. Lett.* **78**, 177 (2001).
- ⁵⁸⁵ M. A. Reshchikov, P. Visconti, H. Morkoç, R. J. Molnar, and C. W. Litton, *Proceedings of the International Workshop on Nitride Semiconductors, IPAP Conference Series, 2000* (The Institute of Pure and Applied Physics, Tokyo, Japan, 2000), Vol. 1, pp. 506–509.
- ⁵⁸⁶ M. A. Reshchikov, Y. T. Moon, and H. Morkoç, *Phys. Status Solidi C* (to be published).
- ⁵⁸⁷ Y. C. Chang, A. E. Oberhofer, J. F. Muth, R. M. Kolbas, and R. F. Davis, *Appl. Phys. Lett.* **79**, 281 (2001).
- ⁵⁸⁸ Y. C. Chang, A. L. Cai, M. A. L. Johnson, J. F. Muth, R. M. Kolbas, Z. J. Reitmeier, S. Einfeldt, and R. F. Davis, *Appl. Phys. Lett.* **80**, 2675 (2002).
- ⁵⁸⁹ I. K. Shmagin, J. F. Muth, J. H. Lee, R. M. Kolabs, C. M. Balkas, Z. Sitar, and R. F. Davis, *Appl. Phys. Lett.* **71**, 455 (1997).
- ⁵⁹⁰ U. Behn, A. Thamm, O. Brandt, and H. T. Grahn, *J. Appl. Phys.* **87**, 4315 (2000).
- ⁵⁹¹ T. S. Kim, S. D. Lester, and B. G. Streetman, *J. Appl. Phys.* **61**, 2072 (1987).
- ⁵⁹² A. J. Kontkiewicz *et al.*, *Appl. Phys. Lett.* **65**, 1436 (1994).
- ⁵⁹³ L. Tsybeskov, Ju. V. Vandyshev, and P. M. Fauchet, *Phys. Rev. B* **49**, 7821 (1994).
- ⁵⁹⁴ M. A. Reshchikov, M. Zafar Iqbal, D. Huang, L. He, and H. Morkoç, *Mater. Res. Soc. Symp. Proc.* **743**, L11.2 (2003).
- ⁵⁹⁵ M. Zafar Iqbal, M. A. Reshchikov, L. He, and H. Morkoç, *J. Electron. Mater.* **32**, 346 (2003).
- ⁵⁹⁶ V. A. Joshkin, J. C. Roberts, F. G. McIntosh, S. M. Bedair, E. L. Piner, and M. K. Behbehani, *Appl. Phys. Lett.* **71**, 234 (1997).
- ⁵⁹⁷ Sample 5 was grown in our laboratory, while sample 6 was prepared at LUMILOG (France).
- ⁵⁹⁸ V. M. Bermudez, *J. Appl. Phys.* **80**, 1190 (1996).
- ⁵⁹⁹ C. I. Wu, A. Kahn, N. Taskar, D. Dorman, and D. Gallagher, *J. Appl. Phys.* **83**, 4249 (1998).
- ⁶⁰⁰ S. Sabuktagin, M. A. Reshchikov, D. K. Johnstone, and H. Morkoç, *Mater. Res. Soc. Symp. Proc.* **798**, Y5.39 (2004).
- ⁶⁰¹ S.-J. Cho, S. Dogan, S. Sabuktagin, M. A. Reshchikov, D. K. Johnstone, and H. Morkoç, *Appl. Phys. Lett.* **84**, 3070 (2004).
- ⁶⁰² T. Sasaki and T. Matsuoka, *J. Appl. Phys.* **64**, 4531 (1988).
- ⁶⁰³ R. A. Beach, E. C. Piquette, and T. C. McGill, *MRS Internet J. Nitride Semicond. Res.* **4S1**, G6.26 (1999).
- ⁶⁰⁴ L. Kronik and Y. Shapira, *Surf. Sci. Rep.* **37**, 1 (1999).
- ⁶⁰⁵ H. Nienhaus, M. Schneider, S. P. Grabowski, W. Mönch, R. Dimitrov, O. Ambacher, and M. Stutzmann, *Mater. Res. Soc. Symp. Proc.* **680**, E4.5 (2001).
- ⁶⁰⁶ S. M. Sze, *Physics of Semiconductor Device*, 2nd ed. (Wiley, New York, 1981).
- ⁶⁰⁷ M. A. Reshchikov, P. Visconti, K. M. Jones, H. Morkoç, R. J. Molnar, and C. W. Litton, *Mater. Res. Soc. Symp. Proc.* **680**, E5.4 (2001).
- ⁶⁰⁸ G. L. Martinez, M. R. Curiel, B. J. Skromme, and R. J. Molnar, *J. Electron. Mater.* **29**, 325 (2000).
- ⁶⁰⁹ E. V. Konenkova, *Vacuum* **67**, 43 (2002).
- ⁶¹⁰ J. O. Song, S.-J. Park, and T.-Y. Seong, *Appl. Phys. Lett.* **80**, 3129 (2002).
- ⁶¹¹ Y.-J. Lin, Z.-L. Wang, and H.-C. Chang, *Appl. Phys. Lett.* **81**, 5183 (2002).